Controlling Realism and Uncertainty in Reservoir Models using Intelligent Sedimentological Prior Information

TEMISTOCLES SIMON ROJAS

Thesis Submitted for the
Degree of Doctor of Philosophy
Institute of Petroleum Engineering
Heriot-Watt University
Edinburgh, December 2013

Abstract

Forecasting reservoir production has a large associated uncertainty, since this is the final part of a very complex process, this process is based on sparse and indirect data measurements. One the methodologies used in the oil industry to predict reservoir production is based on the Baye's theorem. Baye's theorem applied to reservoir forecasting, samples parameters from a prior understanding of the uncertainty to generate reservoir models and updates this prior information by comparing reservoir production data with model production response.

In automatic history matching it is challenging to generate reservoir models that preserve geological realism (obtain reservoir models with geological features that have been seen in nature). One way to control the geological realism in reservoir models is by controlling the realism of the geological prior information.

The aim of this thesis is to encapsulate sedimentological information in order to build prior information that can control the geological realism of the history-matched models. This "intelligent" prior information is introduced into the automatic history-matching framework rejecting geologically unrealistic reservoir models. Machine Learning Techniques (MLT) were used to build realistic sedimentological prior information models.

Another goal of this thesis was to include geological parameters into the automatic history-match framework that have an impact on reservoir model performance: vertical variation of facies proportions, connectivity of geobodies, and the use of multiple training images as a source of realistic sedimentological prior information.

The main outcome of this thesis is that the use of "intelligent" sedimentological prior information guarantees the realism of reservoir models and reduces computing time and uncertainty in reservoir production prediction.

Dedication

To Gaby, Valen and Mariale

To Tin, Gladys, Anita, Pedro and Norbelia

Acknowledgments

First, I want to thank God for all the blessings he has given me.

I would like to express my deepest gratitude to my supervisors Dr. Vasily Demyanov and Prof. Mike Christie for giving me the opportunity to work in this amazing and cutting edge topic and for their support and guidance throughout the meandering path of a PhD.

I would like to thank the financial support provided for this research by the sponsors of the Uncertainty Project (Phase III) at Heriot-Watt: BP, BGG, Conoco-Phillips, Jogmec and Epistemy.

I am very grateful with Prof. Mikhail Kanevski from University of Lausanne and Dr. Alexei Pozdnoukhov from the National University of Ireland for their recommendations on the use of machine learning and with Dr. Alexandre Boucher from Stanford University for his advice on the use of SGeMS. I really appreciate the talk I had with Prof. Sophie Viseur from Marseille University, recommending the use of Deep-Marine data. Thanks to Prof. Dorrik Stow from IPE Heriot-Watt for reviewing part of this work. I am in great debt with Dr. Dan Arnold (my 3rd supervisor) from IPE Heriot-Watt for sharing his experience and knowledge related to geological parameterization, coding with Python and history matching. I also would like to thank IPE PhD students Lorna, Linah, Yasin, Hamid, Mohammad Asaad, Maria Helena, Doaa, and Antonio; and my soul brothers: Jesus, Fucho, Michel, Sebastian and Yonathan. Many thanks as well to the football mates in Heriot-Watt for making easier this journey.

I would like to thank the examiners of this thesis: Prof. Guillaume Caumon from the Nancy School of Geology and Dr. Andy Gardiner from Heriot-Watt University, whose recommendations substantially improved this document.

An endless gratitude to my angels, my wife Gabriela and my daughters Valentina and Maria Alejandra for their support and all the sacrifices they did by leaving the beautiful Buenos Aires to have some economic hard times in the exciting Edinburgh. Finally enormous thanks to my father for inspiring and encouraging me to do this.

Publications

Rojas, T., Demyanov, V., Christie, M. and Arnold, D. (2011) *Use of Geological Prior Information in Reservoir Facies Models*. In Marschaginger, R. and Zolb, F. (eds.) Proceedings of the IAMG 2011 Conference. Salzburg Austria. 266-285.

Rojas, T., Demyanov, V., Christie, M. and Arnold, D. (2012) *Geological Realism of Deep Water Channel Reservoir Models with Intelligent Priors*. Search and Discovery Article #41011. Adapted from oral presentation at AAPG Annual Convention and Exhibition, Long Beach, California, April 22-25, 2012

Rojas, T., Demyanov, V., Christie, M. and Arnold, D. (2012) *Reducing Uncertainty in Modelling Fluvial Reservoirs by using Intelligent Geological Priors*. Ninth International Geostatistics Congress, Oslo, Norway. Expanded Abstract. 11pp.

ACADEMIC REGISTRY
Research Thesis Submission

Name*:*	TEMISTOCLES SIMON ROJAS		
School/PGI:	Institute of Petroleum Engineering		
Version: *(i.e. First, Resubmission, Final)*	Final	Degree Sought (Award **and** Subject area)	Ph.D. Petroleum Engineering

Declaration

In accordance with the appropriate regulations I hereby submit my thesis and I declare that:

1) the thesis embodies the results of my own work and has been composed by myself
2) where appropriate, I have made acknowledgement of the work of others and have made reference to work carried out in collaboration with other persons
3) the thesis is the correct version of the thesis for submission and is the same version as any electronic versions submitted*.
4) my thesis for the award referred to, deposited in the Heriot-Watt University Library, should be made available for loan or photocopying and be available via the Institutional Repository, subject to such conditions as the Librarian may require
5) I understand that as a student of the University I am required to abide by the Regulations of the University and to conform to its discipline.

* *Please note that it is the responsibility of the candidate to ensure that the correct version of the thesis is submitted.*

Signature of Candidate*:*		Date:	27/12/2013

Submission

Submitted By *(name in capitals):*	
Signature of Individual Submitting:	
Date Submitted:	

For Completion in the Student Service Centre (SSC)

Received in the SSC by *(name in capitals):*			
Method of Submission (Handed in to SSC; posted through internal/external mail):			
*E-thesis Submitted (**mandatory for final theses)***			
Signature:		Date:	

Contents

List of Figures

List of Tables

Chapter 1

Introduction

1.1 Motivation

Hydrocarbon exploration and production is a very risky business since the investment necessary to find and develop economical accumulations easily reaches billions of pounds and the uncertainty associated with this business is considerable because available data are usually scarce and inexact. Reservoir data commonly come from two main sources:

(1) Geophysical information: This information does not have yet the resolution required to completely understand the geometry of the reservoir and it is necessary to process this information, e.g. data processing, time-depth conversions and attribute analysis, to have this data in a geologically interpretable version.

(2) Well data: Well-log data is measured by physical methods within the well-bore. These data can be found with different vertical and horizontal resolution.

Well information data are punctual and could be separated from other wells by hundreds of meters. Other reservoir information coming from wells includes well production tests, core-data (core description, petrophysical analysis), side wall samples (for petrophysical and lithological analysis) and fluid analysis pressure, volume and temperature analysis (PVT).

Another source of information is the characterization of outcrops related to the reservoir being studied. Although outcrop characterization makes easier the visualization of the relationships between different reservoir facies, structures and petrophysical properties, outcrops are usually from analogous geological formations deposited in a different geological age and separated by long distances from the studied reservoir. Because of the differences in geological age and the geographical separation between outcrops and reservoirs, outcrop information introduces uncertainty to the geological interpretation of a reservoir.

Summarizing, the information used to characterize a reservoir can be obtained from direct measurements like well information (e-logs, cores, production data, pressure, etc.) and geophysical information (seismic, gravity and magnetic methods). Information can be obtained from indirect sources like outcrops and modern analogue characterization, or information obtained from analogue reservoirs. All this information has different levels of resolution and scale and is subject to different levels of uncertainty.

All the data obtained from a reservoir are used to characterize and understand the reservoir in order to quantify the reserves and to predict the production behaviour. Nowadays the conventional methodology to characterize and understand a reservoir is the generation of reservoir models, which are three-dimensional representations of the studied reservoir. These models can be generated by numerical simulations that consider the geometry of geological features and how the reservoir properties (i.e. porosity, permeability, fluid saturation, pressure, etc.) are distributed within these geological features.

Since 1990’s the advances in computing software and hardware have made it possible to generate multiple models of a reservoir using a single set of data.

Although, the data may be the same, the way they are compiled in the model varies depending on the modelling algorithm, assumptions, interpretation, processing and targets. Generating multiple reservoir models has been useful in analysing the uncertainty associated with the reserves estimation and production forecast of a reservoir.

The conventional methodology used in the hydrocarbon industry to evaluate the reliability of a reservoir model is the so called history match process, which is based on building a reservoir model that is consistent with the production history. History matched models are considered as the models that best represent the distribution of geological and physical properties within a reservoir given the production data. History matched models are used to predict the production behaviour of a reservoir. The forecast of the reservoir production defines the reservoir management.

The history match process is based on changes of reservoir properties within the model (e.g. porosity, permeability, Net to Gross), fluid properties, facies geometry, reservoir structure, pressure, etc.) until production response of the reservoir model is close to the history data (Gavalas, *et al.* 1976). History matching is a complex non-linear, ill- posed, inverse problem, which can have multiple solutions. As any ill-posed problem, using different combinations of reservoir model parameters can generate good matching of reservoir production data (Hajizadeh *et al.,* 2011).

Most of the work related to history matching has been focussed on the variation of reservoir properties like fluid properties, porosity and mainly permeability (Gavalas, *et al.* 1976; Mattax and Dalton, 1990; Gomez et al, 2001; Milliken *et al.,* 2001; Hajizadeh *et al.,* 2011). Less attention have been paid to the variation of geological properties, like sedimentary facies geometry or variation of structural and stratigraphic frameworks (Arnold, 2008, Hoffman and Caers, 2006). This is probably due to the lack of a multidisciplinary approach in the process of history matching which has been traditionally performed by reservoir engineers. History matching studies related to the variation of geological

properties have demonstrated the enormous impact that geology has over the reliability of reservoir models (Park *et al.,* 2013, Arnold, 2008; Suzuki and Caers, 2008; Suzuki *et al.,* 2008; Hoffman and Caers, 2006).

Geological features can be introduced into numerical reservoir models by geological parameterization (Arnold, 2008). Geological parameterization is defined as the methodology used to find the minimum number of characteristics (in order to optimize computing time and hardware use) that can be used to effectively describe a geological event (e.g. channel geometry, fault shape and throw, facies proportions, etc). These parameters can be quantified and introduced into a reservoir model in order to reproduce geological events, like sedimentation, faulting, etc.

The variation of these parameters can produce significant changes in the production profile of a reservoir model and generate models that match the production history of a field. Controlling the variation of such parameters is required to generate reservoir models whose geological characteristics mimic geological information observed in outcrops, modern depositional environments and geological features observed in high-resolution geophysical data. Reservoir models that mimic geological features observed in nature could be considered as geologically realistic. Generating geologically realistic reservoir models is a very important task within the reservoir characterization process; since unrealistic geological models could be history matched but are not reliable predictions and mislead the development plans of a particular reservoir (Hoffman and Caers, 2006).

Carter *et al.* (2006) demonstrated that some history-matched or calibrated reservoir models do not have predictive capability. Models with a high degree of predictive capability are able to forecast reservoir production that should be used in reliable economic analysis.

Reservoir history matching and forecasting, like many problems in earth sciences, has been identified as an inverse, ill-posed problem (Suzuki and Caers, 2008). The solutions of these problems require the specification of the *a*

priori component of a solution (prior information model) to constrain the nature of the inverse solution (Tarantola, 1987). Prior information comprises all the information that is available before the collection of any new data set designed to solve a problem (Curtis and Wood, 2004).

This thesis is based on methodologies that can be included into the history match process, framed within a Bayesian context, to control the realism of geological features. The emphasis on the use of sedimentological prior information (sedimentological concepts, geomorphological descriptions, and geophysical studies) aims to maintain the sedimentological realism in reservoir models. Sedimentological prior information can be used as a tool to control the shape or geometry of sedimentary bodies in reservoir models to contribute to the geological realism of a reservoir model.

In summary, realistic history matched reservoir models should be used in predicting the production behaviour of a reservoir. It is very important to control the parameters that impact the production response of a model within the history matching process, in order to assure that only realistic models are used in forecasting the reservoir production.

1.2 Objectives

The main goal of this thesis is to develop techniques that can control the geological realism of facies geometry and distribution in reservoir models, within the process of automatic history matching. These techniques should be capable of generating geological models with characteristics observed in nature. Figure 1.1 is a comparison between a geologically realistic and an unrealistic reservoir model (fluvial channels that have one meter width and 1000 feet thickness); it is possible that both models history match production data but it is not possible that the facies geometry of the unrealistic model could represent the actual reservoir geometries observed in nature.

The specific objectives of this thesis are:

1) To identify what are the sedimentological parameters that can be used to restrict the geometry of sedimentary bodies or facies in reservoir models.
2) To understand how these sedimentological parameters are related to each other and how these relationships can be introduced into the automatic history matching workflow.
3) To control the geometry of the geobodies within a realistic field by the use of sedimentological prior information.
4) To reduce the uncertainty in reservoir production forecasting by using sedimentological prior information integrated through machine learning techniques.
5) To identify intrinsic parameters within the process of facies modelling (e.g. the use of multiple training images in multiple point statistics and the analysis of continuity of facies) that can improve adequate representation of uncertainty in reservoir models.

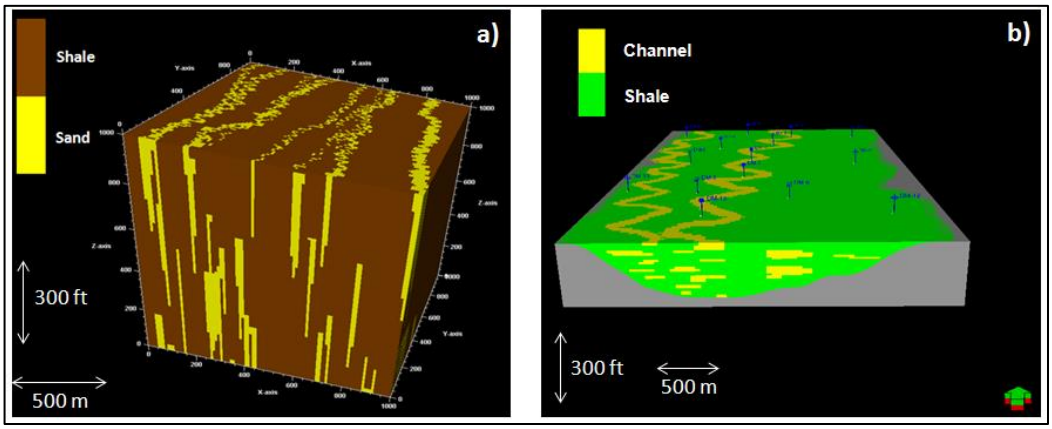

Figure 1.1: Comparing a) unrealistic and b) realistic deep marine channel geometry in facies models generated using object based techniques.

1.3 Thesis overview

This thesis is dived into eight chapters, which describe the path to introduce the techniques that improve the geological realism in reservoir models, within the automatic history match framework:

Chapter 2 presents a review of the reservoir modelling workflow, going from the geological (static) modelling up to the processes of fluid-flow (dynamic) modelling, considering deterministic and stochastic techniques. This chapter presents the most common commercial techniques and some of the techniques that have been developed in the most recent years.

Chapter 3 contains a review of the uncertainty quantification analysis in reservoir history matching, highlighting the main differences between manual and automated history matching. The most commonly used history matching techniques are presented in this chapter, as well as the techniques to reduce the uncertainty in production forecast. The importance of prior information and more specifically sedimentological prior information to control uncertainty in reservoir forecasting is emphasised in this chapter.

Chapter 4 is an introduction to machine learning techniques (MLT). This chapter explains in detail the machine learning techniques used in this thesis to model and compile sedimentological prior information (Multilayer Perceptron - Artificial Neural Networks, Support Vector Machines, for regression and classification and finally One-Class Support Vector Machine, which is a one class-classification technique). This chapter shows as well some of the application of these techniques in geosciences, solving multidimensional problems and reducing uncertainty.

Chapter 5 describes the sedimentology of the reservoirs used in this thesis. Fluvial meandering channels, deltaic and deep-marine channel deposits are analyzed in order to identify the sedimentological and geomorphic parameters that control the geometry of the associated deposits. In this thesis, three synthetic reservoir examples were used to apply the developed methodologies that control the realism in facies models.

These synthetic reservoirs represent fluvial meandering, deltaic and deep-marine channel deposits.

Chapter 6 shows how to control the geometry of facies models generated with multiple point statistics using machine learning techniques. This chapter presents the workflow used in this thesis to build sedimentological prior information related to geobody geometry. The analysed geobodies were formed in different depositional environments: fluvial meandering channels, deep marine channels and deltaic deposits. This chapter describes the methodology to introduce the "intelligent" sedimentological prior information generated using machine learning techniques into the automatic history matching workflow. One of the most important points of this chapter is the uncertainty quantification of production forecast analysis in reservoirs (synthetic cases), demonstrating the advantages of using the intelligent prior models.

Chapter 7 illustrates how the workflow for automatic history matching including "intelligent" sedimentological prior information can be improved by adding some routines that deal with sedimentological processes and interpretation: (1) Different sedimentary environment interpretations within the automatic history match framework, based on multiple training images using Multiple Point Statistics. (2) Generate multiple realizations in order to avoid rejection of models that could match production data. (3) Consider variation of vertical facies proportions as a geo-parameter within the automatic history match are the three improvements added to the automatic history matching workflow.

Chapter 8 summarises the results obtained by discussing their applications, adding concluding remarks and proposing the next steps in controlling and improving geological realism in reservoir models within the process of automatic history matching.

Chapter 2

Reservoir Modelling Workflow

2.1 Introduction

The main objective of reservoir characterisation is to estimate the reserves of a specific reservoir and to forecast the production behaviour with a high degree of certainty. The methodology used to achieve these goals is to build reservoir models that match the data obtained from different sources: well information (e-logs, cores, cuttings, wellbore wall-plugs, production data, well-tests, PVT analysis), geophysical data (seismic and gravity and magnetic methods); analogue models from similar reservoirs and/or outcrop characterisation and production response.

Within the oil industry reservoir modelling traditionally has been divided into two main tasks (1) geological or static modelling which is focused on the description of the physical characterization of the rocks that belong to the reservoir system (structural geology, sedimentology and petrophysical distribution properties); and

(2) dynamic or fluid modelling, which is related to the behaviour of the fluids in a reservoir once the production process begins. Figure 2.1 illustrates the workflow in reservoir modelling.

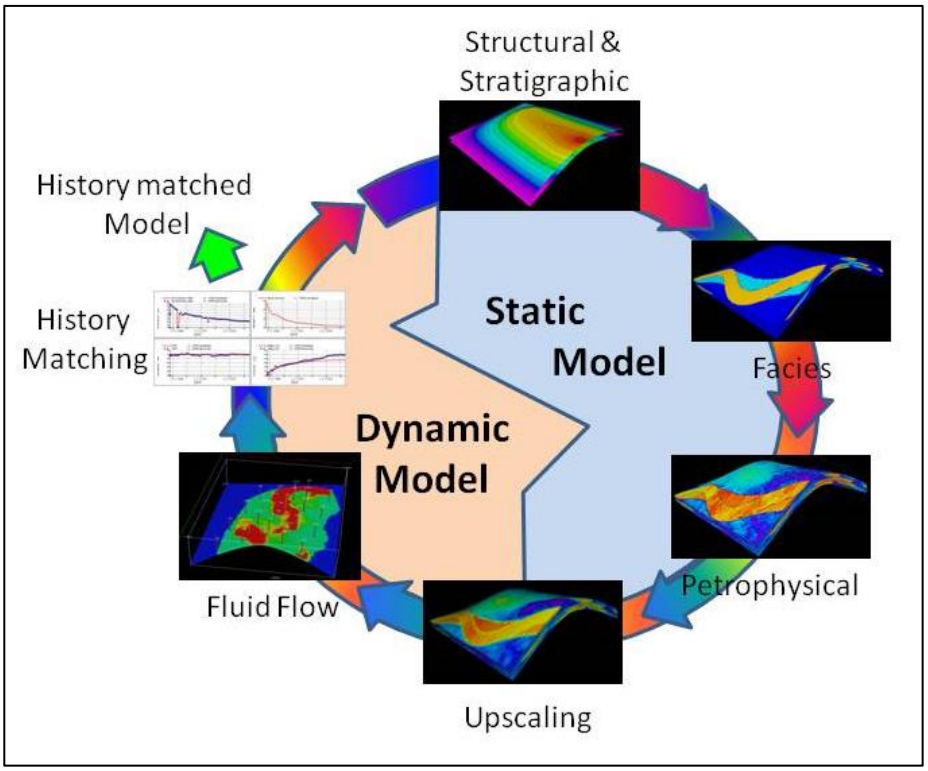

Figure 2.1: Reservoir Modelling Workflow. (Figure built using images from the Stanford VI synthetic reservoir. Castro *et al.,* 2005)

The next step in reservoir modelling is the so-called history match process, where the production response and pressure of the reservoir model are compared to the observed reservoir production and pressure data (Chapter 3). This process places reservoir modelling in an inverse loop, where the objective is to find possible solutions (reservoir models) that generate responses, which match the data (well information, production, and pressure). *i.e.* we try to model the origin of the data, using the data as input (Tarantola, 1987). Tarantola (1987) defined an inverse problem as a general framework that is used to convert observed measurements into information about a physical object or system. Inverse problems involve finding a model for a given output. Inverse problems are ill-posed (Sun, 1994)

since: (1) the solution of the problem is not unique; different variation of the multiple parameters associated with a reservoir model can offer responses that equally match reservoir data and (2) the solution does not continuously depend on the data.

This chapter shows the techniques used to generate reservoir models following the workflow commonly used in the petroleum industry.

1) Analyse the steps of the geological (static) modelling and then going throughout the process of the fluid-flow (dynamic) modelling.
2) Consider the uncertainty associated with each part of the reservoir modelling process.
3) Highlight the parts of the reservoir modelling workflow and the methodologies used in this thesis.

2.2 Geological Model

Reservoir geological (static) models are representations of the distribution and geometry of geological features in the subsurface. Smith and Moller (2003) present the conventional workflow used in the oil industry to generate geological models. These models are built in four main steps, starting with (1) the identification of stratigraphic boundaries of different geological units, (2) identifying the possible structural framework that characterizes a geological region, (3) interpreting the depositional environments that form the reservoir rocks and the distribution of the sedimentary facies within these depositional environments and (4) describing sedimentological and structural features are associated with particular distributions of petrophysical rock properties like porosity and permeability that can determine the capacity of a rock to store fluids or to allow fluid to flow. The distribution of these properties should be mapped in three spatial dimensions.

2.2.1 Stratigraphic Model

The stratigraphic model involves the identification of key regional geological surfaces that can be used to separate geological events (erosional surfaces, boundaries between geological formations or lithology and surfaces with a particular geological importance, like volcanic ash deposits, flooding surfaces, coal seams or palaeosols). The framework of sequence stratigraphy has been used within the petroleum industry as a best practice to identify correlative surfaces within the geological record that can be used to separated different geological events associated with relative sea-level changes. This framework of stratigraphic surfaces is built using well logs, core data, outcrop data adjusted to seismic reflector continuity and terminations (Catuneanu, 2006).

The uncertainty related to the identification of stratigraphic surfaces can be associated with different aspects: the resolution of the seismic data, the velocity model and wavelet used to tie well and seismic data, the ability of the interpreter to identify stratigraphic patterns and sequences and the availability and resolution of palaeontological data to identify potential correlative surfaces. The uncertainty associated with this process has a great impact on the interpretation of the stratigraphic units that contains the reservoir rocks and the correlation between different geobodies (Lallier *et al.,* 2012).

2.2.2 Structural Modelling

After deposition, the geometry of the stratigraphic units is controlled by tectonic events that deform these units, generating folds, joints and faults. The intensity of the deformation of the stratigraphic surfaces is defined not only by the strength of the geological stress, that have been governing a geological region, but also by the competence of the rock. The characterization of the geometry of these geological structures is accomplished basically by using seismic data calibrated with well data (Park, 1997).

The interpretation of structural regimes (extensional, compressional, wrench faults, salt structures, shale structures, etc.) in a geological region allows the identification of structures that can work as hydrocarbon traps and possible path-ways of hydrocarbon migration (Harding and Lowell, 1979). Like in the stratigraphic modelling process, the resolution of the seismic data and the interpreter opinion are the major factors that introduce uncertainty in this process. Uncertainty in the structural model affects the geometry of the reservoir, identification of the trap systems and the associated hydrocarbon reserves (Seiler *et al.,* 2011, Suzuki, *et al.,* 2008 and Cherpeau, *et al.,* 2012).

2.2.3 Sedimentological Modelling

The sedimentological model of a reservoir is the interpretation of the depositional environments that formed the rocks and the distribution of the sedimentary facies through the reservoir. Furthermore, the sedimentological model includes the diagenetic and depositional history of the reservoir rocks. Facies distribution model identifies the possible spatial distributions of porous-permeable and sealing rocks. The sedimentological model is generated by the interpretation and analysis of cores and outcrops and their correlation with well logs. There are techniques used to identify sedimentary facies using well logs (Bridge and Tye, 2000). The extraction of attributes from seismic data is a very useful technique that helps in the identification of geobodies, sometimes associated with sedimentological features. The technique of identifying sedimentological features in the subsurface from seismic data is known as seismic geomorphology (Posamentier, 2005).

2.2.4 Petrophysical Modelling

Petrophysical properties are the rock properties that control the capacity of a rock to store hydrocarbons and to allow fluids to flow (porosity and permeability respectively, Wyllie and Rose, 1950). These properties are measured in

laboratories from rock samples obtained from cores or outcrops and can be estimated from well logs like density, neutron, sonic and nuclear magnetic resonance.

Porosity can be defined as the ratio of voids or pores to the total volume of rock

$$\text{porosity}, \Phi = \frac{volume\ of\ pores}{total\ volume\ of\ rock} \qquad (eq.\ 2.1)$$

The amount of internal space (voids) in a given volume of rock is a measure of the amount of fluid a rock will hold, and is called total porosity. The amount of void space that is interconnected and thus able to transmit fluids is called effective porosity (Asquith and Krygowski, 2004).

Permeability is the ability of a rock to transmit fluids. It is related to porosity but not always dependent upon it. Permeability is controlled by the size of the connecting passages (pore throats) between pores. It is measured in darcys or milidarcys (md) and is represented by the symbol *K* (Asquith and Krygowski, 2004).

The distribution of the petrophysical properties is always associated with the distribution of the sedimentary facies, the diagenetic history of the reservoir rocks and to the structural features in a reservoir (such as joints, faults or folds). As an example, Svirsky *et al.* (2004) identified hydraulic flow units (HFU) within a deltaic reservoir in order to solve productions problems like different oil water contacts in the reservoir and compartmentalization. These HFU's were defined by different petrophysical properties which are associated with the sedimentary facies distribution.

Another important reservoir property that has to be analysed is the water saturation. Asquith and Krygowski (2004) define it as the amount of pore volume in a rock that is occupied by formation water. It is presented as a decimal fraction or as a percentage and has the symbol S_w.

$$S_w = \frac{formation\ water\ occuping\ pores}{total\ pore\ space\ in\ the\ rock} \qquad (eq.\ 2.2)$$

Although, the hydrocarbon saturation is the property of interest, water saturation is usually, estimated as it is easier to calculate through well-log analysis from Archie's (1942) equation:

$$S_w = \left(\frac{R_o}{R_t}\right)^{\frac{1}{n}} \qquad (eq. 2.3)$$

where: R_o is resistivity of water filled formation; R_t is the formation resistivity and *n* is the saturation exponent (see Archie, 1942 for more detail).

Then Hydrocarbon Saturation (S_h) is commonly calculated as:

$$S_h = 1 - S_w \qquad (eq. 2.4)$$

2.3 Cell-based Geological Modelling

Cell-based geological modelling can be defined as the 3D representation of a geological region. This representation is actually a 3D grid composed by a number of 3D cells or small blocks. Each cell has a value related to a geological or reservoir property (facies, porosity, water saturation, pressure, etc.) (Anderson, 1997, North, 1996). The 3D distribution of these properties must have a realistic geological meaning. Within the petroleum industry geo-cellular models are commonly referred to the 3-D representation of the geology of a reservoir, built using cells or 3-D blocks. The subsurface data used to build these models are well and seismic data. As mentioned in Chapter 1 these data have a large associated uncertainty. Geo-cellular modelling is a very dynamic tool in reservoir

characterization, since the model evolves during the reservoir being exploited. The quantity and quality of reservoir data increase with time and the model should be updated. There are a number of techniques that can be used to populate these 3D grids with geological properties, these techniques are mentioned below.

2.3.1 Process based models

Process based models try to reproduce the physics that originated the geological deposits and their alteration or the rock deformations. These models are very realistic and consider a large number of variables. Commonly they are computationally very expensive and applicable only to a very narrow range of geological settings (low generalization). Process based models can be considered as deterministic (Gross and Small.1998) or stochastic (Karssenberg *et al.,* 2001). Figure 2.2 is a representation of fluvial facies distributions obtained from a process based model.

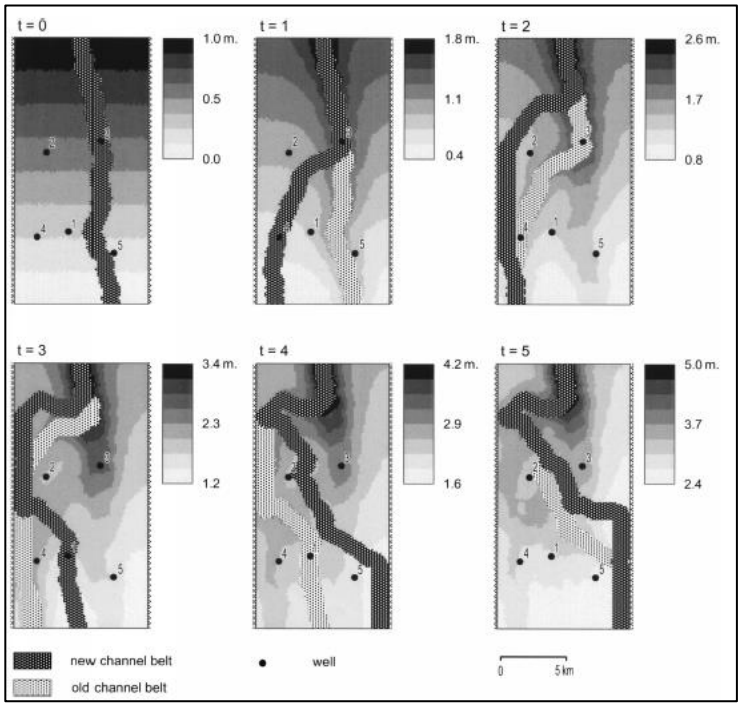

Figure 2.2: Evolution of conditioned process based model of fluvial channel belt migration. From (Krassenberg *et al.,* 2001).

Process-based models are hard to use in reservoir modelling since these models are based on a high resolution framework considering many details of the physics of the geological process. Very often the scale of the reservoir models does not allow the reproduction of detailed geological process. It is very hard to fully apply process based models on reservoir data since within the geological record there is a large uncertainty, which limits precise determination of the underlying physics that generated the geological deposits. Other facts that make difficult the application of process based models in reservoir are the lack of generalization and the difficulty in conditioning these models to a large amount well and seismic, data.

2.3.2 Geostatistical models

Matheron (1971) defines geostatistics as the application of regionalized variable theory to the estimation of mineral deposits. Matheron (1971) states that a phenomenon is regionalized when it spreads in space and exhibits a spatial structure. Then in earth sciences a regionalized variable can be defined as the value of a geological property $f(x)$ (*e.g.* porosity) at a point x. Regionalized variables can be divided as random (marked irregularity and unpredictable value from one point to another) and structured (reflecting the structural characteristics of the regionalized phenomenon) (Matheron, 1971). More recently, Caers (2005) defined geostatistics as a branch of statistical sciences that studies spatial/temporal phenomena and capitalizes on spatial relationships to model possible values of variable(s) at unobserved, unsampled locations. Geostatistics is concerned with a variety of techniques for spatial/temporal data analysis, estimation, and decision making. Some of the most common geostatistical techniques used in reservoir modelling are described in this section.

Modelling continuous variables

A common problem in earth sciences is to create a map of a regionalized variable from limited sample data. This problem was initially addressed by hand-

contouring, which provides insight into trends and empirical relations in the data. Early contouring algorithms evolved from principles of hand-contouring, creating smooth maps that reveal geological trends (Deutsch, 2002).

With advances in hardware and software the application of geostatistical algorithms were used within geoscientific problems, because of their versatility and robustness in finding and describing spatial relationships of geological variables.

Kriging

Daniel Krige, a South African mining engineer, was interested in correcting biased maps in order to solve problems in predicting mine grades. George Matheron (1963) developed an interpolation method named kriging after the pioneering work of Krige in the 1950's. Kriging is the workhorse of traditional geostatistical mapping applications and an essential component of many geostatistical stochastic simulation methods.

Kriging provides a solution to the spatial estimation problem based on a continuous model of stochastic spatial variation. It makes the best use of existing knowledge by taking account of the way that a property varies in space through the variogram model. The aim of kriging is to estimate the value of a random variable, *Z,* at one or more unsampled points or over larger blocks.

Kriging is considered as a linear geostatistical model (*eq*. 2.5) that uses local weighted averaging of neighbourhood measurements in order to make spatial predictions.

In a linear model the unknown value is estimated as a linear combination of the measurement data with weights (λ_α) (Matheron, 1963):

$$z^*(\boldsymbol{u}) = m(\boldsymbol{u}) + \sum_{\alpha=1}^{n} \lambda_\alpha . [z(\boldsymbol{u}_\alpha) - m(\boldsymbol{u}_\alpha)] \qquad (eq. 2.5)$$

Where $z^*(\boldsymbol{u})$ is the estimate at an unsampled location $\boldsymbol{u}$, $m(\boldsymbol{u})$ is the prior mean value at unsampled location $\boldsymbol{u}$, λ_α witn $\alpha = 1, \ldots, n$ are weights, $z(\boldsymbol{u}_\alpha)$ with $\alpha = 1, \ldots, n$ are the data values, $m(\boldsymbol{u}_\alpha)$, $\alpha = 1, \ldots, n$ are prior mean values at the data locations and n are the number of data points.

There are many types of kriging models, all of them are derived from Simple kriging (SK) (*eq*. 2.5). The Simple kriging model assumes that the mean value of the stationary random function (or prior value at the unsampled location) is constant and known.

In order to calculate the kriging estimate it is necessary to obtain the weight values λ_α, for each value $z(\boldsymbol{u}_\alpha)$. It is required then to estimate the spatial variance of the variable which can be estimated using a variogram.

Following Matheron's (1963) definition, a variogram is a function representing the degree of continuity of a variable. Plotting lag distance in the abscissa (x-axis) and the square of the difference between two samples in the ordinate (y-axis) picked at a distance *h*. In general variogram is an increasing function of the distance between points: the more separated two samples are one from the other, the more the values Z are different. Thus, variogram is defined as a 2-point statistical moment:

$$2\gamma(h) = E\{[Z(\boldsymbol{u}) - Z(\boldsymbol{u} + h)]^2\} \qquad (eq.\,2.6)$$

Where: γ is the variogram, h is the lag distance or distance between two samples, $Y(\boldsymbol{u})$ is the residual of the property value z at location *u* minus the constant prior mean $m(\boldsymbol{u})$: $Y(\boldsymbol{u}) = (Z(\boldsymbol{u}) - m(\boldsymbol{u}))$

Sequential Gaussian Simulation (SGS)

Sequential Gaussian Simulation (SGS) is adopted to generate maps of continuous variables in the petroleum industry like porosity or permeability in petroleum reservoirs., the most common approach adopted is sequential Gaussian simulation, because of its simplicity, flexibility and efficiency.

SGS uses the simple kriging estimator and the covariance between the kriging estimate and one of the data value to estimate the statistics of the random variable distribution. This covariance is calculated and fixed when the variance is too small by proceeding sequentially (i.e. using previously predicted values in subsequent prediction.

Deutsch (2002) describes the SGS algorithm as follows:

1) Transform the original Z data to a standard normal distribution Y (all work will be done in normal space).

2) Go to a location **u** and perform kriging to obtain kriging estimate and the corresponding kriging variance:

$$Y^*(\boldsymbol{u}) = \sum_{\beta=1}^{n} \lambda_\beta . Y(\boldsymbol{u}_\beta) \qquad (eq.2.7)$$

$$\sigma_{SK}^2 = C(0) - \sum_{\alpha=1}^{n} \lambda_\alpha C(\boldsymbol{u}, \boldsymbol{u}_\alpha) \qquad (eq.2.8)$$

3) Draw a random residual $R(\mathbf{u})$ that follows a normal distribution with a mean of 0.0 and a variance $\sigma^2_{sk}(\boldsymbol{u})$.

4) Add the kriged estimate and residual to get simulated value:

$$Y_s(\boldsymbol{u}) = Y^*(\boldsymbol{u}) + R(\boldsymbol{u}) \qquad (eq.2.9)$$

5) Previously simulated values are added to the conditioning data to achieve the joint posterior (pdf) of the regionalized variable. Add $Y_s(\mathbf{u})$ to the set of data to ensure that the covariance with this value and all future predictions are correct. As stated above, this is the key idea of sequential simulation,

that is, to consider previously simulated values as data so that we reproduce he covariance between all the simulated values.

6) Visit all grid locations in a random order, to populate the entire grid.

7) Back transform all data values from normal space to the original Z variable distribution and simulated values when the model is populated.

8) Create any number of realizations by repeating with different random number seeds. A different seed leads to a different random numbers and as a consequence, a different random path and a different residual for each simulated node, each realization has the same probability of being correct. The realisations describe inherent uncertainty of the Gaussian random field model representation.

Facies Modelling

Modelling facies distribution in a reservoir is one of the most important steps in reservoir modelling. Sedimentary facies distribution will define the geometry of the reservoir rocks and the distribution of their related petrophysical properties (porosity and permeability). The physical and chemical conditions that generated a specific facies would affect the petrophysical properties associated with that facies (e.g. in a fluvial environment reservoir rocks are associated with coarse grained channel deposits and flow barriers or rock seals are associated with fine grain deposits typically found in floodplain or channel plug deposits).

This section will present some descriptions of the most common variogram based techniques to model facies in a cell-based approach.

Sequential Indicator Simulations (SIS)

The concepts of sequential simulation, described in the context of Gaussian (SGS) distribution can be extended to the indicator-based model of uncertainty.

The key idea for indicator formalism is to code all the data in a common format, that is, as probability values (Journel, 1983).

Figure 2.3 illustrates the sequence followed by SIS to populate a grid with facies distribution. The indicator approach for continuous variables requires significant additional effort versus Gaussian techniques. The indicator formalism applied to categorical data has seen wide application to facies modelling. This approach estimates a distribution (pdf) to describe probability of facies at each unsampled location.

The probability distribution consists of estimated probability for each category:

p(k), k*=1, … , K. The probability values are estimated by first conditioning the data as indicators or probability values:

$$i(\boldsymbol{u}_\alpha; z_k) = \begin{matrix} 1, & if\ facies\ k\ is\ present\ at\ \boldsymbol{u}_\alpha \\ 0, & otherwise \end{matrix} \qquad \textit{(eq. 2.10)}$$

$i(\mathbf{u}_\alpha; z_k)$ = Prob {facies k being present}

The expected value of this indicator variable is the stationary prior probability of facies k, that is p(k).

Kriging (2.7) of the residual data at sampled locations (eq. 2.11) is used to derive the probability of each facies k=1, .. K at an unsampled location. Once again a variogram measure of correlation is required for each facies $k=1, \ldots, K$. (Journel, 1983). Modelled variogram (2.6) is then used to estimate the correlation between two locations considering direction and separation between them.

Residual data are calculated as follow:

$$Y(\boldsymbol{u}_\alpha, z_k) = i(\boldsymbol{u}_\alpha; k) - p(k), \quad \alpha = 1, \ldots, n, \quad k = 1, \ldots, K \qquad \textit{(eq. 2.11)}$$

Where: $Y(\boldsymbol{u}_\alpha,z_k)$ is the residual, $i(\boldsymbol{u}_\alpha,k)$is the indicator α are data points and k the type of facies.

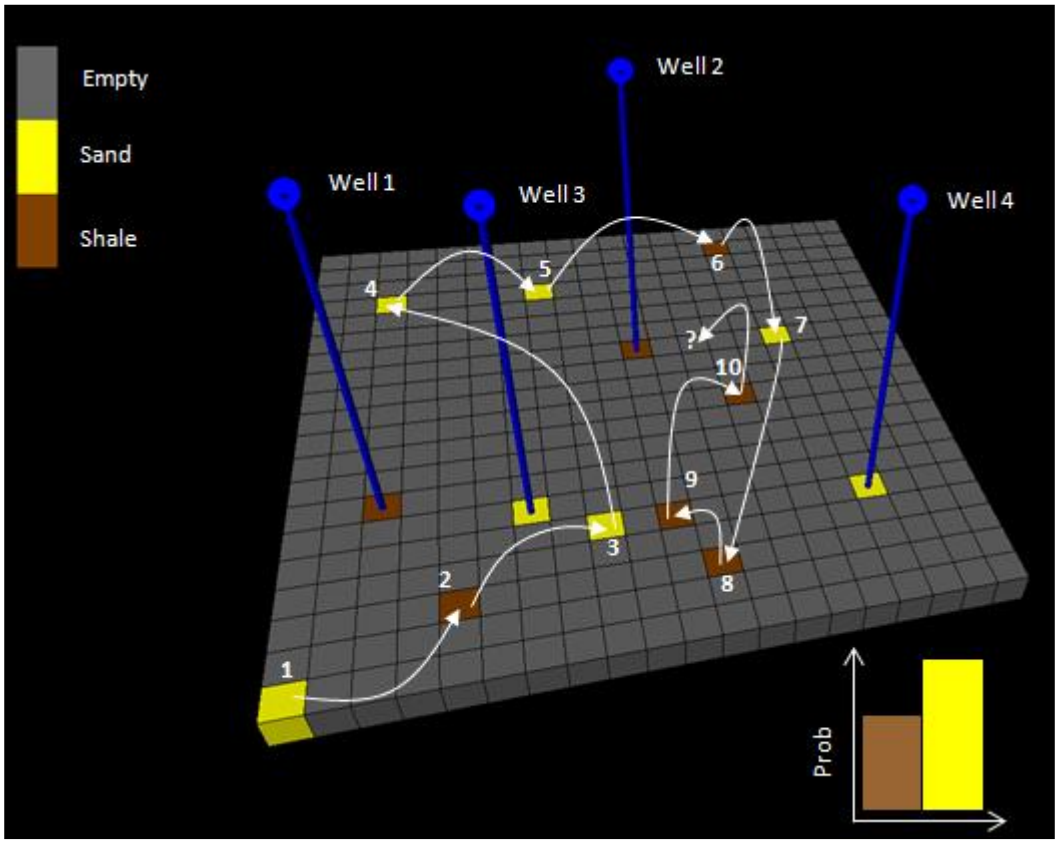

Figure 2.3: In the SIS process cells are visited in a random sequence. In each step the simulated facies is selected randomly from the local PDF. This illustration is a sand/shale simulation, where well data (blue sticks) is honoured (Modified from *Doyen et al.*, 1994)

In order to generate multiple realizations, grid nodes are visited sequentially in a random path and at each grid node:

1) Search for nearby data and previously simulated values.
2) Perform indicator kriging to build a distribution of uncertainty.
3) Draw a simulated value from the distribution of uncertainty.

4) Add the simulated value to the data pool.

Multiple realizations are then generated by repeating the entire process with a different random number seed. Figure 2.4 shows a picture of a facies model obtained using SIS.

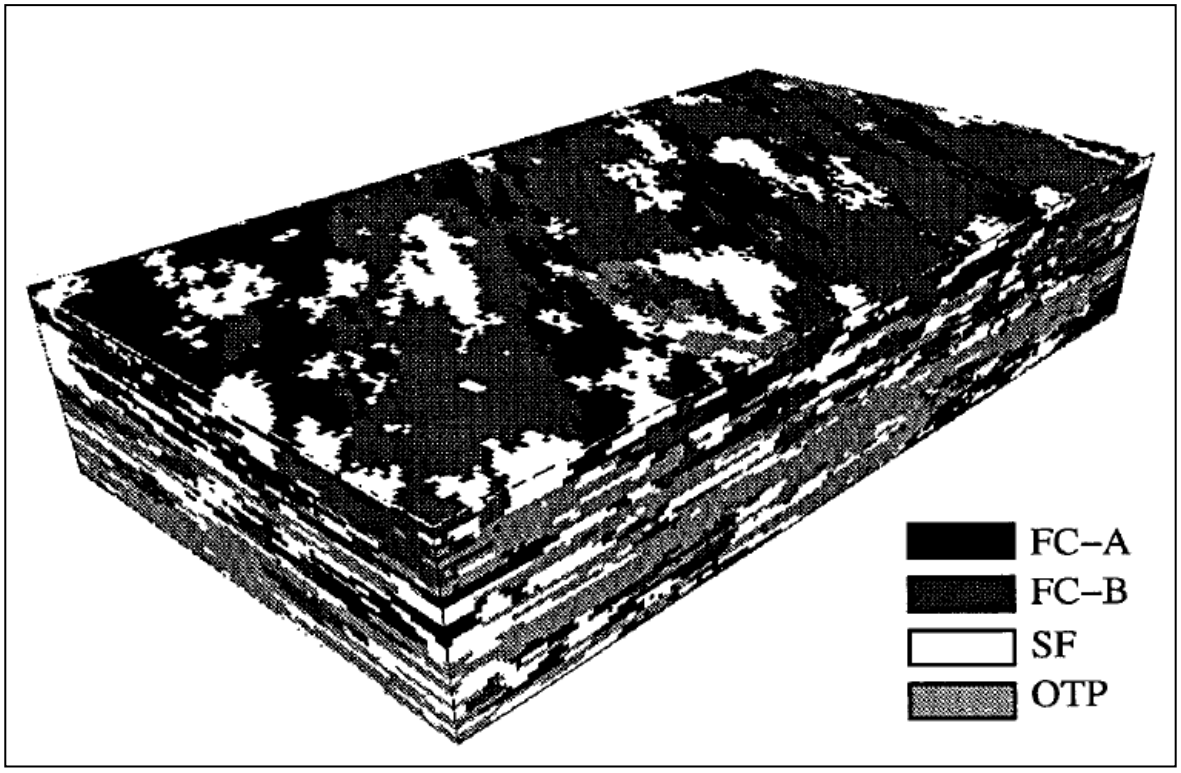

Figure 2.4: A 4-facies braided fluvial model developed using SIS. Where FC is “Fluvial Channel”; SF is “sheetflood” and OTP is “Other than Pay”. (From Seifert and Jensen, 1999)

Truncated Gaussian Simulation (TGS)

The key idea of Truncated Gaussian simulation is to generate realizations of a continuous Gaussian variable and then truncate it at a series of thresholds to create categorical facies realizations (Beucher *et al*., 1993). This technique was designed to apply the concepts of simulating continuous variables (sequential Gaussian simulation) to categorical variables like facies (Beucher *et al*., 1993). Figure 2.5 shows how TGS works in a 1-D example. The categorical simulation, shown in the lower axis, is derived from a continuous Gaussian simulation shown

by the black curve. The threshold for truncating the Gaussian variable need not be constant across the reservoir grid.

TGS is faster than SIS as only one Gaussian distribution is calculated for the entire model, but at the same time the fact that TGS has only one Gaussian distribution it is harder to impose different correlation structures on different facies than using SIS. Note, that the sequence of facies is always the same in TGS following the threshold order, while it can be arbitrary in SIS.

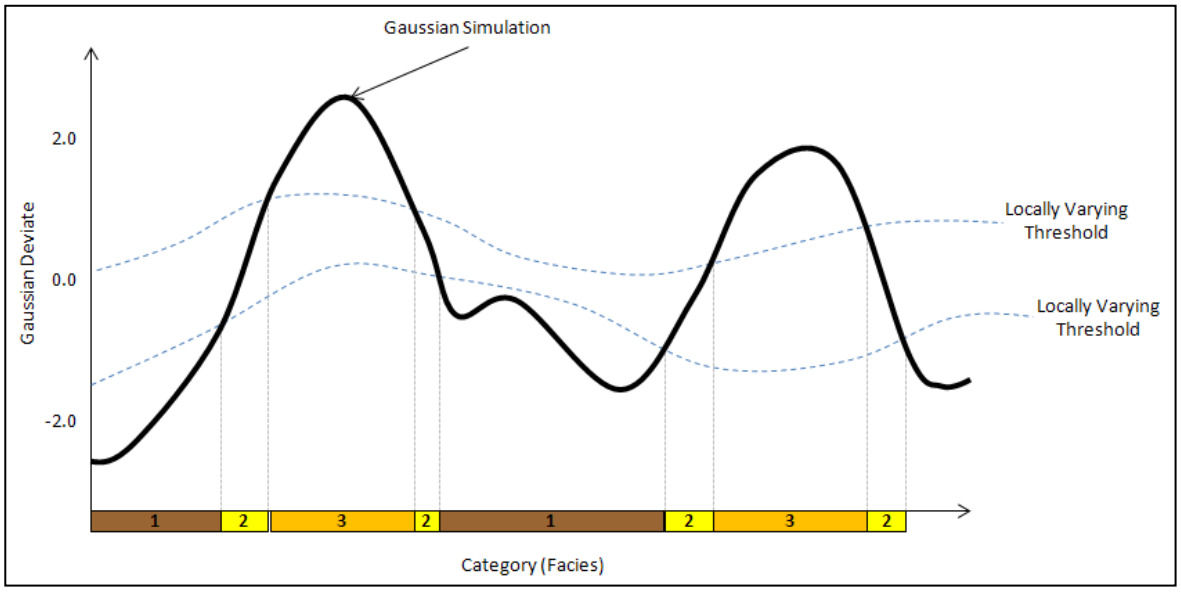

Figure 2.5 Schematic illustration of how TGS works: a continuous Gaussian simulation is truncated at a series of thresholds to create a categorical variable realization. (From Deutsch, 2002).

Object-based models (Boolean models)

Object-based models are built using predefined objects that are distributed over the reservoir model grid. The object shapes reproduce the geometry of geobodies (sinuous channel-like bodies, ellipsoids, cylinders, parallelepipeds, etc, or of another specific 's design.

These objects can be modified in size, orientation and proportions in order to honour the input data used in the model (well data, seismic interpretation or information coming from analogue reservoirs or outcrops).

Models built with object-based techniques are visually more attractive than models built using variogram-based techniques, because the resulting facies mimic idealized geometries interpreted from outcrops and modern analogues better than the models built using two-point statistics techniques. The facies geometries obtained from object-based techniques are sharp and follow regular deterministically defined shapes (that at some degree could be considered as geologically unrealistic.

Deutsch (2002) explains that the basic algorithm underlying object-based facies modelling is the Boolean placement object. The objects may accumulate from the stratigraphic base. Alternatively objects may be embedded within a matrix facies according to some stochastic process and erosional rules imposed afterwards. Unconditional simulation is straightforward; objects are placed randomly until the global proportions of the facies are reproduced. Reproduction of dense well and seismic data conditioning was considered difficult, but many algorithms have been developed to address this challenge, modifying the size and shape of the objects to honour local conditioning data (Hauge *et al.,* 2006; Viseur *et al.,* 2001). Figure 2.6 is an example of a facies model developed using object based-modelling.

2.3.3 Multiple Point Statistics (MPS)

Although, multiple point statistics is considered as a geostatistical technique used to simulate facies or discrete variables, it is described in a separated section since MPS is the core algorithm used in this thesis for modelling facies. MPS is generally better in representing the geological realism of the facies models (Strebelle, 2002). than other cell-based stochastic algorithms (SIS, TGS)The advantages of using MPS instead of any of the technique mentioned before are expressed in the following paragraphs. Geostatistical 2-point statistics techniques mentioned before present some problems that were highlighted in Section 2.3.2.

Journel and Alabert (1989), Guardiano and Srivastava (1993), Strebelle and Journel (2001) and Strebelle (2002) have worked on a technique named Multiple-

Point Statistics (MPS) that can generate realistic facies geometries and facies distribution that are easily conditioned to well and seismic data.

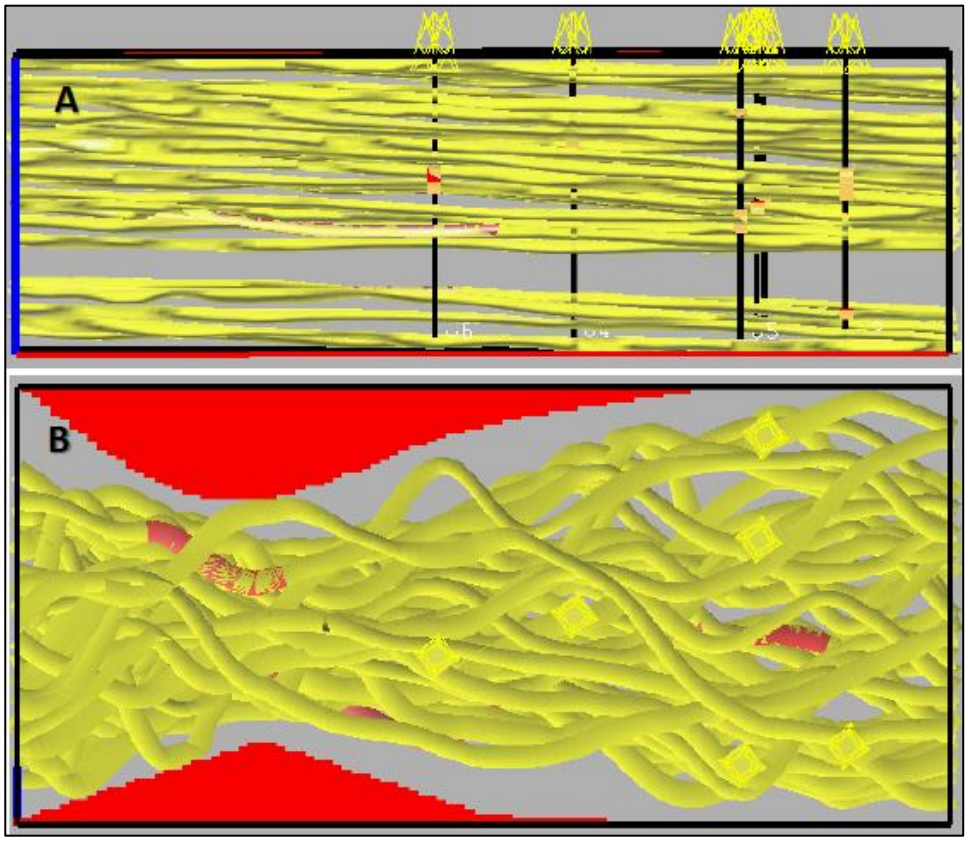

Figure 2.6 Fluvial Channels simulated using Object-Based Technique (A) is a vertical cross section and (B) the Plan view of the model. Geobodies are more realistic than the ones simulated using SIS. See Figure 2.4 (Viseur, *et al.,* 2001).

Multiple point statistics is a technique that expresses joint variability in more than two locations at a time and cannot be inferred by typical sparse well data but could be extracted from training images that represent the subsurface heterogeneities.

A training image does not need any local information of the reservoir, training images can be considered as concepts of geological property distribution in the reservoir. The statistics inferred from the training image can be exported to a reservoir where they are anchored to well data using pixel-based sequential simulations. Figure 2.7 explains how multiple-point statistics works.

Strebelle and Journel (2001) proposed an algorithm named Sequential Normal Equations Simulation (*snesim)* to implement multiple point statistics. Snesim avoids repetitive scanning of a training image as proposed in Guardiano and Srivastava (1993) by storing all the conditional probability distribution functions (cpdf's), obtained while scanning the training image with a particular arrangement of cells (template τ_n, see Fig. 2.7), in a dynamic data structure called "search tree" allowing fast retrieval as the simulation proceeds.

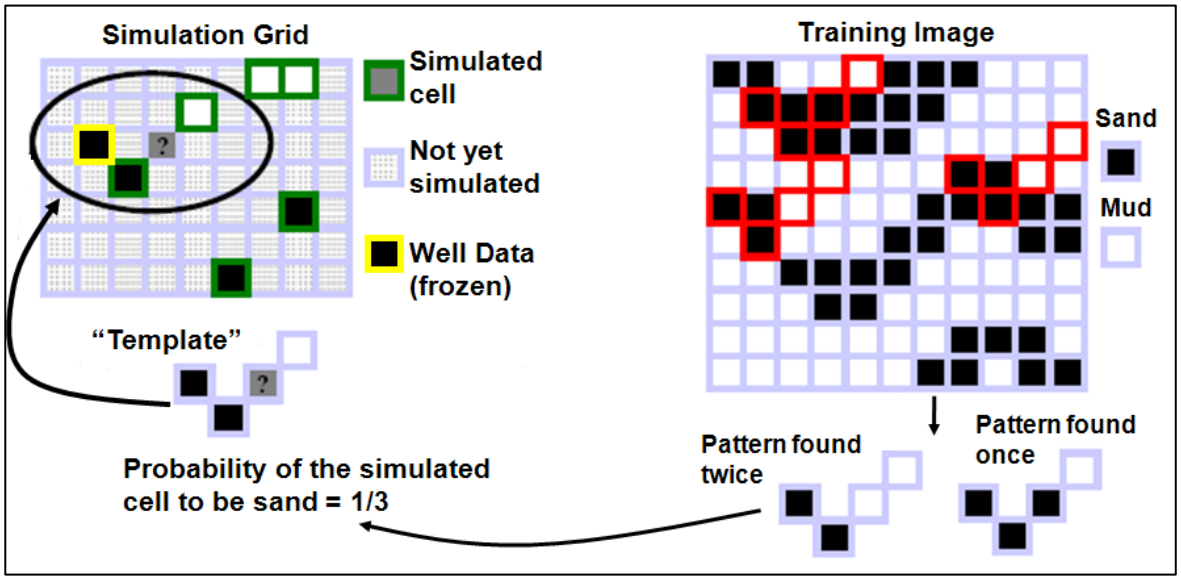

Figure 2.7 How MPS works. MPS is based on a training image (TI), a selected template and well data. TI is canned with a template and the patterns found within this template are statistically analysed indentifying the probabilities of a facies to occur in a grid cell, then this pattern is constrained to the simulated and well data cells, finally the selected pattern is reproduced in the simulation grid (From Caers, 2005).

Such algorithm performs in six steps:

1) Scan the training image(s) to construct the search tree using the data template τ_n (associated with the data search neighbourhood defined by the user. Only the data event that actually occur over the training image are stored in that search tree.

2) Assign the well (conditioning) data to the closest grid nodes. Define a random path visiting only once each unsampled node.
3) At each unsampled location **u**, retain the conditioning data actually present within the template τ_n centred on **u**. Let *n*' be the number of those conditioning data and $d_{n'}$ the corresponding data event. Retrieve from the search tree the proportions of type 1 corresponding to the data event $d_{n'}$. If not enough replicates of $d_{n'}$ are found on the training image, the furthest away conditioning datum is dropped reducing the number of conditioning data to (*n'*-1): the proportion conditions to this lesser data event $d_{n'-1}$ are retrieved again from the search tree and so on. If the number of data drops to *n'*=1 and not enough replicas of $d_{n'}$ can be found yet, the condition probability $p(\mathbf{u}:s_k|d_{n'})$ is replaced by the marginal probability p_k.
4) Draw a simulated value for a node u from the previous conditional probability. That simulated value is then added to the *s*-data to be used for conditioning the simulation at all subsequent nodes (sequential nature of the algorithms).
5) Move to next node along the random path and repeat steps 3 and 4.
6) Loop until all grid nodes are simulated. One stochastic image has been generated. Reiterate the entire process from step 2 from a different random path to generate another realization.

In Figure 2.8 there is an example of a facies model generated using MPS, where it is possible to observe that MPS reproduces the geometry of sedimentary facies and easily adapts the geobodies to well data, solving the problems presented by techniques like SIS, TGS or Object-Based.

2.3.4 Other Techniques

The techniques mentioned before have been used within the oil and gas industry in most of the commercial available software. In research groups or in academia

many other facies modelling techniques have been developed showing important improvement in preserving geological realism, facies continuity and honouring input data (well and seismic data).

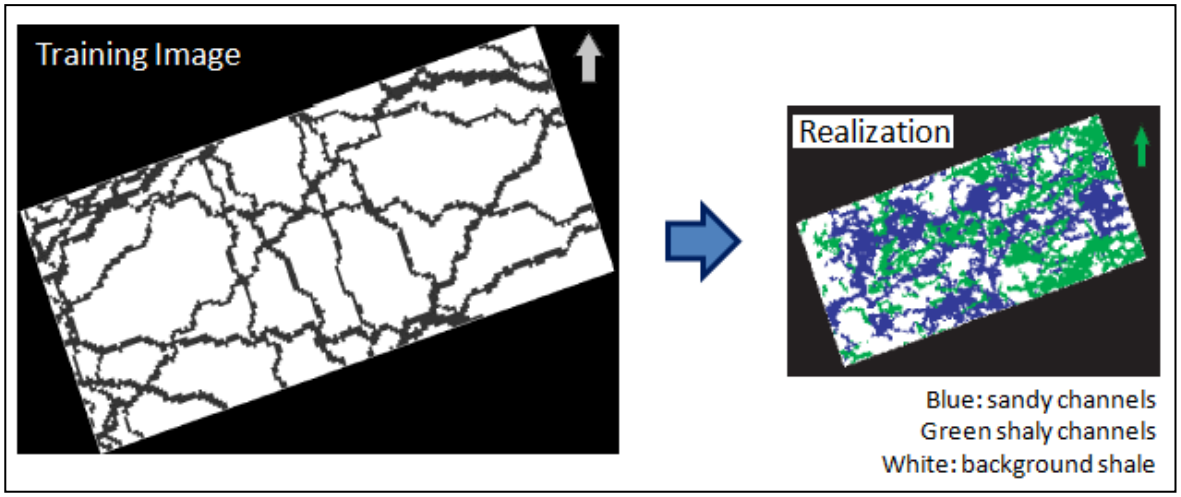

Figure 2.8 Facies Realization of a fluvial system based on a Training image. MPS is a pixel based sequential simulation able to reproduce realistic geological features (From Liu *et al.,* 2004)

Alapetite *et al*. (2005) presented a technique called YACS (Yet Another Channel Simulator). This technique was developed to model fluvial reservoirs, based on the association of a fairway or river bed with the channel to be simulated. A potential field is defined within the fairway. A residual component is stochastically added to the potential field creating sinuosity and meandering channel geometry. This algorithm is based on sequential algorithms guaranteeing convergence and speed. This method honours well data and facies proportions.

Demyanov *et al*. (2008) used Support vector regression (SVR) a machine learning technique to simulate fluvial reservoirs (Figure 2.9). SVR generates a geomanifold based on unlabelled data from seismic information and labelled data from well information. SVR is able to establish spatial relationship between data taking into account the prior information from similar depositional environments and the data

points. Petrophysical properties are the distributed into the grid without generating a facies model.

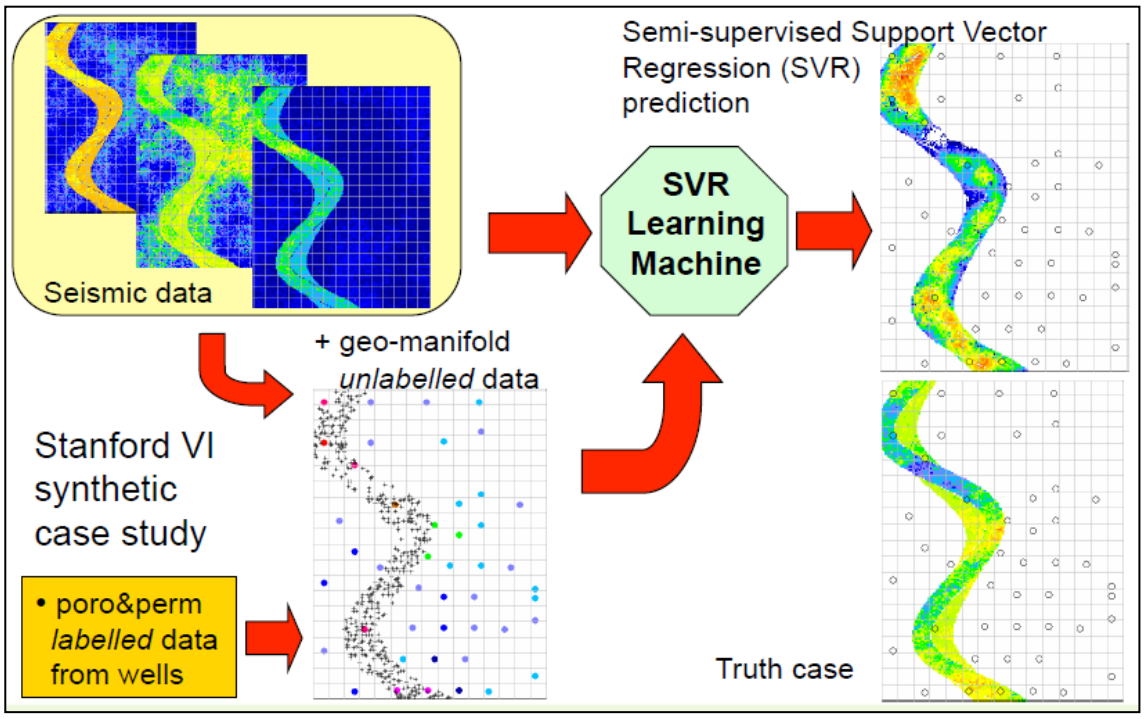

Figure 2.9: Modelling porosity distribution in a fluvial reservoir based on Semi-supervised-SVR, geo-manifold built with seismic information and constrained to well data (From Demyanov *et al.,* 2008).

2.4 Dynamic Model (Reservoir Simulation)

Peaceman (1977) defines reservoir simulation as the process of inferring the behaviour of a real reservoir from the performance of a model of that reservoir. The model may be physical (scaled laboratory model) or mathematical (models presented in this thesis are mathematical model).

In order to estimate the production behaviour of a specific reservoir, reservoir engineers have developed three techniques:

(1) Decline curve analysis, within one of the first techniques used to estimate reserves and predict production in a hydrocarbon reservoir (Arps, 1944). Figure 2.10 is an example of a decline curve analysis. This technique is

based on the observation of the production behaviour of a reservoir through time and fits a curve (harmonic, hyperbolic or exponential) to the production data, in order to estimate what will be the last production point where the reservoir is economically exploitable. The last day of the production plateau is considered as the start point of the decline curves; the production rate is plotted on the y axis and time in the x. This technique only considers the production associated with the existing wells, any production associated with new injection or producing wells; is not going to be predicted by the decline curve analysis (Arps, 1944). This technique does not consider the petrophysical property distribution nor the pressure changes in the reservoir, which makes the production predictions obtained with this technique highly inaccurate.

(2) Material Balance. This methodology is based on the material balance equation presented by Schilthuis in 1936. The equation is derived as a volume balance which equates the cumulative observed production, expressed as an underground withdrawal, to the expansions of the fluids in the reservoir resulting from a finite pressure drop. Figure 2.11 illustrates the changes in volume when the pressure is reduced by a ΔP, allowing the volume to expand in the reservoir.

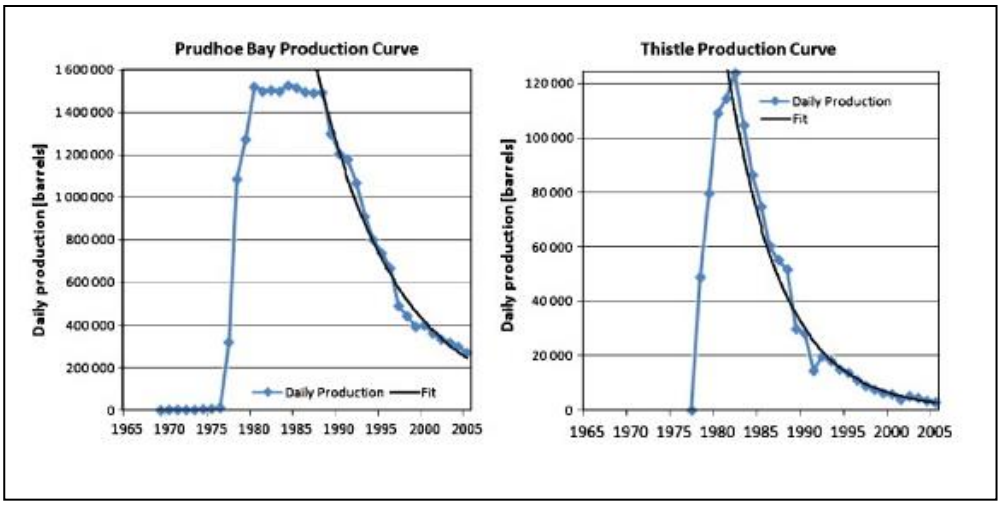

Figure 2.10 Decline curve analysis from Prudhoe Bay and Thistle Fields (From Höök *et al.,* 2002).

The Volume balance can be evaluated in reservoir barrels (rb) as:

$$UW(rb) = Oil\exp(rb) + ODG(rb) + GC\ exp + HCPVred \qquad (eq.2.12)$$

Where:

UW: Underground withdrawal, *Oil exp*: Expansion of oil

ODG : Originally dissolved gas, *GC exp*: Gascap gas expansion

HCPV red: Reduction in HCPV due to connate water expansion.

(3) Reservoir Simulation is a mathematical model which parameterizes the reservoir into grid-cells, each cell has different reservoir properties (facies, porosity, permeability, water saturation, pressure, etc.) that condition the fluid flow. Reservoir properties of each cell, like porosity and permeability are obtained from the geological model. The reservoir model is used then to estimate a mathematical approximation of the field fluid flow, by calculating flows between adjacent cells of the model.

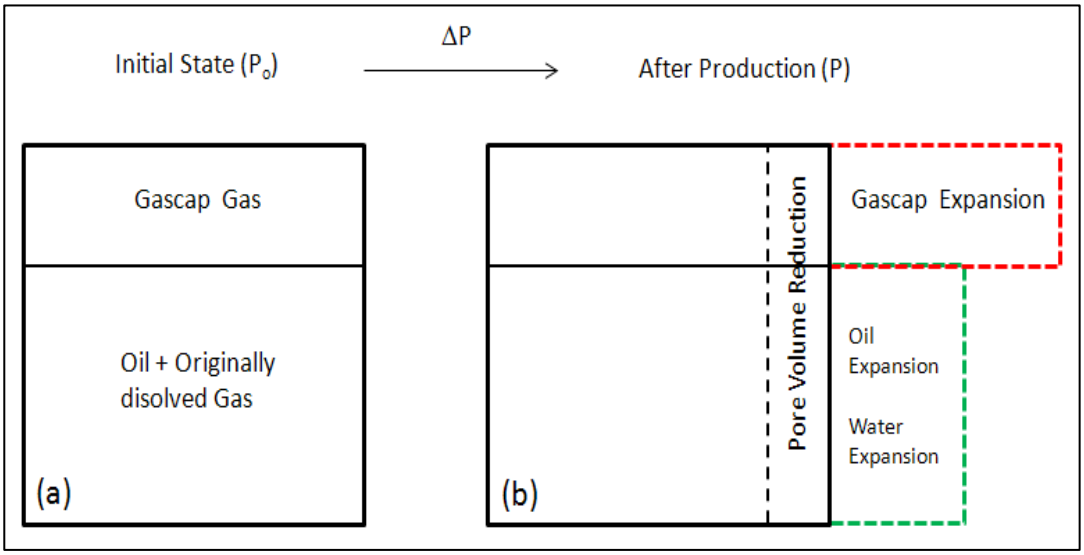

Figure 2.11 Volume changes in a reservoir associated with a finite pressure drop ΔP; (a) volumes at initial pressure, (b) volumes at the reduced pressure (From Dake, 2002).

This thesis will consider only the third approach since reservoir simulation contemplates the geological heterogeneities of a reservoir, modelled using the techniques mentioned in Section 2.3. More detail about reservoir simulation is given in the following sub-section.

For most petroleum companies, reservoir simulation is the next step in the reservoir characterization process observed in Figure 2.1

2.4.1 Upscaling

One of the first steps in reservoir simulations is to identify the number of cells necessary to generate the grid. Since the reservoir property distribution comes from the geological model it is necessary to preserve the geological heterogeneity in the reservoir model, but it is computationally expensive to use the same number of cells in the flow simulation model as that in the geological model. A balance between the grid resolution (number of cells) and the time consumed by the flow simulation is necessary. The resolution of the grid will be dictated by the objectives of the simulation.

In general, for reservoir simulation it is necessary to provide a grid with cell-dimension that retain the geological heterogeneity of the reservoir and not being computational expensive. It is possible to use a detailed geological grid in a reservoir simulation if the number of cells is not too large (Christie, 1996) or to average the physical properties of the grid to capture the fine scale effects in a coarse grid. This averaging process is call upscaling.

Christie and Blunt (2001) presented a worthy discussion about upscaling. The most used techniques of upscaling are averaging methods, over the reservoir properties obtained in the static model (porosity, permeability). Porosity and initial water saturation are averaged using arithmetic average; permeability is averaged using a combination of methods that depends on the permeability tensor.

The geological features presented in this thesis are considered to have dimensions in the order of tens of meters. The grid resolution (less than 500.000 cells) used in the geological models of this thesis can be used in flow simulation, there was no need to apply any upscaling to the geological reservoir models.

2.4.2 Mathematical Methods for Reservoir Simulation

After upscaling the static properties from the geological grid to the simulation grid it is necessary to use some mathematical techniques in order to simulate the fluid movements inside the reservoir (grid cells). The mathematical methods must consider the physical properties of the fluids (viscosity, gravity and capillary).

Peaceman (1977) defines a mathematical model of a reservoir as a model of a physical system composed by a set of differential equations, with a set of boundary equations, which describe the significant physical processes taking place in that system. The processes occurring in a reservoir are basically fluid flow and mass transfer.

Since reservoirs contain oil, gas and water the flow equations must consider necessary to include the interaction of these three phases within the reservoir simulation. The interaction between water and oil is described by relative permeability curves, which reduce the permeability of a fluid in the presence of another. Peaceman (1977) states that the differential equations are obtained by combining Darcy's law for each facies with a simple differential material balance for each phase.

The 1-D description of a single phase fluid flow through a porous medium in a horizontal system is described by the Darcy equation which uses the permeability value to calculate volumetric flow rate q by the equation:

$$q = -\frac{kA}{\mu}\frac{\Delta P}{L} \qquad (eq.2.13)$$

where: k is a homogeneous permeability and ΔP the pressure differential over distance L, μ the fluid viscosity and A the cross-sectional area through which the flow is passing.

For flow in three dimensions, say axes x, y *and* z, the Darcy equation can be written as:

$$u_x = -\frac{k}{\mu}\left(\frac{\partial P}{\partial x} - \rho g \frac{\partial D}{\partial x}\right) \qquad (eq.2.14a)$$

$$u_y = -\frac{k}{\mu}\left(\frac{\partial P}{\partial y} - \rho g \frac{\partial D}{\partial y}\right) \qquad (eq.2.14b)$$

$$u_z = -\frac{k}{\mu}\left(\frac{\partial P}{\partial z} - \rho g \frac{\partial D}{\partial z}\right) \qquad (eq.2.14c)$$

where: D is depth, ρ is the density of the fluid and g is the acceleration due to gravity.

Fluids within hydrocarbon reservoirs are usually gas, oil and water, so the interactions between these three phases must be integrated with the flow equations.

Relative permeability is the property that quantifies the permeability of a fluid within a porous medium, when this fluid is in the presence of another fluid in the same porous medium, and both fluids are immiscible. Curves that illustrate the relationship between relative permeability and the saturation of a fluid (relative permeability curves) are included into the flow simulator to mimic the production of oil, gas and water when these phases are together in the reservoir.

The fluid-flow simulator solves a set of phase and mass balance calculations as well as 3-dimensional group of flow Darcy equations for every grid-cell in the model.

More recently, a technique called streamline simulation appeared as an alternative to the fluid-flow simulator. This methodology is based on the estimation of the pressure field of a reservoir. Once the pressure field is mapped then the streamlines are traced perpendicular to the pressure contours, these lines form the so-called velocity field (Thiele, *et al.,* 2010). Flow model in streamline simulation goes through the velocity lines instead of from one grid-cell to another like finite difference simulators do. One of the advantages of using streamlines simulation is the use of grids with a very complex geology without the need of upscaling and losing resolution (Datta-Gupta, 2000). Streamline simulation is less accurate than conventional simulation schemes, since the pressure field is updated at a reduced number of time steps to the contrast to conventional simulations where the pressure field is updated almost constantly (Datta-Gupta, 2000).

2.5 Summary

A brief explanation of the reservoir simulation workflow has been presented in this chapter (Figure 2.1). The most common techniques used in reservoir characterization were introduced here: Geological and petrophysical models make representations of the distribution of the geological parameters that have influence on the reservoir performance. Then this understating of the geological and petrophysical properties distribution of a reservoir is placed into a 3-dimensional grid by using geostatistics. A brief description of geostatistical techniques used in this thesis, like multiple point statistics, was presented. The geological models generated using geostatistics are upscaled, if it's necessary, and then the fluid flow is simulated through the reservoir static model.

Chapter 3

Reservoir Model History Matching and Forecast Uncertainty Analysis

3.1 Introduction

Reservoir management has been considered by engineers as an optimization problem, due to the number of variables involved in the production behaviour of a reservoir (oil prices, production costs, field facilities, reservoir depth and pressure, hydrocarbon saturation, porosity-permeability distribution, etc.) and because of the uncertainty associated with these variables.

The best practice for managing a reservoir is assessing the uncertainty associated with the reservoir properties by having different reservoir scenarios. One way of obtaining different reservoir scenarios is by generating multiple reservoir models that honour reservoir data. In the previous chapter, different approaches were

reviewed on how to build reservoir models that consider geological and petrophysical properties' distribution and fluid saturations, as well as models that consider the numerical simulation of the fluid flow through the porous media within a reservoir.

We have seen that multiple reservoir models can be generated based on well, seismic, and production data. The next step is to select some of these reservoir models for assessing the uncertainty associated with the production behaviour of a reservoir. This thesis is focused on the generation of multiple geologically realistic reservoir models that match reservoir production information. Realistic reservoir models (Chapter 4) that match production history can be used to evaluate the future of a reservoir/field.

Most of the methodologies used to analyse the uncertainty in reservoir production and to select the models that better honour the production reservoir data (history matching) and production forecasting are indicated in this chapter. Special consideration is granted to the importance of preserving sedimentological realism of reservoir models within the automated history match process. The methodology used for history matching and production forecasting, used in this thesis is also explained in this chapter.

3.2 Reservoir Model Uncertainties

Prediction of reservoir performance is associated with uncertainties arising from the lack of accurate and reliable knowledge about the reservoir rock and reservoir fluid properties (Gavalas *et al*., 1976).

Reservoir modelling is a process that deals with sparse (or remote sensing) data since the source of information (reservoir rocks and fluids) is physically impossible to reach, because it is in the subsurface. Only few wells can reach the actual

reservoir, and the data is available only after drilling them. The data obtained are direct (cores, cuttings, sidewall-cores) or indirect (well-logs, seismic data) measurements, these data are used to identify or estimate, reservoir properties like: lithology, porosity, permeability, fluid saturation and other physical properties. Once a well has been drilled it is possible to perform reservoir pressure and fluid analysis like formation testers (RFT), PVT samples, dynamic analysis like well-tests and downhole pressure. But it is important to remember that not all these analyses are performed in each well and, in some wells, none of these analyses are performed due to the costs involved.

The main task of a geologist is to analyse the geological properties of a reservoir based on the sparse data obtained from wells, seismic data and prior knowledge. Geological interpretations in reservoir modelling are commonly based on geological prior knowledge obtained from previous work, expert knowledge, outcrop description, or analogue field analysis. All these processes are subject to the associated uncertainty, which makes reservoir prediction modelling process a task of an enormous challenge.

Uncertainty is widespread all along all the steps of the reservoir modelling process. Modellers, as it has been previously mentioned, deal with reservoir uncertainty in many different aspects: number of variables, data measurements, interpretations, modelling algorithms and hardware, physical description of fluid flow, etc.

Challenor and Tokmakian (2011) present a good discussion about the anatomy of uncertainty in climate modelling; their analysis of uncertainty can be applicable to most of the simulation problems related to nature. They divided the model uncertainty in to two classes: Aleatoric and Epistemic uncertainty.

1. Aleatoric uncertainty, which refers to random irreducible uncertainty (Challenor and Tokmakian, 2011), an example in hydrocarbon exploration is the prediction of the depth of fluid contacts. Once a structural trap is identified in seismic data, it is

impossible to precisely detect the depth of the fluid contact, because of many reasons: complexity of the geological history of the reservoir, seismic processing and resolution, time-depth conversion.

2. Epistemic uncertainty is related to the lack of knowledge and can be subdivided into structural and input uncertainty. Structural uncertainty arises because one would never know the exact form of the models, so the structural uncertainty will be reflected by differences between the model and reality. Input uncertainty is associated with the initial conditions, parameters and boundary conditions (Challenor and Tokmakian, 2011).

Data measurement errors and simulation errors make contribution to uncertainty in reservoir modelling (Christie *et al.,* 2005). Data measurement errors are intrinsic of the data measurement process. Measurement error can be caused by humans and by the measurement device during the act of data acquisition as well as by calibration errors. These kinds of errors are reduced by improvement in technology and quality control. Simulation errors were analysed by Christie *et al.* (2005), who classified modelling errors into three types:

- Input error: related to poor quality of the measurement to be introduced into the model and errors in data entry.
- Physical error: caused by the inability of the modeller or the algorithm to describe the physics of the problem (physics of the process that generated the deposits in a particular depositional environment).
- Solution error: can be defined as difference between the exact mathematical solution of the governing equation for the model and the approximate solution of the equations obtained with the numerical algorithms used in the simulation.

Massonnat (2000) points out that in reservoir modelling it is essential to assess the method of sampling the uncertainty since there is a risk of underestimating

uncertainty by using a single modelling technique. Using only one sampling technique does not identify the levels of uncertainty present in reservoir modelling.

Figure 3.1 illustrates the six levels of geological uncertainty described by Massonnat (2000). Starting from (1) data acquisition: this level of uncertainty is associated with the amount of data, tools used to obtain data and their resolution. (2) Data interpretation, this will depend on the interpreter's expertise, the methodology and concepts used during the interpretation, an error in this level could mislead the entire geological modelling; data interpretation is associated with structural interpretation, stratigraphic evolution and depositional environments in a reservoir. (3) Elaboration of a geological concept: at this stage the interpreter (geologist) is able to deliver a good idea of the reservoir geology (sedimentary environments, stratigraphy, facies, structural stiles and framework). (4) Scenario for distributing geological features: at this level the geologist should understand the geological property distribution in the reservoir (3D geometry of the facies, geobodies, and structural features). Level (5) is related to the reproduction of the distribution of the geological features described in level (4) into stochastic models (see Section 2.3) and the level (5) described by Massonnat (2000) is associated with the number of realization a geo-modeller has to produce in order to generate a set of models that would represent the uncertainty associated with in a reservoir model.

In this thesis, the geological uncertainty is levels considered at levels 3, 4, 5 and 6 in all the case studies presented here (Chapters 6, 7 and Appendix E). The data acquisition and interpretation methodology are considered as already established.

3.3 History Matching

History matching is the process used in reservoir modelling to select those models whose simulated production response matches the historical production data of a

reservoir in order to calibrate them to data, to evaluate the uncertainty associated with the reservoir modelling process and predict the reservoir production under uncertainty. History matching to production data is performed by varying a number of reservoir variables/descriptions in a reservoir model, until the reservoir production data are matched by the simulated production response. Production data may include production rates and pressure measurements, tracer data and time-lapse seismic data.

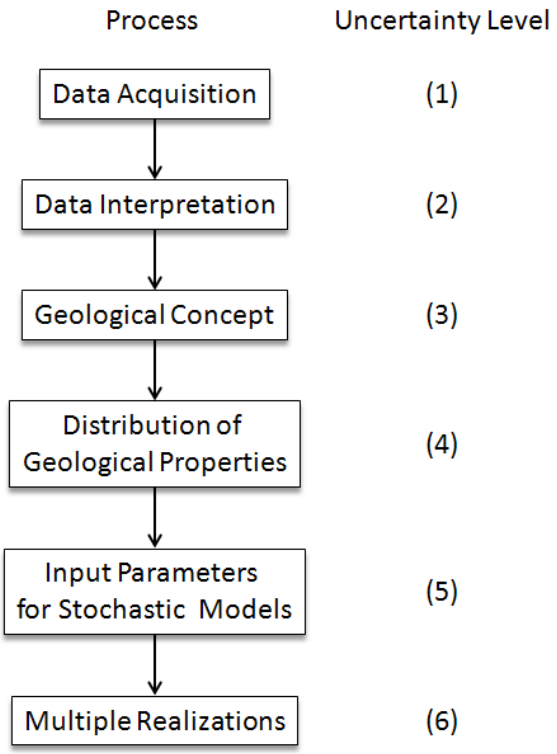

Figure 3.1: Levels of Geological Uncertainty in Reservoir Modelling (from Massonnat, 2000)

History matched reservoir models are used for reservoir production prediction and assessment of different development scenarios for a specific field or reservoir. In

this section, a review of the history matching processes is presented with an emphasis on the automatic history matching framework. This explains the methodology used in this thesis for incorporating geological realism into the automatic history matching workflow.

History match process has been considered as an inverse problem (Suzuki *et al.,* 2006; Christie, 2011; Park *et al.,* 2012; Arnold *et al.,* 2012) since the goal is to find a model that reproduces the production history of a reservoir. I*.e.* the production history of a reservoir is the output of a reservoir, but in reservoir modelling the production history is used as well to infer the actual internal properties of a reservoir.

Tarantola (1987; 2005) explained that the inverse problem consists of using the actual results of some measurement to infer the parameter values of a physical system. Tarantola (2005) stated that while a forward problem has a unique solution, an inverse problem could have multiple solutions. As an example, Arnold (2008) generated facies models of a channelized reservoir using different objects ("pacmans", hammers and channelized geobodies) and found the models, based on each of these three types of geobody shapes, that matched the production data. This is the reason why it is important to use any explicit available prior information in order to ensure geological realism in tackling inverse problems. Tarantola (2005) explains that to solve an inverse problem within the Bayesian framework, it is necessary to present a priori information as a probability distribution over the model space. This prior probability distribution is then transformed into a posterior probability distribution by relating model parameters to some observable parameters and incorporating the actual results of the observations (with their uncertainties).

Finally, the solution of an inverse problem is not a model but a collection of models that are consistent with both the data and the prior information (Tarantola, 2005).

3.3.1 Manual History Matching

History matching started as a manual approach, this means that the reservoir parameters were manually changed or adjusted in order to obtain production responses that matched the reservoir production data. Such trial and error process is time consuming and, in most of the cases, only one history-matched model can be found and used for reservoir forecasting.

Williams and Keating (1998) presented a methodology to manually history match reservoir models. This methodology highlights the hierarchical steps in which a history match process should be performed. Figure 3.2 is an illustration of the history matching stratigraphic method proposed by Williams and Keating (1998). They proposed a 7 step method: (1) Gathering the data; (2) Preparing analysis tools; (3) Identifying key wells; (4) Interpret reservoir behaviour from observed data; (5) Run the reservoir model; (6) Compare model results to observed data (pressure and historic production data), go to step 4 if the model results are different from observed data; (7) If the history data is considered good then adjust model parameters (permeability, rock compressibility, fluid properties, fault sealing, etc.) and run the model again (step 5) after adjusting parameters and then the model will be history matched.

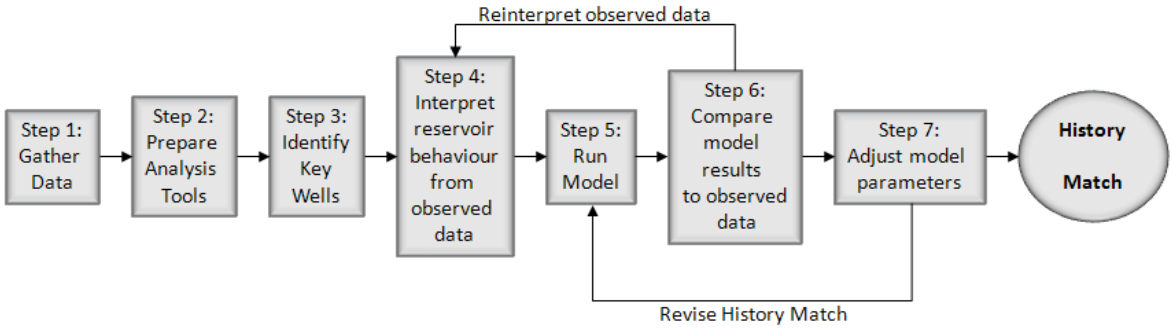

Figure 3.2: History-matching process using the Stratigraphic Method (redrawn from Williams and Keating, 1998)

Using a single history matched reservoir model could bring more problems to the reservoir characterization than solutions:

- A single history matched reservoir model could be unrealistic (very high permeability or negative permeability/porosities, unrealistic sandbody geometry). Unrealistic models have no predictive power.
- Using a single solution does not consider uncertainty, which a very important issue in reservoir modelling (Section 3.2).

Arnold (2008) stated that identifying the true values of reservoir model parameters is an under constrained problem as there could be many equally good possible solutions. Tavassoli *et al.* (2004) demonstrated that history matching is an ill-posed problem (opposed to well-posed problem) and good history match model may fail to predict.

In Tavassoli *et al*. (2004) a model was history-matched several times, producing many models that match the production history. These models produced different reservoir production forecasts, demonstrating that it is practically impossible that a single model could define the uncertainty associated with the reservoir production behaviour.

3.3.2 Automatic History Matching

The development of optimization algorithms has improved the history matching process. Automatic history matching has reduced the amount of manual work that engineers and reservoir modellers used to perform to obtain reservoir models consistent with production data (Thomas *et al.,* 1972; Mohamed, *et al.,* 2010; Hajizadeh, *et al.,* 2011).

Automatic history matching is based on determining the uncertain reservoir parameters linked to the problem of calibrating a reservoir model with observation data. This problem can be tackled by an optimization approach, which tunes the

reservoir parameters and reduces the difference between observation data and simulation outputs.

A measurement of the discrepancy between observed data and simulated production response can be well-defined, e.g. by weighted summation of least squares (least square norm).

$$M = \sum_{i=0}^{N} \frac{(Obs - Sim)_i^2}{2\sigma^2} \qquad (eq.3.1)$$

Where *Obs* and *Sim* are referred to the observed and simulated values of production data respectively, e.g. fluids production rates, bottom hole pressure, water cut, etc. σ is the variance of the observed data.

A least square definition assumes that data errors are Gaussian and independent and does not take into account the modelling errors which require more complex misfit definition (O´Sullivan and Christie (2005)).

Automatic History-Matching Algorithms

The first optimization methods used in assisted or automated history matching were Gradient-based methods (Slater and Durrer, 1972, Thomas *et al.,* 1972 and Anterion *et al.,* 1989). These methods are based on calculating the derivative of the objective function with respect to the model parameters. These are known as gradients.

These gradients are obtained by changing each parameter individually and running the simulation in order to see how a specific parameter affects the change in the objective function.

The conventional optimization methods used later for gradient-based methods are Gauss-Newton, Levenberg-Marquart with the goal of minimize the objective function. These methods are very efficient in converging to a local minimum in the

objective function, but there is no guarantee that this is the global minimum. Gradient based methods are limited for uncertainty quantification because they are able to quantify uncertainty inly in respect to a single local minimum.

Gomez *et al.* (2001) applied a method called “tunnelling” which includes a global optimization method in conjunction with a gradient-based technique. The idea is to escape from all local minima by tunnelling a valley of the objective function to another valley, by sampling far away from the local minima found. Figure 3.3 explains the position of all local minima and a global minimum for a parameter, and how the tunnelling method escapes from a local minimum.

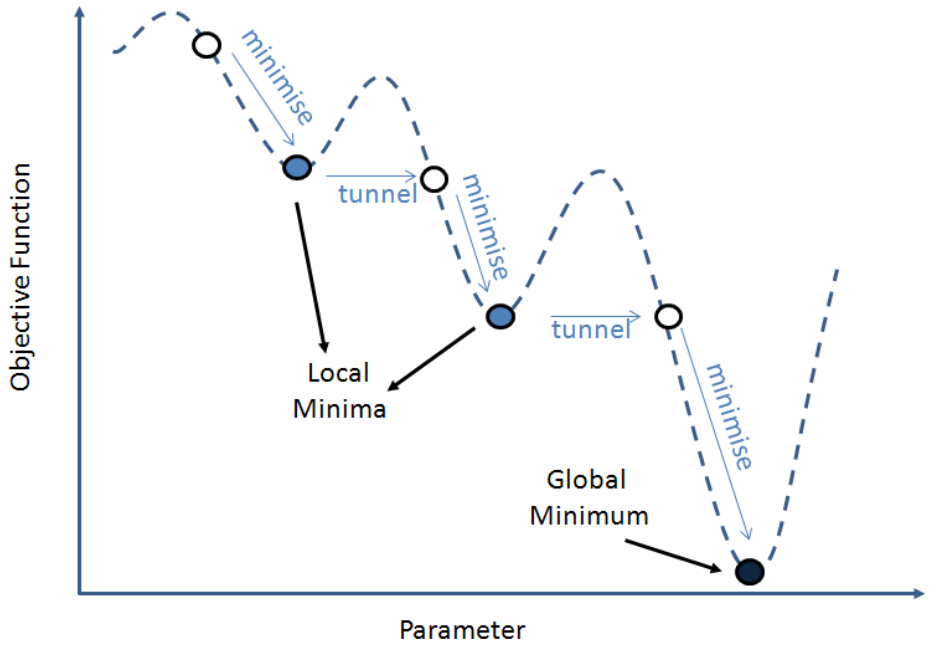

Figure 3.3: Global minimum and two local minima from the objective function, it is possible to observe the tunnelling method. The local minimum at each valley is avoided by tunnelling (sampling far from the local minimum) (from Gomez *et al.,* 2001).

A more popular used approach in sampling algorithms for history-matching is the use of adaptive stochastic optimisation methods, which randomly explore the parameter space, with the following aims:

- Generate evolutionary sequences of sampling parameters that improves the history match process.
- Escape from local minima in order to find global minima.

Some of the most common stochastic optimization algorithms used in the oil industry are:

Simulated Annealing (SA) (Press, et al., 1998) the name came from the annealing process in metallurgy, where, after heating a material, a controlled cooling is applied in order to manage the growth of the material crystals, avoiding the generation of metastable states. Simulated annealing is a numerical method, inspired from metallurgy, for the solving of global optimisation problems by trying to find the global optimum of a given function in a large parameter space. With high temperature values, the molecules of a liquid have a free movement towards one another. When the temperature decreases slowly, the thermal mobility vanishes. If cooling is very fast, the final state can be metastable, where the energy is fairly higher than the energy of the crystallised state. The energy can be translated as the objective function with the temperature as a control parameter. Starting from a point in parameter space, a random update is accepted or rejected according to the energy difference. Hence, the state is accepted if it has improved the objective function. With this method, it is possible that the system state gets out of a local minimum for a global optimum (Press, et al., 1998).

Evolutionary population-based algorithms like: Genetic Algorithm and Neighbourhood Algorithm among others, have brought more attention in the oil industry, because of the ability of these algorithms of generating a population of solutions at each step and then the fitness of each member of the population is ranked (Mohamed, *et al.,* 2010).

Genetic Algorithm (GA) (Holland, 1975) is based on the probability of evolutionary changes of biological species inspired by Charles Darwin's work. Like any evolutionary algorithm , this technique begins with a population of solutions that changes (evolves) based on the objective function values. The evolutionary

process has three operators: reproduction, crossover and mutation. They are able to drive the dynamics of a complex system search. This process is repeated until an acceptable solution (global minimum) is found. The principle feature of GA is the chromosome representation – a type of coding of the model state.

Neighbourhood Algorithm (NA), was developed by Sambridge *et al*. (2009a) to be used in seismic inversion. The aim of this algorithm is to find an ensemble of acceptable models rather than seeking for a single solution. NA is a technique that uses Voronoi cells in a high-dimensional space in order to identify ensemble of parameters that reduce the misfit of the objective function. Erbas and Christie (2007) use NA to find multiple history-match models (Erbas and Christie, 2007).

Gradual Deformation was presented by Roggero and Hu (1998). This technique is based on the inverse theory and composed by an algorithm that gradually deforms continuous geostatistical reservoir models, preserving the overall statistical characteristics of the models. The deformation process is combined with an optimization algorithm developing automatic history matching capability. The inversion of several model parameters and the gradual selection of a new constrained realization can be performed simultaneously. The analytical gradient methods as well as approximated gradients are used to improve the convergence rate of the procedure (Roggero and Hu, 1998). Probability perturbation method was proposed for HM by Caers (ref) as a further extension of gradual deformation approach.

This methodology has been used by Hu *et al.* (1999) in order to reduce uncertainty in reservoir forecasting by gradually deforming the top structure of a reservoir. Hu (2000) presented some variations of gradual deformation and their applications in reservoir history matching and forecasting.

Pilot Points method introduced by de Marsily *et al*. (1984) is based on reservoir parameters that have been estimated in a limited number of points (pilot points) and the remaining values in the other locations of the grid are estimated using

kriging or with another estimator. By adjusting the values on the pilot points the whole realization is affected when the grid is being populated using kriging.

Hamiltonian Monte Carlo (HMC) is a Markov Chain Monte Carlo (MCMC) method for sampling distributions introduced in 1987 by Duane *et al.* HMC is designed to solve some of the problems presented by MCMC algorithms, like slow exploration of the probability distribution if the step size is too small or from excessive rejection of proposed locations if the step size is too high (Christie, 2011). Unlike the above evolutionary algorithms, HMC samples for the posterior rather than from the prior. This allows inferring the uncertainty directly.

Ensemble Kalman Filter (EnKF) (Evensen, 2007) is a data assimilation method which calibrates a number of estimates of model parameters sequentially to points on time-series of observed data. Liu and Oliver (2005) used EnKF to update the facies location in a reservoir model within the automatic history-match process. EnKF has been widely used as reservoir characterisation and history-matching tool (Aanonsen, *et al.,* 2009). A basic feature of EnKF is in gradual assimilation of the initial ensemble of the system state to the observations, which are exhibited to ensemble in a stepwise way. Principle assumptions of EnKF are the linearity of the gradual change and Gaussianity of the perturbation errors.

In this thesis, **Particle Swarm Optimization Algorithm** (PSO) was used for sampling sedimentological parameters within the automatic history matching framework. PSO is considered a swarm intelligence (SI) algorithm because it was inspired on simulation of the social behaviour of a flock of birds. SI algorithms try to find optimal regions of complex parameter spaces through the communications of individuals in a swarm of particles (Clerc, 2006). PSO is easy to implement and computationally efficient (Mohamed, 2011).

Mohamed (2011) explained how PSO behaves: The PSO algorithm starts with the random initialisation of a swarm of particles in the search space. Each particle is

considered as a candidate solution to a problem in d-dimensional space, with the position of particle i represented by x_i. Each particle maintains a memory of its previous best position, $pbest_i$, and a velocity along each dimension, represented by v_i.

The *pbest* vector of the particle with the best fitness in the neighbourhood is designated *gbest*. The importance of these two positions, *gbest* and the $pbest_i$, is weighted by two factors known as the cognitive and social scaling factor parameters at each iteration (Shi and Eberhart, 1998). These two elements govern the swarm behaviour and algorithm efficiency (Suganthan, 1999).

Velocity Update

In the basic PSO algorithm, at each iteration k, particle i*'s* velocity v_i^k is updated using *eq. 3.2*.

$$v_i^{k+1} = v_1^k + c_1 r_1 \left(pbest_i^k - x_i^k\right) - c_2 r_2 \left(gbest^k - x_i^k\right) \qquad (eq. 3.2)$$

in which x_i^k refers to the current position of a particle i at iteration k. c_1 and c_2 are user-defined non-negative constant real parameters which weight the particle's attraction towards its own best known position $pbest_i^k$ and the global best known position of the entire swarm $gbest^k$ up to iteration k, respectively. r_1, and r_2 are two random vectors with each component corresponding to a uniform random number between 0 and 1. Introduction of such random elements into the optimisation is intended to simulate the slightly stochastic unpredictable component of a natural swarm behaviour. In addition to this, the user also chooses the swarm size N.

The velocity update in *eq. 3.2* has three major components (Engelbrecht, 2005).

1. Inertia, component (v_1) that models the tendency of the particle to continue in the same direction.

2. Memory, it is a linear attraction towards the best position (*gbest*) ever found by the particle.

3. Social knowledge, this is a linear attraction towards the best position (*pbest*) found by any particle.

Position Update

The particle's position is added to the particle's velocity once the velocity has been calculated to determine the new position of the particle.

The update equation of the personal best position $pbest_i$ is presented in (*eq. 3.3*), assuming a minimisation problem where f denotes the objective function that is being minimised and k is the iteration (generation) number.

$$pbest_i^{k+1} = \begin{cases} pbest_i^k & if \ \ f(x_i^{k+1}) \geq f(pbest_i^k) \\ x_i^{k+1} & if \ \ f(x_i^{k+1}) < f(pbest_i^k) \end{cases} \qquad (eq.\ 3.3)$$

Mohamed (2011) highlighted the main computational PSO workflow in the following steps:

1) Initialise the swarm of n_{init} models by assigning at locations randomly generated in parameter space. Each particle is also assigned a plausible random velocity.
2) For each model (particle) the forward problem is solved and the relevant objective function value is obtained.
3) For each particle, update the position and value of *pbest* – the best solution the particle has seen. If the current objective function value of one particle is better than its *pbest* value, then its *pbest* value and the corresponding position are replaced by the current objective function value and position, respectively as in *eq. 3.3*
4) Find the global best objective function value and the corresponding best position *gbes*t across the whole swarm's *pbest* and update if appropriate.

5) Update the velocities and positions of all the particles using *eq. 3.2* where c_1 is a weighting factor, termed the cognition component which represents the acceleration constant which changes the velocity of the particle towards $pbest_i$. c_2 is a weighting factor, termed the social component which represents the acceleration constant which changes the velocity of the particle towards $gbest^{k.}$
6) Repeat steps 2–5 until a stopping criterion is met (e.g. the maximum number of iterations is reached or a sufficiently good objective function value).

In this thesis PSO was set up using the parameters mentioned in Table 3.1.

Mohamed *et al*. (2010) indicated that PSO is able to obtain good history matched models in less number of iterations than Neighbourhood Algorithm (NA). And that PSO tends to concentrate more sampling in low misfit regions than NA.

These results have implication in reducing the number of simulated models and reducing computing cost. Therefore, PSO was selected as the sampling algorithm for history matching in this thesis.

3.4 Probability in Reservoir Uncertainty Quantification (Bayes Theorem)

As discussed in section 3.2, reservoir modelling is a task with large uncertainties, due to the scarcity of information and the cost associated with its acquisition. The most common way to quantify the uncertainty of a problem in a statistical way is by assigning a probability distribution to the uncertain parameters related to the specific problem.

PSO Parameter	Characteristic
Number of Particles	Number of models used in the optimization
Group Size	Number of particles for the for each group of particles (the idea is to generate groups of particles)
Initial Inertia	tendency of the particle to continue in the same direction it has been moving
Initial Decay	weight used to reduce the initial inertia in every step
Cognitive Component	Linear attraction towards the best position ever found by the particle
Group Component	Linear attraction towards the best position found by a group of particles
Social Component	Linear attraction towards the best position found by any particle
Minimum steps	Minimum number of time-steps a swarm is allowed to search
Energy Retention	Allows the swarm to retain the strategy used in previous steps
Particle Behaviour	Select between flexible* and conventional behavior of the swarm

Table 3.1: Parameters used to set up the Particle Swarm Optimization Algorithm (PSO).

*Flexible PSO allows the swarm to move more freely through the search space allowing fine tuning in local search (Kathrada, 2009).

Christie *et al.* (2005) stated that, the use of a Bayesian approach for statistical inference provides a systematic procedure to update current knowledge of a system based on available data. In this thesis, a Bayesian framework was used to quantify the uncertainties associated with geological models. This involves a systematic procedure to update the current knowledge of a system based on newly obtained data (Christie *et al.,* 2005). Bayesian inference is based on the Bayes' theorem (after Thomas Bayes), and used to perform inferences about the value of some parameters based on prior and newly observed information.

Bayes' theorem is usually written as:

$$p(m|O) = \frac{p(O|m)p(m)}{\int_M p(O|m)p(m)dm} \qquad (eq.3.4)$$

Where M is considered as the space of the reservoir model, m is a vector of model parameters that compose an arbitrary reservoir model from the space M, O is a vector of the observed (production and pressure data from every well), $p(m)$ is the prior probability distribution, $p(O|m)$ is the likelihood of the data (a measure of the quality of the fit of model m predictions to the observed data and $p(m|O)$ is the posterior probability (PPD) representing our updated knowledge about the model m based on observations O.

Prior probability distribution $p(m)$ as mentioned in Section 3.3 is a very important input used in solving inverse problems. The use of prior information reduces the number of models used in inverse problem solutions (Tarantola, 2005). In this thesis, sediemntological prior information is modelled and included into the automatic-history-matching process, in order to control the realism of reservoir facies models. In Section 3.4.4 there is a discussion about the geological prior information and its importance in solving geoscientific problems.

3.4.1 Likelihood Estimation

Likelihood of a reservoir model can be defined as the probability that reservoir observation data is equal to simulation responses based on a specific reservoir model. In this thesis, likelihood will be calculated using the misfit based on the production data of the reservoir (*Obs*) and the production response obtained from the model (*Sim*). Assuming that measurement errors are independent in each time step and normally distributed, in order to include the information from all well data (gas, oil and water production/injection and pressure changes) likelihood is calculated as the product of the probabilities of individual measurements at all time steps (t).

$$p(O|m) = \left(\frac{1}{\sigma\sqrt{2\pi}}\right)^N \prod_{t=1}^{N} exp\left\{-\frac{1}{2}\frac{(Obs - Sim)_t^2}{\sigma^2}\right\} \qquad (eq.3.5)$$

3.4.2 Posterior Probability Distribution

As explained before the Posterior Probability Distribution (PPD) or $p(m|O)$ in *eq. 3.4* represents our updated knowledge about the model m based on the observations O and the prior knowledge of the model.

Christie (2011) points out that the sampling algorithms used in automatic history matching generates multiple models, but the sampling is not uniform, and there is no guarantee that the samples are samples from the posterior probability distribution (PPD). Sambridge (1999b) deals with this problem by using the so-called Neighbourhood Algorithm-Bayes (NA-Bayes).

NA-Bayes

Figure 3.4 shows how to obtain multiple history-matched reservoir models based on a Bayesian framework. From this *ensemble* of reservoir models it is possible to generate a posterior probability distribution (PPD).

Erbas (2007) identified three methodologies for estimating PPD: (i) Categorisation of PDD around the Maximum Likelihood; (ii) Using a subset of the ensemble of history-matched reservoir models and (iii) sampling from the complete ensemble of history-matched reservoir models.

As explained by Liu *et al.* (2001) and Arnold (2008) the most robust methodology is the one, such as the Markov Chain Monte Carlo, that considers the complete ensemble of history-matched models. The results obtained in this thesis are based on the PPD estimated using a Markov Chain Monte Carlo (MCMC) technique called Bayes-Neighbourhood Algorithm (NAB) (Sambridge, 1999b). This methodology includes the optimization process.

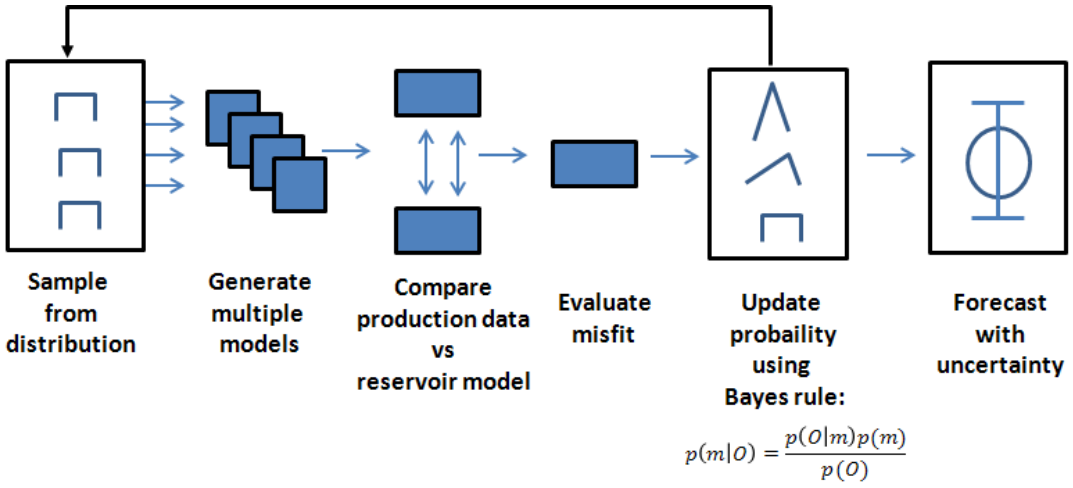

Figure 3.4 Bayesian framework for generating multiple history-matched models: Multiple models are generated after sampling from a prior distribution, the production responses of these model are compared to the actual reservoir production, then the evaluation of misfit allows us to update the probability distribution (PPD) and generate a production forecast with a range of uncertainty (error bar). From Christie *et al.,* 2006.

NAB uses Voronoi cells to interpolate values of misfit away from the known sampled points (models in the parameter space), for which the likelihood is computed exactly. In Figure 3.5 it is shown how NAB uses Voronoi's cells and the Gibbs sampler to estimate PPD. The resulting ensemble of the model with their posterior probabilities is then used to estimate the P10 – P50 – P90 confidence interval (CI to describe the uncertainty envelopes for reservoir performance.

Sambridge (1999b) describes how Neighbourhood Algorithm-Bayes (NAB) proceeds using a Gibbs sampler following the steps:

(i) Choose an initial start point (B) (typically maximum likelihood model)

(ii) Take a series of random steps from B, along each parameter axis

(iii) For each axis an interval is defined that covers the entire parameter range (l_i to ui) a conditional probability distribution function is created (PDF) for this interval by calculating the intersection points of the

interval with the ensemble's Voronoi cells. Producing a PDF like the $P_{NA}(x_i|x_{-i})$ shown in Figure 3.4.

(iv) Each random step is proposed by a random deviation from the uniform distribution along the interval.

(v) The step x_p is accepted or rejected by the equation $r = \frac{P_{NA}(x_i^p|x_{-i})}{P_{NA}(x_i^{max}|x_{-i})}$ where $P_{NA}(x_i^{max}|x_{-i})$ is the Maximum value of the conditional along the interval and r is a second random deviate between 0 and 1.

(vi) If the step is rejected then the process is repeated until a step is accepted.

NAB is be used in this thesis for approximating the PPD, following NAB application for estimating PPD in Erbas and Christie (2007), Demyanov *et al.* (2004), Demyanov *et al.* (2008), Mohamed *et al*. (2010), Hajizadeh *et al*. (2009).

Park *et al*. (2013) used a technique to estimate the PPD based on a **rejection-sampling** sequence. First, they modelled the probability of a reservoir model given the production data in an attempt to reject models with low probability without history matching , and then they used the probability perturbation method (Caers and Hoffman, 2006) for generating model distribution constrained to production data.

3.4.3 Geological Prior Information

Prior information can be defined in probabilistic analysis as the available knowledge about the probability of parameters having a specific value, before having any further information (Swan and Sandilands, 1998). Prior information can be set based on previous knowledge of the problem (expert knowledge) or based

on quantitative data obtained from reliable sources (scientific publications, reports).

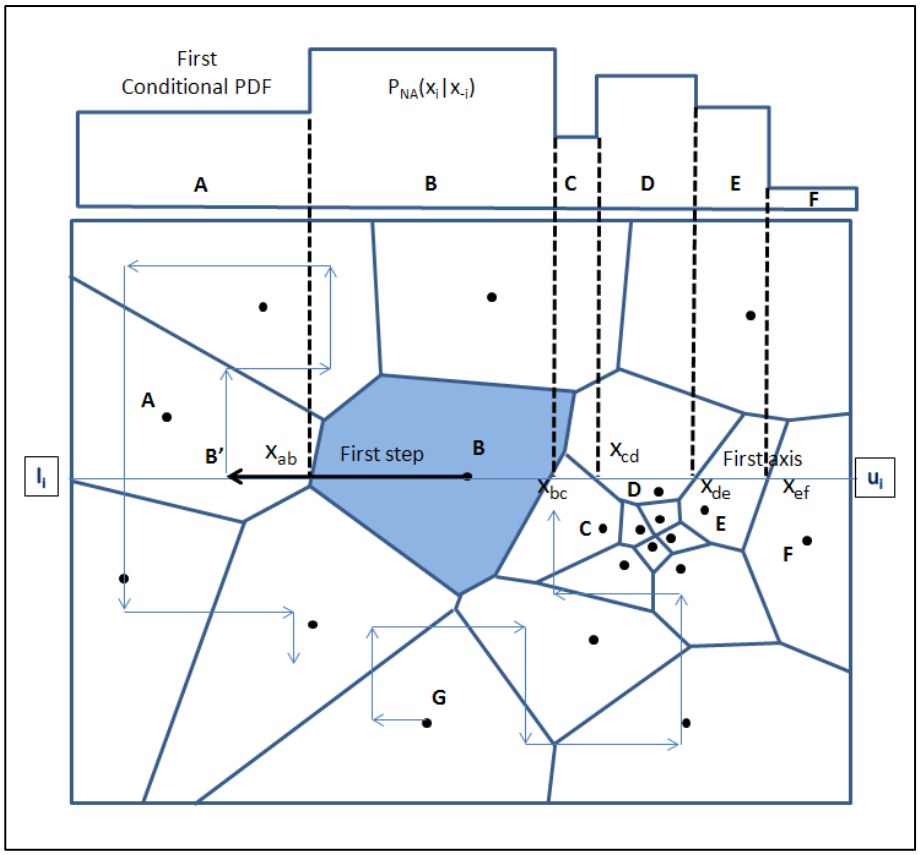

Figure 3.5 Random walk of the Gibbs sampler in NAB (from Sambridge,1999)

Prior information plays an important role in Bayesian analysis; thus, in equation 3.2 we can observe the relevance of this information where the use of prior information will improve the posterior estimation. To highlight the relevance of prior information Jaynes (1968) stated that, once the sampled distribution, the loss function and sample are specified, the only remaining basis for a choice among different admissible decisions lies in the prior probabilities. Jaynes (1968) identified that there is a problem in using prior information based on arbitrariness ("subjectiveness"). It is necessary to identify a realistic distribution of prior information in order to avoid misleading when estimating the posterior distribution.

Gelman (2002) identified three groups of prior distribution:

(1) Non-informative prior distributions. These distributions are usually set as uniform distributions of one or many specific uncertain parameters. This type of distribution assigns the same probability to occur at all the values in the proposed range. This type of priors is named “ignorant”; however, establishing a range of possible responses is an indication of the knowledge of the process that is been analysed.
(2) Highly Informative Priors. This type is used when fairly information about the possible values of a parameter in the model is available. In some cases a normal distribution is given for this type of priors defined by the mean and the standard deviation.
(3) Moderately Informative Hierarchical Prior Distribution. This type of prior distribution is used when information about on the parameter is limited. The prior distribution will make the parameter vary by a specific factor (*a*) between each model and constraining the range of the parameter by a factor (*b*) that could be 10 or 100 times of the mean, factors *a* and *b* are going to depend on the available parameter scientific data.

Another problem identified in setting uniform priors is the so-called **Curse of Dimensionality** (Lee and Verleysen, 2007). As an example, if we consider a uniform prior distribution of a single parameter (one-dimensional parameter space) 80% of the uniform samples fall into one standard deviation. If we consider two parameters, the number of samples that fall into one standard deviation of both parameters is 64%. The number of samples that fall into one standard deviation will reduce exponentially with the increase of the number of parameters (Lee and Verleysen, 2007). The curse of dimensionality is explained in Section 4.4.1.

In the case of analysing uncertainty in geoscience problems, geological prior information was defined by Wood and Curtis (2004) as the geological information provided as an *a priori* component of the solution (i.e. information that existed before the solution was formed and which is incorporated into the solution). The

key to the successful solution of geoscientific problems is to use geological information obtained from sources related to the studied problem or from interpretations based on similar problems.

The use of geological prior information may be subjected to qualitative expert opinion as well as quantitative sources, such as measured data from outcrops, cores, seismic and previous reservoir models of the field under study or analogous fields.

Geological prior information has been used, as a key part of the solution of geological problems by many authors. Wijns *et al*. (2004) generated a stratigraphic model using a set of 9 geological parameters related to the hydrodynamics of a depositional system. The nine parameters were changing during the modelling process in order to find a model that fits the target distribution of sedimentological facies. Wijns *et al*. (2004) used flat or non-informative priors given ranges to the 9 hydrodynamic parameters.

Hodgetts *et al.* (2004) used a set of outcrop digital data where it was possible to identify the geometry and facies relationships of deep-marine fan deposits, to generate geological models of the reservoir developed in the Tanqua Karoo depocentre, South Africa. In their work the prior information related to the geometry of the deep-marine deposits was obtained from the outcrop digital data.

Other examples of geological prior Information applied in uncertainty quantification have used uniform distributions (Erbas and Christie, 2007, Demyanov *et al*., 2004).

Some examples of informative priors used in geosciences are presented here: Arnold (2008) introduces a technique of modelling prior information of fluvial channel geometry based on published equations that relate channel width and thickness, and generating a 2D region that encapsulates a realistic combination of channel width and thickness. This region was used then within the automatic

history match framework and used for rejecting models that were going to use unrealistic combination of channel width and thickness.

Suzuki *et al.* (2007) developed a set of geological structural models and used them as prior information that covered the structural uncertainty of the reservoir. History matched models were generated then by varying the structures based on the structural prior information framework, that was previously accommodated in a parameter space using a “similarity distance”.

A similar example was developed by Park *et al.* (2013), where a set of training images related to the facies geometry and distribution of a deep marine reservoir was used as prior information. The realizations obtained from these training images were flow simulated and the results compared in a Multidimensional Scale plot to the actual production data of the reservoir. The selected realizations, whose production data was close to the actual reservoir production data, were history matched. This work showed how to use multiple geological interpretations as prior information, and to select a geological interpretation to generated history matched models. This work showed as well an improvement in saving computing time by reducing the number of models to history match.

3.5 Summary

The importance of history matching in reservoir modelling has been highlighted in this chapter. Automatic history-matching based on stochastic optimization methods allows the reservoir modeller to select models of a reservoir that match production data, and use them to assess the development plan of a field based on a probabilistic outcome within the Bayesian framework. This allows presenting a range of possible models instead of a single solution (model), which considers the uncertainty associated with the reservoir modelling process.

This methodology is a reliable process to plan for investment and estimate reserves, under uncertain environment like hydrocarbon production. Fast optimization algorithms have been applied to this problem in recent years, saving computing time and avoiding getting trapped in local minima.

In this chapter, it was shown that most of the attention in the probabilistic history-match approach has been paid to find faster and more reliable algorithms for sampling and optimization. Other works have been focussed on varying the petrophysical model properties. It is only in recent years that some research has been done on the impact of geological properties (geological parameterization) on the process of history matching. Less research has been done on how to preserve the geological realism in reservoir models, if the history match process is automatic. Arnold (2008) and Park *et al.* (2013) demonstrated that the use informative geological prior information have the potential of preserving geological realism in reservoir models developed within the framework of automatic history match.

The importance of geological prior information in automatic history matching was presented in section 3.4.3. The use of informative geological prior information to preserve the geological realism in reservoir models is presented in the following chapters.

Chapter 4

Machine Learning Techniques: a Tool for Modelling Geological Prior Information

4.1 Introduction

The use of geological prior information in geoscientific problems was analysed in Section 3.4.3, including a description of the classification of prior information used in reservoir facies modelling. The impact that the prior information has over the posterior distribution was explained.

A new approach for compiling and modelling the interdependencies of the parameters of the geological prior information is proposed in this chapter. The main idea is to generate informative geological prior information based on the intrinsic relationships that exist between the geological parameters that are genetically related (e.g. channel depth and thickness); then use this information prior to control the geological realism of the reservoir facies models in automatic history-match framework.

In this thesis the advantages of Machine Learning Techniques (MLT) were used to model the geological prior. Due to the characteristics of these techniques, it is possible to compile high dimensional interdependencies between geological parameters in a non-linear and non-parametric way. A justification to the use of MLT as the tools for modelling geological priors is presented here.

The sources of geological prior information used in this thesis, as well as the types of geological priors used in geological modelling and automatic history matching are described in this chapter.

Finally, the theoretical basis of the Machine Learning Techniques used in this thesis is explained. Four machine learning techniques have been used here to model geological prior information: Multilayer Perceptron (MLP), which is an Artificial Neural Network (ANN), Support Vector Machine (SVM) for classification, One-Class SVM, which is an extension of SVM, used for novelty detection or sample rejection and Support Vector Regression (SVR) for regression.

4.2 Sources of Geological Prior Information

As mentioned in Section 3.4.4 geological prior information was defined by Wood and Curtis (2004) as the geological information provided as an *a priori* component of the solution to a geoscientific problem (i.e. information that existed before the solution was formed and which is incorporated into the solution).

The determination of the geometry of the sedimentary geobodies preserved in the geological record is one of the most important geoscientific problems faced in reservoir modelling. Verwer *et al*. (2004) and Massonnat (2000) pointed out that one of the major problems in geology is the determination of anatomy of sedimentary geobodies and their related stratigraphic surfaces. It is clear that most of the works in sedimentary geology have been focused on the interpretation of depositional systems rather than on the geobody dimensions of depositional environments. In recent years, many research institutions have acquired an

enormous quantity of data in recent years, considering the dimensions of different geobodies.

The problem of identifying the dimensions and geometry of sedimentary deposits preserved in the geological record has a huge impact in the determination of reserves in the subsurface (minerals, hydrocarbons, groundwater, etc.) and some works have been published on the estimation of the geometry of such deposits.

Understanding the dimensions of sedimentary systems is the second step within the sedimentological model process (Section 2.2.3). First, it is necessary to understand what type of process generated the geobody under study (sedimentary environment). Second, it is necessary to estimate the dimensions and geometry of such geological body and so gain a better idea of the extension of a particular facies or facies association (Massonnat, 2000).

Massonnat (2000) stated that this problem has a high level of uncertainty and the use of reliable geological prior information could reduce the associated uncertainty. Geological prior information related to geobody geometry can be obtained from published data related to geometrical description of geobodies or from measurements taken from outcrops, modern depositional environments or high resolution geophysical data.

Leeder (1973) published one of the first works trying to extrapolate information obtained from modern rivers to fluvial deposits preserved in the geological record, proposing some equations that can be used to predict the width of a palaeo-fluvial channel based on the thickness of their deposits.

Allen (1964) describes the geometry of meandering fluvial channels deposits from the Old-Red Sandstone in the Welsh Borders. Allen's 1983 work has been widely used as prior information to generate facies models of reservoirs deposited in meandering fluvial systems (Robinson and McCabe, 1997 and Clemente and Perez-Arlucea, 1993). Fisk *et al.* (1954) described the facies distribution within the Mississippi river delta and this work has been the base of many further

depositional models of deltaic reservoirs (Le Blanc, 1972 and Curtis and Picou, 1980).

Jones *et al.* (2004) used digital techniques and fuzzy logic algorithms to generate geological maps. They compared their results with maps generated by paper-based methods, which do not consider uncertainty in the interpolation methods. The geological prior information used by Jones *et al.* (2004) to build the digital maps was obtained from outcrops and modern depositional environments. The compilation of the maps obtained from digital techniques gives quantifiable ranges of uncertainty of the geological maps obtained. The paper based map does not offer these ranges of uncertainty.

Jones *et al.* (2004) highlighted the types of geological prior information stating that geological prior information can be divided into: field data, expert knowledge and previous information; and they explained how these three types of priors are related.

Posamentier (2005) described geomorphological features from seismic data (seismic geomorphology). The geometry of the geobodies described by Posamentier (2005) has been used as the prior information for modelling the facies geometry of various depositional environments (Rasmussen *et al.,* 2007 and Moscariello, 2005)

In this thesis, the prior information was modelled using published data. These data came from field observations and a more detailed explanation of the origin and type of data used to model our prior information can be found in chapter 6 and Appendix E.

4.2.1 Geological Prior Information Models

As mentioned in the previous section, the geological prior information used to model geobody geometry is based on published data, existing knowledge and

information obtained directly from outcrops, modern depositional environments and high resolution geophysical data.

In this thesis, published information related to geobody geometry was used to model the interrelationships between the geometrical variables that characterize sedimentary bodies. These models are then used as prior information to generate geological interpretation of the subsurface.

A description of the types of prior information was shown in section 3.4.4. Figure 4.1 illustrates some examples of prior information models that have been used in modelling facies distribution and uncertainty analysis.

The use of geological prior information related to geobody geometry depends as well on the modelling technique used. Most commercial software for geomodelling that have object-based techniques among their modelling algorithms (e.g. Petrel from Schlumbeger or RMS from ROXAR) use as input (prior information) a range of values of specific geological parameters. In the case of modelling channels it is necessary to put a range of channel parameters, like channel width and thickness and meander amplitude and wavelength (Figure 4.1(a)), these ranges can be considered as uninformative priors. Uninformative priors do not have the capacity to describe complex multivariate relations between geological parameters (e.g. relationship between channel depth and channel thickness), or it is possible as well to introduce distribution in a parametric or non-parametric way as informative priors. Prior distribution bounds the space for selecting combinations of geological parameters that are seen in nature (realistic) (Figure 4.1 (b)). The space outside the prior distribution refers to unrealistic combinations of the parameters and increases exponentially with the dimensionality of the problem (curse of dimensionality, see Section 4.4.1). Although, most of the geomodelling commercial softwares have different options to identify the relationships between geomorphic variables some geomodellers use linear relationships (Leeder, 1973 and Williams, 1986) as informative priors (Figure 4.1 (b)). These linear relationships are very restrictive and lead to underestimation of uncertainty. Since linear relationships only include the combination of parameters that are on the

regression line, excluding data that were taken from nature. Figure 4.1(d) illustrates how Arnold (2008) solved this problem by generating a region of realistic combinations of fluvial channel width and thickness, where it is possible to sample and generate multiple realistic models. This region uses some of the linear regression equations as boundaries proposed by (Leeder, 1973, Crane, 1983, Bridge and Mackey, 1993 and Williams, 1986).

Lange *et al.* (2011) proposed a methodology called the Frequency Matched Method (FMM) in a reservoir model built using multiple-point statistics with a training image (prior information). FMM generates multiple training images by randomly changing the original training image but keeping the same facies proportions as the original training image. This method allows the generation and use of multiple training images (prior information) in the reservoir modelling process.

More recently Park *et al.* (2013) used a series of training images as geological prior information to model facies distribution of deep-marine channel reservoirs, using multiple point statistics (Figure 4.1(e)).

4.3 Why modelling priors using Machine Learning Techniques?

In Section 4.2, it was shown that it is possible to generate geological prior information for reservoir modelling by understanding and modelling the relationships among geological variables (Leeder, 1973 and Arnold, 2008). The main problems found in modelling geological prior information are described as well in section 4.2. It was clear that, modelling geological relationships (facies geometry, sediment grain-size, bed thickness, fossil age, etc.) is a non-linear, multivariate problem applied to data coming from multiple sources (outcrops, seismic interpretations, modern depositional environments, well data, and analogous oil fields, etc). Some of the most common modelling approaches used to generate geological prior information are statistical techniques and process

based models, which cannot cope efficiently with the characteristics of geoscientific data:

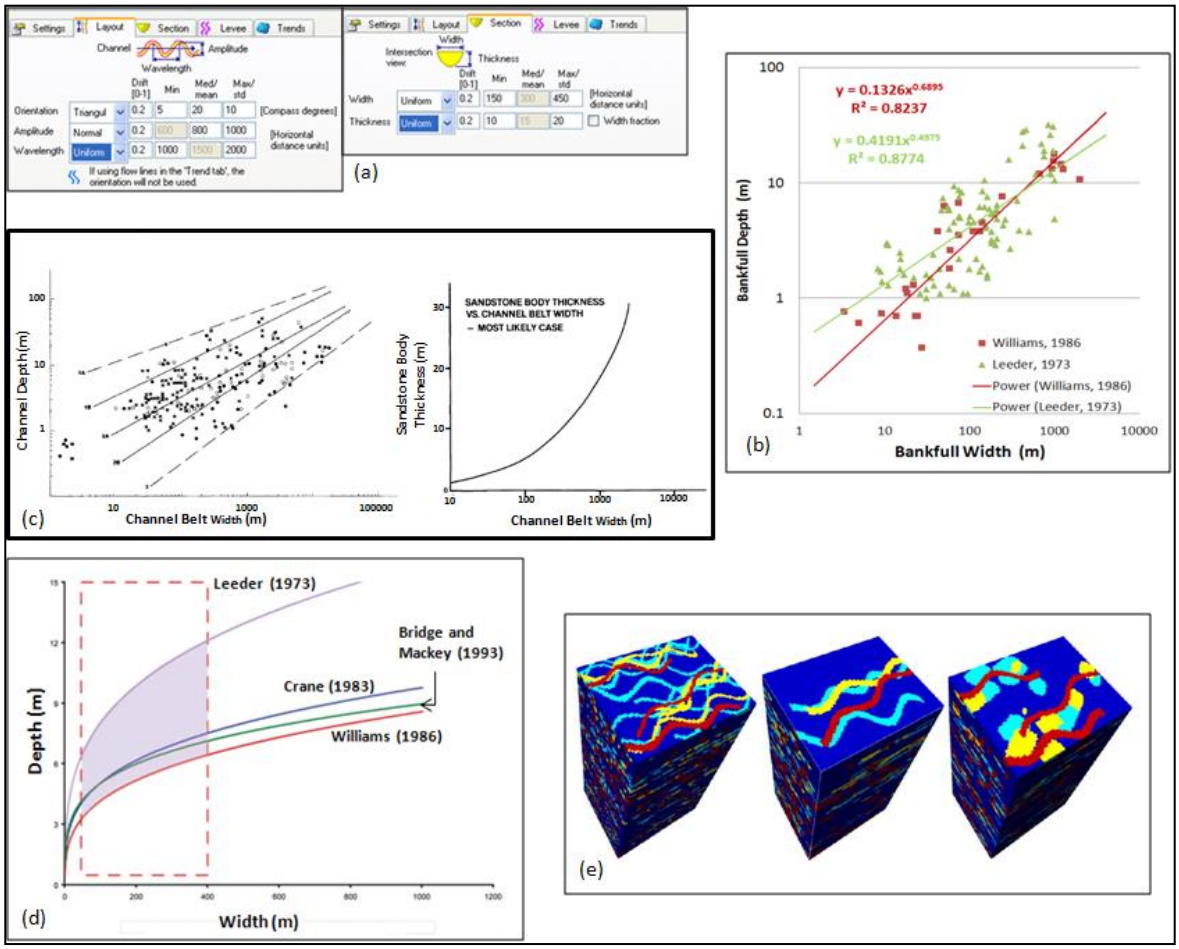

Figure 4.1: Examples of geological prior information that have been used in modelling facies for reservoir characterization: (a) Prior information used in modelling channels using object modelling in Petrel®. Note, that one can use uniform, normal and triangular prior distributions. (b) Empirical linear regressions that relate fluvial channel depth and width, data was obtained from Williams (1986) and Leeder (1973). (c) Plots of the relationships defined by Fielding and Crane (1987) relating channel depth with channel belt width and sandbody thickness with channel belt width. (d) Arnold (2008) used hydrological data for restricting width and depth (channel thickness). The prior range (red dashed line) has a significantly larger area than even the extremities of the hydrological data suggests. The four curves, *Leeder, Crane, Williams and Bridge and Mackey* represent a range of values produced from possible palaeohydrological models for channel dimensions. (e) Park *et al.* (2013) use these three training images (geological concepts) as geological prior information to generate reservoir models.

- The number of observations is commonly low, if it is compared to the whole universe of possible combination of geological parameters. Geologists commonly work with a reduced number of data (well data, outcrops, field samples) or low resolution data (seismic) to generate models of a geological event.
- Geological information is often high-dimensional since many processes and factors are involved in the generation of a specific rock (sediment grain-size, available sediment, temperature, energy, tectonics, etc.) or the distribution of a property within a rock-volume (porosity, chemical composition, and fossil distribution).
- Statistical relationships between the geological variables are non-linear and are not known with a sufficient precision. Although many authors try to use linear relationships in order to explain in a simple way the interaction between some geological parameters (e.g. Leeder, 1997, Bridge and Mackey, 1993, Crane, 1983).
- All the data obtained from geological sources are noisy because the sampling process, preparation and analysis introduce noise to the result. A technique that can cope with the presence of noise in the data is needed.

Kanevski *et al*. (2009) described Machine Leaning Techniques (MLT) as modelling tools that are universal, adaptive to nonlinear data, robust and efficient. MLT can find acceptable solutions for classification, regression and probability, density modelling problem in high-dimensional spaces.

MLT is specially designed to handle finite datasets, embedded in high-dimensional spaces considering noisy data and non-linear relationships between variables (Vapnik, 1995).

MLT have been used in different scientific and engineering disciplines with excellent results. The use of MLT in geosciences is relatively new; some of the work based on MLT has been oriented to environmental analysis, remote sensing, phenomena prediction and uncertainty quantification in geosciences:

In soil science, authors like Shang *et al*. (2004), Kanevski (1999), Kanevski *et al.* (1997) and Buszewski and Kowalkowski (2006) among others used artificial neural networks to map soil contamination and to distinguish the degree of contamination. In other branches of geosciences Bastidas *et al*. (2008) used artificial neural networks to identify the type of deposits within a deltaic system, using a classification arrangement of neural networks. Rogers *et al*. (1992) created a program to identify lithology from well-logs responses based on artificial neural networks. Machine learning algorithms have been used as well in mineral prospecting (Brown *et al.*, 2000) and analysis and classification of landslides (Yesilnacara and Topal, 2005 and Ehsani and Quiel, 2008). These publications are a small sample of the application of MLT in geosciences demonstrating that these techniques can handle multidimensional problems, using noisy data in a non-parametric and non-linear way.

Modelling geological prior information related to reservoir models is a potentially attractive application for MLT. The next sections of this chapter will describe the characteristics of the MLT used in this thesis for modelling geological prior information.

4.4 Learning from Data

Learning from data can be defined as a process of learning complex and hidden statistical dependencies from examples, in other words, obtaining results from a system based on observation of processes that connect the conditions, where the observed event happens (input space), and the observed event or its outcomes (output space). This concept can be considered a definition of Machine Learning (Kanevski *et al.,* 2009). Another property of Machine Learning Algorithms is that they can control automatically or semi-automatically the learning process.

There are various algorithms in machine learning, adopting many methods from non-parametric statistics, artificial intelligence and computer science. In this thesis, two of the most widely applied algorithms in geosciences were used:

Artificial Neural Networks (ANN) (Bishop, 1995; Haykin, 1999) and Support Vector Machines (SVM) (Vapnik, 1995; Platt, 1999; Cherkassky and Mulier, 2007; Kanevski *et al.,* 2009).

In the process of learning from data usually a set of data is use to understand the hidden relationships among data points this is called training data set. Then another set of data points is used to test the relationships found with the training data set.

4.4.1 Curse of Dimensionality

The dimensionality D of an input vector x and the number of data instances N strongly affect the ability of an algorithm to learn input-output data dependencies. This is due to the curse of dimensionality (Lee and Verleysen, 2007), which is defined as the emptiness in space for increasing dimensions. More formally, the number of data samples N, required to estimate a function with sufficient accuracy, increases exponentially with the number of dimensions (see Figure 4.2 a).

The curse of dimensionality affects data analysis and modelling using statistics, *e.g*. the behaviour of volume as dimensionality increases, the ratio between the volume of a hypersphere and its circumscribed hypercube tends to 0 with increasing dimensionality (Lee and Verleysen, 2007).

$$\lim_{D\to\infty} \frac{V_{sphere}(R)}{V_{cube}(R)} = 0 \qquad eq.4.1$$

where R is the radius of the sphere, D is the number of dimensions and V is the volume.

This means that the hypercube becomes spiky and the spherical shape of the hypersphere vanishes in high-dimensional space (see Figure 4.2 b), this causes a problem when evaluating the probability density function (p.d.f.)

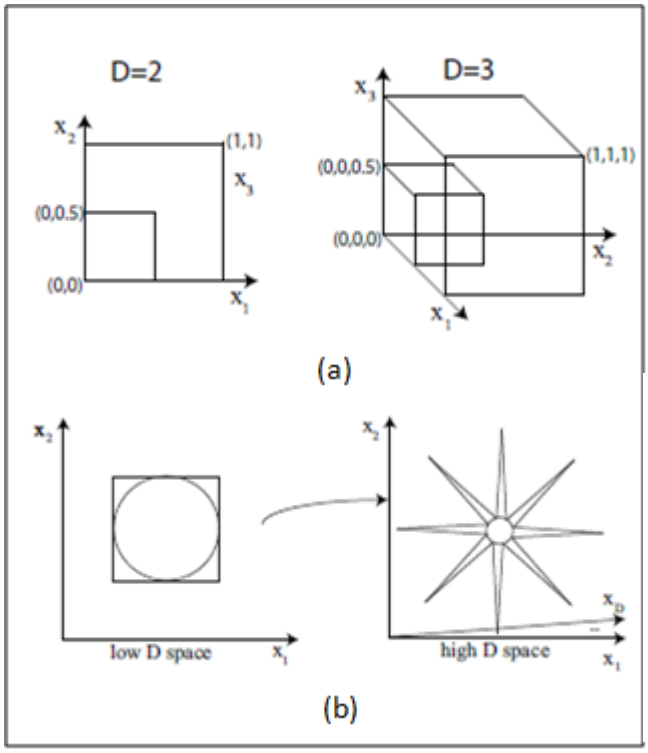

Figure 4.2: Visualization of the curse of dimensionality. (a) Moving from a 2-dimensional space to a 3-dimensional space the number of half unit cubes rises from 4 to 8, which is proportional to 2^D. (b) The body of the *D*-sphere vanishes compare to the body of its circumscription *D*-cube as *D* increases (from Foresti, 2011).

Some of the problems presented when dealing with high dimensional data are:

- Makes harder for any algorithm to learn dependencies from the data.
- The number of data needed to describe the whole input space grows exponentially with its dimension.
- It is more likely to obtain overfitting in high dimensional space, since the training data covers less parameter space when dimensionality increases.
- Testing samples are equally far from the training samples in the data space. So distance-based similarities learned from the training data are not reliable.
- Thus, the predictions are harder to make.
- The parameter space remains poorly sampled.

4.4.2 Unsupervised Learning

Unsupervised learning consists of learning by using inputs only, since no data on the outputs are available. Unsupervised learning is used to find patterns, clusters and structures in a set of N input data samples $\{x_i\}_{i=1}^{N}\ belong\ to\ X$ where X is the input domain $X\ is\ a\ subset\ of\ \mathbb{R}^D$ with a dimensionality D.

Figure 4.3 illustrates how unsupervised neural networks can be used to classify lithology and depositional facies from well-logs.

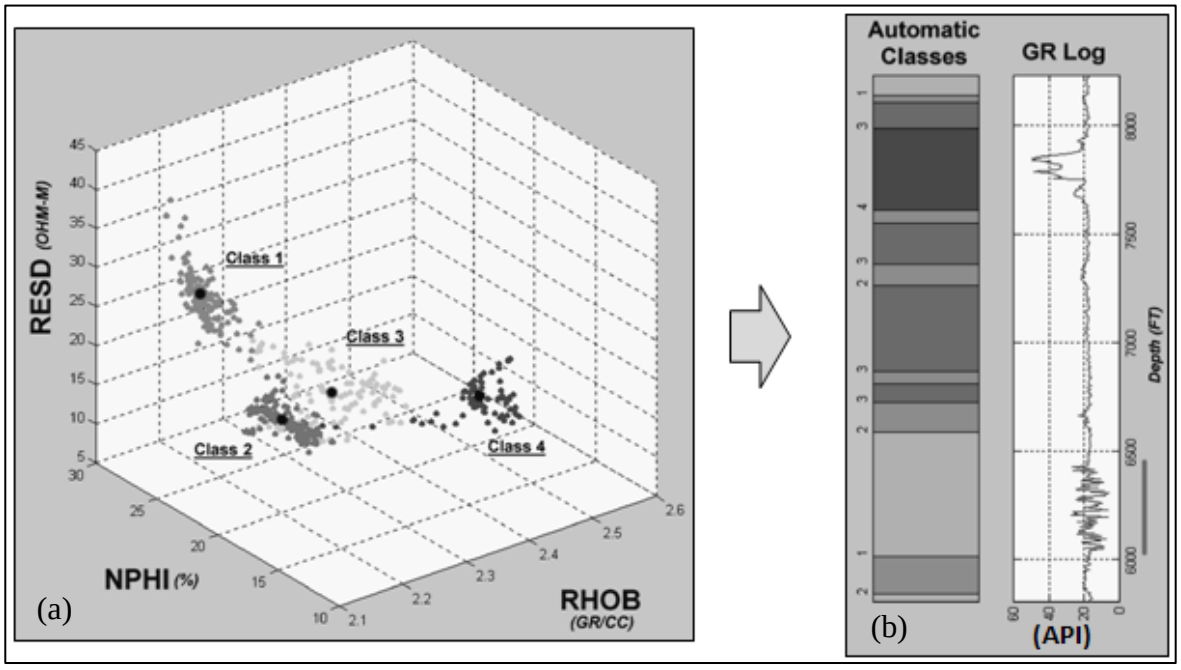

Figure 4.3: Facies Classification from well-log data, using unsupervised artificial neural networks. (a) Data from logs (Resistivity, Neutron-Porosity and Density) cluster in different classes (facies), (b) using ANN it was possible to classify the data and identify sedimentary facies. From Saggaf *et al.* (2000).

Unsupervised learning algorithms are commonly used to find some groups (clusters) of input vectors. Dimensionality reduction is another task where unsupervised learning is useful. The main idea is to find a simpler, low dimensional representation which preserves some geometrical or topological properties of the original space.

4.4.3 Supervised Learning

If the outputs are known for the corresponding limited number of inputs, the learning problem is called supervised; this means that the examples that illustrate the input-output dependence are available to "supervise" the modelling process.

As an example, let's consider a one-dimensional categorical output, $y = \{1,2,3,\dots,M\}$ in a multi-class classification problem, as every observed input x is known to belong to some class y. The idea is to use the available examples, to build a classification model (i.e. to generate a rule that assigns a class label to any previously unseen input vector). Figure 4.4 shows an example of classification problem in supervised learning.

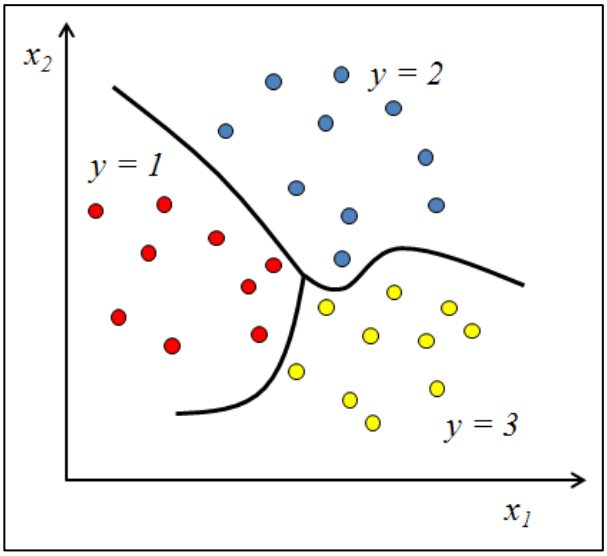

Figure 4.4: Supervised learning in a classification problem. Consider each (x_1,x_2) samples of soils with y characteristics. The classification algorithm identified three classes and separated them in the x_1-x_2 space (from Kanevski *et al.,* 2009).

Qi *et al.* (2007) used supervised neural network to predict oolitic facies in uncored wells from image logs. Figure 4.5 demonstrates how they applied supervised neural networks to predict oolitic facies.

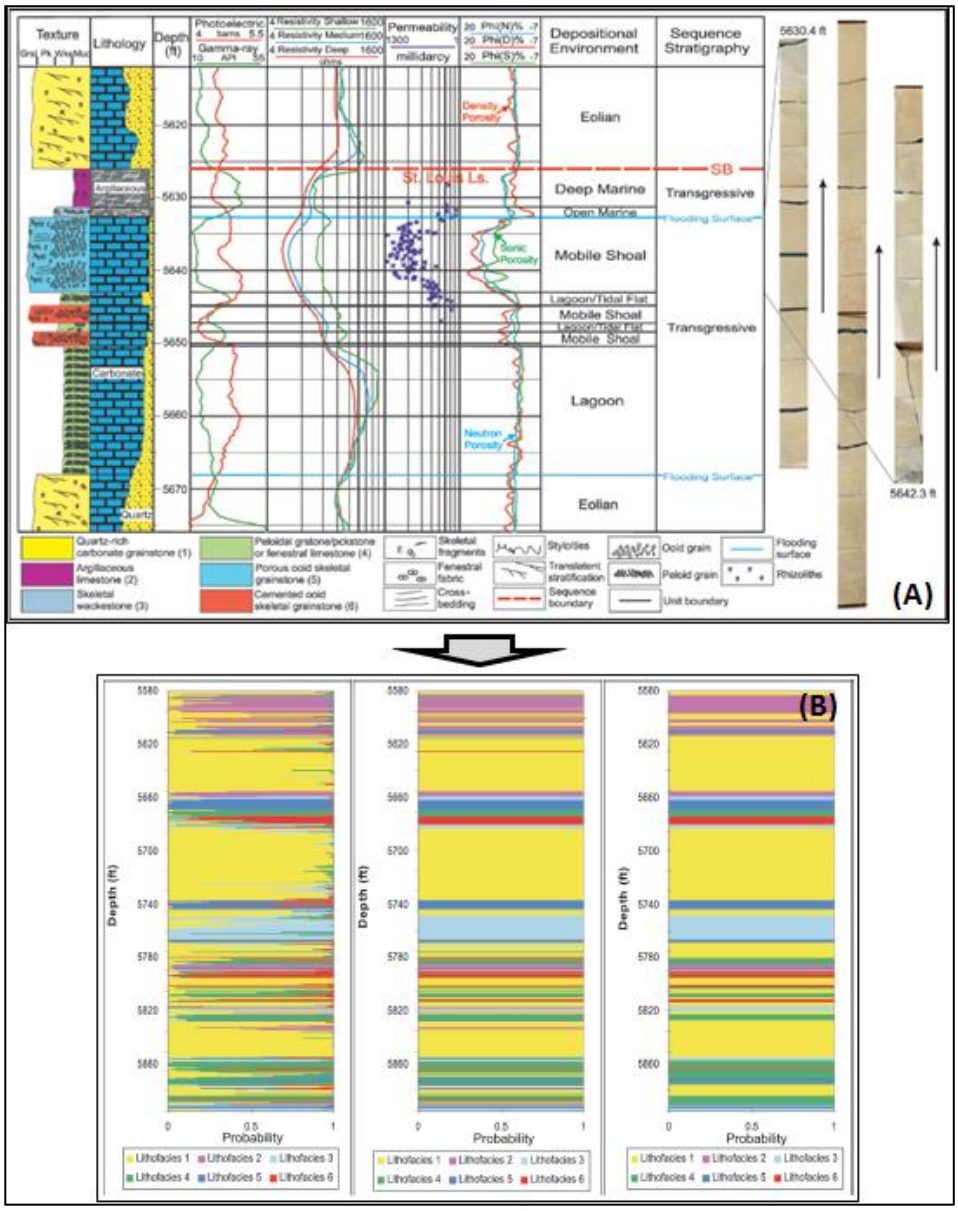

Figure 4.5 Predicting oolitic facies from core data to uncored wells based on image logs using supervised neural networks. Neural networks were trained using data from cored wells (A); Neural networks were used to predict oolitic facies in uncored wells using image logs as input (from Qi *et al.,* 2007).

Figure 4.6 is an example of solving a regression problem using supervised learning. This problem is solved by drawing a line through a cloud of points. Regression problems can have a one-dimensional continuous output (modelling

the conditional mean). If the problem has high-dimensional outputs then it is called a multivariate problem.

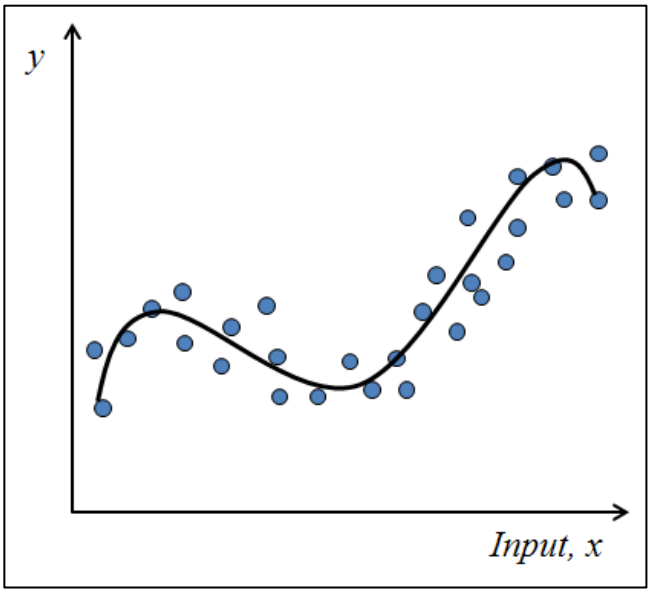

Figure 4.6: Supervised learning. Regression problem (from Kanevski *et al.*, 2009).

4.4.4 Semi-supervised Learning

Real-life data analysis does not often offer a complete set of inputs and outputs, which makes these types of problem more interesting. It is common to observe data sets with a small proportion of labelled data (outputs are known) accompanied with a large set of unlabelled data (inputs with unknown outputs). This setting is known as semi-supervised learning. The information obtained from the unlabelled part of the dataset mainly concerns the geometrical properties or the structure of the input space. Figure 4.7 presents two solutions of a classification problem (a) without unlabelled data and (b) with unlabelled data, we can observe that the differences in the classification boundary geometry are ruled by the structure given by the unlabelled data. Although, unlabelled data do not have output values, these data can identify the structure that relates samples from different populations.

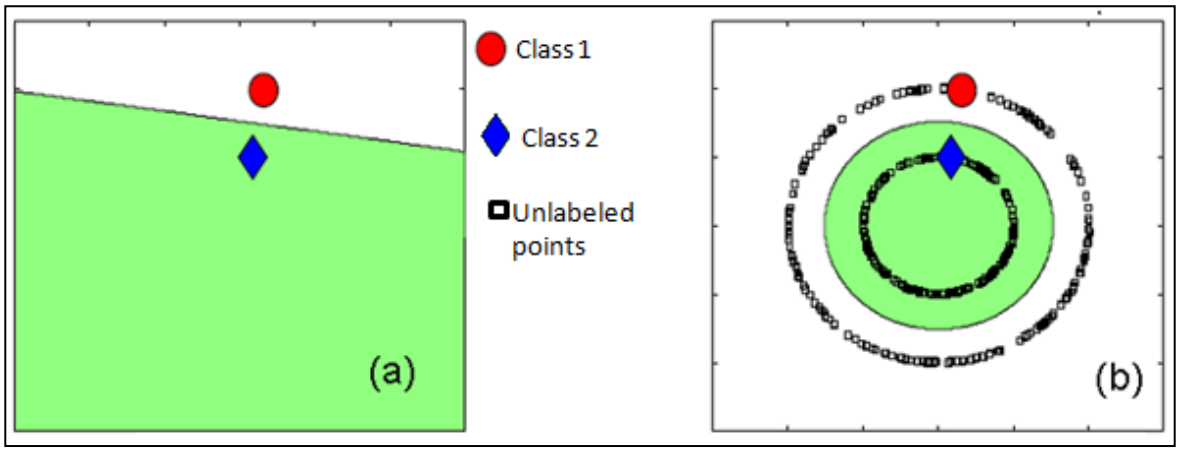

Figure 4.7: Semi-Supervised learning. (a) Classification problem solved without (a) and with (b) unlabelled data. Unlabeled data give the information about the geometry or structure of the boundary between classes (from Belkin *et al.,* 2006).

Demyanov et al. (2008) used semi-supervised Laplacian Support Vector Regression (after Belkin *et al.,* 2006), based on porosity and permeability data from wells and unlabelled data from seismic in order to generate permeability distribution maps in a fluvial reservoir (Figure 4.8).

4.4.5 Learning from data - Summary

Machine Learning algorithms have a wide field of applications since the problems that can be tackled with these types of algorithm are very broad and it is possible to work with one of the types of problem mentioned above (unsupervised, supervised or semi-supervised) covering most of the statistical problems and datasets present in real-life. Multidimensional classification and regression problems can be solved using Machine Learning Techniques (MLT) which select the best function from a set of available functions, given sets of training and testing data and a loss function to compute training and testing errors (Kanevski, *et al.,* 2009).

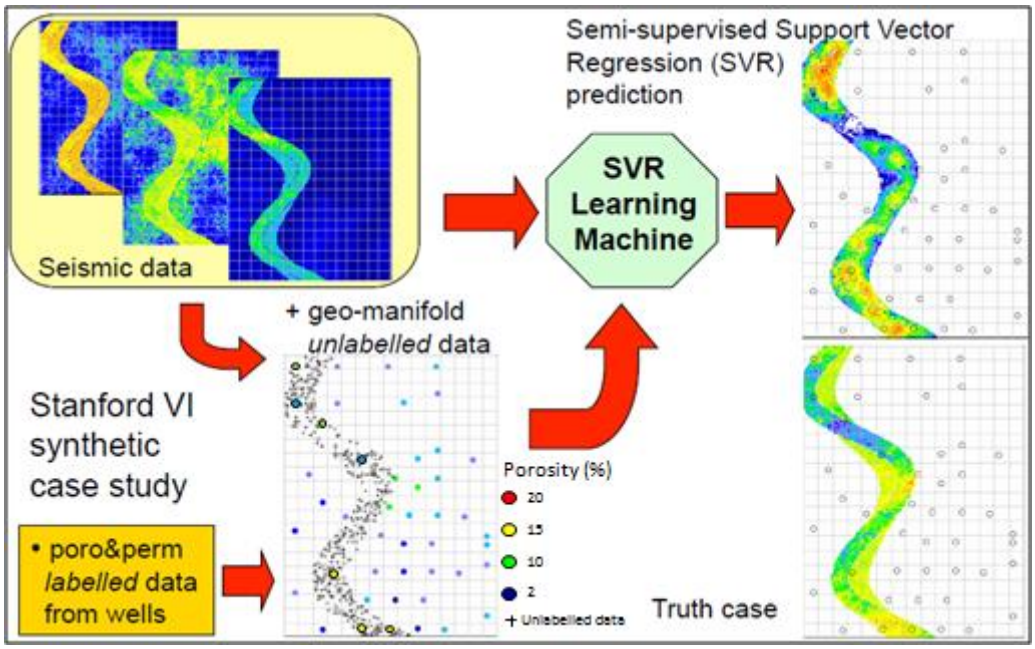

Figure 4.8: Porosity distribution maps using semi-supervised vector regression. Note that unlabeled data points are obtained from the geobody extraction of seismic data. Labelled data come from well data. Unlabelled data points give the structural information of the geobody (geo-manifold) this geo-manifold is populated with the data obtained from wells (from Demyanov *et al.,* 2008).

4.5 Artificial Neural Networks (Multilayer Perceptron)

Models developed using artificial neural networks (ANN) are now used in many scientific and engineering fields. Artificial Neural network models overlap heavily with statistics, especially nonparametric statistics (Kanevski *et al*., 2009). Artificial neural networks consist of numerous connected simple process units called “neurons” (motivated by biological neurons) that one can program for some desired computation. One can train or program a neural network to store, recognise and retrieve patterns; to filter noise from measurement data and to control ill-defined problems. Unlike statistical estimators, ANNs can estimate a dependent function without an explicit mathematical model of how outputs depend on inputs (Kanevski *et al*., 2009; Bishop, 1995; Govindaraju, 2000a).

In this thesis, I used a traditional model of multilayer perceptron (MLP), considered as a network with no feedbacks and no lateral connections (Kanevski *et al*., 2009) where the information flows in only one direction from the input to the output (Figure 4.9). Multilayer perceptron is a fully connected network of neurons organised in several layers. A MLP can learn with a supervised learning rule using the backpropagation algorithm (Kanevski *et al*., 2009). The backpropagation algorithm gave rise to the iterative gradient algorithm designed to minimize the error measure between the actual output of the neural network and the desired output using a pre-computed error on the forward pass of information through the network (Kanevski *et al*., 2009).

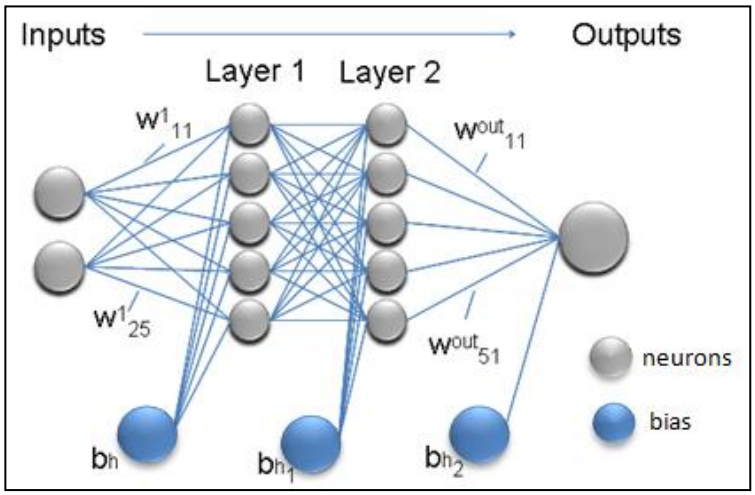

Figure 4.9 MLP with 2 inputs, 2 hidden layers with 5 “neurons” (process units) each and one output. w_i are the weights given to each connection. The input data go into the input neurons, this information is processed by two interconnected layers of 5 neurons each, and influenced by bias (b_{hi}), after processing the information one output is obtained. From Kanevski *et al*. (2009).

Tuning MLP

A conventional practise is to use training and testing data to achieve the optimal balance between goodness of training data fit and prediction accuracy on validation data. The way used to achieve this balance is to measure and compare errors obtained from training and testing data. *Training Error* can be defined as the difference between the outputs (t) obtained using training data inputs and the ideal

value of the output variable (i) in training data. The network is then tested against a set of *testing* data; the difference between the *testing* data values and the outputs obtained from the MLP using the *testing* data inputs is named *Testing Error.*

In this thesis, training and testing errors are calculated using the mean square error equation (*eq*. 4.2) (Kanevski et al., 2009):

$$error = \frac{(i_1 - t_1)^2 + (i_2 - t_2)^2 + \cdots + (i_n - t_n)^2}{n} \qquad (eq.\,4.2)$$

n is the number of outputs.

The combination of neurons that generates the lowest testing and training errors is considered as the optimal neural network which gives good predictions without overfitting data (Kanevski et al., 2009).

A trained neural network as a computational model can be represented with a formula for computing predictions based on learned/tuned weights and the inputs, *i.e.* for a two-layer perceptron (Haykin, 1999):

$$F^m(x^1, x^2, \dots, x^k)$$

$$= f^{out}\left\{\sum_{h_2=1}^{H_2} w_{h_2,m}^{(out)} f^{h_2}\left[\sum_{h_1=1}^{H_1} w_{h_2,h_1}^{(2)} f^{h_1}\left(\sum_{k=1}^{K} w_{k,h_1}^{(1)} x_k + b_k\right) + b_{h_1}\right] + b_{h_2}\right\} \qquad (eq.\,4.3)$$

where:

$w_{h_q,h_p}^{(H)}$ is the weight of the link from the neuron h_p of the previous layer to neuron h_q in the layer H.

m is the index of an output,

H_1,H_2 are the number of hidden units (neurons) in the first and second layers,

K is the number of inputs,

b_k, b_{h1} and b_{h2} are the biases of the layers.

f^{h_i} are the transfer function for the hidden layers and f^{out} the transfer function for the output layer.

The choice of the number of hidden neurons can be consider as a common problem in the use of ANN, as there is not a straightforward unique solution. This is tackled by generating different ANN structures changing the number of layers and the number of neurons in order to find a solution avoiding generalization and overfitting.

4.6 Support Vector Machines

This section presents a brief introduction to the Statistical Learning Theory and then will show how this concept is applied to develop the support vector machines for classification, regression (SVR) and novelty detection One-Class SVM (OC-SVM). Statistical Learning Theory was formulated a generalisation theory for a wide range of learning based algorithms: ANNs, SVMs, etc.

4.6.1 Statistical Learning Theory

Vapnik (1995) developed a statistical learning framework in order to generate highly generalized, statistical, predictive models. In statistical learning theory the term "learning" means the process of estimation of some function $y = f(x)$ where $x \in \Re^N$ and, depending on the problem, $y \in \Re$ for regression, $y \in [1,2, \ldots M]$ for *M-class* pattern recognition or $y \in \{-1,1\}$ for binary pattern recognition.

Kanevski *et al*., (2009) stated that the process of learning is considered as follows: A learning machine must choose from a given set of function $F = \{f(x,\alpha), \alpha \in \Lambda\}$ one of which best approximates the unknown dependency. Λ is an abstract set of parameters, chosen beforehand. This choice is actually an optimization problem in the parameter space of α.

Learning algorithm. To generate a learning algorithm it is necessary to define a learning problem with an associated loss function, then an induction principle and a set of decision functions. Kanevski *et al*. (2009) defined the induction principle as a routine that provides a method for generalizing some particular observations into a general rule, i.e. it allows one to construct a decision rule that can classify every point in the space given only a finite number of examples (points) from the space (the training set).

Loss functions and risk minimization. A loss function as defined by Vapnik (1998) is a measure of the discrepancy between the estimate and the actual value of a parameter. Learning was defined previously as the estimation of the function *f(x)* from the set of functions $F = \{f(x, \alpha \in \Lambda)\}$ defined *a priori*, which provides the minimum value of the risk function (Vapnik, 1998):

$$R(\alpha) = \int Q\big(y, f(x,\alpha)\big)p(x,y)dxdy \qquad (eq.4.4)$$

Where $Q(y, f(x, \propto))$ is the loss function, *i.e*. a measure of the discrepancy between the estimate and the actual value y given by the unknown function at a point x and $p(x,y)$ is the joint probability distribution.

The goal here is to minimize the risk function, which means that the objective is to minimize the expected average loss (chosen loss function) for a given problem.

For classification problems the loss function is:

$$Q(y,f) = \begin{cases} 0, & if\ f(x) = y \\ 1, & otherwise \end{cases} \qquad (eq.4.5)$$

For regression:

$$Q(y,f) = \big(y - f(x)\big)^2 \qquad (eq.4.6)$$

Empirical risk minimization principle. It is necessary to minimize the risk function (eqs. 4.5; 4.6) by using a function that provides the minimum deviation. In order to approximate the risk function with training data, Kanevski *et al*. (2009) use the so called empirical risk function:

$$R_{emp} = \frac{1}{L}\sum_{i=1}^{L} Q(y_i, f(x_i, \alpha)) \qquad (eq.\,4.7)$$

Then, a function f that gives the minimum value to empirical risk is chosen as an optimal decision function. This induction principle is called empirical risk minimization (ERM).

Vapnik-Chervonenkis dimension. The VC-dimension is a useful method to characterize the complexity of a model. VC-dimension is used to calculate the complexity of nonlinear models in the parameter space (Kanevski *et al.,* 2009). Christie *et al*. (2011) pointed out the importance of complexity in modelling. Incorporating more detail into a model may allow a more accurate description, but over-complex models tend to lose generality, and thus, lead to poor predictions, while a poorly identified model does not describe well the data. It is necessary then to strike the right balance between too much simplicity and too much complexity (Christie *et al.,* 2011).

In classification VC-dimension can be considered as a number of possible separations of the data samples with the function from this set. As illustrated in Figure 4.10 there is a classification problem on a 2D plane where, with a linear decision function one can classify three samples, whatever labels have been assigned to them. However, there exists a labelling for 4 samples so they cannot be classified by a linear function in other words the linear decision function is not powerful enough (or complex) to perform this task. The VC-dimension of the linear decision functions in $\Re^N$ is $N+1$, *N* is the number of dimensions, $\Re^N$ is the *N*-dimensional feature space.

Generalization is considered as the ability to describe the actual underlying functional dependency from finite empirical data. Choosing a set of functions, which can perform many possible separations, will achieve a low empirical risk but

could give a poor generalization. The phenomenon of choosing a false (too complex) structure is called overfitting. On the other hand, choosing a weaker set of functions can result in better generalization, but a too weak set of functions would not describe the actual dependencies in the data.

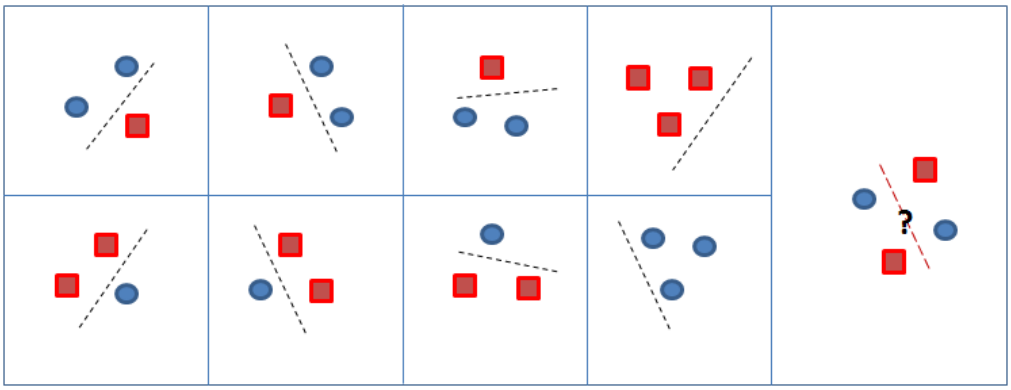

Figure 4.10 Three samples in 2D can be separated with a linear decision function. However, there is a combination of 4 samples which cannot be separated by a linear function. (from Foresti, 2011).

Figure 4.11 illustrates the overfitting and the generalized phenomena. In this case, a data set and a regression function is used to describe the phenomenon. First, it is necessary to select the set of functions $F = \{f(x, \alpha)\}$ that can describe the data. One set (Figure 4.11 (b)) are linear decision functions $f(x, \{w, b\}) = wx + b$ and the other set (Figure 4.11 (c)) are sine functions $f(x, \{w, b\}) = b.\sin(wx)$. The first set only describes linear dependencies while the second set can describe any dependency with high frequency sine curve, but with a very low generalization.

Linear and sine functions sets have the same number of parameters, w and b, but different generalization properties. VC-dimension of the sine function is infinite, since w can be high enough to fit any data set.

A learning machine needs to fit the data (minimize empirical error) while keeping the complexity of the machine low (rise of generalization).

Considering a problem of classification where the bound on the expected risk holds with the probability $1 - \eta$ (Vapnik, 1998):

$$R(\alpha) \leq Remp(\alpha) + \sqrt{\frac{h\left(\log\left(\frac{2L}{h}\right) + 1\right) - log\,\frac{\eta}{4}}{L}} \qquad (eq.4.8)$$

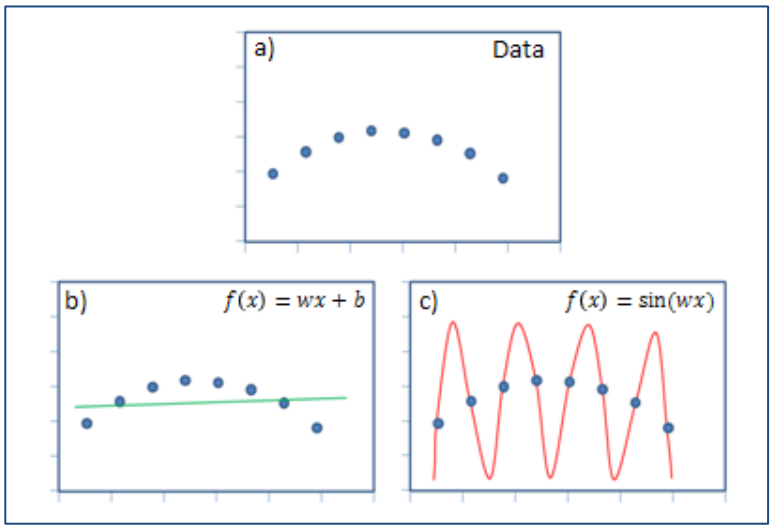

Figure 4.11: Tackling a regression problem: a) Data set for regression problem. b) Linear regression is not powerful enough to fit the data. c) Sine function fits the data, but the generalization ability is very low (From Kanevski, *et al.*, 2009).

The parameter h is the VC-dimension of the set of decision functions parameterized by α. Knowing the exact value of h and choosing a sufficient small value for η, allow to calculate the best choice for α (the best function to select from the set of decision functions).

The ERM principle, which minimizes the first term, gives a small value of expected risk when $\frac{L}{h}$ is large (the ratio of the number of training samples to the VC-dimension of the functions set). In order to minimize over both terms of eq. 4.8, it is necessary to set the VC-dimension as a controlling variable and not just used *a*

priori. Generalization ability is then controlled by choosing the VC-dimension or some other related embodiment of capacity in the set of functions.

Structural risk minimization (SRM) principle. The aim is to minimize both the empirical risk and the confidence interval (in *eq.* 4.8). If we have a structure:

$$S_1 \subset S_2 \subset \ldots \subset S_T \qquad (eq.4.9)$$

Using the set of decision functions F whose VC-dimension satisfy

$$h_1 \leq h_2 \leq \cdots \leq h_T \qquad (eq.4.10)$$

and the chosen S_{opt} of the structure to minimize the bound (*eq.* 4.8). Thus, the SRM principle defines a trade-off between the accuracy (empirical risk or training error) and the complexity of the approximation by minimizing over both terms in *eq.* 4.8.

4.6.2 SVM Classification

Support vector machines (SVMs) are constructive learning algorithms based on the statistical learning theory (Vapnik, 1995). SVM implements the set of decision functions and uses the SRM principle. SVM uses the VC-dimension to build a set of functions whose detailed description does not depend on the dimensionality of the input space. This is possible by generating a special loss function (*margin*) to have control on the complexity (VC-dimension). The margin is known as the distance between two labelled classes.

The simplest approach to the classification problem is to separate two classes with a linear decision surface (a line in 2D, a plane in 3D or a hyper-plane in higher dimensions). Data separable without misclassification can be called linearly separable. Large margin classifier is an algorithm that can find the optimal decision hyperplane for linearly separable data. Ssoft margin classifiers are algorithms that allow for training errors and find linear decision hyperplane for data that is not linearly separable (real data). This problem is avoided by using the

kernel trick, which generates a nonlinear classifier known as Support Vector Machine (SVM), the kernel trick will be explained later in this section.

Considering the following basic set of linear functions:

$$f(x) = w.x + b, \qquad (eq.\,4.11)$$

Where x is a vector in $\Re^N$ to be optimized. For classification the sign of the function $f(x)$ is considered as the output of the classifier. As mentioned before, the VC-dimension is $N + 1$, this condition is fixed and cannot be controlled by the choice of parameters. In order to use SRM it is necessary to overcome this inconsistency by introducing the large margin idea.

Large margin classifiers

Considering the following decision function:

$$y = \begin{cases} 1, & if\ w\,.x - b \geq 1 \\ -1, & if\ w\,.x + b \leq 1 \end{cases} \qquad (eq.\,4.12)$$

In this case, the decision is taken considering the position of the sample with respect to a margin along the hyper-plane defined by w and b. Then if the training set of vectors in $\Re^N$ belongs to the sphere with a radius$R$, the VC-dimension h of the set $(eq.\,4.12)$ is bounded with:

$$h \leq \min([R^2\|w\|^2], N) + 1 \qquad (eq.\,4.13)$$

The separating constrains of the classes can be defined as:

$$\begin{matrix} w.x_i + b \geq 1, & if & y_i = 1 \\ w.x_i + b \leq -1, & if & y_i = -1 \end{matrix} \qquad (eq.\,4.14)$$

The scaling of w and b is arbitrary and fixed as above, such that the value of the decision function equals one for the samples closest to the boundary ($eq.$ 4.14) can be written as a single constraint:

$$y_i(w.x_i + b) \geq 1 \qquad (eq.4.15)$$

Figure 4.12 illustrates how to calculate the margin between samples of different classes. Where the margin ρ can be estimated as the distance between hyper-planes $f(x) = 1$ and $f(x) = -1$

$$\rho = \frac{2}{\|w\|}(x) \qquad (eq.4.16)$$

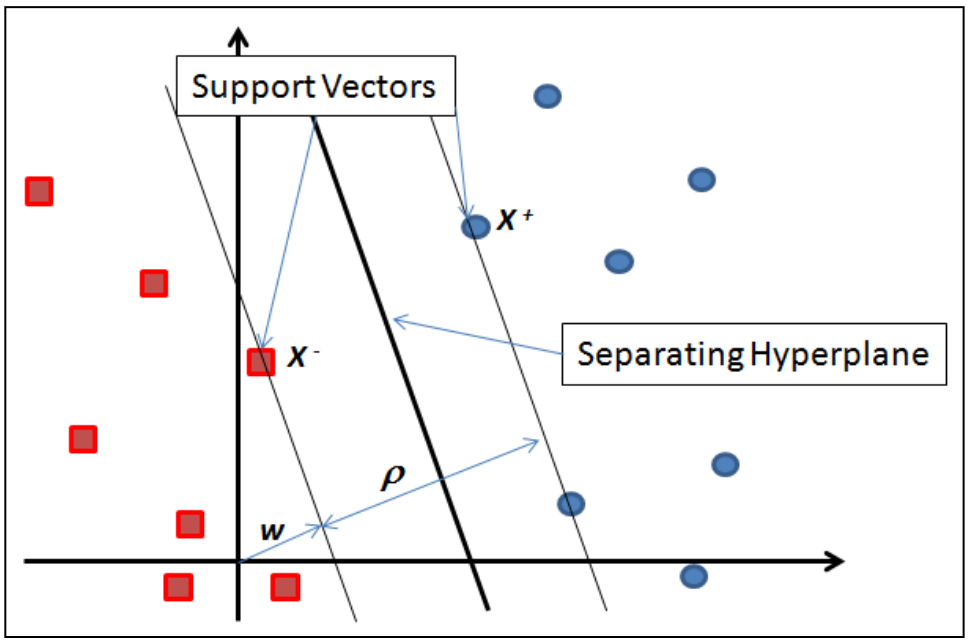

Figure 4.12: Calculating the margins from samples of different classes, using Support Vectors. This Figure explains graphically the formulation of the margin as a linear separating hyperplane. Support vectors are the only points which contribute to define the separating hyperplane (from Kanevski, *et al.* (2009)).

SVM not only separates two classes but also maximizes the margin between the two classes by minimizing $\|w\|$ (eq. 4.16). The main idea is that a large margin should be more resistant to noise and should have better generalization than a small margin.

It is necessary then to optimize the SVM algorithm, by maximizing the margin ($eq.$ 4.16) within the constrains ($eq.$ 4.15). This is possible by minimizing the squared norm $\|w\|^2$. The optimization problem has been addressed using Lagrangian formulation. Lagrange multipliers α_i are used for the constraints, then the Langrange functional Lp is minimized with respect to *w* and *b* and maximized with respect to α_i:

$$L_p = \frac{1}{2}\|w\|^2 - \sum_{i=1}^{L} \alpha_i \, y_i(w.x_i + b) + \sum_{i=1}^{L} \alpha_i \qquad (eq.4.17)$$

subject to the constrains

$$\alpha \geq 0, \qquad i = 1, \dots, L \qquad (eq.4.18)$$

Having:

$$\frac{\partial L_p(w,b,\alpha)}{\partial b} = 0, \qquad \frac{\partial L_p(w,b,\alpha)}{\partial w} = 0 \qquad (eq.4.19)$$

Provides:

$$\sum_{i=1}^{L} \alpha_i y_i = 0, \qquad \sum_{i=1}^{L} \alpha_i y_i x_i = w \qquad (eq.4.20)$$

Replacing them in the Lagrangian ($eq.$ 4.17) will give a dual formulation:

$$L_D = \sum_{i=1}^{L} \alpha_i - \frac{1}{2} \sum_{i=1}^{L} \alpha_i \sum_{j=1}^{L} \alpha_i \alpha_j y_i y_j x_i . x_j \qquad (eq.4.21)$$

$$\sum_{i=1}^{L} \alpha_i y_i = 0, \qquad \alpha_i \geq 0 \qquad (eq.4.22)$$

If the solution of the optimization problem depends only on the dot product of the data with non-zero weights/coefficients, the decision function becomes:

$$f(x) = \sum_{i=1}^{L} \alpha_i y_i x_i . x + b \qquad (eq.4.23)$$

Following the Kuhn-Tucker theorem explained by Schölkopf and Smola (2002) if $\alpha_i = 0$ then $y_i(w.x_i + b) \geq 1$ and for $\alpha_i > 0$ the equality holds: $y_i(w.x_i + b) = 1$. These two possibilities $\alpha_i = 0$ and $\alpha_i > 0$ give the name of the Support Vector method. Samples from the training data corresponding to $\alpha_i > 0$ will fall on the hyper-planes $f(x, \{w, b\}) = +1$ or $f(x, \{w, b\}) = -1$ of the decision surface. They are called the ***Support Vectors***. If the SVM is trained using all the training data set except the support vectors (SVs) or if the SVM is trained using only the SVs the same decision boundary would be obtained.

Soft Margin Classifiers

It is possible to apply the classification theory described above to non-separable data sets by adding slack variables $\xi_i \geq 0$ to the constraints (*eq.* 4.15). This application was proposed by Cortes and Vapnik (1995), who called these classifiers *soft margin classifiers*:

$$y_i(w.x_i + b) \geq 1 - \xi_i \qquad (eq.4.24)$$

Now the aim is to minimize the function:

$$\tau(w,\xi) = \frac{1}{2}\|w\|^2 + C\sum_{i=1}^{L}\xi_i \qquad (eq.\,4.25)$$

where the first term corresponds to minimizing the VC-dimension (complexity) and the second term corresponds to minimizing the number of misclassified points of the training set.

Soft margin classifiers are used to moderate the hard margin SVM in order to admit some misclassification of data (Figure 4.13).

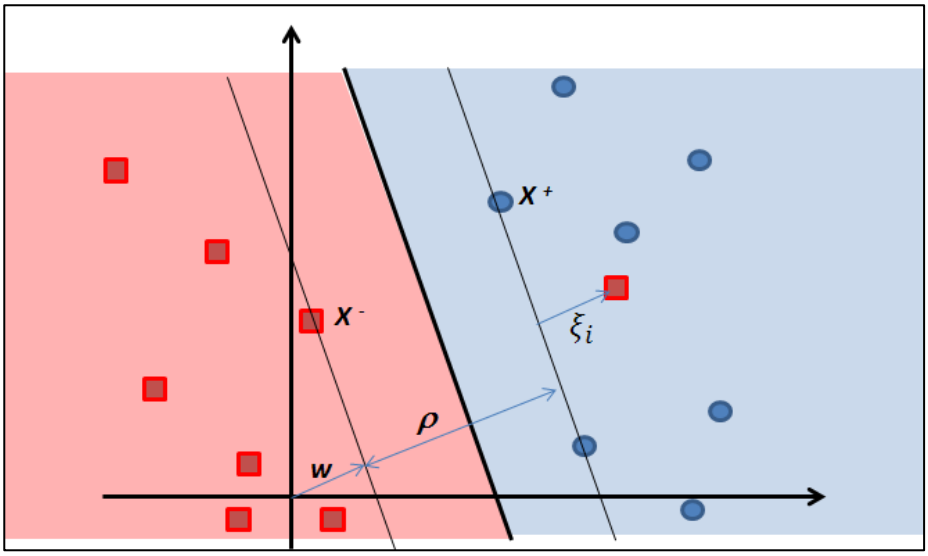

Figure 4.13: In soft margin classifiers the slack variables ξ allows noisy samples to lie inside the margin or on the other side of the decision hyper-plane (from Lampert 2009).

C-Regularization term

The positive regulirisation constant C weights the second criterion (misclassification) with respect to the first criterion (complexity) in *eq*. 4.25. The

trade-off constant C becomes an upper bound for the weights in the dual formulation, resulting in the constraints $C \geq \alpha_i \geq 0, i = 1, \ldots, L$.

"Kernel Trick"

Kernel Methods (Scholkopf *et al.,* 1999) are designed for mapping data into a high-dimensional feature space, transforming the data into a set of points in a Euclidean space. In that space, multiple methods can be used to find relationships among the data-points. Support vector machines can be considered as a natural field to apply kernels. Given a training set $\{(x_1, y_1), (x_2, x_2), \ldots (y_L, y_L)\}$ of L samples, kernel methods typically model SVMs with this hypothesis:

$$f(x) = \sum_{i=1}^{L} \alpha_i K(x_i, x) + b, \qquad (eq. 4.26)$$

where $K(x_i, x)$ is a kernel function and α_i and *b* are the parameters to be optimized.

Figure 4.14 shows how the so called ***kernel trick*** is used to solve a 2D classification problem that is not possible to solve by a linear decision function, but can be solved by transforming the data into a higher-dimensional space (3D), where the data can be classified with a linear hyper-plane.

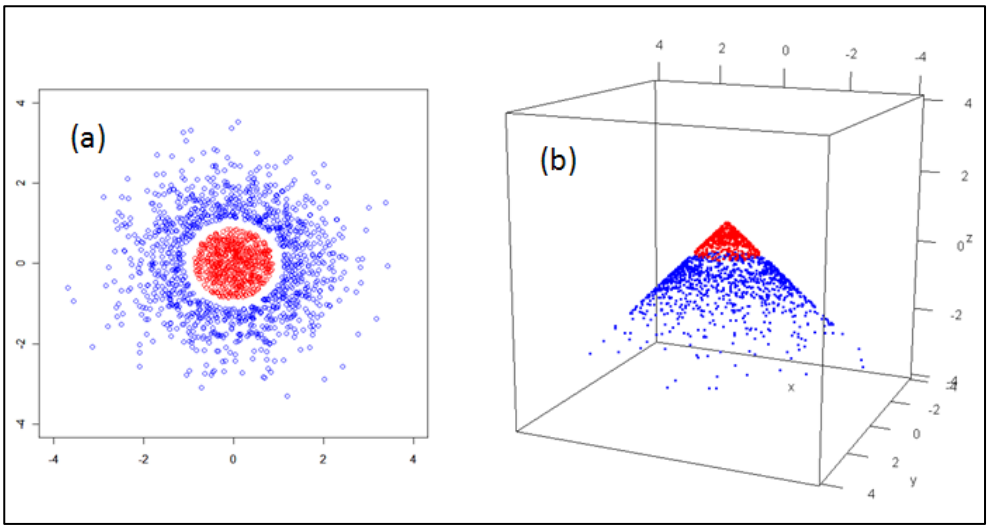

Figure 4.14. Use of the kernel trick to discriminate between two classes: (a) it is not possible to discriminate them in 2D with a linear function; (b) but mapping these classes in 3D solves the problem with a hyper-plane. This linear hyper-plane in the feature space corresponds to a non-linear decision in the input space. (Pictures obtained from the website www.stackoverflow.com)

The kernel trick is justified by considering a continuous symmetrical function $K(x, x')$: $X^2 \rightarrow \Re$ where an input space is denoted as X. if for any function $g \in L_2(C)$ where C is a compact subset of X, then the function $K(x_i, x')$ is:

$$\iint_{CxC} K(x_i, x')g(x)g(x')dxdx' \geq 0, \qquad (eq.4.27)$$

Then it can be expanded in converging series

$$K(x_i, x') = \sum_{k=1}^{\infty} a_k \psi_k(x)\psi_k(x'), \qquad (eq.4.28)$$

where $\psi_k(.)$ and $a_k \geq 0$ is the eigensystem of the corresponding integral operator with a kernel (x, x') .

The expansion of *eq.* 4.28 can be considered as a scalar product:

$$\sum_{k=1}^{\infty} a_k \psi_k(x)\psi_k(x') = \langle \sqrt{a_k}\psi_k(x), \sqrt{a_k}\psi_k(x')\rangle = \langle \Phi(x), \Phi(x')\rangle \qquad (eq.4.29)$$

That means that for every $K(x,x')$ exists a feature space, where it acts as a dot product. If it is necessary to use a feature space, the kernel function would be just a dot product in this feature space. Given a kernel function and some learning algorithm formulated in terms of the dot products between input samples, it is easy to obtain a nonlinear form of the algorithm by substituting the dot product for kernels:

$$x.x' \rightarrow K(x.x') \qquad (eq.4.30)$$

If the kernel trick is applied to the decision function (*eq.*4.23), the formulation of the ***support vector machine*** classifier will be written as:

$$L_D = \sum_{i=1}^{L} \alpha_i - \frac{1}{2}\sum_{i=1}^{L} \alpha_i \alpha_j y_i y_j K(x_i.x_j), \qquad (eq.4.31)$$

$$\sum_{i=1}^{L} \alpha_i y_i = 0, \qquad C \geq \alpha_i \geq 0 \qquad (eq.4.32)$$

And for the decision function:

$$f(x) = \sum_{i=1}^{L} y_i \alpha_i K(x_i, x) + b, \qquad (eq.4.33)$$

Kernel Parameters

It is important to choose from different kernel functions, because kernel functions define the feature space and the capacity of the model.

- Gaussian RBF Kernel: $K(x, x') = e^{-\frac{(x-x')^2}{2\sigma^2}}$, $\sigma \in R^+$,
- Polynomial kernel $K(x, x') = (x.x' + 1)^P, P \in N$

σ is called the bandwidth or width of the Gaussian RBF, and this parameter defines the width of the "bell". The order P of the polynomial kernel defines the smoothness of the functions.

Probabilistic outputs

SVM classifiers do not include any probabilistic interpretation of the outputs (Kanevski *et. al*, 2009). This interpretation can be obtained by modelling the class densities.

In some applications it is required to produce a continuous indicator of the class membership and to estimate the uncertainty of the prediction. This is possible to produce by using some post-processing of the decision function.

The samples beyond the margin are the most uncertain, the decision function inside the margin is such that $-1 < f(x) < 1$, equals +1 or -1 at the boundaries (and correspondingly the support vectors), and $|f(x)| > 1$ for normal samples that are correctly classified. Thus, the value of the decision function can be used as a class membership indicator.

To obtain a probability of class membership it is common to scale it to the interval of (0,1) using the sigmoid transform:

$$P\big(y = 1 \big| f(x)\big) = \frac{1}{1 + \exp(Af(x) + B)} \qquad (eq. 4.34)$$

Constants A and B need to be tuned from data using some appropriated criterion. Figure 4.15 illustrates the use of the sigmoid transformation of the SVM decision function, proposed by Platt (1999), where A and B are derived to maximize the likelihood (or to minimize the negative log-likelihood to simplify the optimization)

on the testing data set, because the use of training samples only may lead to overfitted biased estimate.

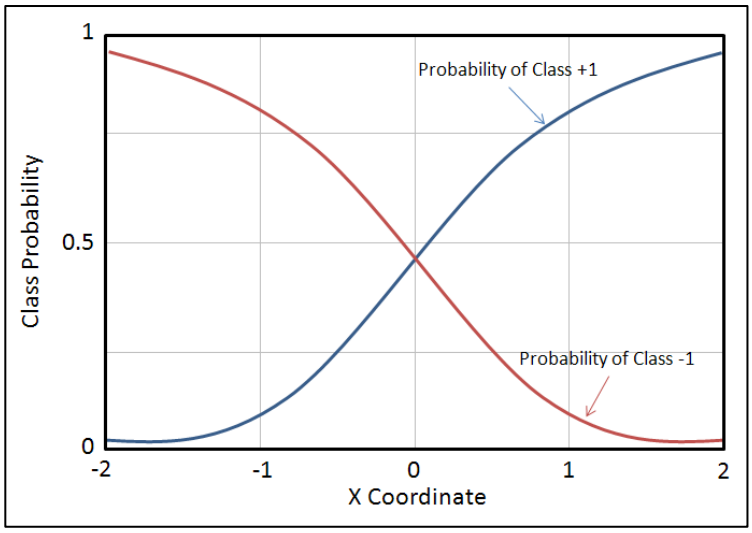

Figure 4.15. Representation of the use of the sigmoid function to estimate the SVM outputs probabilities, taking the sigmoid from the linear decision function (from Kanevski *et al.,* 2009).

4.6.3 One-Class Support Vector Machine (OC-SVM)

One-Class SVM is the SVM extension to one-class classification. This new method is very powerful in solving novelty and target detection tasks.

Schölkopf *et al*. (2001) defined OC-SVM as an unsupervised kernel-based method, which is used to estimate the support of probability density distributions. The main application of this technique is to detect novelty, outliers and rare events in a high-dimensional feature space. OC-SVM can be applied, as well, for target detection by rejecting all points with different statistical distribution from the target class.

This technique is based on the necessity of an algorithm that returns a density function, which takes the value +1 in a small region capturing most of the data points and -1 elsewhere. The strategy is to map the data into the feature space corresponding to the kernel, and to separate them from the origin with maximum

margin. For a new point x the value of $f(x)$ is determined by evaluating which side of the hyperplane it falls on, in the feature space.

The following quadratic problem is solved to separate the data from the origin:

$$\min_{w \in F, \xi \in \mathbb{R}^N, \rho \in \mathbb{R}} \quad \frac{1}{2}\|w\|^2 + \frac{1}{\nu N}\sum_i \xi_i - \rho \qquad (eq.4.35)$$

subject to $$\left(w.\Phi(x_i)\right) \geq \rho - \xi_{i,} \quad \xi_{i,} \geq 0 \qquad (eq.4.36)$$

where ν is a parameter controlling the factors of support vectors and outliers (complexity) and ρ is an offset.

When data are mapped in the kernel space by means of a kernel function, the data are linearly separated from the origin by maximizing the margin of the hyperplane. Outliers are constrained to be close to the origin, while the core of the distribution is pushed away with a maximum margin.

This problem can be solved in a dual way as a two-class SVM problem.

$$\min_{\alpha} \frac{1}{2}\sum_{ij} \alpha_i \alpha_j \, k(x_i x_j) \quad \text{subject to} \quad 0 \leq \alpha_i \leq \frac{1}{\nu N}, \sum_i \alpha_i = 1 \qquad (eq.4.37)$$

The decision function for a point x is computed as:

$$f(x) = \sum_i \alpha_i \, K(x, x_i) - \rho \qquad (eq.4.38)$$

The hyper-parameter ν controls the amount of data that is considered as outliers. That is, for $\nu \to 0$, all points are constrained to be part of the support composing the underlying probability density function. In this case, all data points including the outliers are separated from the origin in the kernel space. Furthermore, when $\nu \to 1$, only the very central part of the distribution is considered as part of it and all the other points (outliers) are kept close to the origin in kernel space. Figure

4.16 shows how tuning OC-SVM hyper-parameters affects the results of the decision function.

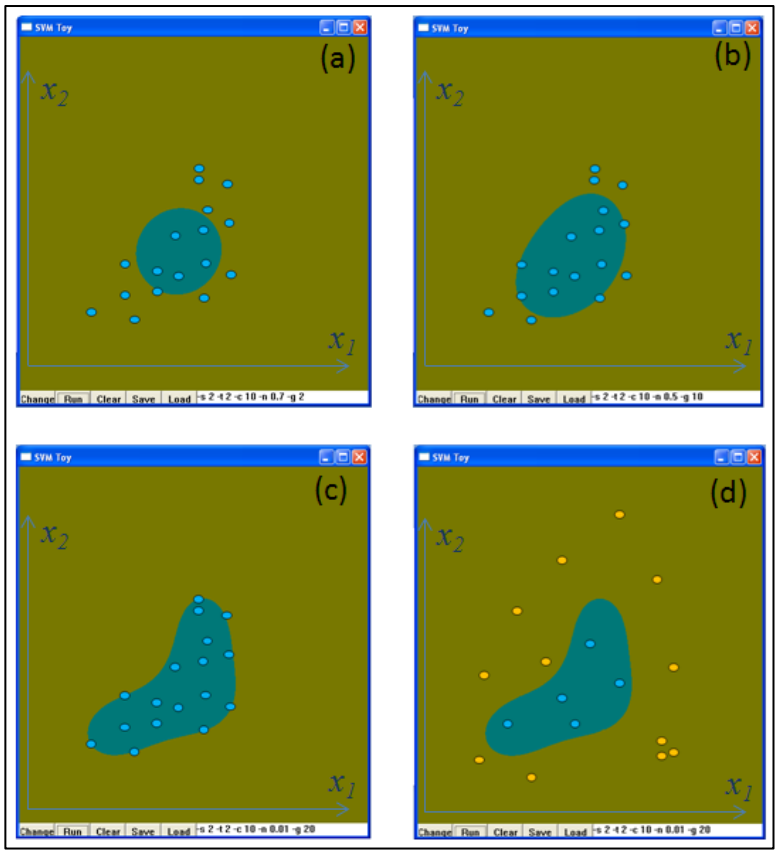

Figure 4.16: One-Class SVM "toy" example: (a), (b) and (c) illustrate the evolution of tuning of the One Class-SVM to identify the region in the parameter space that encloses the blue point (points from a single class) by modifying the hyperpameters – Kernel type, Cost, and *nu* factor. In (d) it is possible to observe how this One-class previously generated (blue) region can be used to separatethe points from a random set of points belong to the modelled (blue) class from points that do not (yellow points). Figures were obtained using libsvm from: http://www.csie.ntu.edu.tw/~cjlin/libsvm/.

4.6.4 Support Vector Regression (SVR)

Regression problems can be solved using a machine learning technique called Support Vector Regression (Smola and Schölkopf, 2004; Vapnik, 1998). Support vector regression (SVR) uses support vector machine algorithms, to solve regression problems by implementing a set of linear decision functions and using

the structural risk minimization (SRM) principle in order to minimize both the empirical risk and the confidence interval. Thus, the SRM principle defines a trade-off between accuracy (empirical risk or training error) and the complexity of the approximation by minimizing over both terms (Kanevski *et al.,* 2009).

Smola and Schölkopf (2004) stated that the basic idea of SVR is based on the computation of a linear regression function $f(x)$ in a high dimensional feature space where the input data are mapped via a non-linear transformation (kernel trick). The function $f(x)$ must be as flat as possible (finding a small w) and fit the data in the best possible way.
In the case of a linear function f takes the form:

$$f(x) = \langle w, x \rangle + b \quad with \quad w \in X, b \in R \qquad (eq.4.39)$$

where $\langle\ .\ ,\ .\ \rangle$ denotes the dot product.

Flatness in the case of $(eq.4.39)$ means that one seeks a small w that means to minimize $\|w\|^2$:

minimize: $\frac{1}{2}\|w\|^2$;

Subject to:

$$\begin{aligned} y_i - \langle w, x_i \rangle - b \leq \varepsilon \\ \langle w, x_i \rangle + b - y_i \leq \varepsilon \end{aligned} \qquad (eq.4.40)$$

Similar to this conclusion, Vapnik (1995) introduced an error using some slacking variables ξ to cope with otherwise infeasible constrains of the optimization problem (Somola and Schölkpof, 2004).

Minimize:

$$\frac{1}{2}\|w\|^2 + C\sum_{i=1}^{l}\langle \xi_1 + \xi_i^* \rangle ; subject\ to: \quad \begin{matrix} y_i - \langle w, x_i \rangle - b \leq \varepsilon + \xi_i \\ \langle w, x_i \rangle + b - y_i \leq \varepsilon + \xi_i^* \\ \xi_i, \xi_i^* \geq 0 \end{matrix} \qquad (eq.4.41)$$

The constant $C > 0$ determines the trade-off between the flatness of f and the amount up to which the deviations larger than ε are tolerated. This corresponds to dealing with a so called ε-insensitive loss function $|\xi|_\varepsilon$ described by:

$$|\xi|_\varepsilon = \begin{cases} 0 & if \quad |\xi| < \varepsilon \\ |\xi| - \varepsilon & otherwise \end{cases} \qquad (eq.4.42)$$

The support vector regression model is based on the ε-insensitive loss function. As we have seen, this function measures the discrepancy between the estimate and the actual value of y given an x. Figure 4.16 describes graphically this situation, where the points outside the shaded region contribute to the cost.

By introducing Lagrange multipliers we can obtain the following dual formulation of the problem:

Maximize:

$$\begin{matrix} -\frac{1}{2}\sum_{i,j=1}^{l}(\alpha_i - \alpha_i^*)(\alpha_j - \alpha_j^*)\langle x_i, x_j \rangle \\ -\varepsilon\sum_{i=1}^{l}(\alpha_i - \alpha_i^*) + \sum_{i=1}^{l} y_i(\alpha_i - \alpha_i^*) \end{matrix} \qquad (eq.4.43)$$

subject to

$$-\varepsilon\sum_{i=1}^{l}(\alpha_i - \alpha_i^*) = 0, \ \ and \ \ \alpha_i, \alpha_i^* \quad \in [0, C]$$

Collobert and Bengio (2001) and Smola and Schölkpof (2004) solved this quadratic programming problem by deriving (*eq*. 4.38), and then obtaining the prediction as a linear regression function:

$$f(x) = \sum_{i=1}^{l} (\alpha_i - \alpha_i^*) \langle x_i, x \rangle + b \qquad (eq. 4.44)$$

The nonlinear support vector regression is easily derived by applying the kernel trick to the linear algorithm. The kernel trick allows us to solve problems in a dimensional space higher than their actual space by substituting dots products for kernels (see Kanevski *et al.*, 2009). The kernel trick allows us to restate the SV optimization problem:

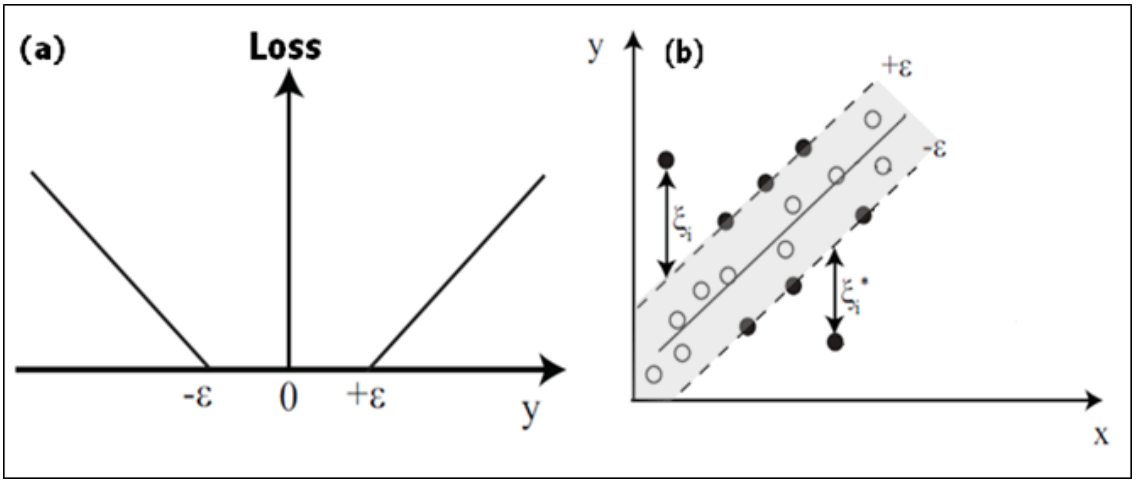

Figure 4.17: Representation of the soft margin loss settings for SVR (ε-tube) (modified from Foresti, 2011). (a) ε-insensitive cost function; (b) SVR in a linear problem. Support vectors are represented with filled dots; the noisy data inside the ε-tube (empty dots) are not involved to define the prediction function. If the problem is not linear SVR should act in the Kernel space in order to find a linear solution, and then go back to the actual problem space. The slack margin ξ allows for some amount of noise in the data, which deviate from the regression model.

Maximize:

$$-\frac{1}{2}\sum_{i,j=1}^{l}(\alpha_i-\alpha_i^*)\left(\alpha_j-\alpha_j^*\right)K\langle x_i,x_j\rangle \\ -\varepsilon\sum_{i=1}^{l}(\alpha_i,\alpha_i^*)+\sum_{i=1}^{l}y_i(\alpha_i-\alpha_i^*) \qquad (eq.4.45)$$

subject to

$$-\varepsilon\sum_{i=1}^{l}(\alpha_i,\alpha_i^*)=0,\ \ and\ \ \alpha_i-\alpha_i^*\ \in\ [0,C]$$

The prediction then becomes a kernel expansion:

$$f(x)=\sum_{i=1}^{l}(\alpha_i-\alpha_i^*)\,K\langle x_i,x\rangle+b \qquad (eq.4.46)$$

Where K is subject to the choice of the kernel function used as in eq. 4.33.

4.7 Summary

This Chapter reviews the importance of geological prior information in modelling geoscientific problems and which methodologies have been used to model geological prior information. The main problems of modelling geological information and use it as prior are: 1) statistical relationships between the geological variables are non-linear and unknown; 2) process-based models of the relationship between geological parameters have proved to be very accurate, but computational expensive and with a very narrow field of applicability or low generalization.

Based on the characteristics of the geological data (high-dimensional, finite number of samples, non-linearly related, etc) machine learning techniques are recommended to find and to model the relationships between geological parameters. These geological relationships can be used as geological prior information, when introducing probabilities and uncertainty analysis to a geological problem. Various applications of MLT to modelling geological prior information are described in the next chapters.

At the end of this chapter the Machine Learning Techniques used in this thesis are described (Multilayer Perceptron, Support Vector Machines for classification and regression and the One-Class SVM novelty detector) in order to understand how they work and how they can be applied in the problems presented in this thesis.

Chapter 5

Facies and Depositional Environments of the Reservoirs Modelled in this Thesis

5.1 Introduction

In this chapter I describe the sedimentological features of the reservoirs used in this thesis. The parameterization of sedimentological features has a big impact on reservoir history-matching (Arnold, 2009). Understanding the origin and characteristics of the sedimentological parameters makes clearer the parameterization process.

Synthetic reservoirs are datasets that include all the properties that an actual reservoir possesses. These synthetic reservoirs are used to test new techniques or algorithms for reservoir modelling, characterization or history matching (Castro *et al.,* 2005). All the techniques developed in this thesis were applied to synthetic reservoirs. These techniques automatically and realistically vary sedimentological properties of a reservoir in order to find history matched models. That is the main reason for describing the sedimentology of the reservoirs used here.

Three synthetic reservoirs representing different depositional environments were used in this thesis: (1) The intermediate stratigraphic unit of the Stanford VI Reservoir (Castro *et al.,* 2005) which was deposited in a fluvial meandering system; (2) a synthetic reservoir formed by deep marine channel deposits (DM_Field); this synthetic reservoir was built using the description of the Balliste-Crécerelle Canyon Fill (Wonham *et al.,* 2000) and (3) a reservoir deposited in a fluvial-dominated deltaic system (Mitare_Field), based on the description of a modern fluvial-dominated delta (Rivas *et al*., 1997).

The next sections of this chapter describe the sedimentological features of the reservoirs used in this thesis in order to understand the characteristics of sedimentological parameters when varying them during the history match process.

5.2 Fluvial Meandering Channel Deposits

As mentioned in Chapter 2, one of the most important tasks in reservoir exploration and development is determining the geometry of the sandbodies. Fluvial sandstone bodies, when preserved in the geological record, are excellent reservoirs for oil and gas (Bridge and Tye, 2000). To estimate reserves and production performance in this type of reservoir, it is necessary to characterize these deposits (*i.e*. geometry, orientation, spatial and internal physical property distributions). These data are used in the process of reservoir modelling, in order to maintain the geological realism of the models.

The main problem in determining the geometry of these deposits is the uncertainty associated with the available sparse data (Chapter 3). One of the first stages in the study of a reservoir is the identification of the sedimentary environment. This process can be done by describing well-cores, high resolution seismic data, using analogue outcrops or published information. The main indicators of the sedimentary environment in fluvial settings are the absence of marine fossils, the presence of palaeobotanic fossils like roots in growing position, coal seams, palaeosols or ichnofacies associated with continental environments in addition to

erosion-based, generally upwards-fining sandbodies dominated by current-generated structures (Figure 5.1). After the identification of the reservoir sedimentary environment it is necessary to interpret the dimension of the associated geobodies, their spatial locations and the distribution of the reservoir petrophysical properties. This thesis is focussed on the variation of the geobody geometry as a factor that influences reservoir production profiles.

5.2.1 Description of meandering channels preserved in the geological record

Figure 5.1 illustrates how meandering channels are developed and describes the type of sediments that are deposited in the inner part of the channel loops (point-bars). Point-bars are developed when the fluvial channel migrates laterally, eroding the outer part of the channel and depositing mainly sand and gravel in the inner part of the channel.

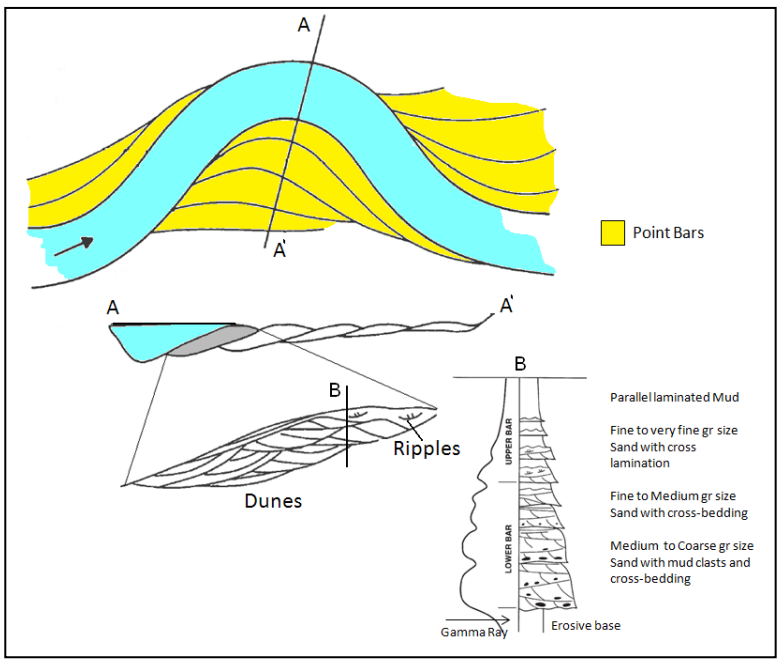

Figure 5.1. Point bar geometry and sediments. A-A' is a cross section of a river meander, showing the geometry of a point bar, B is the typical sequence of sediments deposited in a point bar and a gamma ray response of these deposits (from Bridge and Tye, 2000).

Point-bar deposits are characterized by an erosive base with poorly sorted conglomeratic deposits over it. These conglomeratic deposits are commonly composed of clay intraclasts. The deposits that overlie the erosive base are part of a fining upward facies sequence cycle. This sequence of deposits can be preserved in the geological record and is used as a key feature in recognising meandering channel sedimentological environment (Allen, 1965; Leeder, 1973).

Many authors have explained how to interpret meandering channel in outcrops. This interpretation is extrapolated to well-cores and well-logs (Leeder, 1973; Bridge and Tye, 2000; Miall, 2006). The major challenge in this process is to interpret the geometry of these deposits. Leeder (1973) proposed a methodology based on data from modern rivers, using equations that related the interpreted thickness of a meandering channel deposit from cores or well-logs to the width of the channels. In the second step Leeder (1973) used the equations proposed by Leopold, Wolman and Miller (1964) that related channel width with channel wavelength and amplitude, to estimate the channel belt width. Later Lorenz *et al.* (1985) estimated the meander belt width of channels using a similar technique to the one proposed by Leeder (1973) but included a degree of uncertainty in the dimensions of the sandbody by estimating the average of the dimensions of the channels and the standard deviation of the measurements. Their results, compared to outcrop data, established a good agreement with the outcrop measurements. Fielding and Crane (1987) identified empirical relationships between channel width and depth for different type of rivers and related them to the sandstone body width and thickness. Bridge (1975), Crane (1983) and Bridge and Tye (2000) suggested various empirical equations to estimate the channel belt width based on the meander amplitude and wavelength or curvature radius.

A different way of estimating channel geometry in subsurface deposits was published by Doyle and Sweet (1995), who measured the dimension of sand bodies from outcrops, close to the producing field and used this information to delineate the sand body geometry using well information (channel thickness).

Gibling (2006) collected a large dataset of fluvial sandbody dimensions considering width and thickness and classifying the sandbodies based on geomorphic settings, geometry and internal structure. The work presented by Gibling (2006) provided plots of width vs thickness of fluvial sandbodies and encapsulated the data points into envelopes that can be used as *validity domains* (see Apendix E.2.2) of width and thickness combinations of different fluvial systems.

A more realistic approach to estimate the geometry of fluvial sandbodies (when they are sufficiently thick) is the use of seismic geomorphology (Ethridge and Schumm, 2007; Posamentier, 2005), where it is possible to extract the geometry of fluvial deposits from high-resolution seismic data (high-resolution seismic data of a vertical resolution of about 10 to 20 meters). The disadvantages of this technique would be that a high-resolution seismic data is necessary, and the seismic volume should cover all the area of interest. Also, seismic data is in time domain, which implies that sandbody thickness estimation would be then conditioned to the time-depth conversion methodology and many fluvial systems consist of sandbodies below the seismic resolution.

From the works mentioned in Appendix E, it is clear that the geometry of meandering deposits depends on the geometry of the fluvial (meandering) channels that generated such deposits and their behaviour through time. Single channel belt dimensions are related to channel thickness and width and the meander amplitude and wavelength (Figure E.7).

In this section, single channel belts are considered as the sedimentary units that built the channel sandbodies. Based on Miall´s (1991) classification, a single channel belt can be considered as 5^{th} order sedimentary process, which develops a thickness between 10 and 100 m.

Fluvial Sequence Stratigraphy

Over the past 20 years, sequence stratigraphy has become the preferred methodology for stratigraphic analysis of sedimentary rocks. The origin of sequence stratigraphy was attached to seismic stratigraphy analysis. The seismic reflection patterns, their cyclicity through the geological record in combination with well and outcrop data made it possible to generate a stratigraphic framework that explains the genesis and evolution of depositional patterns. Sequence stratigraphy is based on the detection of bounding correlative surfaces that enclose a particular sequence of deposits (Sequence Boundaries, Flooding Surfaces, depositional hiatus or erosive surfaces).

Figure 5.2 describes the general framework of sequence stratigraphy following the EXXON sequence depositional model (Baum and Vail, 1988), showing surfaces that separate different depositional systems or system tracts, and their relation with sea-level changes.

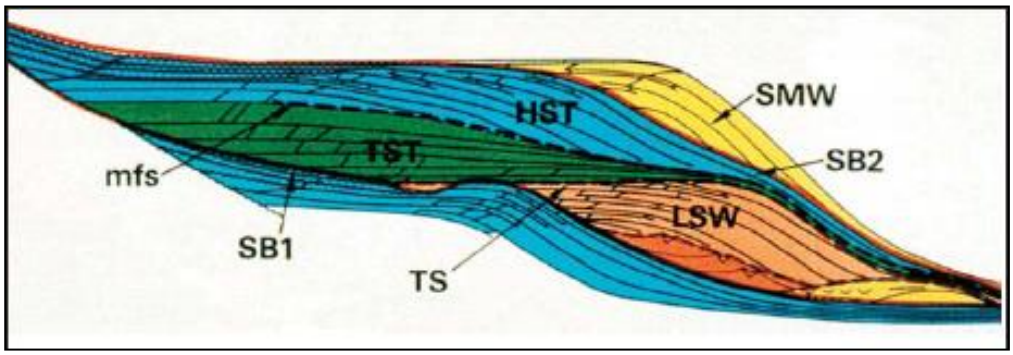

Figure 5.2: EXXON Depositional Sequences or Systems Tracts: Low Stand System Tract (LST); Transgressive System Tract (TST); Highstand System Tract (HST) and Shelf Margin Wedge (SMW). These sequences are limited by major bounding surfaces, Sequence Boundaries (SB), Maximum flooding surfaces (mfs) and Transgresive Surfaces (TS) (Baum and Vail, 1988).

The Lowstand System Tract (LST) is generated, when the sea-level has dropped and part of the platform is eroded. The deposits of this system lie over a major erosive surface (Sequence Boundary).

Once the sea level begins to rise, the sediments find that the accommodation space increases and the deposition occurs over zones that were previously eroded. Such depositional system is called the Transgressive System Tract (TST). This system ends when the sea level has reached its maximum and a muddy marine surface covers all the previous deposits. This mud-prone surface has been called a Maximum Flooding Surface (Catuneanu, 2006)

When the sea level has reached its maximum and remains relatively constant, a large accommodation space for the sediments has been created, where progradational sequences start filling up this space. This major depositional system has been named the Highstand System Tract (HST).

In the specific case of fluvial deposits, where deposition may be a long way from the sea, the sequence stratigraphic framework has been given a special treatment by various authors (*e.g*. Shanley and McCabe, 1994, and Ramon and Cross, 1997). The key factors controlling the deposition of fluvial sequences are: (1) change of the base level (water-table), which would be the equivalent to the sea-level changes in marine environments; (2) tectonics and (3) sediment supply (Shanley and McCabe, 1994, Miall, 1992 and Ramon and Cross, 1997).

Figure 5.3 illustrates how fluvial deposits change when changes in the base-level occur. If the base level (sea-level) drops, erosion occurs in the fluvial basin, generating a so-called Incised Valley (Zaitlin *et al.,* 1994). Figure 5.3 helps to understand the influence of sea/base-level changes on vertical facies proportions in reservoirs developed in fluvial settings.

Ramon and Cross (1997) stated that, when the base level begins to rise, the accommodation space (A) increases; and if the sediment supply (S) is constant, then A/S >1, allowing the deposition of single-story channels. Then the base-level drops again, reducing A and increasing the proportion of sandy and gravelly deposits (multi-story and multi-lateral channels). The base-level could drop until generating a sequence boundary, repeating the sedimentary sequence.

Changes in the base-level thus produce changes in the facies proportions of fluvial systems. These changes in base-level could be associated mainly with tectonic and secondly with eustasy (Miall, 1992). In the case of new fields with very few wells or poor understanding of the geological history of an ancient fluvial basin, modelling base level changes would assess the uncertainty of the vertical variation of facies distribution.

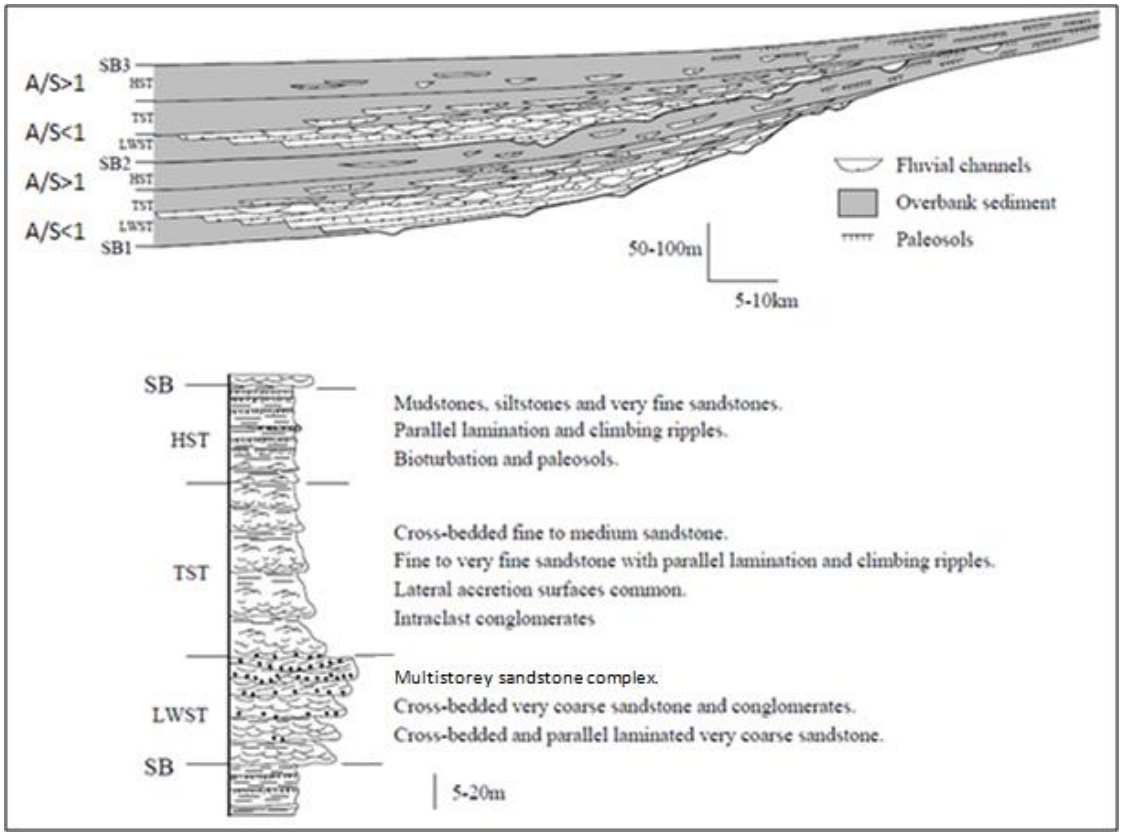

Figure 5.3: Schematic cross-section and columnar section of Alluvial Depositional Sequences from the Mesozoic of Argentina. (From Shanley and McCabe, 1994).

5.2.2 Meandering Fluvial Facies Description

The term Facies was first introduced by Nicholas Steno in 1669 to describe the aspect of a part of the Earth's surface during a period of the geological time. Later Gressley, in 1883, defined facies as the sum of the paleontological and lithological characteristic of a stratigraphic unit (Teichert, 1958). The term facies can be used

in both a descriptive and an interpretive sense. Facies can be used to describe rocks or sediments aspects detectable in the field: lithology, structures and organic content (*e.g*. Facies "A" is a sedimentary unit composed of medium grained sand, with parallel lamination and bioturbated with *Ophiomorpha nodosa*). Also the term facies is used to give an idea of the interpretation of a group of rocks. For example, "fluvial facies" or more "fluvial facies association" encompasses a set of features including (in the fluvial example) sharp-based fining-upward successions with lags at their bases; thin siltstones with root traces, abundant trough and planar tabular cross bedding, and the absence of marine indicators. It is normally obvious from the context whether the term facies is being used in a descriptive or an interpretive sense.

In this thesis the term facies associations is going to be related to a series of deposits genetically related and limited by bounding surfaces of third-fifth order. These bounding surfaces represent the beginning and ending of a depositional process (Miall, 1992).

As mentioned before, the deposits of meandering channels preserved in the geological record have been described by many authors, and have been classified into a number of facies associations. As explained in Section 5.2.1, meandering channel deposits are originated by the dynamics of the channels. Although these deposits are genetically related, different processes dominate in the sedimentation of each of the facies associations. Some of the facies associations (architectural elements) described by Miall (1996) that could be found within meandering fluvial systems are channel deposits, point bars, floodplain, crevasse splays and natural levees. The origin and description of these facies is explained in Table 5.1.

In this thesis the facies associations used to model fluvial meandering depositional environment will be related to channel, point bar and floodplain deposits.

Facies	Processes	Lithology	Sedimentary Structures	Fossils
Channel Deposits (CH)	Finning-upward successions due to progressive abandonment or flash floods.	Sand-fine Sand Silt and Clay.	Ripples, parallel lamination.	Plant debris, reworked fossils.
Floodplain (FF)	Overbank deposits, sheet flow, swamps and ponds.	Clay, silt, fine sand.	Parallel lamination, ripples, massive muds	Coal, plant debris, roots, continental ichnofacies, insects.
Point Bars (LA)	Lateral accreation of sediments due to the helical pattern of the flow .	Gravel, coarse – medium grain size sand.	Cross stratification, ripples, planar lamination.	Reworked fossils, timbers.
Crevasse splay (CS)	Break in main channel margin.	Sand , Silt and Mud.	Plannar cross-beds, lamination, very small ripples.	Plant debris, reworked fossils.
Natural Levee (LV)	Overbank Flooding.	Sand , Silt and Mud.	Planar cross-beds, lamination, very small ripples.	Plant debris, reworked fossils.

Table 5.1: Description of the architectural elements that can be found in fluvial meandering deposits. Compiled from Miall (1996).

Figure 5.4 illustrates the architectural elements (Miall, 1985) that can be identified within meandering channel depositional systems modelled in this thesis.

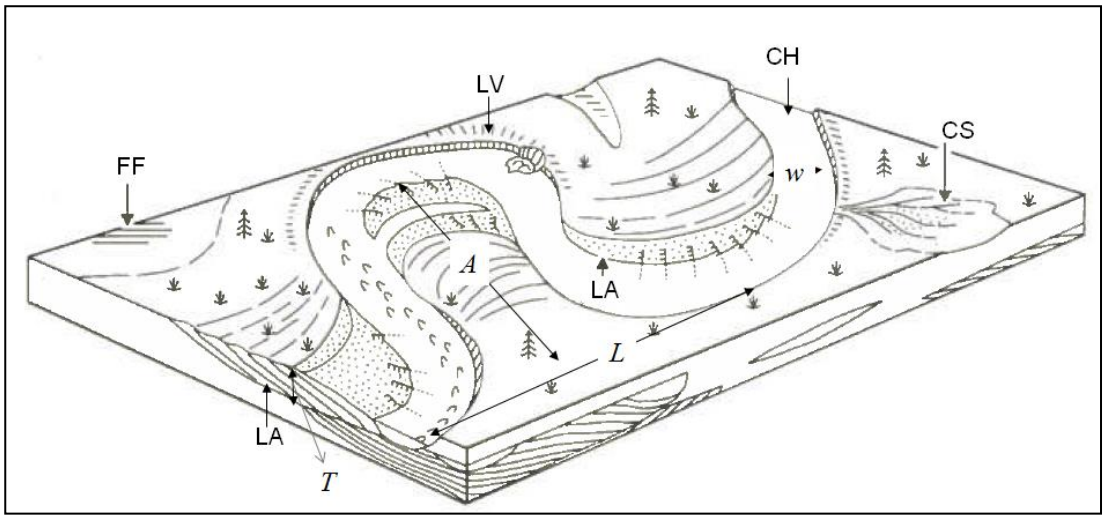

Figure 5.4: Description of the architectural elements and geomorphic parameters that could be found in fluvial meandering deposits (Miall, 1985). CH: Channel, LA: Point Bar, FF: Floodplain, CS: Crevasse splay, LV: Levee. In this thesis the Facies used to model fluvial meandering deposits are Channels, Point Bars and Floodplain. Geomorphic Parameterized are: Meander Length (L); Meander Amplitude (A); Channel Width (w) and Thickness (T).

5.3 Deep Marine Channel Deposits

Figure 5.5 shows a photograph of meandering fluvial channels in Argentina and an amplitude extraction map of a seismic horizon of deep-marine sediments in the Gulf of Mexico, where it is possible to observe geomorphic similarities between these two very different depositional environments.

Although fluvial meandering channels look very similar to deep-marine channels, their origins are very different. The origin of fluvial meandering channel deposits has been described in Section 5.2. Deep Marine channels have been developed by different physical processes than fluvial channels, as will be described in this section.

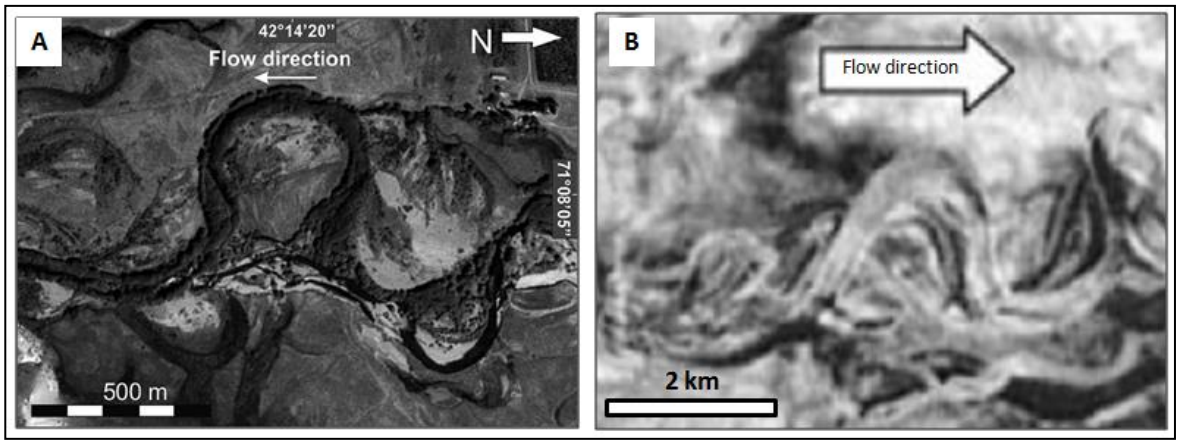

Figure 5.5: Visual comparison between fluvial meandering and deep-marine channels. A: Meandering channel,Chubut river, Argentina (from Foix et al., 2012); B: Deep-marine channel, De Soto Canyon, Gulf of Mexico (from Posamentier and Kolla, 2003).

Figure 5.6 illustrates the deep marine settings, ranging from the slope to the basin plain as described. The sinuous channels considered in this section are developed between the canyon and the basin plain.

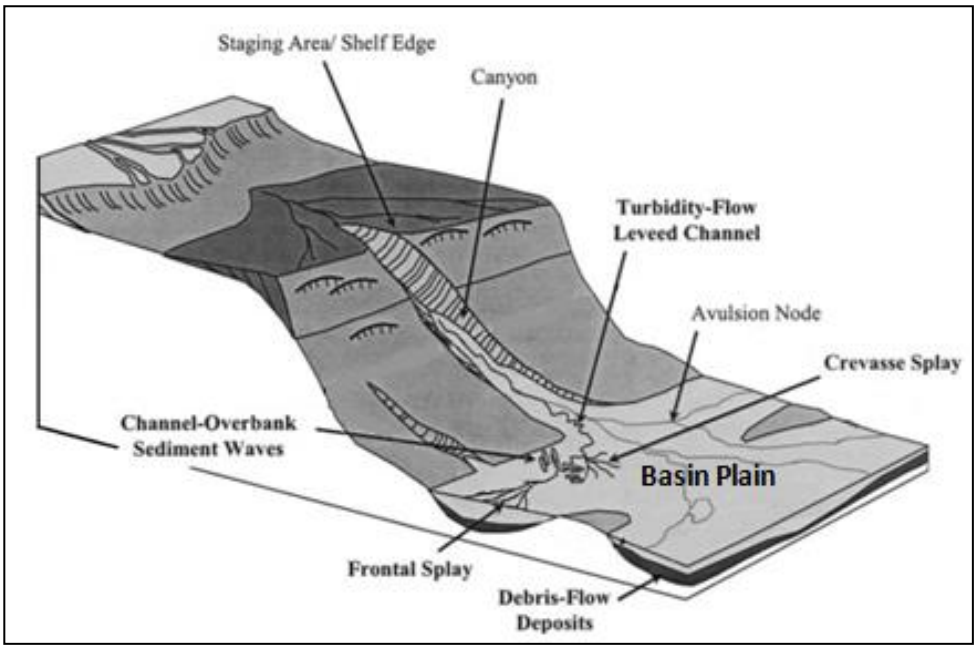

Figure 5.6: Deep-Marine settings (Posamentier, 2003).

Deep marine channels can be developed from the canyon to the submarine fan. They are part of a re-sedimentation process originated by the movement of pre-existing deposits in continental to shallow marine environments into deep water specifically by turbidity currents (Stow *et al.,* 1996).

Turbidity currents are suspensions of sediment that are sustained by fluid turbulence. They are the most important transport mechanism of coarse grained sediment into deep water. Within an active turbidity current, the upwards components of turbulent fluid motion provide the main grain support mechanism and this behaviour can be sustained over long distances through a feedback loop called *autosuspension* (Southard and Mackintosh, 1981). In this dynamic equilibrium: (i) turbulence is generated by the flow; (2) flow results in the excess density of the suspension; (iii) excess density results from the suspended load; and (iv) the suspended load is maintained by turbulence (Pantin, 1979).

Figure 5.7 is a representation of a turbidity flow and a deposition that illustrates the processes associated with transportation and deposition in turbidity currents.

Deposition in these systems occurs from deceleration of the flow and occurs most commonly from the body and tail.

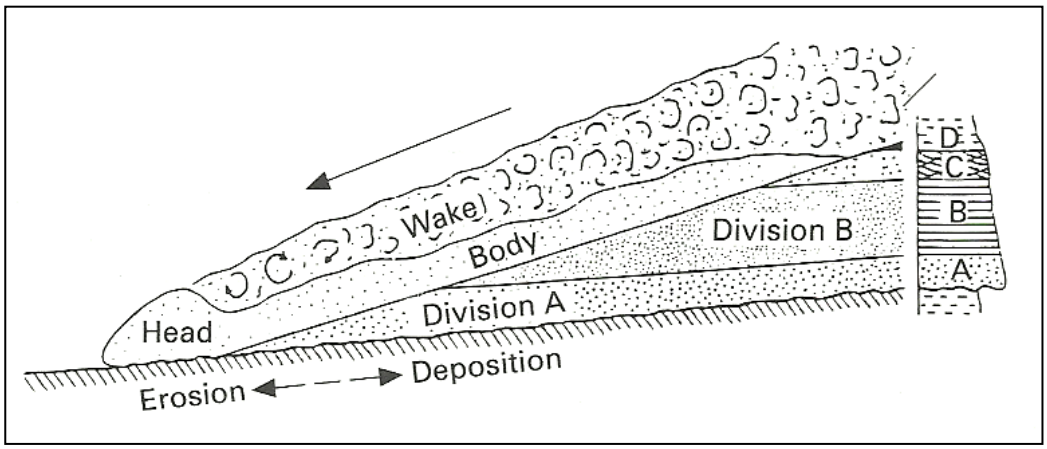

Figure 5.7: Turbidity current profile, showing its zones and sites of deposition of the Bouma intervals. Interval A, lacks depositional lamination and may show grading, A results from of the upper part of the upper flow regime. B, parallel lamination, results from plane bed transport in the upper flow regime Sequence B to D reflects desacceleration. Interval C, with rippled cross-lamination reflects a fall out of sand or silt from suspension while lower flow regime ripples were moving on the bed. (From Allen,1991).

Deep marine channels' spatial scale ranges from meters to kilometres. Most channels are filled by the coarsest sediments in the system: lag deposits, thick bedded sandstones and pebbly sandstones, thin bedded turbidities particularly at the channel edges and chaotic deposits (Southard and Mackintosh, 1981).

Deep marine channel deposits have a high potential to be preserved in the geological record due to the physical conditions of the depositional processes: (i) deposition occurs deep below sea- level, small changes in sea-level will not affect these deposits; (ii) deposition of mud covering channel deposits can be considered as constant, protecting channel deposits from erosion; (iii) younger channels deposit sediments over older channels instead of eroding them, like in the fluvial realm (Posamentier, 2003).

5.4 Deltaic Deposits

Deltas are shoreline protuberances formed where a river meets a large body of water (Bhattacharya and Walker, 1992). Deltas are formed by the velocity reduction of the fluvial stream produced when the flow abandons the channel and is expanded in a body of water (Dabrio-Gonzalez, 1984). This process allows the sediments to settle and build up until reaching the surface.

The concept of a delta was originated by Herodotus (ca. 400 B.C.) who recognized that the alluvial plain at the mouth of the Nile River had the form of the Greek letter Delta (Δ) (Figure 5.8, Whateley and Pickering, 1989 and Bhattacharya and Walker, 1992).

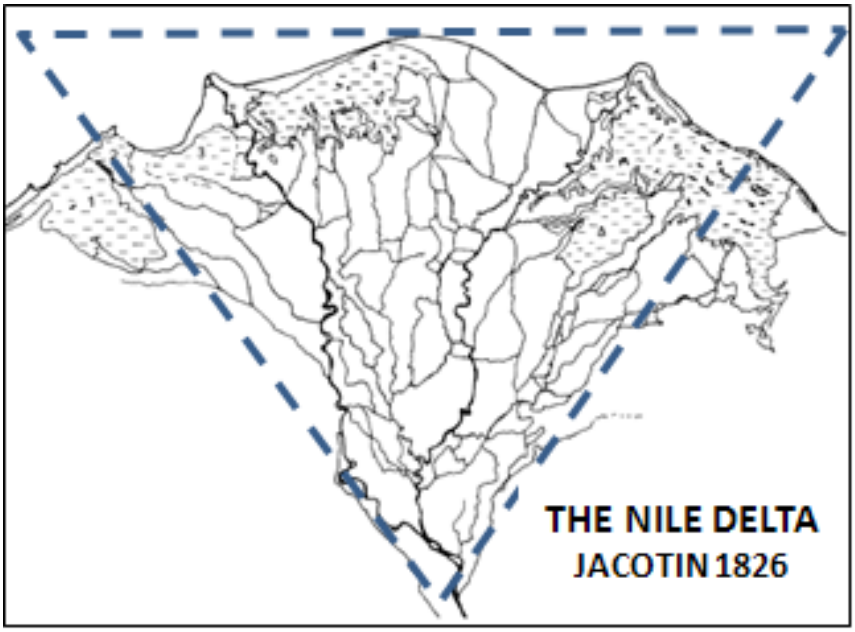

Figure 5.8: Nile Delta map from Jacotin in 1826 (Sestine, 1989).

Deltas are generated by the interaction of multiple sedimentological processes: river currents, waves and tides. The different agents that work on deltaic sedimentation control the delta's shape.

In this section, a brief description of deltaic facies models is presented in order to set up the environment to describe a case study of a deltaic synthetic reservoir (Section 6.4) built to history match its production using realistic geological prior information.

5.4.1 Deltaic Facies Description

The term delta includes the delta plain, delta front and prodelta deposits as shown on Figure 5.9, most deltaic deposits come from a particular river (Figure 5.10). A delta may be composed of different lobes which stack irregularly or shingle side by side as the distributary channels change their positions from time to time.

Deltas basically consist of a sandy framework fleshed out with finer grained deposits. Depending on the dominant process in deltaic sedimentation, the shape of the sandy deposits could vary. Deltas dominated by fluvial processes develop more elongated sand bodies associated with elongated distributary channels and associated mouth-bars perpendicular to the coastline, with fine material deposited between distributary channels. With an increasing effect of waves, the sand fraction of the delta tends to be reworked alongshore and the fine fraction is swept out to sea. The sandbodies generated by these deltas are therefore aligned parallel to the coast line (Coleman and Wright, 1975).

As described by Coleman and Wright (1975) and shown in Figure 5.9, a deltaic sequence comprises an upwards-coarsening vertical facies succession from the prodelta to the delta front and thence to the delta plain. These facies have variations depending on the type of the delta.

Delta classification

As mentioned above, deltas can be classified based on the dominant process that acts on the coast. Commonly, a tripartite classification of deltas has been used to distinguish between them: Fluvial, Tidal or Wave dominated (Coleman and Wright, 1975). As observed in Figure 5.10 the geometry of a deltaic system depends on

the dominant physical process and the sandbodies generated by each deltaic system will depend on the geometry of the deltaic system.

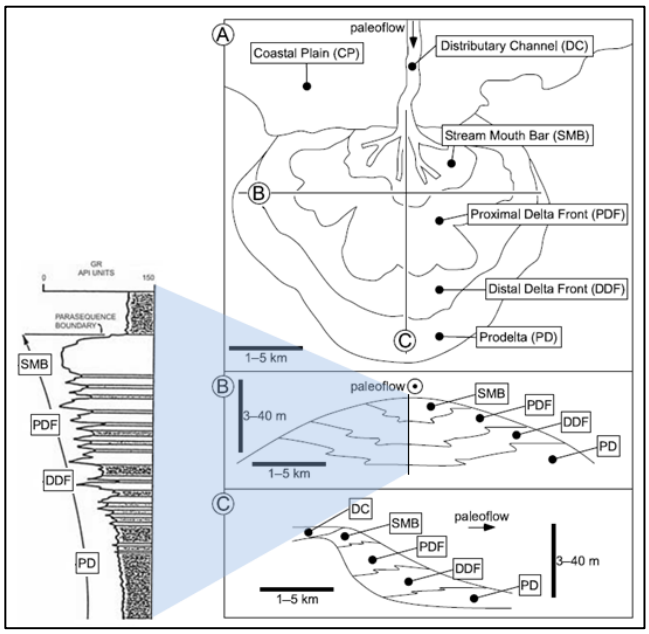

Figure 5.9: Conceptual model of a delta lobe. A: Plain view; B: Axis perpendicular cross section; C along-axis cross-section. Note the theoretical gamma ray log describing the coarsening upwards sequence of a deltaic system (Deveugle *et al.,* 2011).

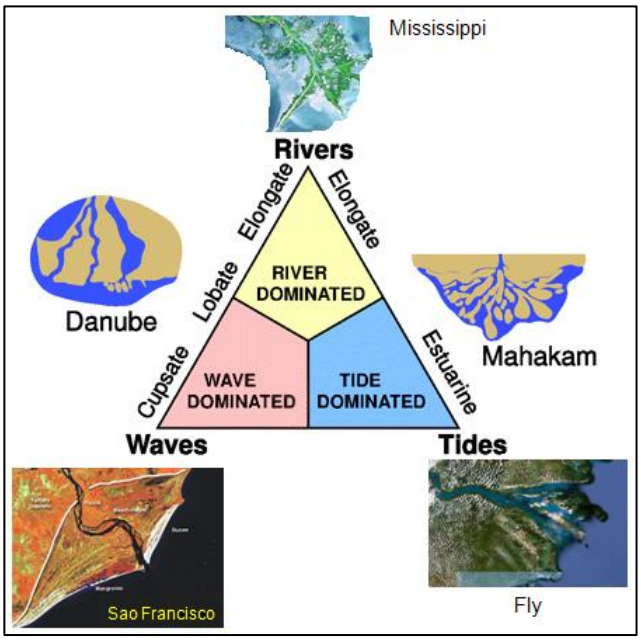

Figure 5.10: Triangular classification of deltaic systems based on the key depositional processes. (From Galloway, 1975).

Fluvial dominated (highly constructive) deltas

In fluvial dominated deltas, prodelta deposits are massive to well stratified muds and silts. Delta front facies are mainly composed of sand, which is deposited in the mouth bar sub-environment (Figures 5.9 and 5.10). These sands are characterised by unidirectional current ripples and cross-bedding or massive graded beds (depending on the relation between frictional and inertial processes (Martinensen, 1990).

Figure 5.11 is a representation of the subenvironments associated with fluvial dominated deltas. The deltaic plain is composed by distributary channels and interdistributary areas. The base of the distributary channel is erosive and their sequence is fining upwards or blocky (Miall, 1976). The filling of these channels is commonly sand and is reworked by tidal or transgressive processes once the channel is abandoned and the distributary channel moves to a new location. Areas between distributary channels (interdistributary bay) are filled with overbank deposits of fine grain material from the river during flood stages (Miall, 1976).

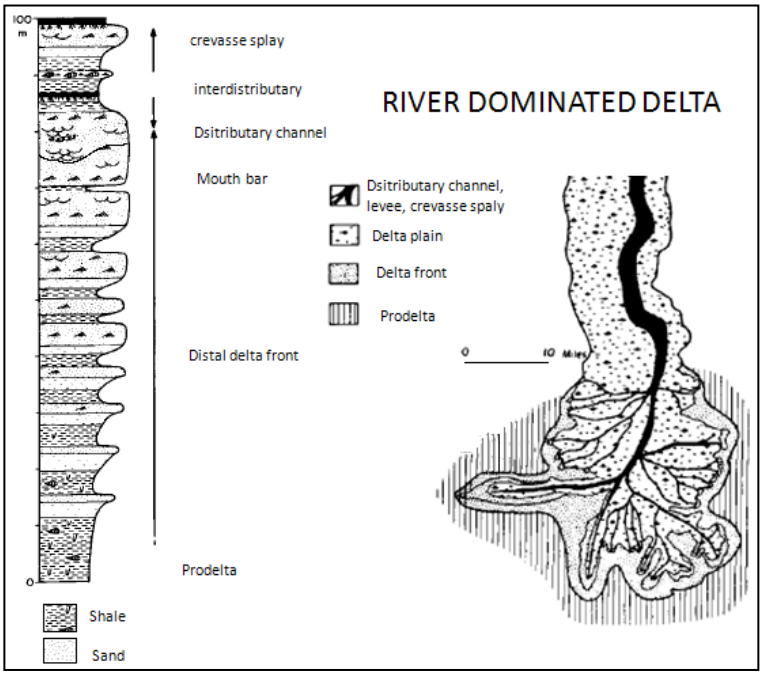

Figure 5.11: Fluvial dominated delta morphology and stratigraphic column for a Mississippi type delta (after Miall, 1976).

Tidally influenced deltas

Figure 5.12 illustrates how the deltaic subenvironments are distributed in deltas dominated by tides, as well as the sediment composition in each of these subenvironments. Allen (1997) stated that tide-influenced delta fronts have a dominant coarsening upward trend, with facies reflecting tidal influence (rythmites, herringbone cross-bedding, reactivation surfaces and tidal bundles). Rythmites and cyclicity can be developed in the prodelta fine sediments (muds, silts and very fine grained sands). Interdistributary areas in tide-influenced deltas can develop facies like tidal flats and tidal channels (Allen *et al.,* 1979).

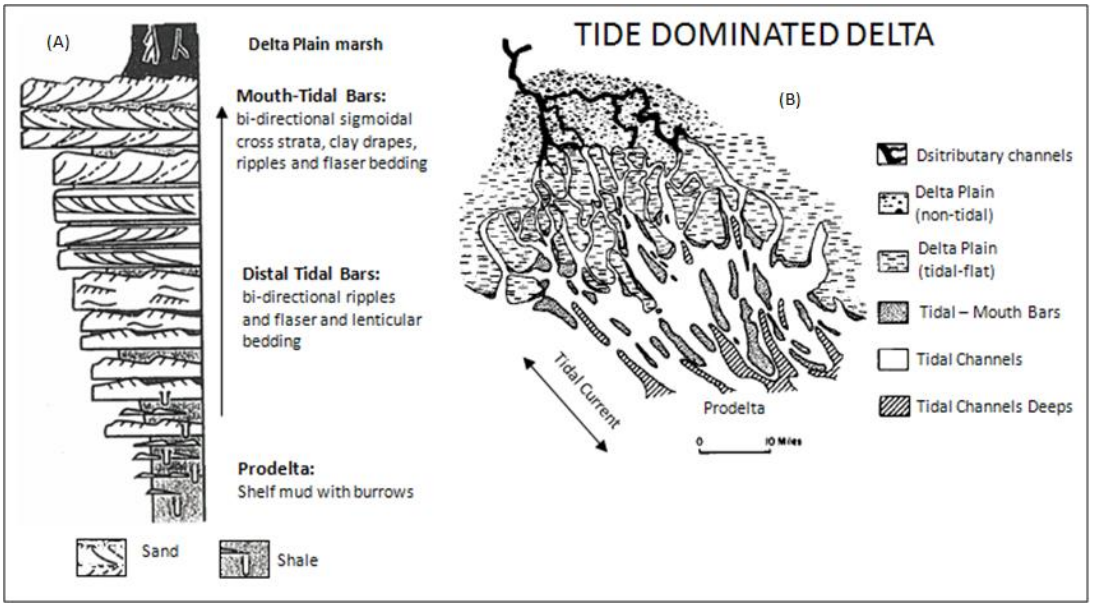

Figure 5.12: Tide dominated deltas, Gulf of Papua Type, morphology and stratigraphic column (after (A) Allen, 1997 and (B) Miall, 1976).

Wave Influenced Deltas

Wave dominated deltas are described in Figure 5.13. This type of deltas commonly consists of a series of prograding beach and beach-ridge complexes. The delta front is characterized by a continuous coarsening upwards facies succession characteristic of a wave dominated shoreface. The prodelta muds in

wave-dominated deltas are thinner and sandier than the prodelta muds in fluvial dominated deltas (Miall, 1976).

Interdistributary areas may be completely closed off by barrier/beach complexes in wave-dominated deltas, resulting in back barrier lagoons. Deposits in these areas tend to be organic-rich.

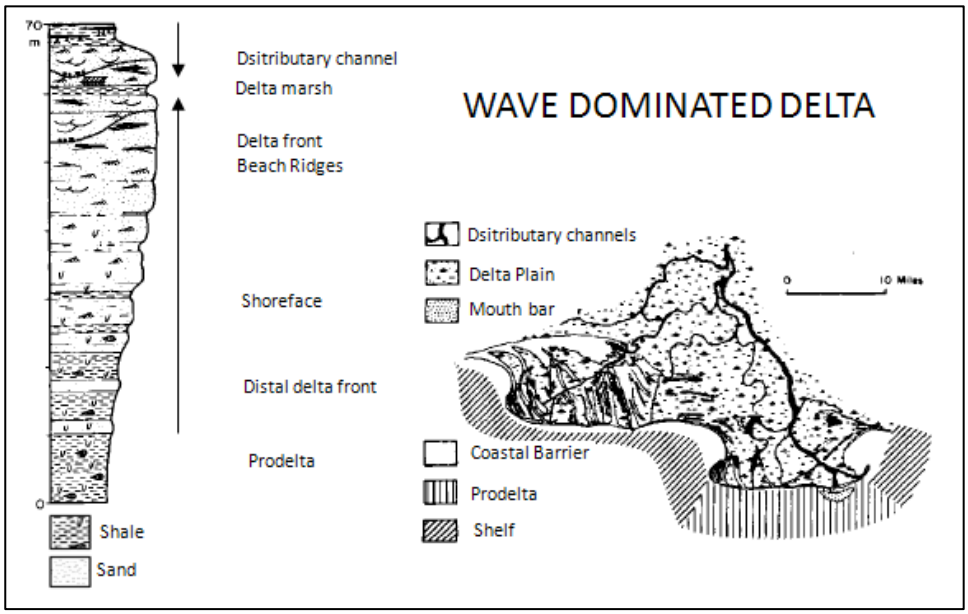

Figure 5.13 Wave dominated deltas morphology and stratigraphic column. Rhone type Delta (from Miall, 1976).

5.5 Summary

This chapter presented a description of the sedimentological processes that generated the sandbodies present within the reservoir case studies used in this thesis. As shown in Chapters 6 and 7, the techniques developed in this thesis were applied to synthetic reservoirs which feature different depositional environments: (1) fluvial meandering settings (Stanford VI Reservoir); (2) deep-marine channels (DM_Field); and (3) deltaic deposits (Mitare_Field).

For the Stanford VI reservoir, the facies that are going to be simulated are channel, point bars and floodplain deposits. The geometry of the meandering

channels is modelled using: meander wavelength, amplitude, channel width and thickness. In this chapter the process that generated these deposits were described.

For the deep marine channels a comparison was made between fluvial meandering and deep-marine channels, explaining that the processes that generated these deep-marine channels were totally different from the process associated to fluvial meandering channels. In the DM_Field the deposits considered for simulation were channel deposits and deep-marine shale.

In the case of deltas, the basic processes that generated the three main types of deltas are: river current, wave and tide processes. These processes were described as well as the geometry of the sandbodies generated by the interaction of these processes.

This chapter has described the geometry of the deposits and sedimentation processes of three depositional systems. From this chapter it is possible to select the geomorphic parameters of these depositional systems to be used in reservoir history matching in the next two chapters. The use of these geomorphic parameters in history matching will be described in the following chapters.

Chapter 6

Use of Intelligent Sedimentological Prior Information in Automatic History Matching of Reservoir Models

6.1 Introduction

The relationships between fluvial channel geomorphic parameters (channel depth and width, meander wavelength and amplitude) were modelled using Machine Learning Techniques in Appendix E. These models were used as sedimentological prior information to control the realism of geobody geometry in reservoir models (Appendix E.4 and Rojas *et al.,* 2011). In this Chapter, these sedimentological prior models are used to control the geological realism in reservoir facies models. These sedimentological prior models were included into the automatic history matching process, where the modeller did not have direct control on the geobody geometries due to the automation of the process.

The relationships between different geomorphic parameters, from different depositional environments (fluvial meandering, deltaic and deep-marine channel

deposits) were modelled using machine learning techniques (MLT). These models are used as prior information within the automatic history match workflow (Section 3.4). The geomorphic parameters are sampled using stochastic sampling (Section 3.3.2) from the prior models (Section 3.4.4) in the Bayesian framework, and the posterior information is updated based on the misfit calculation of the model and historic production data of a reservoir.

The sedimentological prior information was modelled using One-Class SVM, which is a classification Machine Learning Technique used to identify a one particular class (group of samples with specific characteristics). Therefore, the samples that do not belong to such class can be rejected (Section 4.6.3). The idea is to model a region composed of realistic combination of geomorphic parameters using One-Class SVM. Then, this region acts as a prior to accept any combination of geomorphic parameters that could be considered as geologically realistic, assuring then the realism of geometry of the facies in the reservoir models. The samples outside the prior region are rejected as unrealistic.

The reservoir data used in this chapter are synthetic, like the Stanford VI reservoir (Castro *et al.,* 2005). The second stratigraphic unit of this reservoir was used as the *truth case* for modelling reservoirs developed in fluvial meandering settings. Two other synthetic reservoirs were generated in this thesis to be used as *truth cases* for modelling reservoirs developed in deep-marine (DM_Field) and deltaic settings (Mitare_Field). The fluid properties, pressures, relative permeability curves and capillary pressures for these two reservoirs were taken from the Stanford VI reservoir (Castro *et al*., 2005).

6.2 Meandering Channel Models (Synthetic case: Stanford VI)

Meandering channels deposits preserved in the geological record have been described by many authors (Allen, 1965, 1983; Bridge and Tye, 2000; Miall, 2006) due to the importance they have in prospecting mineral and hydrocarbon resources.

Rojas *et al.* (2011) showed examples of modelling the geometry of this type of channels using different sets of geomorphic parameters as prior information. Rojas *et al.* (2011) selected combinations of geomorphic parameters that could be considered as realistic, based on the compilation of geomorphic information using Machine Learning techniques (Appendix E).

The compilation of geomorphic parameters (channel width and thickness and meander wavelength and amplitude) was used in this Section as geological prior information within a Bayesian framework for uncertainty quantification and history matching in reservoir production and forecasting.

6.2.1 Sedimentological Prior Information

Sedimentological prior information, for modelling meandering channels, can be defined as the knowledge of the natural relationship between channel parameters (e.g. channel width and thickness and meander wavelength and amplitude), before making a model of meandering channels.

As observed in Appendix E and in Rojas *et al.* (2011) Support Vector Regression (SVR) is a powerful tool to model the relationships among the channel geomorphic parameters. These relationships can be used as prior information for modelling channels.

One-Class Support Vector Machine (OC-SVM)

Another useful technique to identify realistic combination of geomorphic parameters is the previously described OC-SVM (Section 4.6.3). OC-SVM is capable to identify which combination of geomorphic parameters is realistic and to reject any unrealistic combination of parameters.

OC-SVM has been used not only as a one-class classification technique but is also used to distinguish anomalies or novelty detection in new data.

Channel geomorphic parameters, channel width and thickness and meander wavelength and amplitude, are genetically related (Appendix E) due to the hydrodynamics that controls the channel geometry. In order to obtain realistic reservoir models, it is necessary to use a realistic combination of all these parameters. By using OC-SVM it was possible to generate a four-dimensional region that comprises realistic combinations of the channel geomorphic parameters. Each of the four geomorphic parameters (channel, width and thickness and meander amplitude and wavelength) is a dimension in the 4-D space. This region or "cloud" can be used as a prior distribution to sample from and generate meandering channel models based on the realistic combination of the geomorphic parameters (see Figure 6.1). This yellow "cloud" looks very similar to the validity domain obtained using General Regression Neural Networks (GRNN) (Appendix E.2.2). The difference between GRNN and OC-SVM is that OC-SVM is a classification technique that can identify novelty faster than GRNN and can generate probabilistic outputs which is explained in the next sub-section. The OC-SVM hyper-parameters used to tune this 4-D "cloud" are shown in Table 6.1 (page 155).

One-Class SVM probability output

The output of a classifier should be a calibrated posterior probability to enable post processing. Constructing a classifier to produce a posterior probability is very useful in practical recognition situations (Platt, 1999); a posterior probability output allows decisions that include uncertainty (Duda and Hart, 1973). One-Class SVM does not provide such probabilities. In this thesis, the results of One-Class SVM were transformed into a probabilistic form using the methodology proposed by Platt (1999). In order to probabilistically generate a "window" that includes part of the parameter space that was not included in original One-Class SVM realistic "cloud", this "window" of the parameter space could exist in nature as is part of the uncertainty associated to the number of data points used. It is important to clarify that the prior information used in this thesis for history matching come from the posterior of the SVM classifier as explained above.

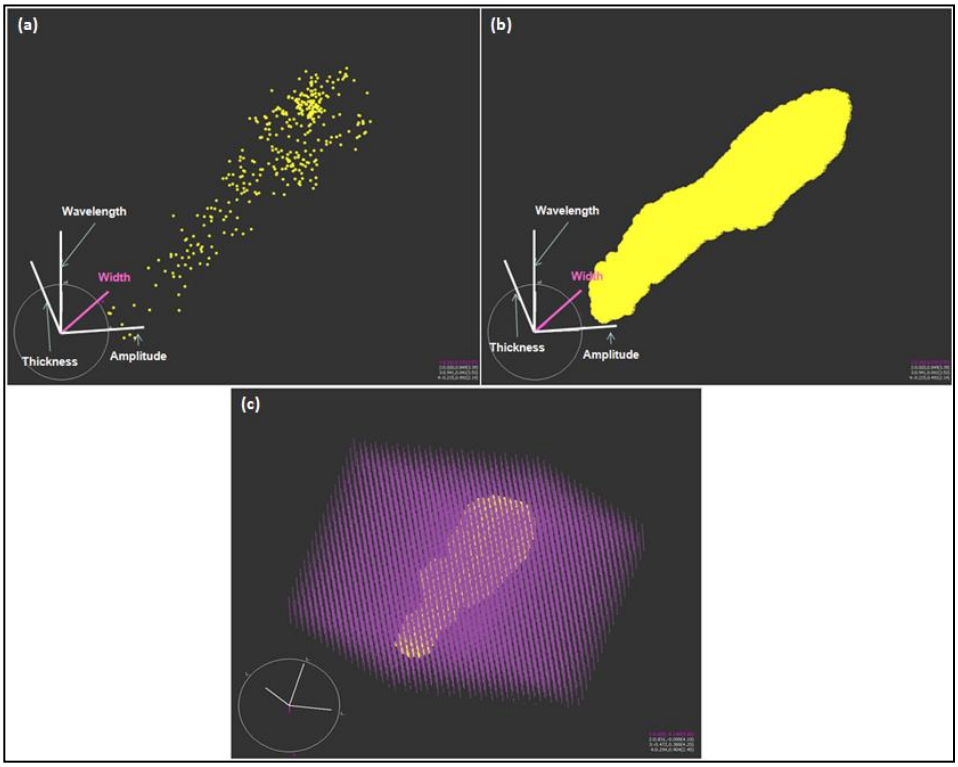

Figure 6.1: 4D region (cloud) of realistic combination of the channels geomorphic parameters. (a) 715 data points used to generated the 4D region; (b) In yellow the 4D region or cloud that encapsulate the realistic combination of geomorphic parameters; (c) in purple points outside the OC-SVM region (Yellow) these purple point are unrealistic combinations of parameters. This yellow cloud

Platt (1999) points out that the class-condition densities between the margins in a SVM classifier, are apparently exponential. Indicating that Bayes' rule on two exponentials suggests using a parametric form of a sigmoid (*eq.* 4.32):

$$P(y = 1|f) = (1 + \exp(Af + B))^{-1}$$

Where $P(y=1|f)$ is the posterior probability (an analytic function of f) and f is the decision function. This posterior probability obtained from the SVM classifier is used to build the intelligent prior information.

This sigmoid model (eq. 4.32) is equivalent to assuming that the output of an SVM is linearization of the posterior probability (Platt, 1999).

Figure 6.3 illustrates the methodology used to transform the One-Class SVM results into a probabilistic output:

(1) A series of data points that do not belong to the "one class" was generated (purple points) and mixed with the points that belong to the "one class" (points inside the yellow region).

(2) One-Class SVM was used to separate these two classes. The *decision values* generated by SVM were used to be included into the sigmoid function:

$$P(y) = (1 + \exp(Af + B))^{-1} \qquad (eq\ 6.1)$$

where: P is the probability, f are the *decision values* obtained with the two classes SVM classification, parameters A and B were tuned using maximum likelihood estimation.

Decision Value can be defined as the value obtained from the SVM decision function (eq. 4.9) in the parameter space, during the SVM classification process.

(3) The probability used in all the prior models generated in this thesis was 0.1. Any point with a probability lower than 0.1 was considered as a point with an unrealistic combination of geomorphic parameters.

The probability of 0.1 is the point where the sigmoid function crosses the decision value of 0. It is possible to move this probability "cut-off" in the code in order to change the size of the "cloud" of realistic combination of geomorphic parameter.

(4) Extend the region of realistic combination of parameters in order to analyse uncertainty.

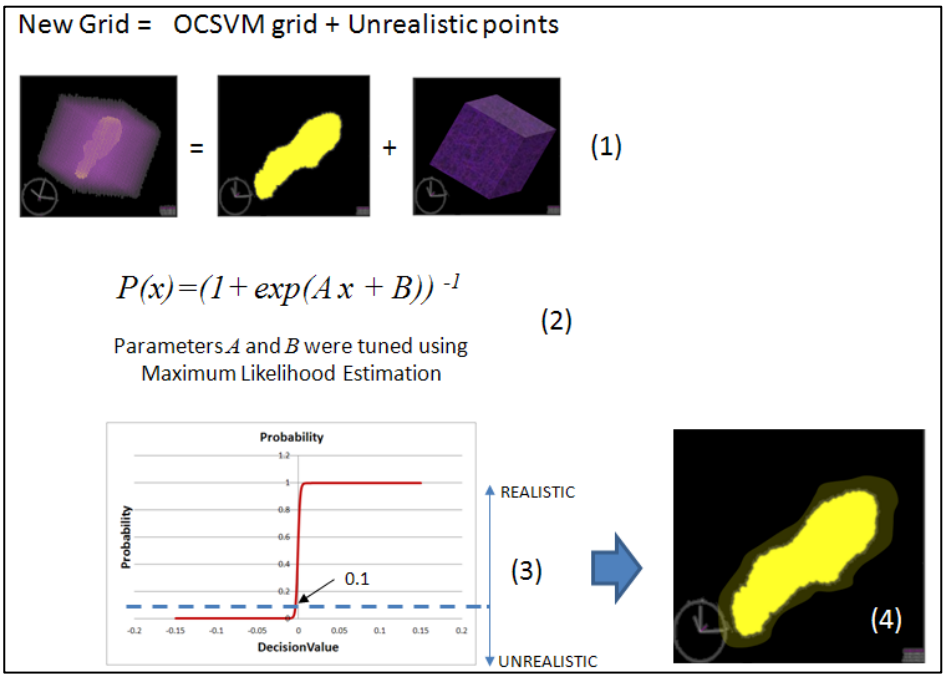

Figure 6.2: Methodology to transform One-Class SVM into probabilistic outputs: (1) Generation of a hyper-region of unrealistic and realistic combination of geomorphic parameters; (2) an (3) Application of the sigmoid function to the One Class-SVM outputs and (4) obtaining region "cloud" of realistic combination of parameters with uncertainty.

6.2.2 Meandering Geometry using Multiple Point Statistics

As mentioned in Chapter 4, the technique used in this thesis for modelling facies is Multiple Point Statistics (MPS). Chapter 4 demonstrated how the use of MPS solves the problems occurring in other techniques. Like object models, Truncated Gaussian Simulation (TGS) or Sequential Indicator Simulations (SIS). In object based modelling it is very difficult to adapt the geometry of the objects to the well data or to seismic interpretations. While, the models obtained from SIS or TGS suffer from the lack of geological realism of the facies geometry (Chapter 2). In this thesis the MPS-SNESIM algorithm (Remy *et al.,* 2009) was used to simulate the facies distribution within a reservoir grid. As explained in Chapter 2, MPS is

based on sampling the facies distributions from a Training Image (TI), and populating the model grid considering the facies geometry presented in the TI and conditioned to the well and seismic information.

In order to generate models with different facies geometries based on a single training image, SNESIM has the capability of varying the geometry of the facies in the model by modifying the geometry of the training image using the "affinity" parameter (Liu, 2006). Figure 6.3 shows the impact of the affinity parameter on the MPS realisations. The "affinity" parameter is a combination of three numbers (x, y and z), which correspond to each axis of the 3D grid model. Combination of the affinity parameter values, such as (2, 0.5, 1) will generate a model with the facies dimensions increased by 2 in the x axis, reduced by 0.5 in the y axis and keep the same dimension as the TI in the z axis).

Figure 6.4 demonstrates that in the case of modelling sinuous channels the relationship between the affinity parameter variation and the geometry observed in the model is not always a linear relationship. For example, having some sinuous channel in a TI, with amplitude of 1000 m and changing the affinity parameter to 2 in the axis that affect the amplitude will generate a range of amplitudes (1600 - 2400 m) instead of a single output of 2000 m in amplitude. This is due to the template size (small), or the sequential population of the cells.

The problem in the use of MPS for modelling channelized geometries is in relating the physical geometry of the facies in the model, which are measurable parameters, to the changes in the affinity parameter, which is the model parameter not supported by observation. This problem was solved by designing an Multilayer Perceptron (MLP) ANN predictor (Chapter 4) of affinity parameter values given the channel geometry based on generated 1500 realizations with different "affinity" parameter based on a single TI, and measuring the variations of the channel geometry in them. The obtained results are shown in Figure 6.4. The Multilayer Perceptron (MLP) relates the actual dimensions of the geomorphic parameters (channel width and thickness and meander wavelength and amplitude) to the SNESIM "affinity" parameter (TI transformation parameter). One

of the problems observed in this approach is that, it is very difficult to change independently the geomorphic parameters, like channel width and meander amplitude (Figure 6.3). However, varying the affinity in the three axes can offer a good degree of independency for varying each parameter. A different approach is to use multiple training images (Park *et al,* 2013). Using multiple training images with multiple channel geometries allows the selection of the training image that better represents the geometry of the reservoir geobodies.

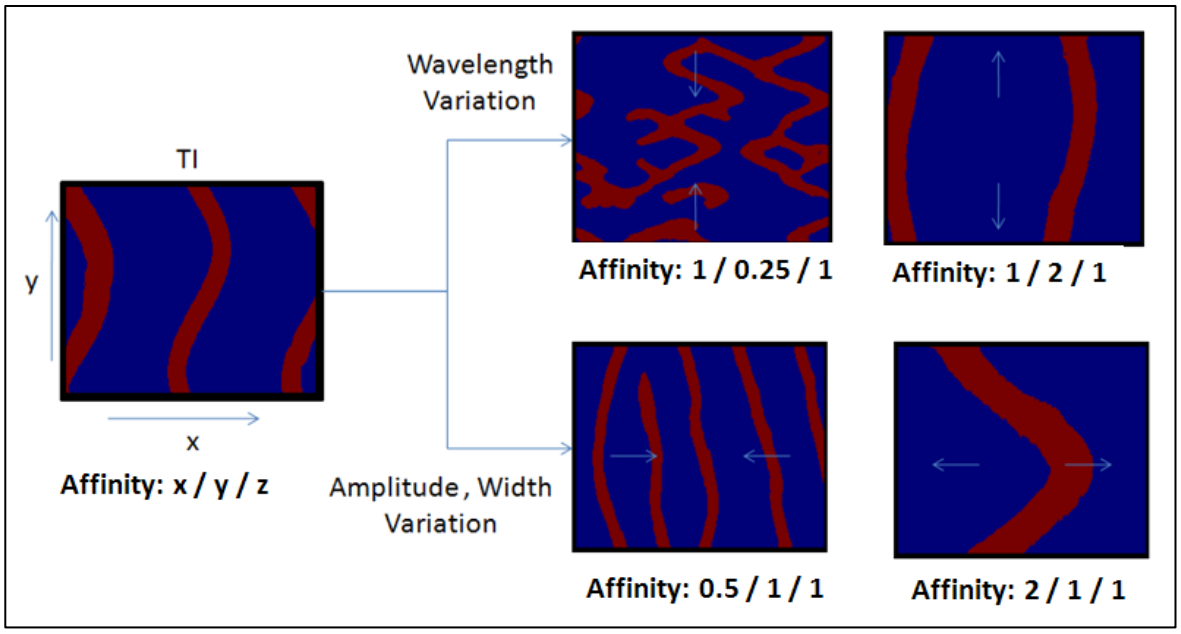

Figure 6.3: Variation of channel geometry changing the SNESIM affinity parameter. The variation is subject to the effect of the affinity parameter over the Training Image (TI).

Figure 6.5 illustrates the MLP network trained to find the relationship between channel geomorphic parameters and variations in the affinity parameter in the x axis. The MLP-network has four inputs (geomorphic parameters: channel thickness and width and meander wavelength and amplitude) and 3 outputs ("affinity" in x, y and z). With this network it is possible to translate the geomorphic parameters into affinity parameters and use them as input in MPS to generate facies models.

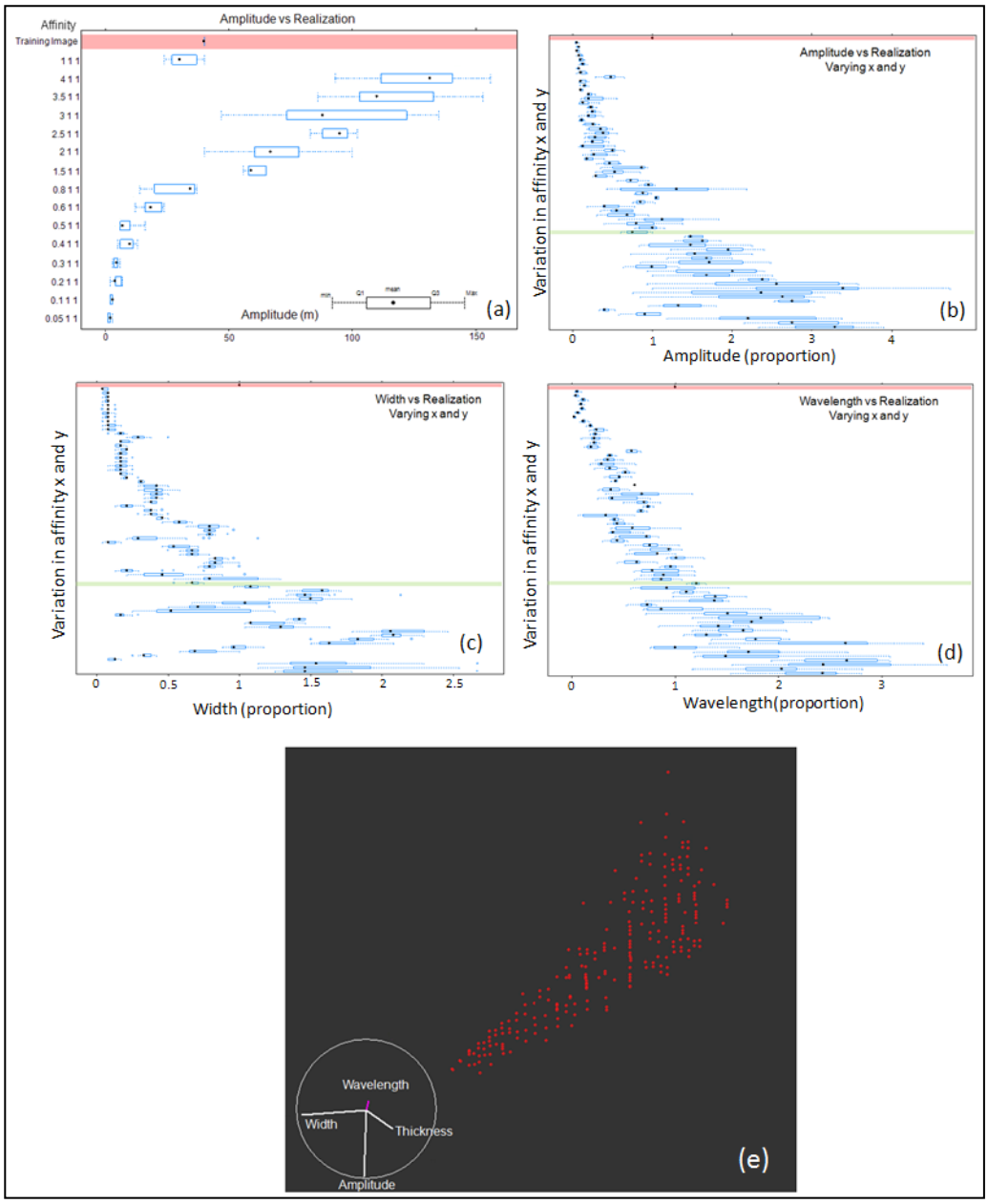

Figure 6.4: Different responses of the channel geometry after varying affinity. (a) variation of meander amplitude while varying affinity in x; (b), (c) and (d) illustrate the variation of amplitude, wavelength and channel width while varying affinity in x and y. Note that the values of the channel parameters in the training image are represented in red and in green the values of the parameters using affinity 1/1/1. In (b), (c) and (d) the geomorphic parameter is measured in proportions referred to the values of the parameter in the training image (i.e. the value of the parameter in the model is divided by the value of the parameter in the training image). (e) 4D Plot of the combination of geomorphic (channel width and thickness, meander wavelength and amplitude) parameters obtained from the perturbed realizations.

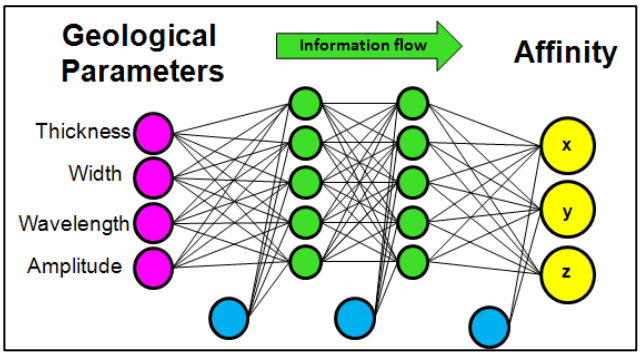

Figure 6.5: Multilayer Perceptron used to convert geomorphic parameters into affinity parameters, this network was built using the data obtained from the simulations varying affinity (Figure 6.2).

6.2.3 Reservoir Modelling and History Matching

As highlighted in Chapters 2 and 3 and discussed by Arnold (2008), one of the main problems faced by geological parameterization in automatic history matching is to keep the realism of the facies geometries in reservoir models.

As discussed in Sections 4.3, authors like Arnold (2008), Rojas *et al.* (2011) and Park *et al.*, (2013) have developed some techniques to use geological prior information as a constraint to keep the geological realism of facies geometry in reservoir simulations.

Hyper-parameter	Value
Kernel Type	Gaussian
Gamma	0.01
η	0.001
Cost (C)	10

Table 6.1: Hyper-parameters used in One-Class SVM, after tuning.

In this chapter, a new approach is proposed: the use of the 4-D region built with OC-SVM as prior information that can control realism of the combination of

geomorphic parameters. Figure 6.6 shows a workflow illustrating the idea of using the realistic 4-D “cloud” to reject combinations of geomorphic parameters that are unrealistic, accepting only the combination of parameters that are within the “cloud”. The selected realistic combination of parameters is used to generate facies models of meandering channel deposits. These facies models are then used to generated reservoir and fluid flow models, and history match these models in order to select the best match models, to predict the behaviour of the reservoir.

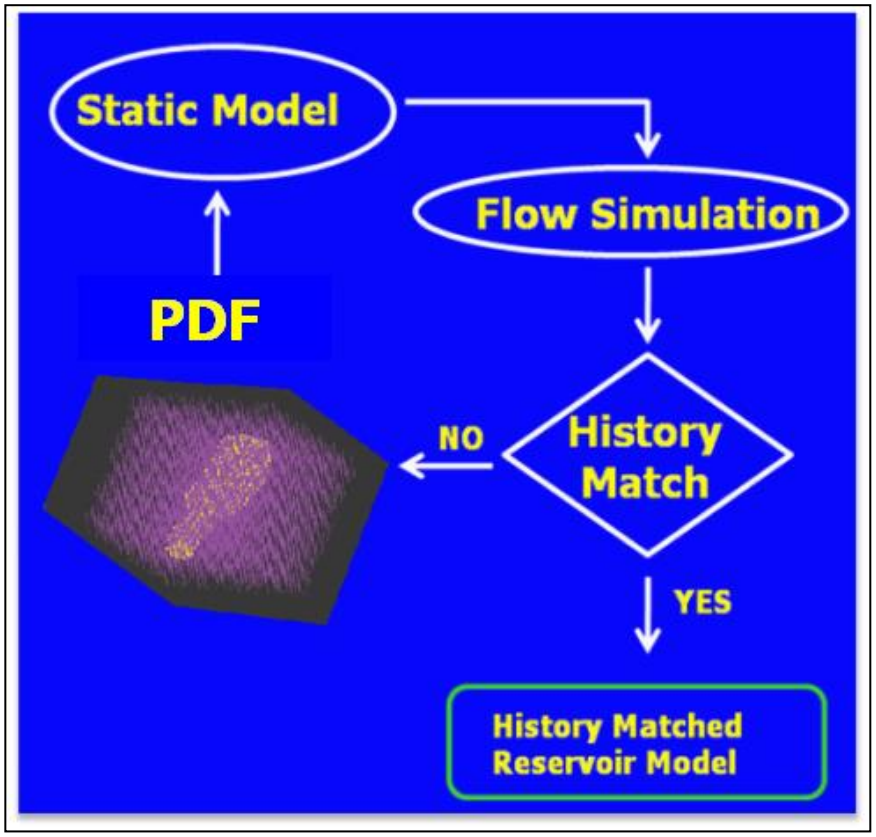

Figure 6.6: Workflow for History matching, illustrating the use of a region of realistic combination of geomorphic parameters (yellow region) as the probability density function to sample (Geological Priors) and build the reservoir model. Purple points are unrealistic combinations of geomorphic parameters.

Truth Case

In order to apply this methodology, a synthetic reservoir, composed of meandering channel deposits was used as the reference case (Truth Case). The advantage of using a synthetic case is that the internal geometry of the sedimentary facies is known as well as the production history. In this example the second stratigraphic unit of the Stanford VI synthetic reservoir (Castro *et al.,* 2005) was used as the truth case (see Table 6.2 for the reservoir properties). Stanford VI has 29 wells, 11 injectors and 18 producers. The facies present in this reservoir were channel, point bars and floodplain deposits and the petrophysical properties (porosity, vertical and horizontal permeability were assigned as constant for each facies (Table 6.3) in order to observe only the effect of varying facies geometry on the history matching results. Figure 6.7 is a 3D visualization of the Stanford VI synthetic reservoir, specifically the second stratigraphic unit. This stratigraphic unit was built by process based modelling using the software SBED (Castro *et al.,* 2005). The characteristics of the channel geomorphic parameters are shown in Table 6.4. Synthetic seismic data are available for Stanford VI to generate soft conditioning for each facies.

Stanford VI Props Meandering Channels	Values	Stanford VI Props Meandering Channels	Values
Wells	18 Producers 11 Injectors	**Number of Cells**	100 000 50x50x40
Fluids Density (lb/ft^3)	Oil: 45.09 Water: 61.8	**Cell size**	X: 75 m Y: 100 m Z: 1 m
Fluids Viscosity (cp)	Oil: 1.18 Water: 0.325	**Top Reservoir Depth**	2000 ft (TVD)
Formation Volume Factor	Oil: 0.98 Water: 1.0	**OWC**	6000 ft (TVD)

Table 6.2: Reservoir Properties of the Stanford VI (Castro *et al.,* 2005).

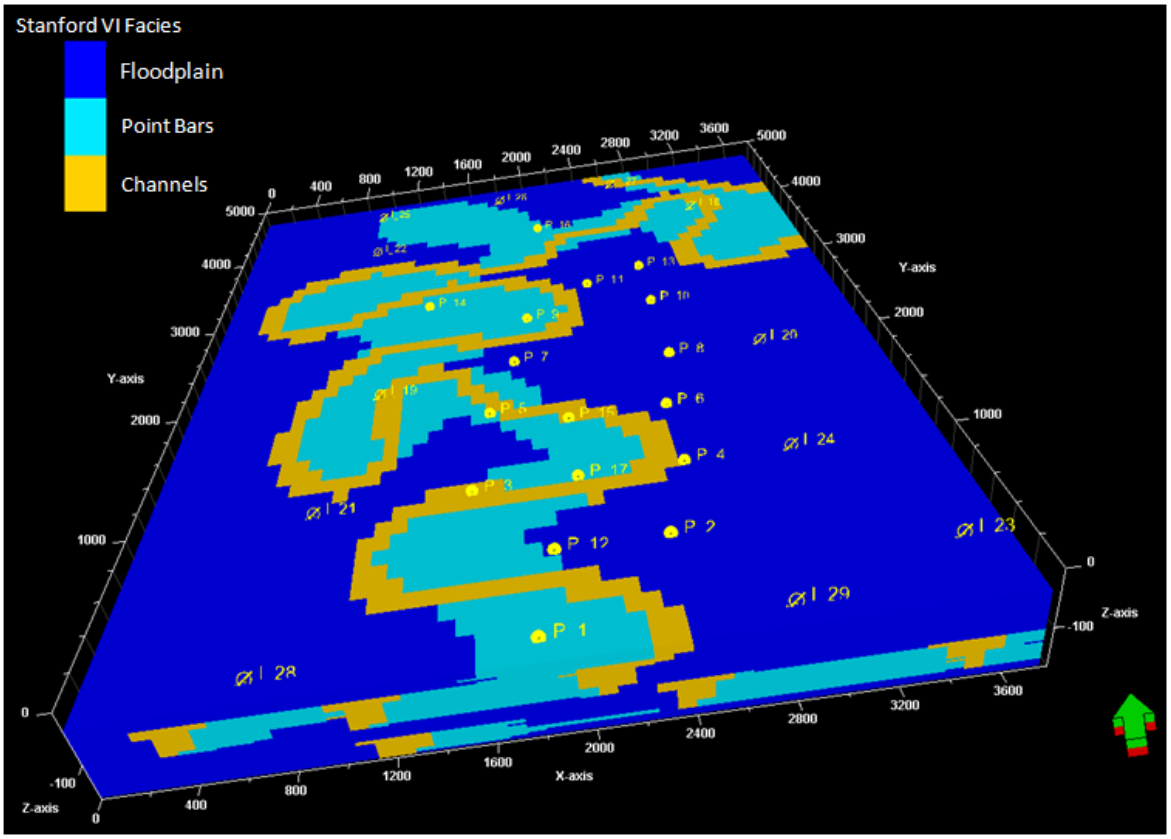

Figure 6.7: 3D representation of the "Truth Case", the second stratigraphic unit of the Stanford VI reservoir (Castro et al., 2005). Reservoir developed in a fluvial meandering system, with three facies: Floodplain, Point Bars and Channels.

Facies	Porosity (%)	Horizontal Permeability (mD)	Vertical Permeability (mD)
Channel	5	50	25
Point Bar	20	500	250
Floodplain	0.1	0.001	0.0005

Table 6.3 Petrophysical properties for each sedimentary facies

Parameter	Max (m)	Average (m)	Min (m)
Channel Width	150	180	200
Channel Thickness	15	15	15
Meander Amplitude	900	1080	1150
Meander Wavelength	1100	1500	1700

Table 6.4 Channel Geomorphic Parameter Properties (Truth Case).

Automatic history matching:

In this thesis the software RAVEN developed by Epistemy Ltd. (www.epistemy.com) is used for automatic history matching. Table 6.5 presents the characteristics to set up the history match process, where the variables to measure are field oil production rate (FOPR), field water production rate (FWPR), wells production and pressure, and the sampling algorithm was Particle Swarm Optimization PSO (Section 3.3). PSO samples from the parameter ranges shown in Table 6.5. The selected combination of the parameter values is compared with the OC-SVM prior information model. If the combination of the parameter values is not within the "cloud" of the realistic combination, then it is considered as unrealistic and its is penalised with a very high value to avoid its use in the forecasting. Thus, unrealistic models are not inferred in forecasting.

The fluid flow simulator used in this thesis is the black oil simulator Eclipse 100 from Schlumberger; the production time was set as 2000 time steps (days). Figure 6.8 is a summary of the Field oil and water production profile of this reservoir (Truth Case), within a production interval of 2000 days.

Figure 6.9 shows relative permeability and water saturation curves used in the fluid flow simulation. These curves were taken from the Stanford VI synthetic reservoir (Castro *et al,.* 2005) and capillary pressure (Pc) was considered 0.00.

History Match Set Up		
Geomorphic Parameters and Ranges	Chanel Width Channel Thickness Meander Amplitude Meander Wavelength	100 – 600 m 5 – 200 m 500 – 3000 m 500 – 3000 m
Total Number of Models	1000	
Minimum Misfit (*eq*. 3.1)	2000	
Sigma (σ in *eq*. 3.1)	6000 (STBD)	
Sampling Algorithm:	**Particle Swarm Optimization**	
No of Particles	20	
Group Size	4	
Initial Inertia	0.9	
Initial Decay	0.9	
Cognitive Component	1.333	
Group Component	1.333	
Social Component	1.333	
Min steps	5	
Energy Retention	0.8	
Particle Behaviour	Flexible	

Table 6.5: History Match set up for Meandering Channel Reservoir

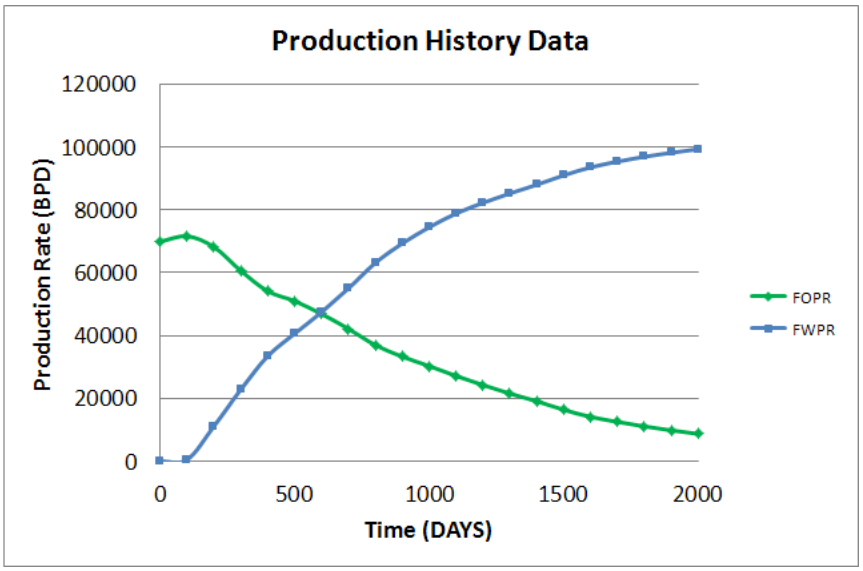

Figure 6.8: Oil and water production profile of the "Truth Case".

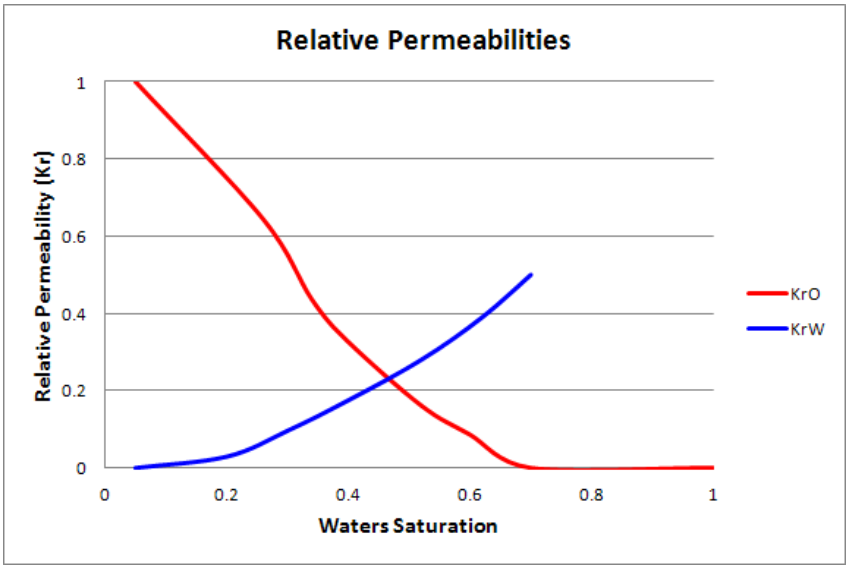

Figure 6.9 Relative Permeability curves. Stanford VI Reservoir (Castro *et al.*, 2005)

An ensemble of 1000 models was generated with PSO for this case with misfit calculated using a Least Squares misfit function (equation 3.1).

As shown in Figure 6.6 the workflow for history matching starts by selecting a combination of channel geomorphic parameters (channel width and thickness and

meander wavelength and amplitude, the ranges of the geomorphic parameters are shown in Table 6.5). This combination is compared to the 4D "cloud" of realistic combination of parameters obtained in with OC-SVM. If the selected combination of parameters is inside the 4D "cloud" then the model will be geologically realistic otherwise the model will be rejected. If the combination of geomorphic parameters is considered realistic, then they are used as input in a Multilayer Perceptron (MLP) network to generate their equivalent in the MPS-SNESIM "affinity" parameter (as explained in Section 6.2.2) and then introduced into the SNESIM input parameters.

MPS simulations are based on a training image, specifications given in Figure 6.10, well data and seismic conditioning. Then the facies model is populated with constant petrophysical properties for each facies as previously described in Table 6.3. The model is taken to the flow simulator and the results are history matched.

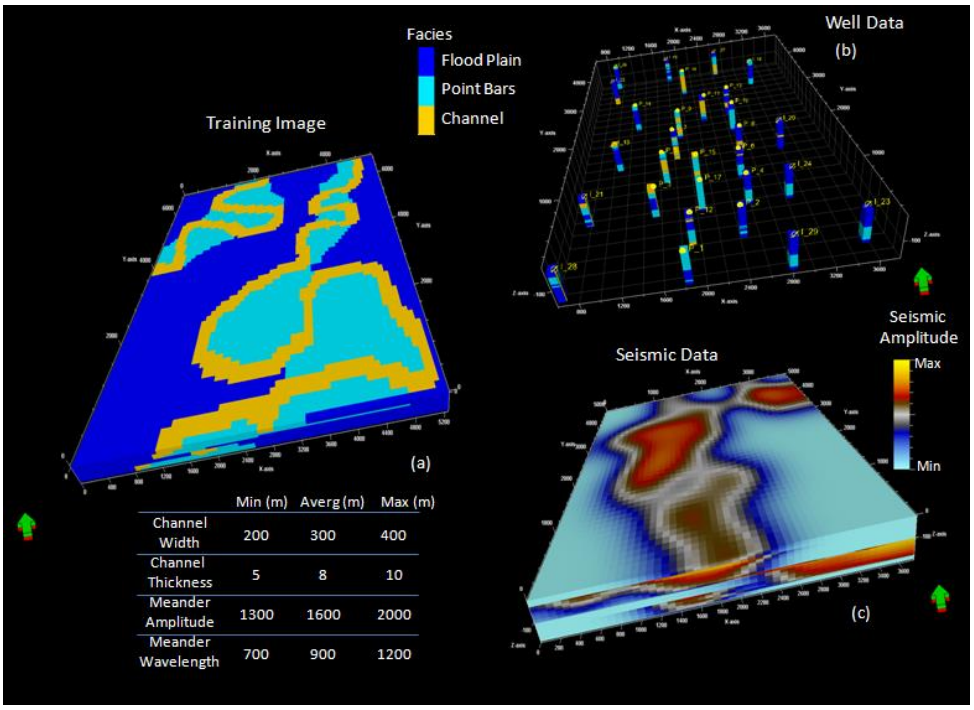

Figure 6.10: Input data for MPS Simulation using SNESIM: (a) Training Image with table specifying channel geomorphic parameters; (b) Well Data (Facies); (c) Seismic Data used as soft conditioning data.

Settings for uncertainty analysis in production forecast

After history matching, NA-Bayes (Sambridge, 1999b) was used to infer the uncertainty for production forecast (Section 3.4.2). The parameters for setting up NA-Bayes are described in Table 6.6.

6.2.4 Results

Figure 6.11 shows the convergence behaviour to a lower misfit during the history match process considering misfit and iterations. There were 126 iterations rejected as unrealistic, the lowest misfit was reached after 223 iterations and more history matches of similar quality were generated thereafter.

NA-B Set Up	
Chain Length	200,000
Burning Period	100,000
Number of Chains	8
Cell visits	56

Table 6.6: NA-B set up for forecasting and uncertainty quantification.

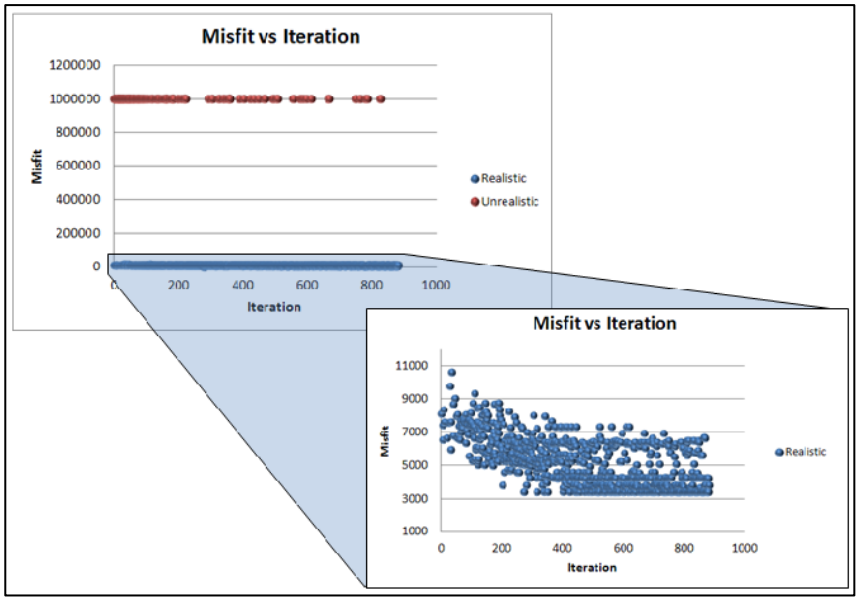

Figure 6.11: Misfit vs Iteration. In the zoom, it is possible to observe a convergence trend during the history match process.

Figure 6.12 compares the truth case geomorphic parameters and the parameters corresponding to the models with the lowest and the highest misfits, and an example model obtained with an unrealistic combination of parameters.

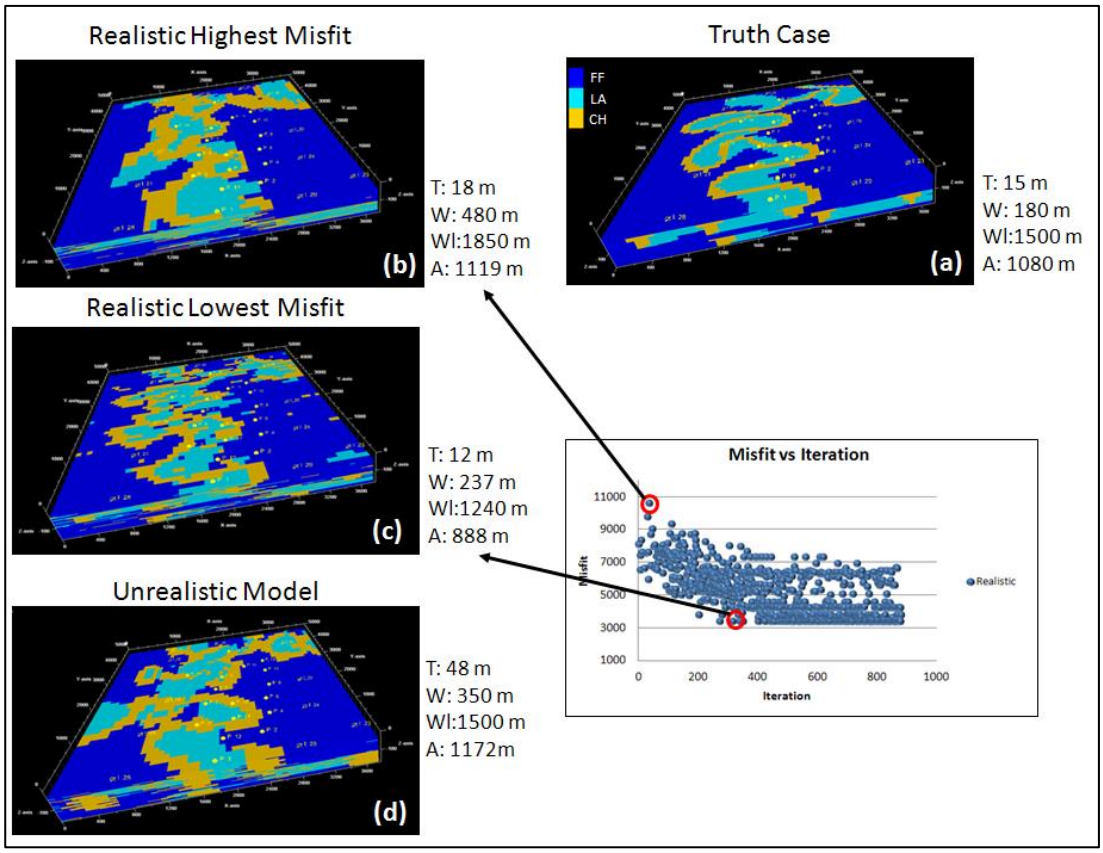

Figure 6.12: Comparison between models and truth case geomorphic parameters: (a) Truth Case; (b) Model with the highest misfit and realistic combination of parameters; (c) Model with the lowest misfit and realistic combination of parameters. (d) Model rejected because of the unrealistic combination of parameters. The misfit associated to models (b) and (c) can be located in the plot Misfit vs iteration. The averages of the parameters are shown for every model T: Channel thickness; W: Channel Width; Wl: Meander wavelength; A Meander Amplitude. Facies: FF: Flood Plain Facies; LA: Point Bar Facies; CH: Channel Facies. The dimensions of geomorphic parameters in the models were manually measured, using the measurement distance tool in Petrel.

Figure 6.12 shows that the dimensions of the geomorphic parameters of the realistic model with the lowest misfit (c) are closer to the dimensions of the

parameters of the “truth case” than the other models. In the case of the unrealistic model (d) the channel thickness value was considered as unrealistic given the corresponding channel width, meander amplitude and wavelength.

Figures 6.13 and 6.14 illustrate the difference of history matching the Stanford VI reservoir considering the sedimentological prior information model generated using OC-SVM (Section 6.2.2), and the models obtained using flat priors (ranges in Table 6.6).

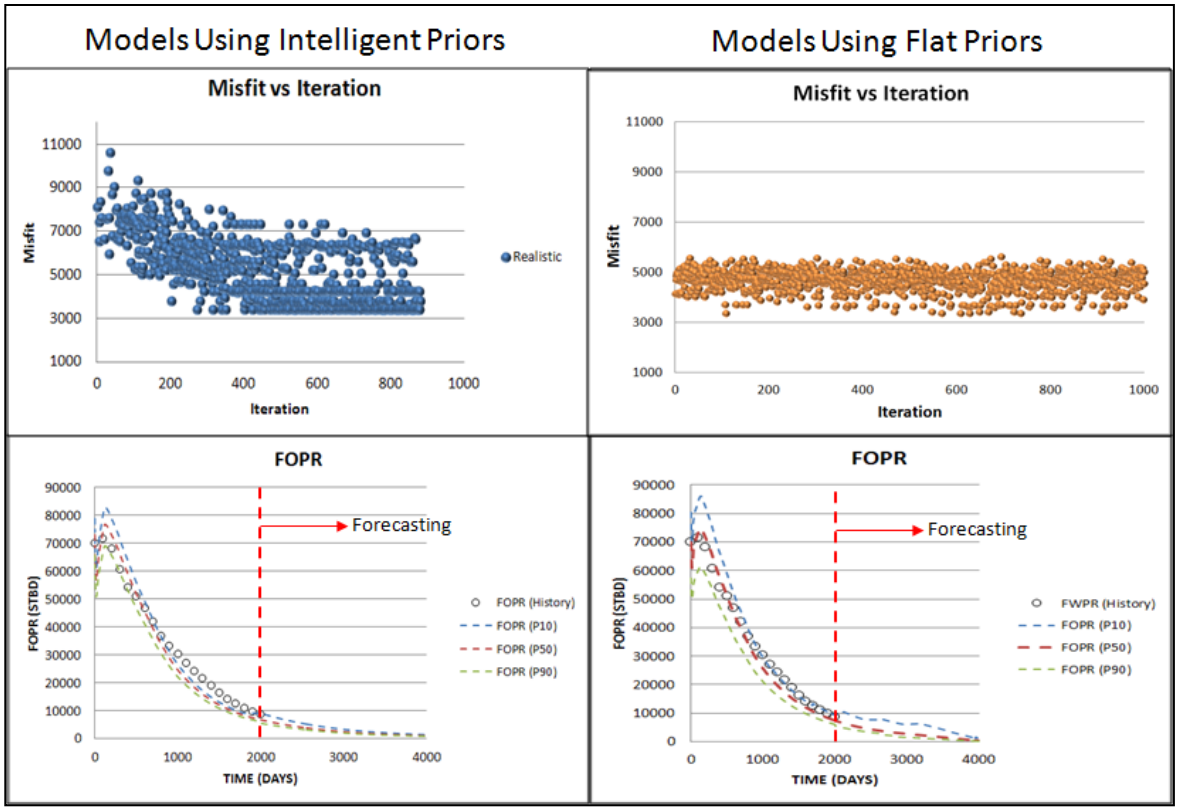

Figure 6.13: Comparison between history matching and forecasting models using intelligent geological prior information and models generated using flat priors.

From Figure 6.13 (Top) it is possible to observe that, when using intelligent priors, there is a trend for convergence of the match quality that is not seen in the case of using flat priors. The lowest misfit was reached twice faster in the case of

intelligent priors (realistic model #223) than in the case of using flat priors (model #586). In the forecasting of Field Oil Production Rate, the range of P10-P90 is lower in the case of realistic prior information than in the case of flat prior which suggests a reduction in uncertainty when using intelligent prior Information.

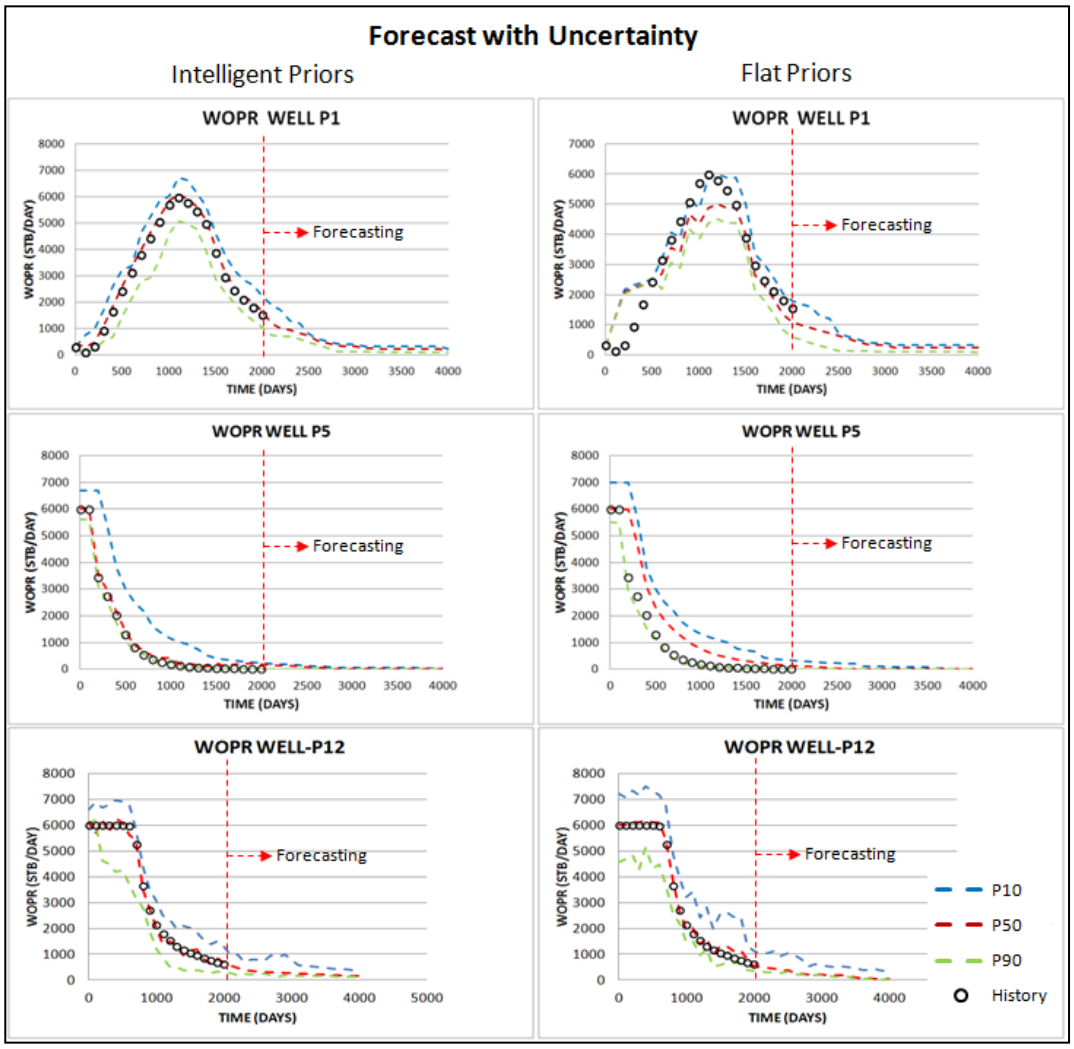

Figure 6.14: Comparison between history matching and forecasting Well Oil Production Rate (WOPR) in some wells of the Stanford VI synthetic reservoir, using intelligent sedimentological prior information and models generated using flat priors.

Figure 6.14 shows the oil production rate history match and forecast of the wells 1, 5 and 12 from the Stanford VI synthetic reservoir. This is a comparison between oil rate production response of the models generated using intelligent sedimentological prior information and flat priors. In general, the range P10-P90 of the well oil production rates (WOPR) in models generated using intelligent prior information is smaller than the range P10-P90 of the models using flat priors. Another important aspect is that the P50 curve is closer to the history data of the model with intelligent sedimentological priors than the models that used flat prior information.

Time consumed in the processes of history matching and forecasting for models using intelligent sedimentological prior information and uninformative prior is presented in Table 6.7. The use of intelligent priors reduced the time spent in history matching and forecasting. It is clear from Figure 6.13 that the history matching process converges faster when using intelligent sedimentological prior information.

	Intelligent Priors	Uninformative Priors
History Matching	89 hs	126 hs
Forecasting	37 hs	42 hs

Table 6.7: Time consumed in the processes of history matching and forecasting for models generated using intelligent sedimentological prior information and models generated using uninformative priors, time is measured in hours (hs).

It is important to mention that these experiments were performed in a desktop work station of 32 GB RAM and 1T Hard Disk Memory, performing these experiments in a cluster will speed-up these processes.

The Gibbs sampler (Sambridge 1999b) was used for forecasting, 26 models were resampled for the case of uninformative priors and 21 models were resampled for the case of using “intelligent” prior information.

Figure 6.15 shows that the models with geomorphic parameters dimensions closer to the “truth case” values were generated using “intelligent” priors. The ranges of values for each geomorphic parameter are narrower when using realistic prior information than when using uninformative priors.

Figure 6.16 illustrates in 4-D space the differences in shape of the intelligent prior information (yellow) and the region obtained with the 21 models resampled in red (posterior) after forecasting. Figure 6.15 suggests that the choice of prior is important, since sampling with uninformative prior is not able to find best models.

6.3 Deep Marine Channels (Synthetic Reservoir)

Deep marine channel deposits preserved in the geological records are excellent reservoir rocks (Wonham *et al.,* 2000, Posamentier and Kolla, 2003). As described in Section 5.3 the geometry of deep marine channels is very similar to fluvial meandering channels (Figure 5.5), although their origins are completely different.

Sedimentological prior information for deep marine channels was used in order to include “intelligent” prior information into the automatic history match process. In this section, a model of the prior information related to the geometry of deep marine channels was developed and used for generating facies models of a reservoir developed in a deep marine environment.

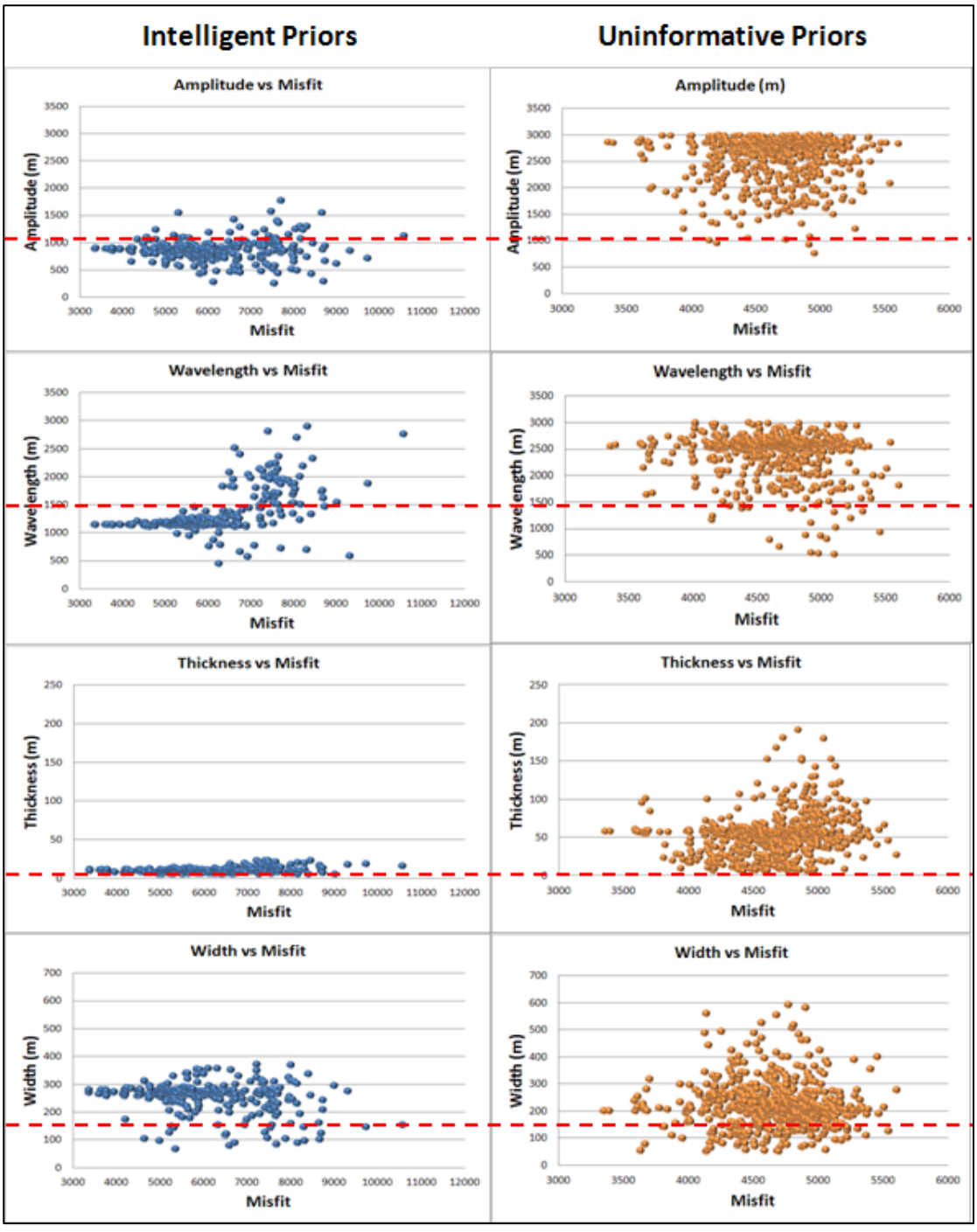

Figure 6.15: Geo-parameters of the models using Intelligent and “flat” priors and compared to the “truth case” value (Red dashed line).

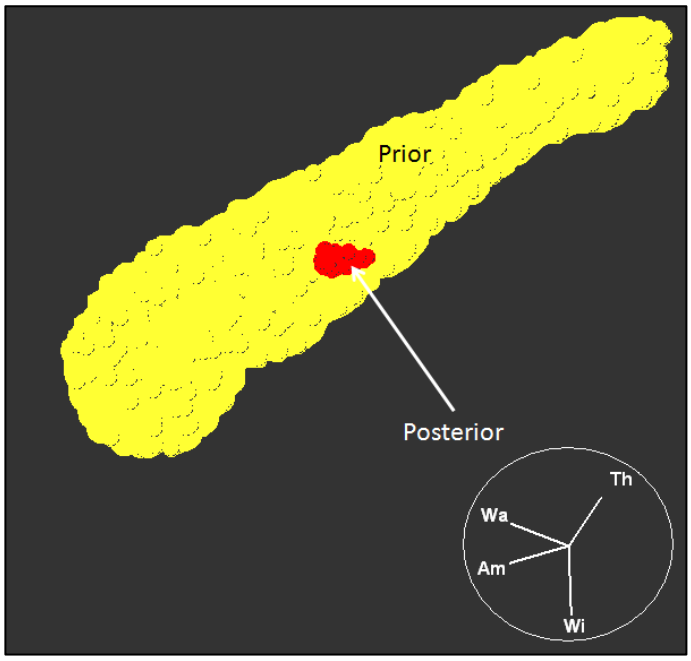

Figure 6.16: Comparison between the shape in 4-D of the Prior information (yellow) and the posterior (red). Am= amplitude, Wa= Wavelength, Th=Thickness and Wi= Width.

The truth case for this example is a synthetic reservoir built based on the work of Wonham *et al*. (2000), where the geometry of the channels deposited in a deep marine conditions and the relationships among the geomorphic parameters of these channels were described. This synthetic reservoir, called DM_Field, is composed by sandy channels and deep marine muddy deposits. The reservoir rocks are represented by sandy deposits, while the muddy deposits generate seal and permeability barriers between channels.

6.3.1 Prior Information

As observed in Figure 5.5, deep marine channels develop meander like geometry but, contrary to most of the fluvial meandering channels the coarse grained deposits are related to the channels and not to the point bars.

The prior information model built for fluvial meandering channels in Sections 6.2.1 were based on the geomorphic parameters: channel width and thickness and meander wavelength and amplitude. The same set of parameters can be used as well to describe the geometry of deep marine channels. As was explained in Chapter 5 meandering channels and deep marine channels are formed under very different physical conditions and by very different sedimentological processes. Therefore, the relationships between the geomorphic parameters vary for different depositional environments.

Figure 6.17 highlights the geomorphic differences when plotting together channel geomorphic parameters of meandering fluvial channels and deep-marine channels. The dimensions of the geomorphic parameters of fluvial meandering channels and deep marine channels overlap in a wide area, whereas, there is a clear difference between the geometry of fluvial meandering channels and deep marine channels towards the extremes. Prior information models for deep marine channels were generated with data from actual deep-marine channel deposits, taken from seismic interpretation and outcrops. Appendix B includes all the 675 data points obtained from the literature that was used to build the prior information models for deep marine channels used to build the prior distribution model.

As was explained in section 4.4, some data sets were incomplete (*i.e* they have missing data-points). This problem was solved by using semi-supervised learning (see Section 4.4.1). The geological priors for deep marine channels were modelled then using OC-SVM, the same technique used to model the prior information for fluvial meandering channels (Section 6.2). The hyper-parameters selected after tuning the OC-SVM are shown in Table 6.8

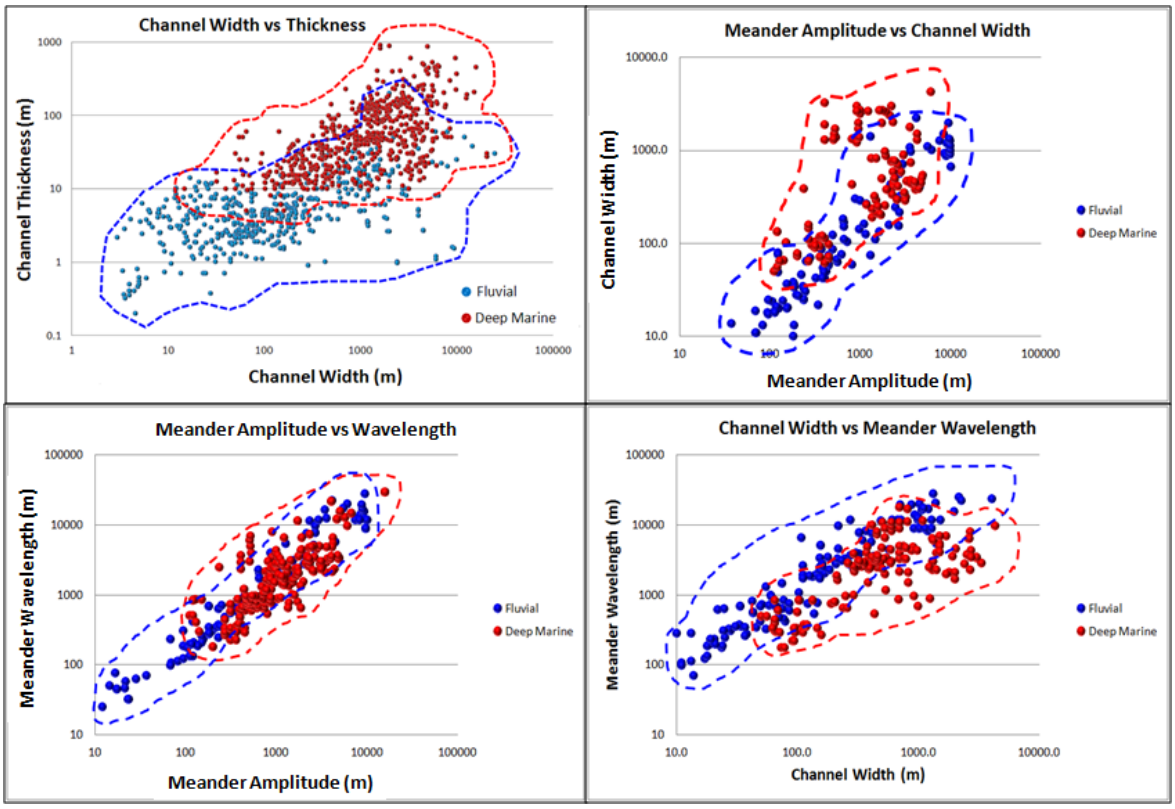

Figure 6.17: Channel dimension comparison between fluvial meandering and deep-marine channels. In red data points measured in deep marine channels and in blue data from fluvial meandering channels. Data collected from publications related to outcrop description and seismic analysis (Appendix B).

6.3.2 Reservoir Modelling

A synthetic reservoir (DM-Field) with facies geometry reflecting the description of deep-marine channels of the Balliste-Crécerelle Canyon Fill (Wonham *et al.*, 2000) was used to demonstrate the application of informative priors in HM).

Hyper-parameter	Value
Kernel Type	Gaussian
Gamma	0.015
η	0.001
Cost (C)	12
A	-827.097
B	0.0727

Table 6.8: Hyper-parameters selected to model the geological prior information using One-Class SVM. The values of A and B for the use of the sigmoid function to control the probabilities in One-Class SVM are shown in this table.

A 3D representation of this reservoir is presented in Figure 6.18. The reservoir data are presented in Table 6.9.

DM_Field Props	Values
Wells	6 Producers 4 Injectors 5 Dry Holes
Fluids Density (lb/ft^3)	Oil: 45.09 Water: 61.8
Fluids Viscosity (cp)	Oil: 1.18 Water: 0.325
Formation Volume Factor	Oil: 0.98 Water: 1.0
Number of Cells	280 000 80x140x25
Cell size	X: 100 m Y: 100 m Z: 2 m
Top Reservoir Depth	2000 ft (TVD)
OWC	6000 ft (TVD)

Table 6.9: DM_Field reservoir and “truth case” model properties.

The reservoir sedimentary facies in the DM_Field were generated using unconditional object modelling with sinuous channels. There are basically three facies in this reservoir (1) pre-canyon deep marine pelagic and hemipelagic shales, (2) muddy channel levees and canyon fill pelagic shales, and (3) Deep marine channel sandy deposits (Figure 6.18). Table 6.10 shows the dimensions of the deep-marine channel geomorphic parameters in the DM_Field.

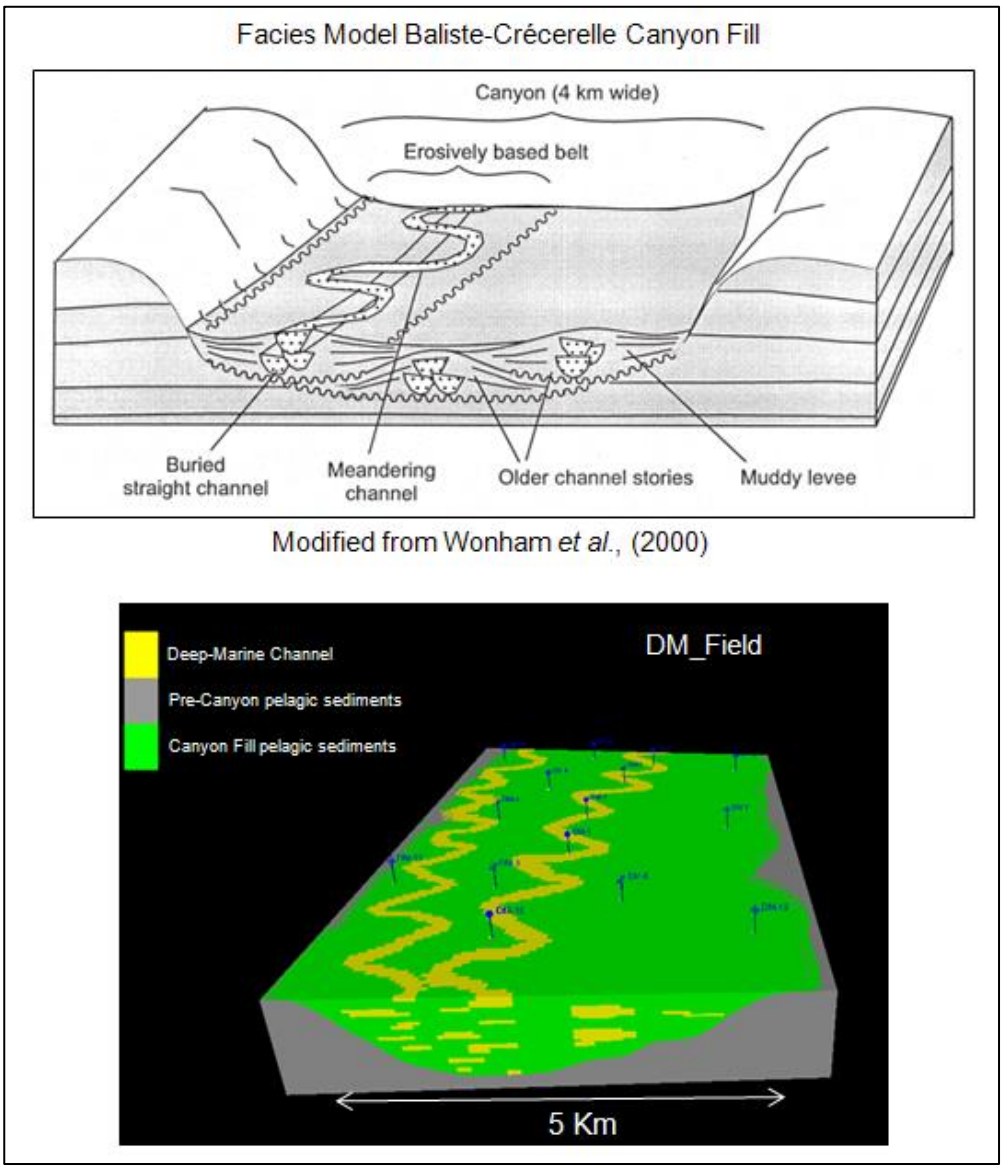

Figure 6.18: 3D representation of the DM_Field and the facies model of the Balliste-Crécerelle Canyon fill (Whonham *et al*. (2000).

Parameter	Min (m)	Average (m)	Max (m)
Channel Width	150	180	250
Channel Thickness	20	30	50
Meander Amplitude	600	700	1000
Meander Wavelength	800	950	1200

Table 6.10: Deep-Marine channel geomorphic properties in DM_Field reservoir.

Petrophysical properties for these facies were set constant for each facies to analyse the effect of varying facies geometries on history matching processes, and avoid a smearing effect possibly introduced by the variation of the petrophysical properties. Table 6.11 shows the relationships between sedimentary facies and petrophysical properties.

Facies	Porosity (%)	Horizontal Permeability (mD)	Vertical Permeability (mD)
Channel	20	500	250
Pelagic Canyon-Fill	0.01	0.01	0.01
Pre-Canyon Pelagic	0.01	0.01	0.01

Table 6.11: Petrophysical Properties associated to Deep Marine Facies in DM_Field.

Fluid properties and reservoir properties were taken from the Stanford VI synthetic reservoir (Castro *et al.,* 2005), see Table 6.10 for more detail and Figure 6.8 for

relative permeability curves. Capillary pressure was set to zero like in the Stanford VI case.

6.3.3 History Match and Uncertainty Quantification

The idea of history matching this reservoir is to evaluate the changes in facies geometry within a realistic geology (similar to Section 6.2). The input parameters for the facies simulations in MPS are shown in Figure 6.19: a training image generated using unconditional object based modelling, 15 wells for hard data conditioning and seismic data for soft conditioning. Facies proportions were set as pelagic shale canyon fill 65% and deep-marine channel sands 35% as described by Wonham *et al.* (2000) for the Balliste-Crécerelle Canyon facies model.

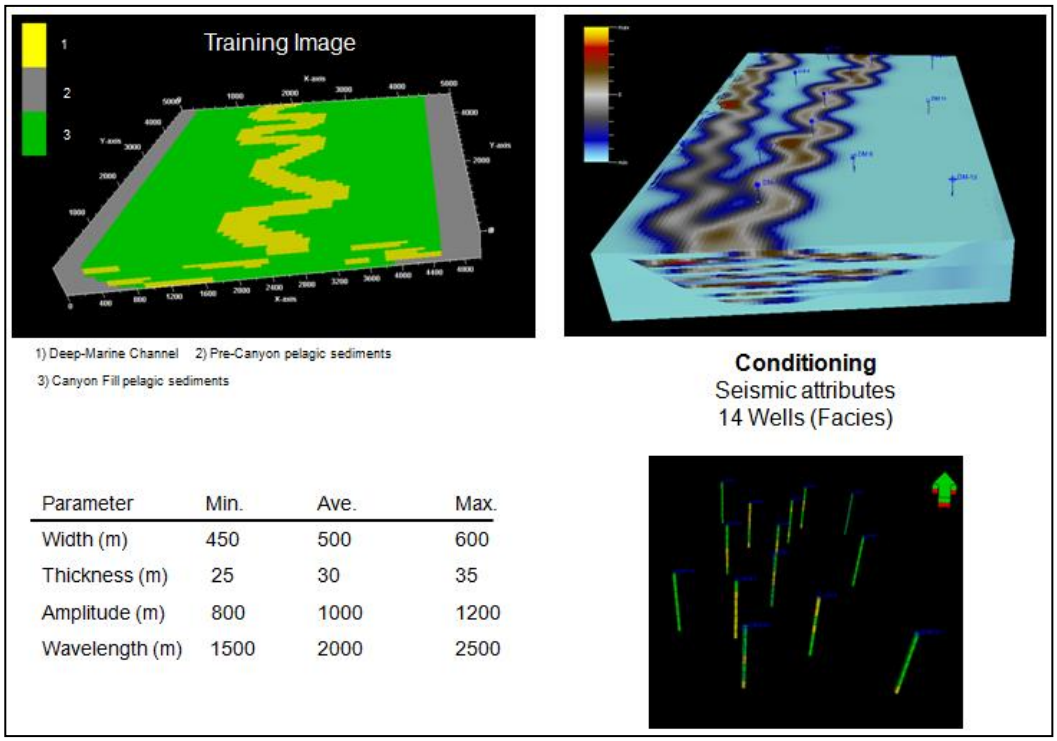

Figure 6.19: Input Data for modelling Deep-marine facies using MPS: Training Image with their characteristics (geomorphic parameters dimensions) and hard and soft conditioning data, well data (Facies logs) and seismic information respectively.

The history matching setup is presented in Table 6.12, the Misfit was estimated using the Least Squares function (equation 3.1). In this case the data to match were: oil and water field production rates (FOPR and FWPR) as well as pressure and production rates (WBHP, WOPR and WWPR) for injector and producer wells. The sigma error of the production data was set to 200 STDBPD. The production data are for 600 days.

History Match Set Up DM_Field		
Geomorphic Parameters and Ranges	Chanel Width Channel Thickness Meander Amplitude Meander Wavelength	150– 1000 m 20 – 280 m 200 – 5500 m 200 – 4500 m
Total Number of Models	1000	
Minimum Misfit	1500	
Sigma	500 (STBD)	
Sampling Algorithm:	**Particle Swarm Optimization**	
No of Particles	20	
Group Size	4	
Initial Inertia	0.9	
Initial Decay	0.9	
Congnitive Component	1.333	
Group Component	1.333	
Social Component	1.333	
Min steps	5	
Energy Retention	0.8	
Particle Behaviour	Flexible	

Table 6.12: Automatic history matching setup for DM_Field.

Uncertainty quantification and production forecast.

NA-B (Sambridge, 1999) was used to generate the forecast of this reservoir based on the history match results (Chapter 3). The setup of NA-B is shown in Table 6.13. the period for forecasting was of 600 days more than the history matching production days, which means a total of 1200 days.

NA-B Set Up	DM_Filed
Chain Length	200,000
Burning Period	100,000
Number of Chains	8
Cell visits	123

Table 6.13: NA-B setup for production forecast and uncertainty quantification in DM_Field.

6.3.4 Results

Figure 6.20 shows the results of history matching and forecasting DM_Field using "intelligent" and uninformative geological prior information. Using the same workflow as proposed in Figure 6.6 the "intelligent" prior information rejected the models that were going to be built using unrealistic combination of geomorphic parameters. In this case 156 out of 1016 models were rejected by the use of intelligent prior information.

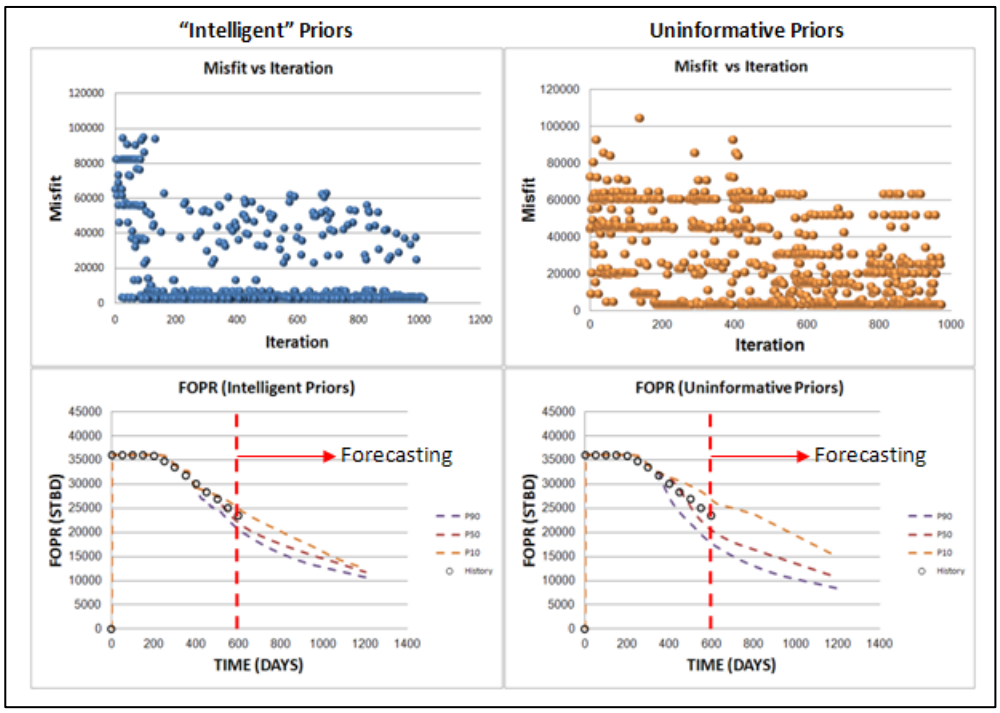

Figure 6.20: Comparison of the history-match process and forecasting production rate for the DM_Field using "intelligent" prior information and uninformative priors.

In Figure 6.20 (top) it is possible to observe that the history-match process converges faster to the lower misfit values using intelligent priors than using uninformative priors, just like it was observed in the case of fluvial meandering channels in Section 6.2. It is also possible to observe the reduction of uncertainty in the forecasted field oil production rate by using intelligent priors (see Figure 6.20 bottom). Figure 6.21 shows a comparison between the values of the geomorphic parameters obtained using "intelligent" and uninformative prior information vs the corresponding model misfit.

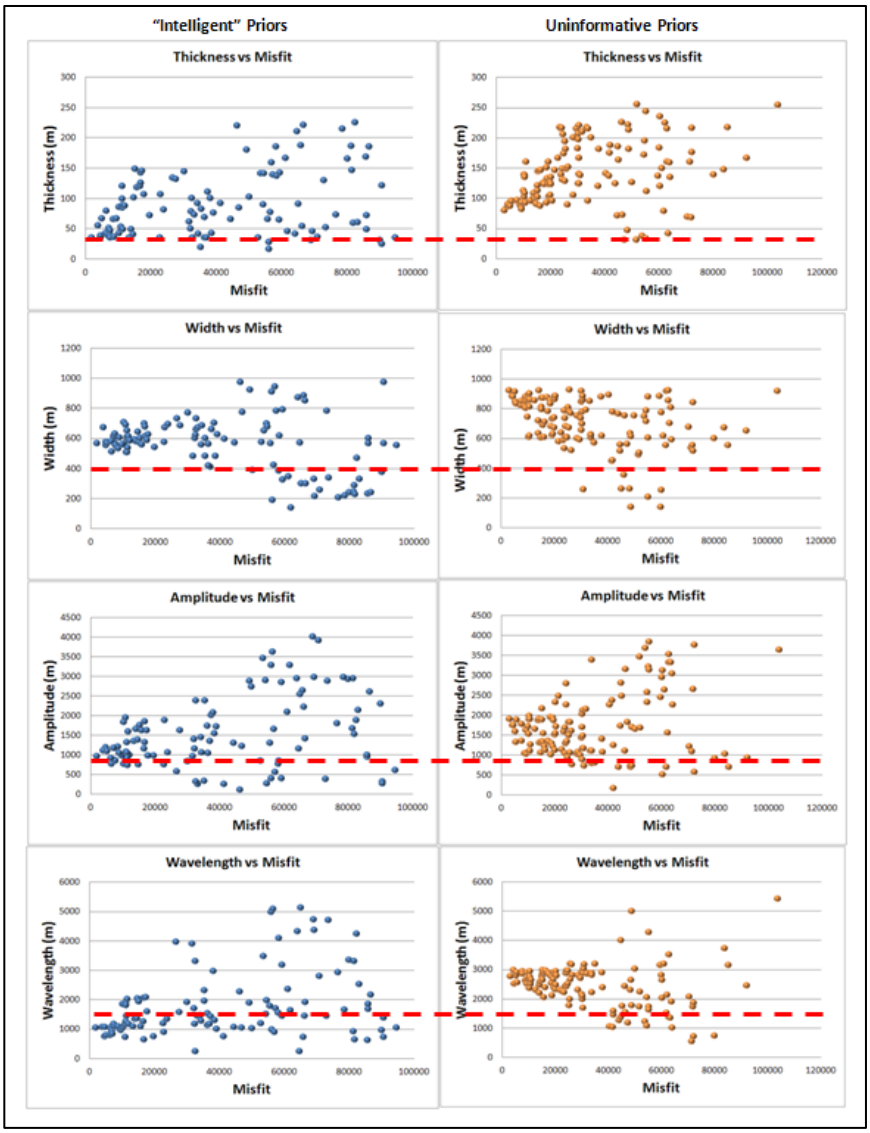

Figure 6.21: Comparison of the plots Parameter vs Misfit related to the models generated using intelligent and uninformative geological prior information.

From Figure 6.21 it is clear that the models with the lowest misfit generated using "intelligent" priors have the geomorphic parameter values closer to the truth case than the models generated using uninformative priors.

The duration of the history match and forecasting processes for the models generated using intelligent sedimentological prior information and the models using uninformative priors are presented in Table 6.14. Although, the duration is similar in both cases (intelligent and uninformative priors) it is clear that there is a reduction in time when using intelligent prior information. As mentioned before, it is important to highlight that these experiments were performed in a desktop work station of 32 GB RAM and 1T Hard Disk Memory, performing these experiments in a cluster will speed-up these processes.

	Intelligent Priors	Uninformative Priors
History Matching	76 hs	104 hs
Forecasting	23 hs	31 hs

Table 6.14 Time used in the processes of history matching and forecasting for models generated using intelligent sedimentological prior information and models generated using uninformative priors, time is measured in hours (hs).

Figure 6.22 illustrates the differences of the facies geometry obtained from different models with realistic combination of geomorphic parameters and their misfits, for the models obtained using flat geological priors compared to the truth case. The facies geometry of the model with the lowest misfit obtained using the intelligent prior information (Fig. 6.22 a) is very similar to the truth case (Fig. 6.22 b). In this case one of the models generated using flat priors (Fig. 6.22 d) had the lowest misfit, however the combination of its geomorphic parameters was

considered as unrealistic. This shows the risk that using uniform priors can generate unrealistic models that can, however, still match history.

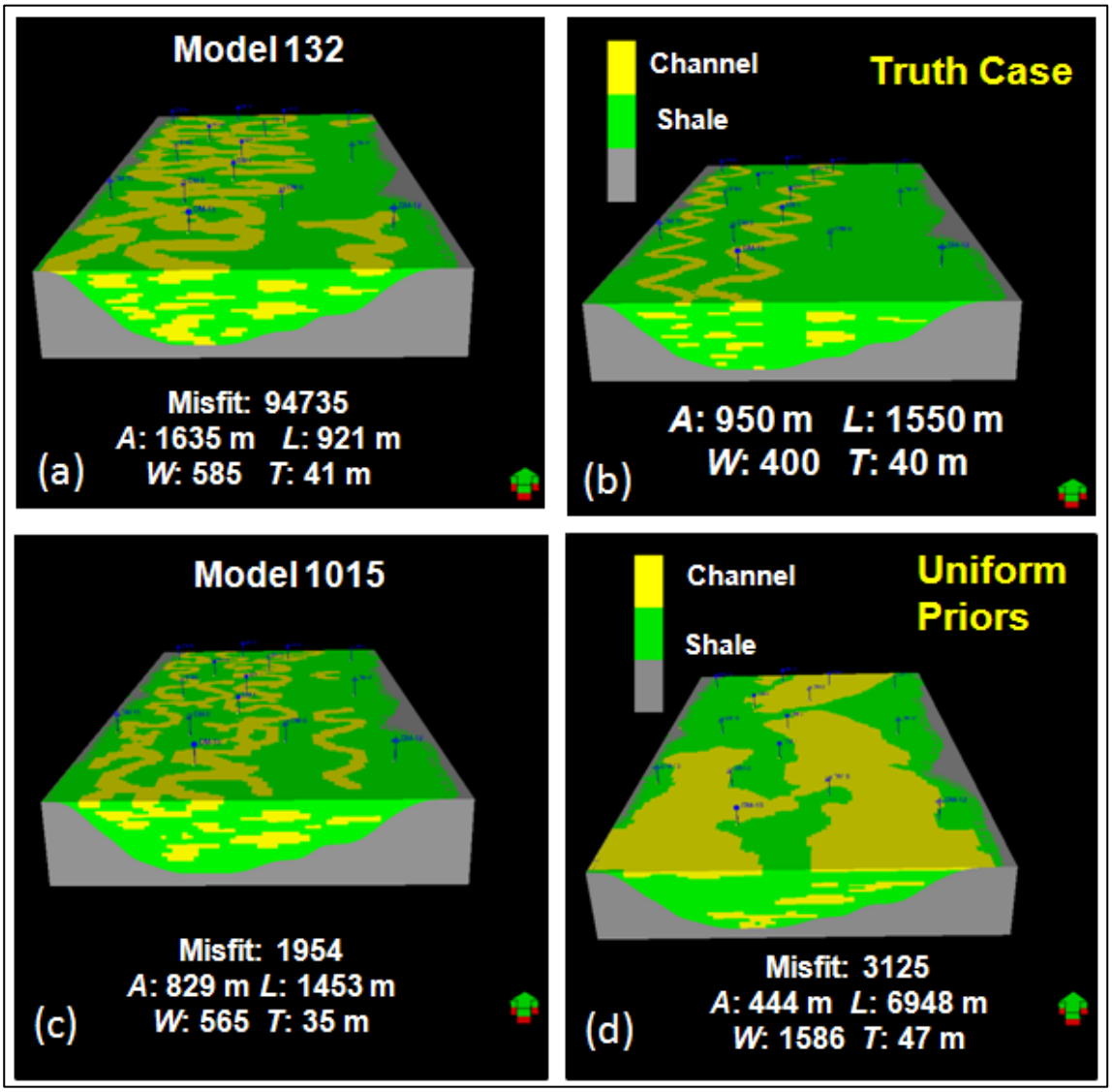

Figure 6.22: 3D Facies distribution in models of the DM_Field. (a) Model with the largest misfit using intelligent Prior Information; (b) Truth Case (c) Model with the lowest misfit using intelligent Prior Information and (d) Model with the lowest misfit using uniformative Prior Information.

6.4 Deltaic Reservoir (Mitare_Field)

Ancient deltas are economically important because they are commonly associated with coal, oil and gas resources (Whateley and Pickering, 1989). That is why deltas have been deeply studied (Bhattacharya and Walker, 1992). Many

hydrocarbon reservoirs have been developed in ancient deltaic sequences preserved in the geological record (Helland-Hansen *et al.,* 1989; Brown and Richards, 1989)

In this section, a synthetic deltaic reservoir is used to history match and forecast its production behaviour, varying geomorphic parameters within a realistic domain. This synthetic reservoir is called Mitare_Field since the geometry and facies distribution was based on the observation of the Mitare river delta, which is a relatively small modern delta developed on the western part of Venezuela described by Rivas *et al.,* (1997).

Sedimentological prior information for deltaic deposits was modelled using the same technique used to model the sedimentological prior information for fluvial meandering channels (Section 6.2) and for deep-marine channel facies (Section 6.3). These sedimentological prior models were used to keep the realism of the facies geometry within the reservoir models produced whilst history matching for uncertainty quantification.

6.4.1 Sedimentological Prior Information

The deltaic geomorphic parameters collected for modelling the prior information to control the facies geometry of a deltaic reservoir model, were taken from 210 observations of modern deltas. The geomorphic information was based on measurement of the main deltaic sub-environments: delta plain and delta front. In this case, prodelta deposits were considered as composed only by shale and no geomorphic measurements were taken from this sub-environment. Table 6.15 shows the geomorphic parameters used to build geological prior models. Appendix C includes all the geomorphic measurements of the delta facies used and their sources.

Deltas Geomorphic Parameters	
Delta Plain	Width (Dw) Thickness (Dt) Length (Dl)
Distributary Channels	Width (Cw) Thickness (Ct) Sinuosity (Cp)
Mouth Bar	Width (MBw) Thickness (MBt) Length (MBl)
Beach Ridges	Width (BRw) Thickness (BRt) Length(BRl)

Table 6.15: Geomorphic parameters used to model the deltaic sedimentological priors

Figure 6.23 is a compilation of 2D plots showing the relationships between all the deltaic geomorphic parameters considered in this thesis to build the geological prior models. From these plots one can infer a direct relationship among most of the geomorphic parameters, which indicates that the hydrodynamic conditions that govern the flow of water and sediments in a deltaic system control as well the geometry of the different deltaic sub-environments. This observation allows the generation of only one region of realistic combination of geomorphic parameters using OC-SVM (Chapter 4). The regions for the realistic prior were created for fluvial meandering and deep-marine channels in a similar way as in the previous section. In the case of deltaic systems the region of realistic combination of geomorphic parameters is within a nine-dimensional space. Each dimension corresponds to a geomorphic parameters for one of the sub-environments: (delta plain: width, thickness and length; distributary channels: width, thickness, sinuosity; mouth bar: width, thickness and length). The values of the One Class SVM hyper-parameters to develop the region of realistic combination of parameters are shown in Table 6.16.

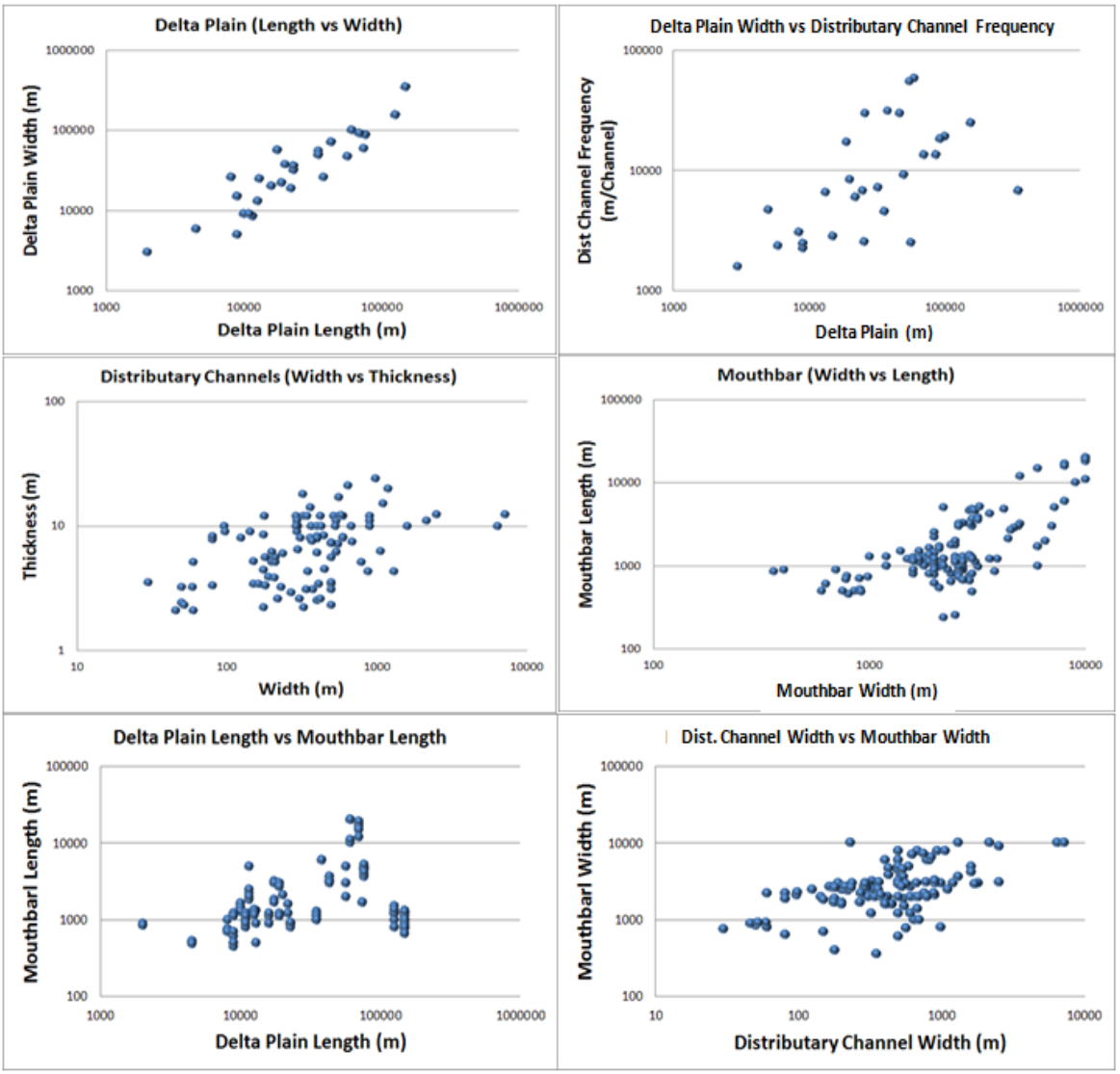

Figure 6.23: 2D Plots of the relationships between delta geomorphic parameters

Hyper-parameter	Value
Kernel Type	Gaussian
Gamma	0.01
η	0.001
Cost (C)	15
A	-75.708
B	2.66178

Table 6.16: One-Class SVM hyper-parameters used to model realistic prior information for deltaic facies geometry.

6.4.2 Delta Geometry using MPS

Like in previous examples (Sections 6.2 and 6.3) the reservoir facies modelling for the deltaic reservoirs was performed using Multiple Point Statistics. One way of modelling sedimentary environments composed by facies with different geometries using MPS is generating regions inside the modelling grid (Remy *et al.,* 2009) and associating these regions to a specific training image.

Figure 6.24 shows that, in the case of the deltaic facies, the simulation grid was separated into 6 regions, regions 1 and 5 are part of the coast surrounding the deltaic plain, sediments that come from the river are reworked and deposited by shoreline currents and waves along the coast, so a training image of beach ridges facies is used for regions 1 and 5. Regions 2, 3 and 4 are part of the deltaic plain where the development of distributary channels is the main characteristic. The shape of the distributary channels is controlled by a training image with sinuous channels. Variation on the *affinity* parameter (Section 2.3.3) controls the width,

thickness and sinuosity of the distributary channels. Region 6 is associated with the deposition of the mouth bars in the deltaic front, a training image with oval-shaped bodies represent the sandy deposits of mouth bars. It is necessary to highlight that in a deltaic progradational process, mouthbar sandy deposits will be connected, generating a finger-shape sand body for each mouth bar/channel.

Variation of the geometry of this facies within each region is controlled by the intelligent priors modelled using OC-SVM.

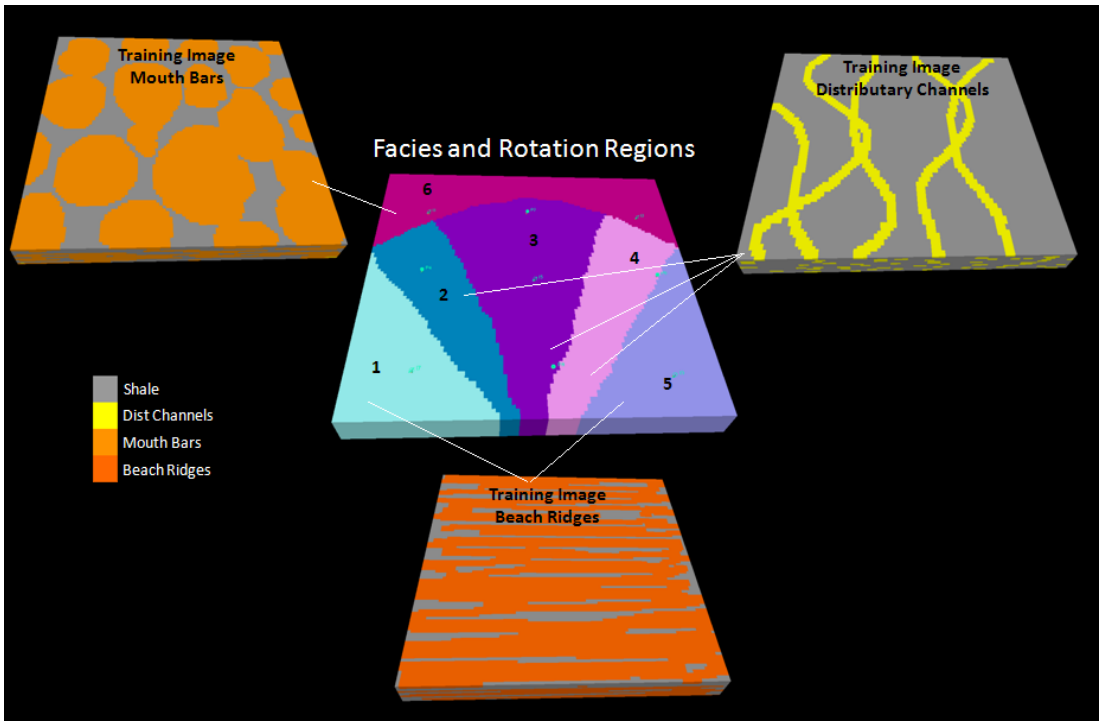

Figure 6.24: Grid regions and training images used for facies models of deltas.

As observed in Figure 5.10 the geometry of the delta system depends on the sedimentological processes that interact in the area where the delta is developed. Varying the shape of the training image in SGeMS (Remy *et al.,* 2009) was the way to model automatically the variation of the delta system geometry. Figure 6.25 illustrates how the variations of the training image geometry can reproduce different geometries of deltaic systems.

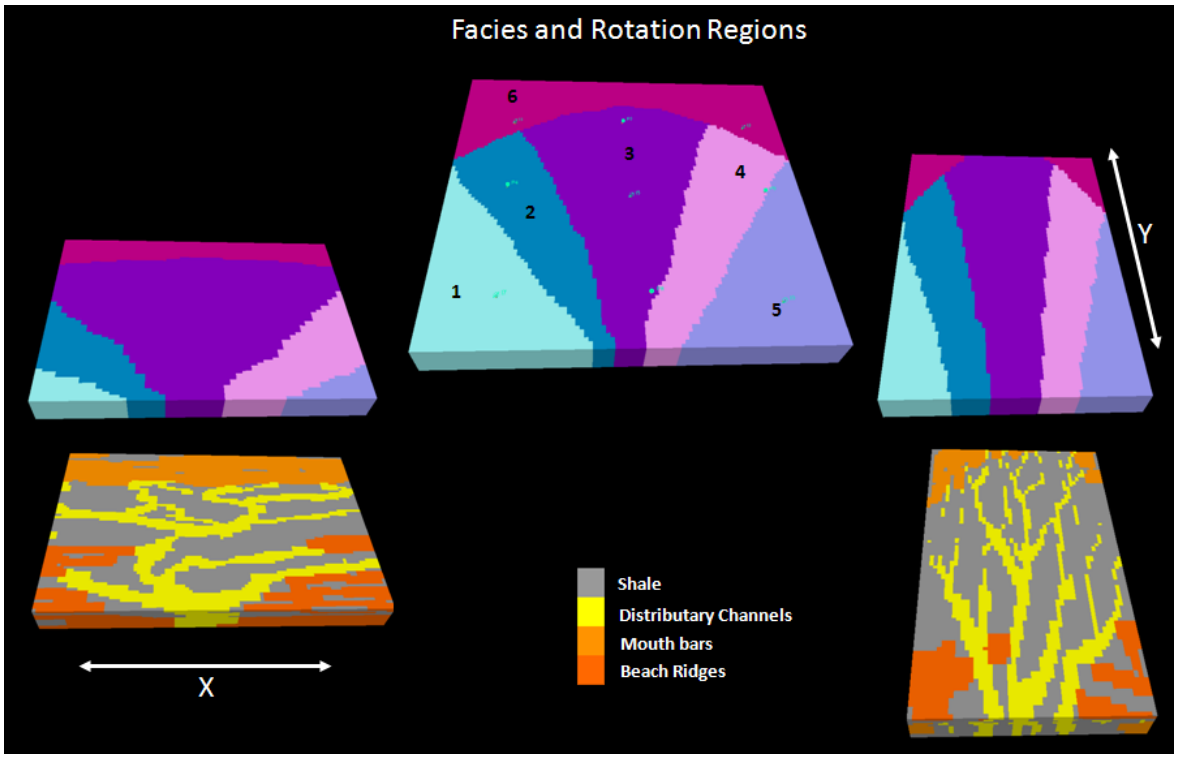

Figure 6.25: Geometry variation of the simulation zones will allow reproduction of different delta geometries. If increasing dimensions in X of the grid would generate geometries similar to cuspate deltas dominated by waves; increasing dimension in axis Y will generate elongated deltas which can be associated to deposits of deltas dominated by rivers. Generating coast-parallel channels would be challenging using this methodology, an extra modelling channel geometry code must be written to allow channels run parallel to the coast.

6.4.3 Reservoir Modelling and History Matching

The truth case used in this example was a synthetic reservoir developed in a deltaic environment and the model was built based on the geometry of a modern delta developed in the western part of Venezuela, the Mitare River Delta (Rivas, *et al.,* 1997). The Mitare River delta was originally a cuspate delta (Section 5.4.1) which had developed beach ridges associated with the effect of the waves over the coast and the river mouth (Rivas *et al.,* 1997). (Section 5.4.1). After changing the hydrological conditions on the coast, the Mitare River delta was transformed

into a fluvial dominated delta (Section 5.4.1), the distributary channels eroded part of the beach ridges deposits and the delta plain prograded (Rivas *et al.,* 1997).

The geomorphic parameters that vary in the automatic history match process are separated in two main steps; the first step is related to the variation of the geometry of the main sub-environments: delta plain and delta front and the second step is based on the variation of the facies geometry and proportion inside every sub-environment. As was shown in Figure 6.23 all the deltaic geomorphic parameters used here are genetically related, by using OC-SVM it is possible to select only realistic combination of these parameters.

Tables 6.17 and 6.18 compile the information about the truth case Mitare-Field and the settings for the automatic history match process respectively. Figure 6.26 is an image of the Mitare-Field (Truth Case) showing the Facies distributions and the different subenvironments present in this synthetic reservoir, as well as the dimensions of the geomorphic parameters of this deltaic system. Fluid and reservoir properties are the same used for the Stanford VI synthetic reservoir (Castro, *et al.,* 2005).

Settings for uncertainty in production forecast

The set-up of the production forecasting and uncertainty quantification was very similar to the one use in sections 6.2 and 6.3 (Table 6.19).

6.4.4 Results

In this section facies proportions were included as geological parameters for history matching. Figure 6.27 is a comparison of the history matching results obtained in the case of using the 9 geomorphic parameters of deltaic facies and the case of including facies proportions within the history-match process.

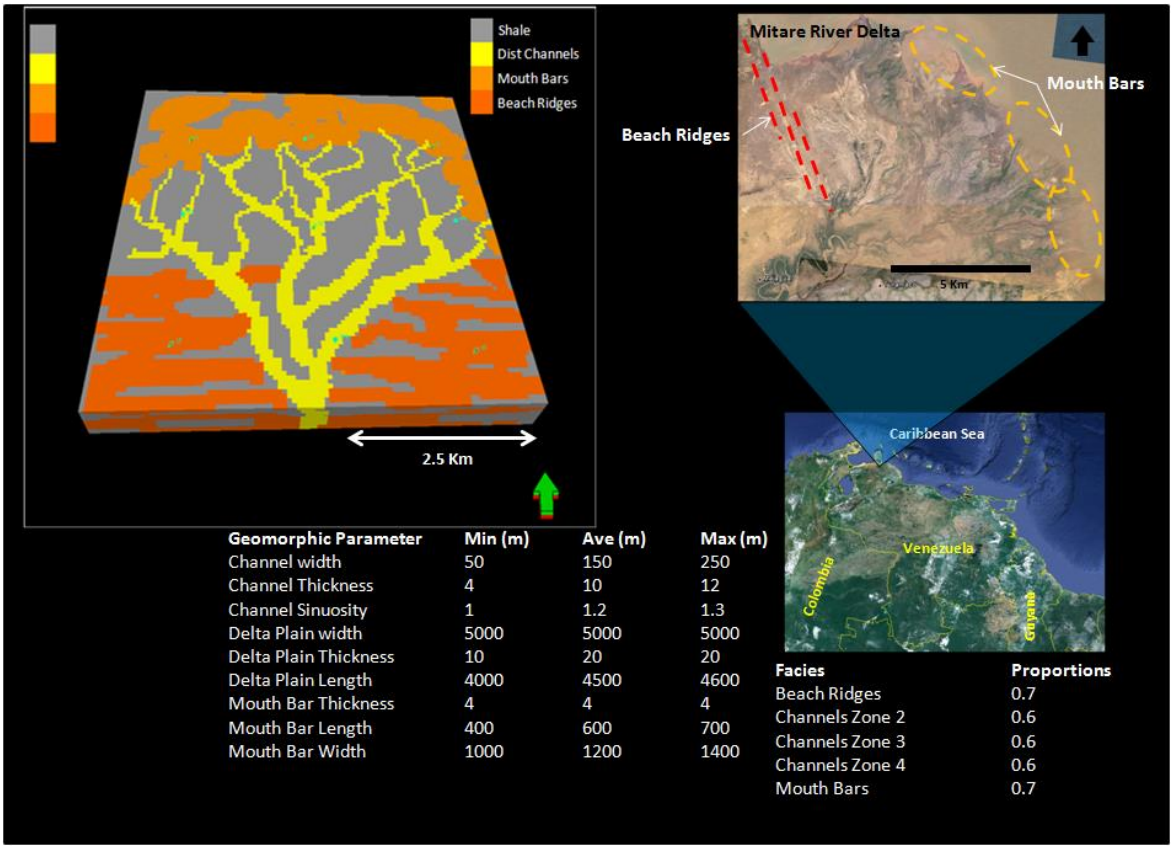

Geomorphic Parameter	Min (m)	Ave (m)	Max (m)
Channel width	50	150	250
Channel Thickness	4	10	12
Channel Sinuosity	1	1.2	1.3
Delta Plain width	5000	5000	5000
Delta Plain Thickness	10	20	20
Delta Plain Length	4000	4500	4600
Mouth Bar Thickness	4	4	4
Mouth Bar Length	400	600	700
Mouth Bar Width	1000	1200	1400

Facies	Proportions
Beach Ridges	0.7
Channels Zone 2	0.6
Channels Zone 3	0.6
Channels Zone 4	0.6
Mouth Bars	0.7

Figure 6.26: Mitare Synthetic Reservoir, with the current location of the Mitare river delta in Western Venezuela. Images of Mitare River Delta were taken from **Google** earth 2012. Beach ridges are highlighted in red and mouthbars in yellow on the Mitare satellite image.

We can observe that, when facies proportions are included as parameters, the history match process converges slower than in the case of using fixed facies proportions. This is due to the increment in the number of dimensions of the parameter space. Increasing the dimensions of the parameter space requires more models to explore a larger space. It is important to highlight that in both cases of this study (fixed and variable facies proportions) the number of models rejected by the use of “intelligent” prior information were similar in both cases: 177 and 187 for fixed and variable facies proportion respectively.

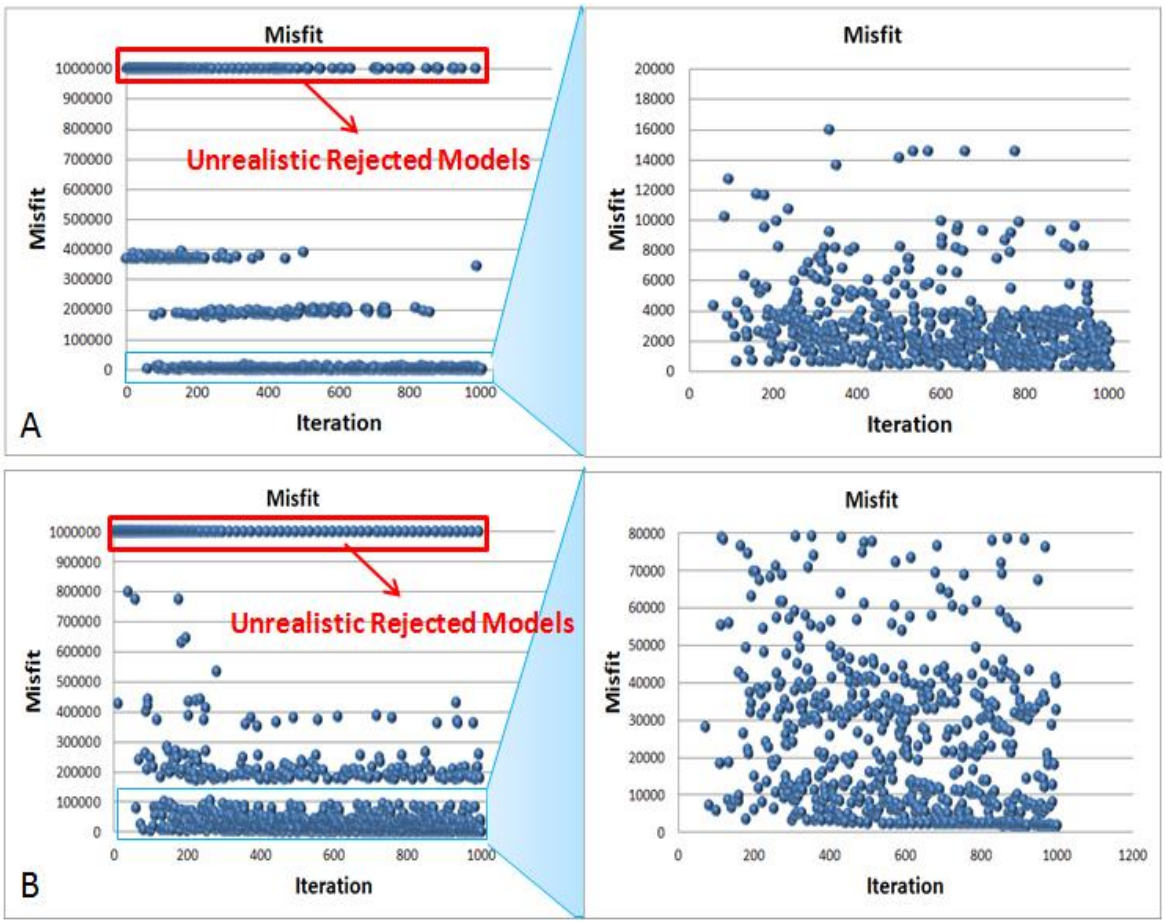

Figure 6.27: Effect of including facies proportions as a parameter in the automatic history-match process: Plots of Misfit vs Iteration (and zoom in the range of the lowest misfits) in the history match process. A) Using fixed facies proportions; B) Including uncertain facies proportions as additional geological parameter for history-matching. Within the red rectangle are the models rejected by the use of intelligent prior information. History matching with uncertain facies proportions (B) converge slower than the when the facies proportions has been fixed (A), since including facies proportions increases the dimensions of the parameter space.

Mitare_Field Props	Values
Wells	4 Producers 5 Injectors
Fluids Density (lb/ft^3)	Oil: 45.09 Water: 61.8
Fluids Viscosity (cp)	Oil: 1.18 Water: 0.325
Formation Volume Factor	Oil: 0.98 Water: 1.0
Number of Cells	200 000 100x100x20
Cell size	X: 50 m Y: 50 m Z: 2 m
Top Reservoir Depth	2000 ft (TVD)
OWC	6000 ft (TVD)

Table 6.17: Reservoir Properties Mitare Field.

Figure 6.28 is a comparison between the forecasting of the Mitare_Field reservoir, considering fixed and variable facies proportions as a geological parameters. It is possible to observe that the uncertainty increases when facies proportions are included in the history-match process. Increasing the number of parameters to sample increases the dimensions of the parameter space. In this case, if 5 proportion parameters for each facie are included in the history match framework (Table 6.18), results in a larger uncertainty in forecasting compared to the case that considers the facies proportions being fixed. Reducing the ranges of facies proportion by using “intelligent” prior information would make the sampling process more efficient.

History Match Set Up Mitare Field		
Geomorphic Parameters and Ranges	Chanel Width Channel Thickness Channel Sinuosity Mouth Bar Thickness Mouth Bar Width Mouth Bar Length Delta Plain Length Delta Plain Width Delta Plain Thickness	50– 1000 m 5 – 20 m 1 – 2 m 5 – 50 m 300-5000 m 300-5000 m 3000-30000 m 3000-30000 m 20-200 m
Facies Proportions Ranges	Channel - Zone 2 Channel - Zone 3 Channel - Zone 4 Mouth Bar Beach Ridges	20 - 80 % 20 - 80 % 20 - 80 % 20 - 80 % 70 -90 %
Total Number of Models	1000	
Minimum Misfit	500	
Sigma	500 (STBD)	
Sampling Algorithm:	**Particle Swarm Optimization**	
No of Particles	20	
Group Size	4	
Initial Inertia	0.9	
Initial Decay	0.9	
Congnitive Component	1.333	
Group Component	1.333	
Social Component	1.333	
Min steps	5	
Energy Retention	0.8	
Particle Behaviour	Flexible	

Table 6.18: History Match setup for Mitare Field.

NA-B Set Up Mitare_Field	
Chain Length	200,000
Burning Period	100,000
Number of Chains	8
Cell visits	23

Table 6.19: Forecasting NA-B setup for Mitare Field.

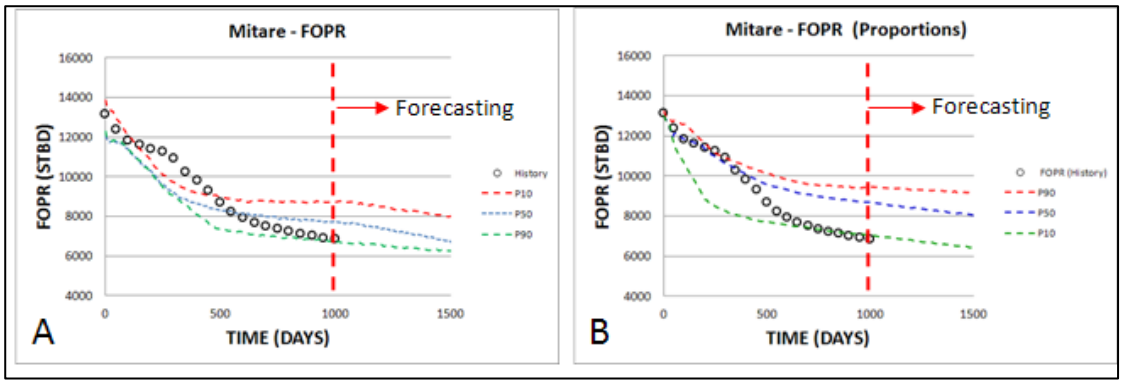

Figure: 6.28 Comparison of forecasting and uncertainty quantification between (A) the case of fixed facies proportions and (B) the case of varying proportions. It is clear that in the case of the Mitare_Field reservoir, P10-P90 ranges were wider than P10-P90 ranges in other cases (DM_field and Stanford VI) this is due to the fact that Mitare_Field does not have seismic data to condition facies simulation.

Figure 6.29 illustrates some of the parameters associated with the lowest misfit models obtained through the process of automatic history-matching for the study cases using fixed (blue points) and variable (red points) facies proportions.

In Figure 6.29 values of delta plain length and mouth bar width seem to be trapped in a local minimum away from the truth case value. This is due to the fact that the geomorphic parameters like Delta Plain Length and Mouth bar width have relatively large dimensions and a high connectivity. These local minima generate models whose facies geometry does not produce big changes in the reservoir model fluid flow.

Figure 6.30 (A) compares the geomorphic parameters of the truth case and the geomorphic parameters obtained in the models with the lowest misfit, for fixed facies proportions (Case A) and variable proportions (Case B). Figure 6.30 (B) compares the facies proportions obtained in the models with the lowest misfit and the truth case (only for Case B). Figure 6.30 shows that the parameters obtained in the models with the lowest misfit are very similar to the parameters in the truth case apart from the proportions in Zone 2.

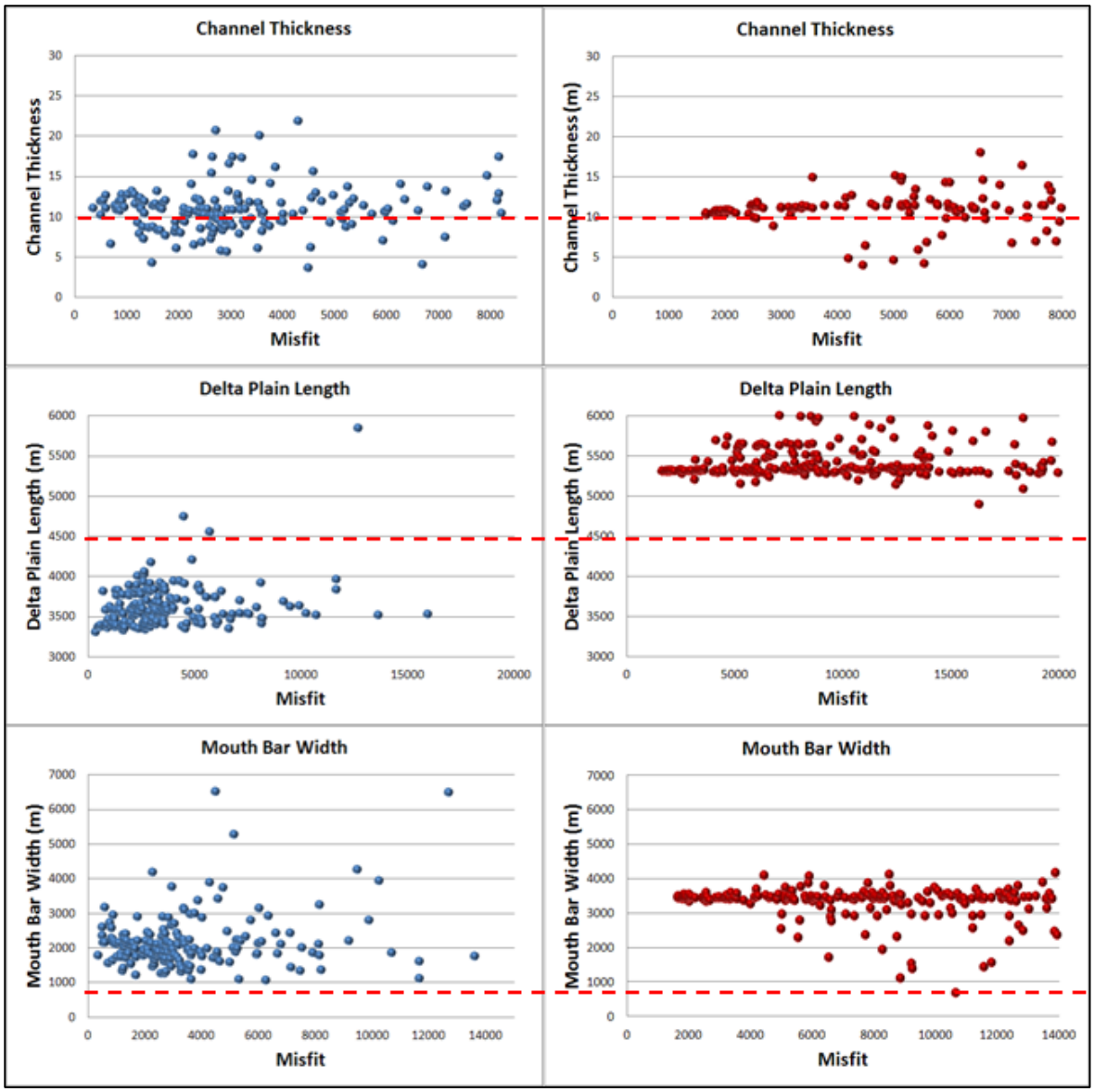

Figure 6.29: Plots of geomorphic parameters vs misfit, comparing results obtained with fixed (blue points) and variable (red points) facies proportions. Dashed red lines are the truth case values. For fixed facies proportions we can observe that the values of the geomorphic parameters try to converge towards the truth case value, with the exception of the delta plain. This can be due to the fact that in a delta plain with these dimensions (5400 m length) it is possible to develop very similar deltaic deposits to the deposits generated in a delta plain with a length of 4500 m (truth case). In the case of variable facies proportions, the values of the geomorphic parameters converge far from the truth case value; this can be due to the necessity of more models in order explore the parameter space and escape from the local minimum.

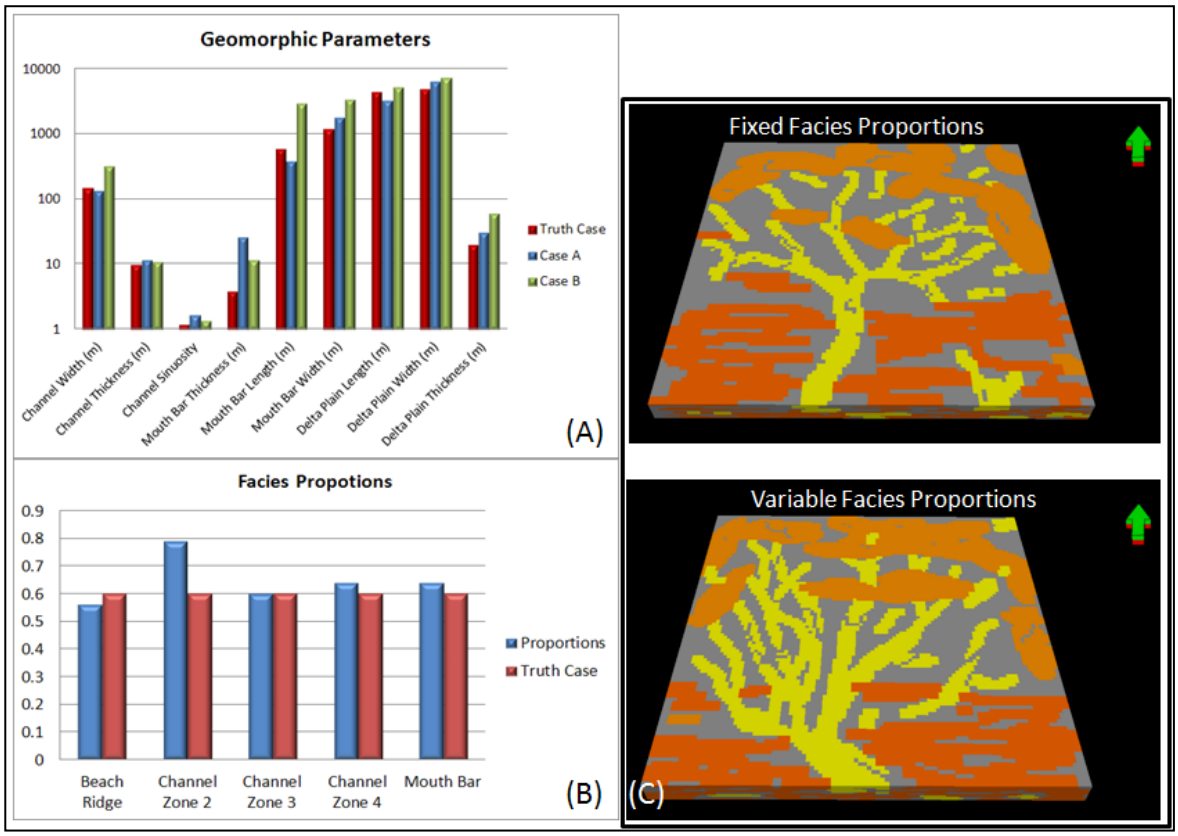

Figure 6.30: Differences between geological parameters of the truth case and the models with the lowest misfit. (A) Geomorphic parameters Case A is for models with fixed facies proportions and Case B is for models with variable facies proportions; (B) is only for models with variable facies proportions; (C) Models with the lowest misfit: Model 834 of fixed facies proportions and Model 923 of variable proportions.

6.5 Summary

In this chapter it was shown how to include the geological prior information on different depositional environments within the history matching workflow. The depositional environments modelled in this chapter were: meandering fluvial channels, deep-marine channels and deltaic deposits.

There were generated geological prior distribution models for each of these environments. The prior models were built using One-Class SVM, a machine learning technique that is used to detect novelty and one-class classification.

The workflow for automatic history matching begins by selecting a combination of model parameter values and these parameters are compared to the “intelligent” priors. If the combination of the parameter values is considered as realistic, then the model is generated stochastically, flow simulated and history matched. If the combination of the parameters is considered as unrealistic, then the model is rejected and a penalty misfit value of 1,000,000 is assigned to this model to mitigate its impact in the inference for the forecasting.

The use of intelligent prior models allowed the rejection of models that were going to be generated using an unrealistic combination of geological parameters, which saved computing time. It was observed that the when using “intelligent” geological priors the history match process converges faster than when using uninformative priors, since the algorithm tends to sample from the reduced parameter space controlled by the realistic combination of geological parameters (Sections 6.2 and 6.3).

It was experienced in Section 6.4.4 (Figure 6.28), that adding extra parameters (facies proportions) to the history-matching workflow increases the parameter space and then the exploration of this space results in the increase of the number of iterations to achieve the history-match.

It is necessary to mention that, the Mitare_Field result showed a good improvement in the automatic history match process like: (1) automatically varying the geometry of the deltaic system and (2) modelling different facies in the same reservoir (channels, mouth bar, shale and beach ridges). However, the geometry of some of these facies (e.g. mouth bars) and the spatial relationship between facies (distributary channel- beach ridges) should be improved, in order to obtain more realistic models.

Chapter 7

Improvements in the Workflow for Reservoir Facies Modelling in Automatic History Matching

7.1 Introduction

The workflow for automatic reservoir history matching proposed in this thesis (Chapter 6) suggested the use of intelligent prior information to control the realism of the uncertain geobodies' geometry in the reservoir models. The use of intelligent priors reduced the number of models generated to reach a desired production fit quality in history matching process. This reduces the computational time and guarantees that all the models obtained during the automatic process of history matching feature realistic combination of geomorphic parameters. However, some issues in history matching arose from the results obtained in Chapter 6. The three main problems observed addressed in this chapter using different techniques are:

(1) uncertainty of the geological scenario; (2) variation of the facies proportion; (3) connectivity variation across stochastic realisations.

(1) One of the largest uncertainties in reservoir models is the interpretation of the sedimentary environment. A mistaken interpretation of a depositional environment could mislead the facies and petrophysical distribution in a reservoir model. In Multiple Point Statistics approach the conceptual geological scenario of a reservoir model is represented by a Training Image (Chapter 3). Finding a way to use multiple training images or multiple sedimentological interpretations of a model gives the opportunity to consider different interpretations and allows the workflow to find the interpretation(s) that best matches the production history of a reservoir.

(2) Another important point is the vertical variation of facies proportions. Including the vertical variation of facies proportions within the automatic history-matching workflow (Chapter 2) will help in the interpretation of how the facies distributions vary vertically within the reservoir.

(3) History matching individual well production is a challenge; in fact this is one of the most common problems found in automatic history matching. In this thesis, the main reason for this problem has been associated with the connectivity of the facies bodies. In this chapter, a simple technique that measures the facies connectivity is proposed. This technique can easily be included into the automatic history matching workflow and used to select a facies model from multiple realizations, based on a criterion related to the expected facies connectivity of a reservoir.

7.2 Multiple training images - an internal parameter in MPS

One of the major uncertainties in reservoir modelling or more specifically in facies modelling is the interpretation of the depositional environment (Chapter 1). The interpretation of a reservoir depositional environment has an enormous impact on reserves estimation and on estimating the tortuosity of the fluid flow in a reservoir

model. A reservoir developed in a fluvial-dominated deltaic environment has a different distribution of reservoir facies than a reservoir developed in sandy shoreface settings, which implies differences in fluid accumulations and fluid production behaviour.

Availability of the data for depositional environment interpretation always has been an issue in reservoir characterization. Lack of reliable data for sedimentological interpretation inflates uncertainty of the reservoir description and modelling. Depositional environment interpretation of a reservoir based on outcrops description is always risky, since sedimentary facies may vary from outcrops to the reservoir; thus, one could be generating a facies model very different from the actual reservoir facies distribution. If the sedimentological interpretation is based on core description the risk of a misinterpretation could be related to the lateral extension of the facies. Cores are partially continuous vertical rock samples that have a diameter no larger than 6 inches, which gives plenty of space to introduce uncertainty within the lateral extension of facies. Based on expert criteria and with the use of other data if available, (palaeontology and high resolution seismic attributes) the uncertainty in facies interpretation could be reduced.

As discussed in Chapter 2, MPS is a geostatistical technique based on a training image. In facies modelling using MPS, the training image represents a geological concept of the facies distribution. Training images could be based on modern depositional environments, object based models, high resolution seismic or process based simulations (Chapter 2).

The use of multiple training images in the automatic history matching process could give a new insight to the problem of the facies interpretation and modelling. Since a training image is a geological concept, if it is possible to consider different geological concepts (i.e. sedimentary environment interpretations) to generate a facies model and history match it, then it would be possible to validate the selection of the training image or the geological concept by matching the historical production data of a reservoir.

This alternative has been presented by Park *et al.* (2013), where they compared the production profile of a reservoir developed in deep-marine settings with the production response of reservoir models obtained using different training images (geological concepts). This comparison is made within the Euclidian space, using Multidimensional Scaling (MDS). With this comparison the training images that generate models non-consistent with the production data are rejected (without history matching). Finally, the training images that lead to the models with production profiles very similar to the actual reservoir production data were identified.

In the next section a similar methodology is presented, but here the idea is to use the optimization algorithm (Particle Swarm Optimization) described in Chapter 3, to select the training images that correspond to the models that best reproduce the historical production data of a reservoir.

7.2.1 Sampling from multiple Training Images

The main problem is to generate a robust and consistent way of sampling from a number of training images. The simplest option is to let the algorithm (PSO) sample from a discrete succession of training images. However, this methodology could bring the problem of identifying the optimal number of training images that can be used in the process of training image selection. Also, there would be a problem with identifying the metric and establishing the continuity in the sampling space. A possible answer to this problem can be found by generating a manifold of realizations, where the realizations generated for a specific training image are clustered and can be separated from the realizations generated from different training images.

An example of choosing from different training images was presented by Park *et al.* (2013). Figure 7.1 is a 2D plot using Multidimensional Scaling (MDS) extracted from the work of Park *et al.* (2013) relating the production responses of the models generated with multiples training images and the actual production data of the

field. Park *et al.* (2013) used MDS to compare different responses of production data obtained from different simulations (discretized by the training image that was used to generate the models) with the actual production data. This allows selection of the training images that generated models whose production response is close to the actual production data.

Multidimesional Scaling (MDS) is considered as a family of methods that construct a configuration of points in a target Euclidean space (Leeuw and Heiser, 1982) from information about interpoint distances (Lee and Verleysen, 2007). The theory of MDS is explained in Appendix D.

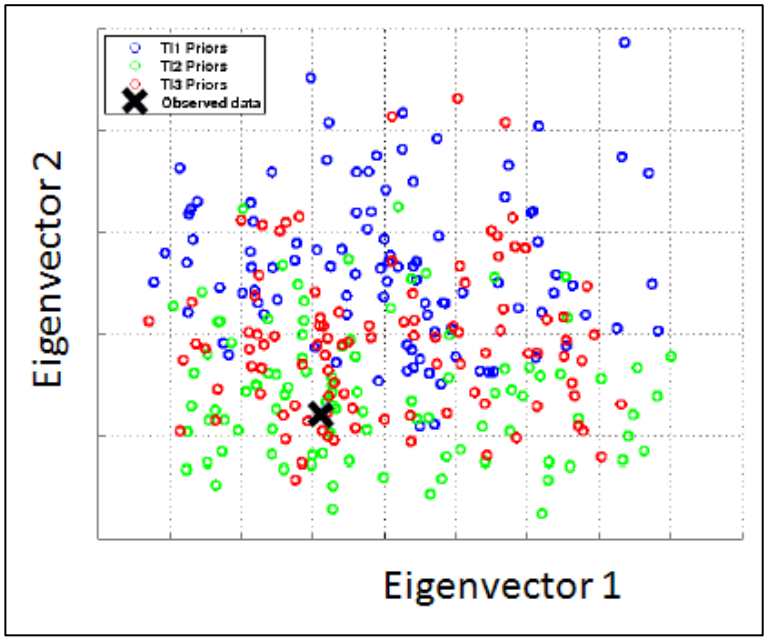

Figure 7.1: MDS plot in 2D of the production response of model generated with different training images. **X** is the production history of the reservoir; the coloured circles represent the production behaviour of the models generated with different training images: blue production behaviour of models generated using TI 1; green production of the models using TI 2 and red production of the models using TI 3 (from Park *et al.,* 2012).

In this Section, MDS is used to generate a configuration in the Euclidean space (Figure 7.2) in which 150 facies models are generated by three different training images. MDS provides a metric to establish the relation between the realisations.

These models cluster in three different regions of this Euclidean metric space. The models of each cluster were generated with a particular training image. This can be observed in Figure 7.2 (a) where each point represents a model realisation; the models are colour coded to the corresponding training image that originated the model (i.e. red points are the models generated with training image 2, blue points were generated with training image 1 and green points with training image 3).

The metric space was defined with the first 8 eigen-vectors (dimensions), which are the vectors that explain 99% of the data analysed (Figure 7.2 b). For visualization purposes, the matrix space was illustrated in a two-dimensional plot (Figure 7.2 a and c) using the first 2 eigen-vectors.

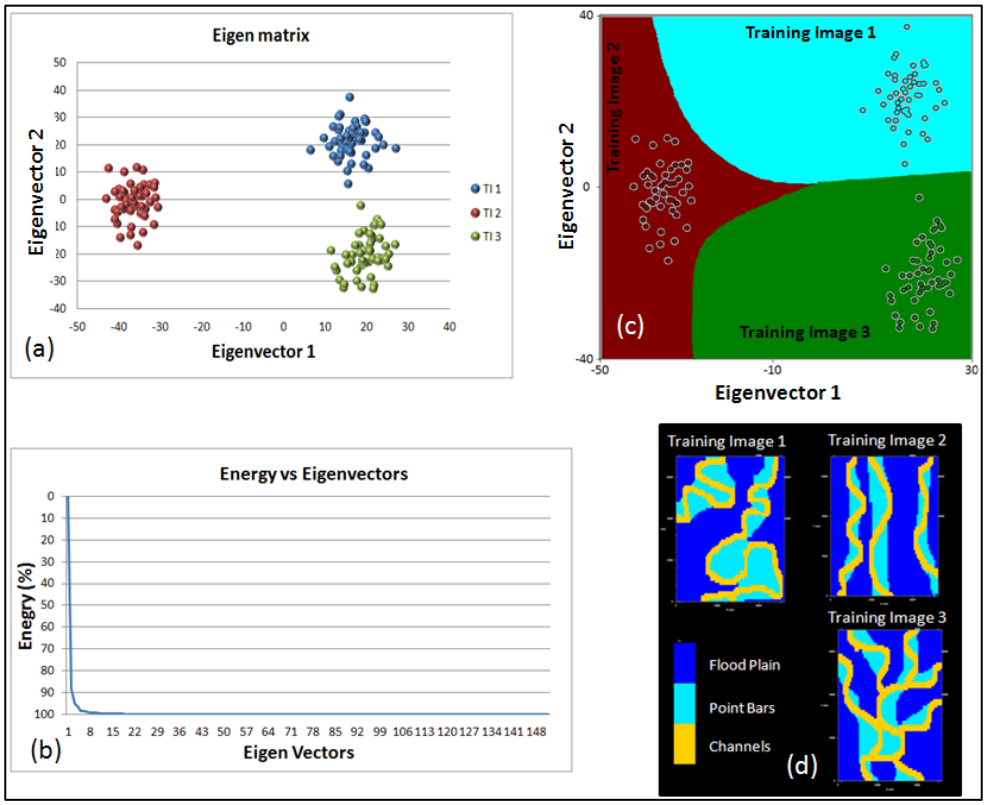

Figure 7.2: MDS plot comparing the facies models generated using three different training images (d). (b) is the representation of the energy of the MDS system described by the 150 eigen-vectors, with 8 eigen-vectors it was possible to describe 99% of the energy data. The energy of the system is the number of the eigen-vectors that better describe the data (Appendix D.4) (c) SVM classification to identify the regions in the eigen space that belong to each of the training images.

After generating an eigen-value matrix in an 8-dimensional space, the regions of this matrix are classified depending on the number of training images used for modelling by using Support Vector Machine (SVM) (Chapter 3). Figure 7.2c is a representation of this matrix in 2D, where it is possible to distinguish between the models generated with different training images.

Each training image represents a different geological interpretation. Using this methodology it is possible to observe the region in Euclidean space described with a specific training image (geological concept).

Figure 7.2c can be considered as a representation of the geological regions in the Euclidian space described by different training images. Training Image "1" is a representation of a meandering channel system (this training image was used in the reservoir modelling process in Section 6.2); training image "3" is characterized by a network of anastomosed channels with development of meanders and point bars and training image "2" is a 3D exemplification of straight channels with the development of some meanders and point bars. These three training images represent three different concepts of facies distributions that could be hard to distinguish with a core description. A new training image could be included, by plotting the facies models generated with the new training image. A new training image could be included as a plausible geological concept if it describes a region not explored by the previous training images, or should be excluded if models based on the new training image describe areas in the Euclidean space that already were described by the previous training images.

7.2.2 Application (Meandering Channels)

The use of multiple training images was implemented within the automatic history matching framework proposed in Chapter 6. Figure 7.3 illustrates the arrangement of the workflow including multiple training images.

In this case, a realistic combination of geomorphic parameters for fluvial meandering deposits is selected for the MPS mode input. Also, the metric space is

then adaptively sampled for a location and the corresponding training image is selected according to the classified region in the metric space to generate a further MPS realisation for flow simulation. By evaluating the misfit function between the model response and the production history (*eq*. 3.1) the optimization algorithm will update the posterior distribution in order to select the training image that generates the reservoir model that better reproduce the field production history.

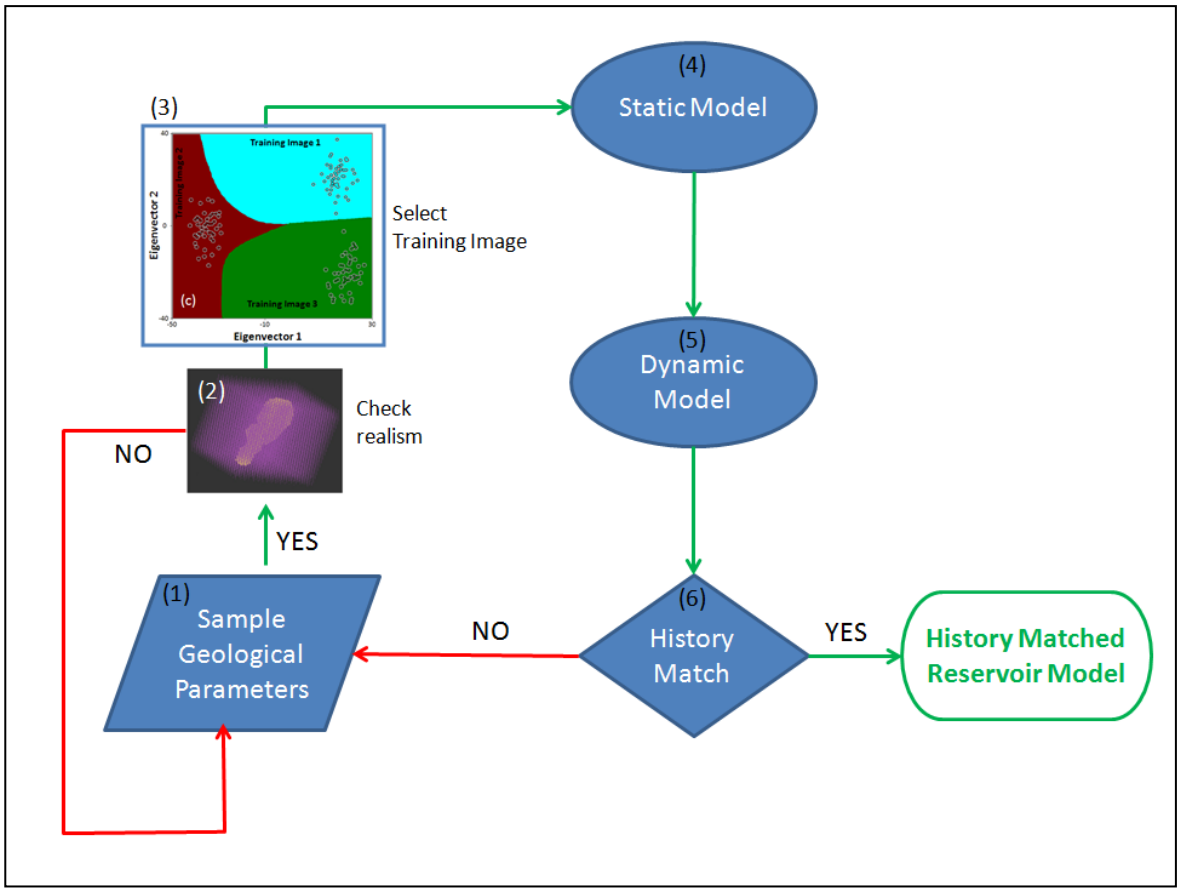

Figure 7.3: Workflow for history matching including Multiple training images selection: (1) Sample a combination of geomorphic parameters from an uniform; (2) Analyze if the combination of parameters is realistic; (3) Select a training image using the MDS-SVM technique; (4) Generate a geological model; (5) Flow simulation; (6) History Match the model; Begin the cycle again until the stop criterion is met (e.g. number of iterations, good history match models).

In order to use this workflow, the selected truth case was the second stratigraphic unit of the Stanford VI synthetic reservoir (Section 6.2). This stratigraphic unit is composed of fluvial meandering deposits. This synthetic reservoir is going to be used throughout this chapter to apply the proposed workflow improvements and make coherent the comparison of the obtained results.

7.2.3 History Match and Uncertainty quantification

The properties of the Stanford VI reservoir are the same as shown in section 6.2. In this section the eight eigenvalues are included as parameters to sample from and select the selected training image. Table 7.1 summarises the history match settings for this case. The forecasting using NA-Bayes was setup using the same parameters as in the case shown in Section 6.2.

History Match Set Up		
Geomorphic Parameters and Ranges	Chanel Width Channel Thickness Meander Amplitude Meander Wavelength	100 – 600 m 5 – 200 m 500 – 3000 m 500 – 3000 m
eigenvalues	All 8 eigen values have the same range (-50 to 50)	
Total Number of Models	1000	
Minimum Misfit	2000	
Sigma	6000 (STBD)	
Sampling Algorithm:	**Particle Swarm Optimization**	
No of Particles	20	
Group Size	4	
Initial Inertia	0.9	
Initial Decay	0.9	
Congnitive Component	1.333	
Group Component	1.333	
Social Component	1.333	
Min steps	5	
Energy Retention	0.8	
Particle Behaviour	Flexible	

Table 7.1: History Match setup

7.2.4 Results

This methodology differs from the one proposed by Parks *et al.* (2012) mainly in the sense that the MDS-SVM classification plot. In this thesis, identification of the geological regions within the Euclidian space corresponding to each training image prevents the use of different training images that do not lead to good history match.. Parks *et al.* (2013) used the MDS plot to compare the production of few models with the actual production of a reservoir (pre-history matching any model) and select the training images that generate the models with production closest to the actual reservoir production. As explained before, the inclusion of multiple training images into the automatic history match framework gives the option of using different possible geological interpretations (prior information). This provides more flexibility in history matching to find better models realisations from different geological scenarios.

Figure 7.4 illustrates the misfits obtained with the reservoir models in the history matching process and a compares with the misfit obtained in Section 6.2, when modelling the same reservoir but with a single training image. We can observe that a lower misfit is reached in the case of multiple training images and that the range of misfit (under 3000) is narrower when using multiple training images. Figure 7.4 illustrates how the inclusion of multiple training images (b) reduced the misfit when compared to history matching models with a single training image. From Figure 7.4 it is clear that the lowest misfit has been reduced from 3366 in case (a) to 2794 in case (b). This can be associated with the fact that in case (b) the models with the lowest misfit were generated with a training image that describes the facies distribution of the reservoir better than the models generated with the single training image used in case (a). This is only possible by having the opportunity to sample from different training images.

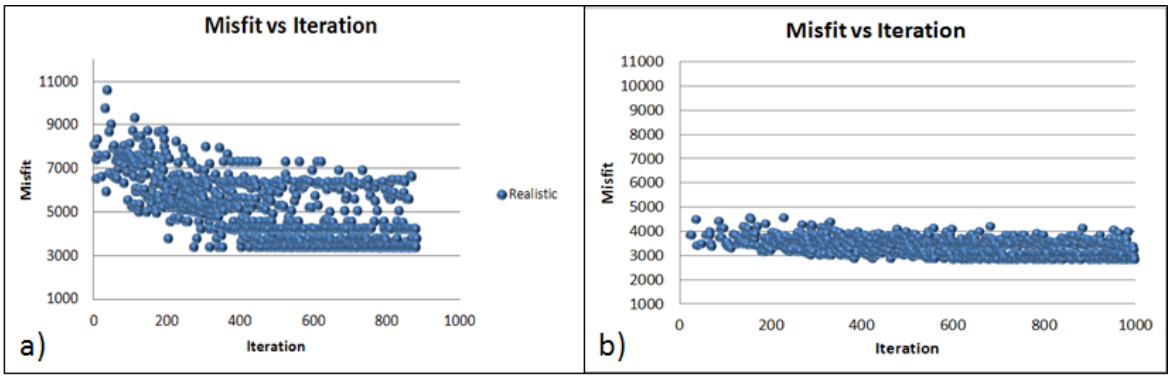

Figure 7.4: Comparison between the misfit evolution of the case of using a) one training image and b) the case of using multiple training images. Note that case b starts better than case a, this is due to the randomness in the parameter selection associated with the optimization algorithm, PSO.

Figure 7.5 is a comparison between history match and the forecast of the oil production rate (WOPR) of three wells, obtained when using one training image and multiple training images.

The use of multiple training images reduced the uncertainty in wells 12 and 5, but in well 1 the uncertainty (range P10-P90) increased. This can be due to local effects of the facies distribution close to Well-1.

Figure 7.6 compares the geomorphic parameters obtained with the models with the lowest misfit using multiple or a single training image. The results shown in Figure 7.6 are very similar and very close to the truth case. Note, channel wavelength and amplitude for the best history matched obtained with multiple training images are closer to the ones of the truth case, because the choice between multiple training images provides a better control over planar/lateral variation of the meander geometry. However, the width and the thickness for the best history match with a single training image are closer to the ones of the truth case because these parameters are less variable across the multiple training images. .

In Figure 7.7, we can see the eigen-values (red dashed square) of the first and second eigenvectors that are converging during the process of history matching

and when plotting them within the MDS plot it is possible to observe that the training images selected are TI 1 and TI 3, which are the geological concepts that best describe the reservoir and are more similar to the truth case (Figure 6.7).

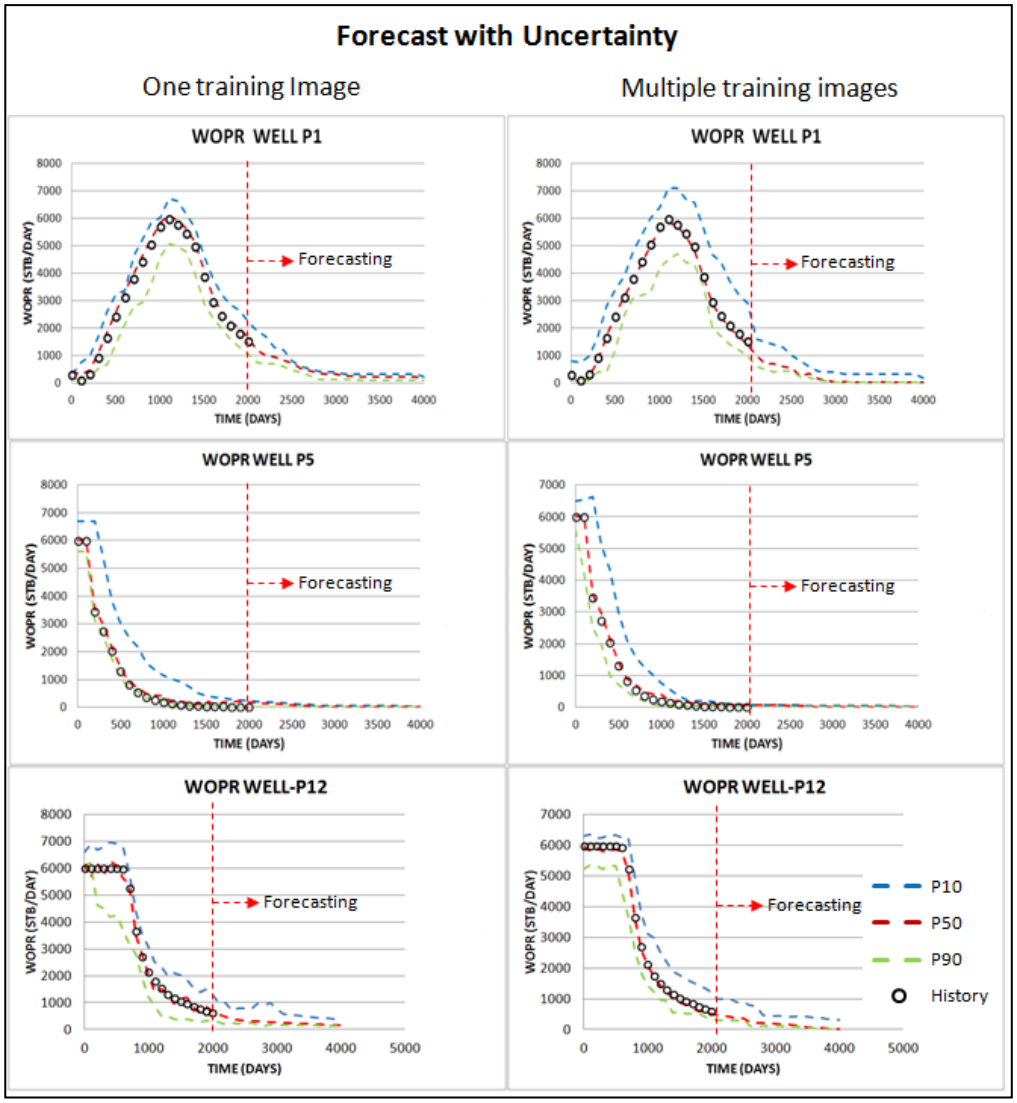

Figure 7.5: Comparison between the history matching and forecasting of the oil production rate (WOPR) in three wells, considering models using a single training image and using multiple training images.

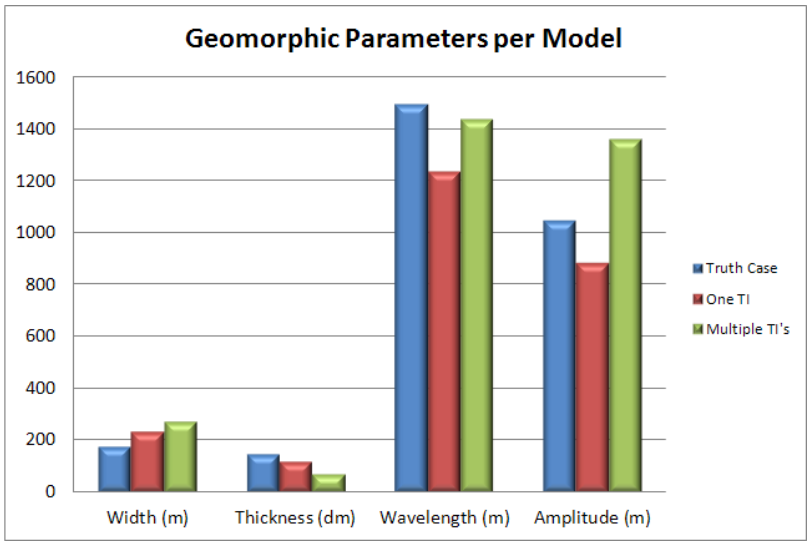

Figure 7.6: Comparison of geomorphic parameters with minimum misfit with the models generated with one and multiple training images.

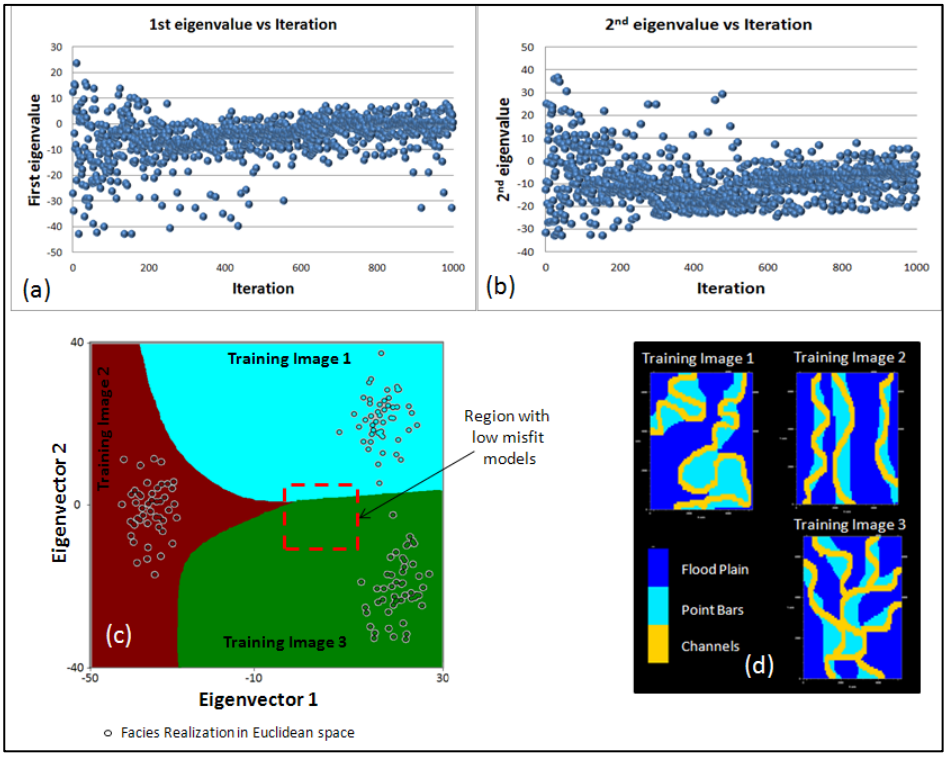

Figure 7.7: Convergence of the values for first and second eigenvalues (a) and (b); (c) area (red square) with the eigenvalues that generated the models with the lowest misfit. Training mage regions were defined using SVM, these regions represent the fields of the Euclidean space described by each training image. (d) facies geometry in the training images.

Comparing the production forecast of the models using a single training image (Figure 7.8) and the models that include multiple training images it is possible to observe that there is a reduction in uncertainty when using multiple training images. This reduction could be associated to the selection of a different training image (TI 3) from the one used in the models with one training image (TI 1). This is suggested in Figure 7.7.

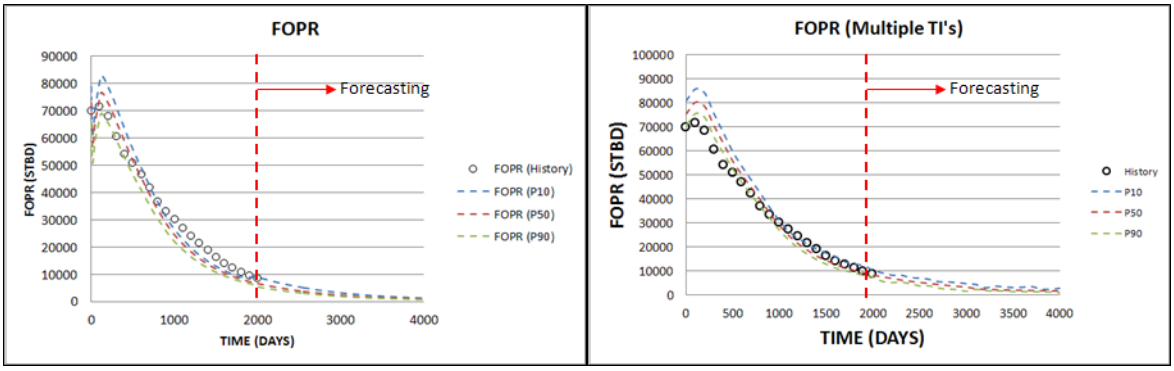

Figure 7.8 Forecast of the FOPR for the models generated using one and multiple training images.

7.3 Modelling vertical facies proportions

In sequence stratigraphy of fluvial environments variations of the base-level (Chapter 5) have a great impact on the control of the facies distribution in a fluvial system (Shanley and McCabe, 1994; Ramon and Cross, 1997). The relation between base-level and facies distribution can be explained by the variations of the relationship between Accommodation space and Sediment supply (*A/S*).

Ramon and Cross (1997) explained that, when the accommodation space (*A)* is larger than the sediment supply (*S*), there is plenty of space for the channels to deposit their sediments, the connectivity between channel sandbodies is low and the proportion of channel facies is low compared to the flood plain facies. Contrary to this, when (S) is larger than (A), there is no space for the channels to deposit their sediments then the channels erode the earlier deposits, including the deposits of the previous channels. When this is preserved in the geological record

a large multi-storey/multi-lateral geobody channels is generated. This evolution of channel deposits was illustrated in Figures 5.15 and 5.17.

Varying the Accommodation space/Sediment supply relation (A/S) in a fluvial system will vary the facies proportions of the fluvial deposits. When modelling fluvial reservoirs with few wells or where the geological history of base level changes is not clear, it is necessary to consider the uncertainty associated to the vertical variation of facies, since this has an important impact production response of a reservoir.

Changes in vertical facies proportions can be modelled by analysing well data, or changes in net to gross. The methodology presented in this section is an alternative that can be applied in reservoir with low density of wells, where it is difficult to interpret vertical proportion curves.

7.3.1 Function that models vertical proportion variation.

Facies vertical proportion variation is directly related to variation on the net to gross ratio in a reservoir (*i.e*. volume of reservoir facies over the bulk rock volume of a geological unit). Vertical proportion variation of facies can be approximated by a periodic curve. Demicco (1998) and French (1993) used sine functions in order to model the vertical proportions of carbonates and salt marsh sediments. Indicating that vertical variation of facies can be modelled as cyclic events. In this Section, a sinuous function S (*eqs*. 7.1; 7.2) was used to reproduce the periodic behaviour of vertical facies proportions variation:

$$S = \sin(A * j + k) \qquad eq.7.1$$

$$FVP = a * S + b; \qquad a = \frac{vp2 - vp1}{2} \quad and \quad b = vp2 - 2 \qquad eq.7.2$$

where A is the continuous value (in radians), of a grid cell in a column of the modelling grid, j is the parameter that controls the wavelength of the sine function, k is the parameter that controls the vertical position of the maximum and minimum of the sine function within the reservoir; FVP is the facies vertical proportion, $vp2$ and $vp1$ are maximum and minimum facies proportion values respectively.

This sine function is used to model the changes in the vertical facies proportions. Then the variation in the facies proportions can be controlled in the automatic history-match process by sampling the parameters of j, k, $vp1$ and $vp2$ using PSO within the Bayesian framework. Figure 7.9 illustrates the how the vertical proportion of facies can be described by a sine function, Figure 7.9 is a vertical proportion curve of reservoir facies in the Athabasca Oil Sands, Canada.

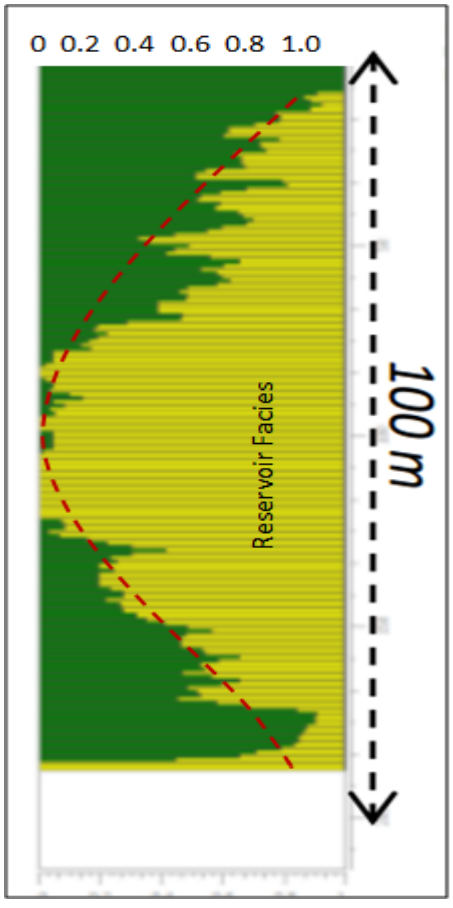

Figure 7.9: Vertical proportion curve of the reservoir facies (in yellow) in one filed of the Athabasca Oil Sands in Canada, taken from Bujor *et al.* (2011). The dashed red line is a sine curve that could describe the reservoir facies vertical proportion.

7.3.2 Application (Meandering Channels)

In this Section, the fluvial meandering stratigraphic unit of the Stanford VI synthetic reservoir (Castro *et al.,* 2005) is used as a "truth case". In this section, the vertical facies proportion varies within the automatic history matching workflow. History match and Forecasting setups were the same as used in section 7.2, but in this case PSO will be sampling s of the parameters *j, k, vp1* and *vp2* of equations 7.1 and 7.2 in addition to multiple Tis and the geomorphic parameter to generate different curves of changes in vertical facies proportions.

The ranges for the geomorphic and vertical proportions parameters used in history matching are displayed in Table 7.2.

History Match Set Up		
Geomorphic Parameters and Ranges	Chanel Width Channel Thickness Meander Amplitude Meander Wavelength	100 – 600 m 5 – 200 m 500 – 3000 m 500 – 3000 m
Vertical Proportion Parameters	*j* *k* *vp1* *vp2*	0 – 1.6 0 – 25 0 – 0.8 0 – 0.8

Table 7.2 Parameter used in history matching and their ranges.

Figure 7.10 compares the production forecasts of the models with and without varying vertical facies proportions. There is more uncertainty related to changes in facies vertical proportions than in keeping the proportions constant. The increase in the number of parameters to sample from widens the uncertainty in production forecasting.

In Figure 7.11 we can observe the values of the parameters of the equations 7.1 and 7.2, which converge during the process of automatic history matching and a comparison of the models vertical facies proportions that have the lowest and highest misfits.

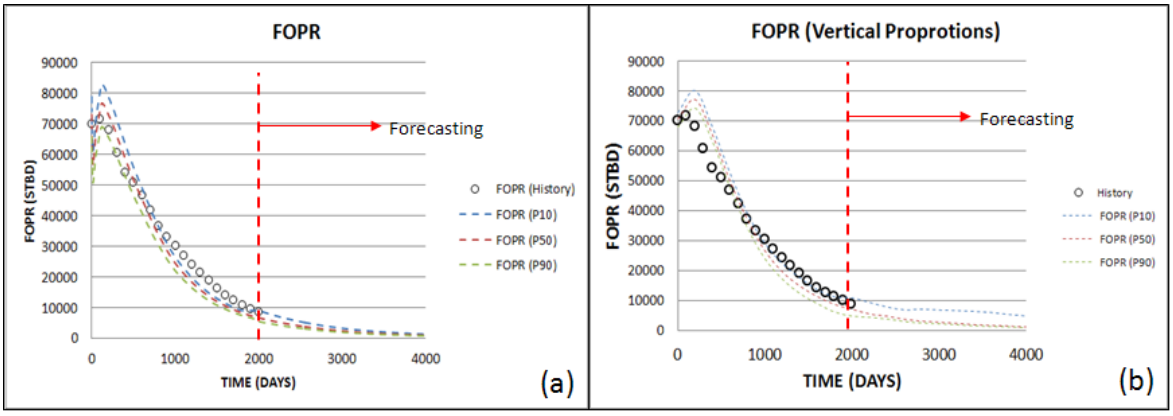

Figure 7.10: Forecasting of the field oil production rate. (a) no-variation of facies vertical proportions and (b) varying vertical proportions. “Intelligent” geological prior information for channel geomorphic parameters was used in both cases.

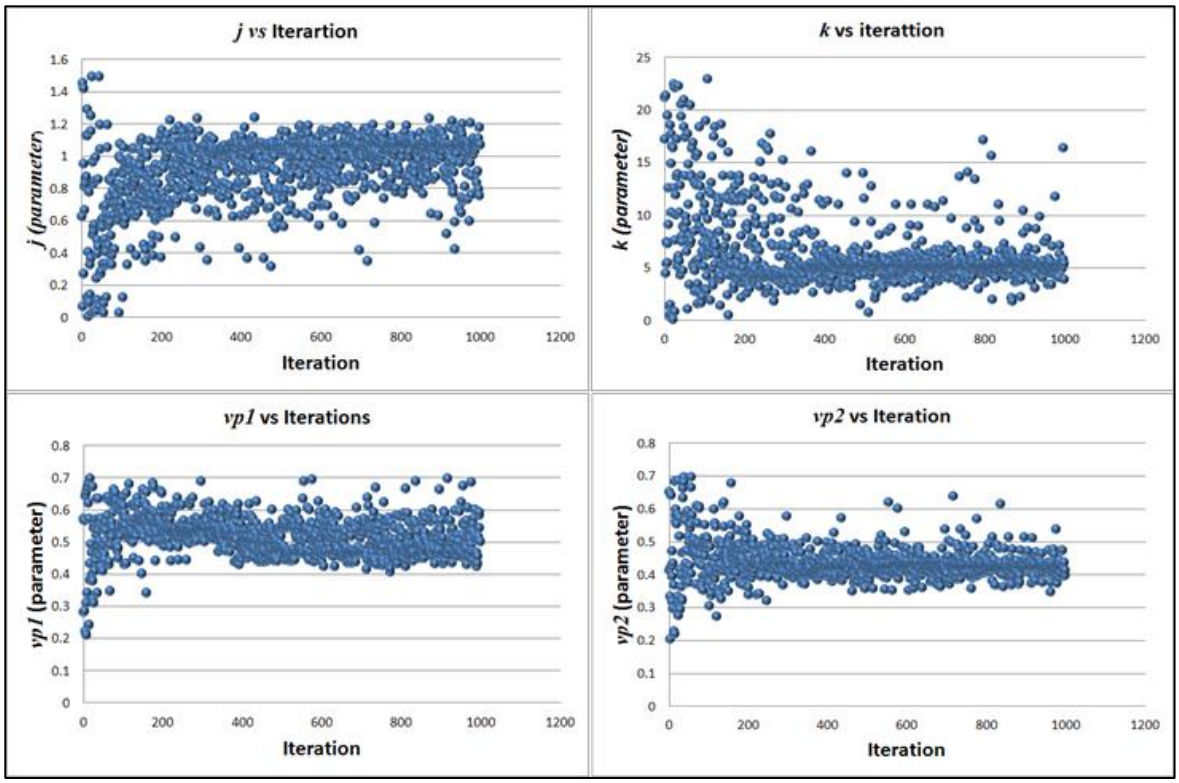

Figure 7.11: Convergence trends of the Vertical facies proportion parameters.

Figure 7.12 compares the point bar vertical proportion curves estimated using equations 7.1 and 7.2 for the best model (Model 500) and the two models with high misfit. Note, that the trend of the vertical proportion curve for “Model 500” for the point bars follows the vertical proportion variation of the truth case, although the values of facies (proportions are not the same).

With the application of this technique within the framework of automatic history matching it is possible to identify which vertical facies distribution can be history-matched and select the ones that could represent better the actual vertical distribution of facies in a reservoir.

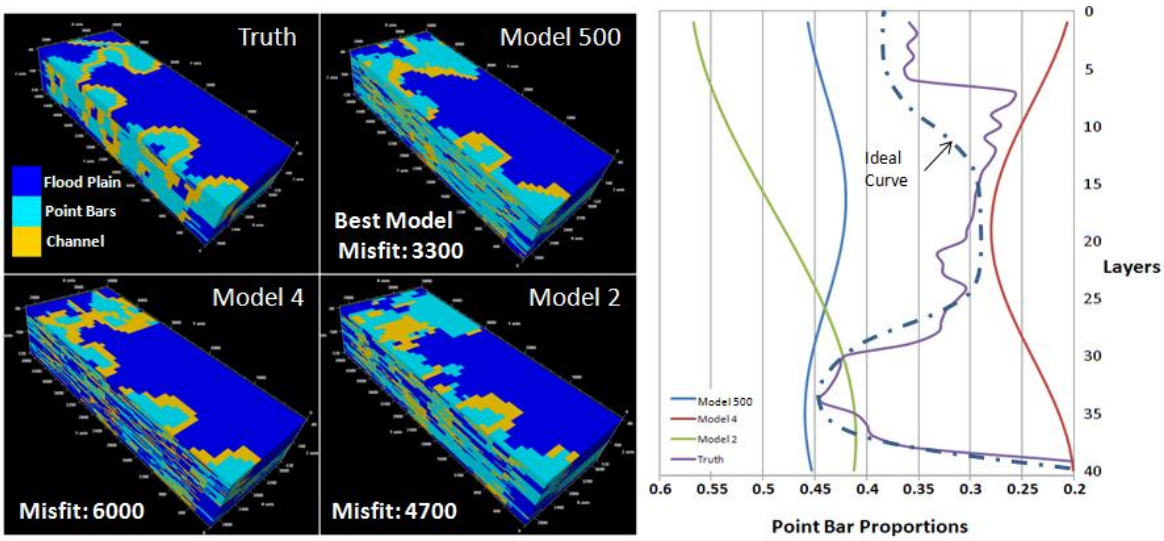

Figure 7.12: Comparing point bars vertical proportion curves of best model (Model 500) and models with high misfit (Model 4 and Model 2). 3D representations of the models cut half-way through from North to south in order to show the vertical distribution of the facies. The sine function is not flexible enough to reproduce the dash and dot ideal curve.

7.4 Analysing connectivity in facies models using MPS

The application of geological parameterization within the automatic history matching framework (Arnold, 2008) is based on the generation of multiple geomodels varying different geological parameters in order to obtain multiple possible models of a reservoir and history match them. In this thesis, it has been

shown that the facies geometry of reservoir models can be controlled by the use of “realistic” prior information. In consequence all the multiple models obtained by varying the geological parameters related to facies geometry, can be considered as geologically realistic.

Figure 7.13 shows that the geobody connectivity may cause problems in history matching. Even though the selection of geomorphic parameters can be considered realistic, the simulation technique (MPS) could generate discontinuous geobodies; this discontinuity affects the production response of a model in specific wells. Works like Maucec *et al.* (2012), Renard *et al.* (2011) Demyanov *et al.* (2012), Demyanov *et al.* (2008) and Honarkhah and Caers (2012) raised concerns associated with this connectivity problem and present different approaches to deal with it. In Figure 7.13 well P1 is isolated in Model 38 while in the Truth case Well P1 is part of a point bar belt.

In this section, this problem was tackled by using one of the advantages of geostatistics, where it is possible to generate multiple realizations from the same set of parameters, and then choose the model whose geobody connectivity is the closest to the connectivity sampled by the optimization algorithm. The chosen realization is selected by comparing the facies connectivity from each realization and compared to the connectivity (new parameter) sampled from a uniform prior distribution. The realization with the facies connectivity most similar to the sampled connectivity is selected it’s connectivity measure is the optimised further whilst history matching.

7.4.1 Measuring Facies Connectivity in a 3D grid

Connectivity represents one of the fundamental properties of a reservoir that directly affects recovery. Larue and Hovadik (2006) defined two types of connectivity used in reservoir modelling. One is reservoir connectivity which is associated with the percentage of the reservoir that is connected to wells and the other definition is geobody or sandbody connectivity which is defined as the

percentage of the reservoir that is connected. Renard and Allard (2011) reviewed the most recent techniques used to measure reservoir connectivity. They identified two types of connectivity: (1) static connectivity, which is associated with the structural parameters of the field (hydraulic conductivity or geological facies); and (2) dynamic connectivity, which is related to physical processes such as flow or transport.

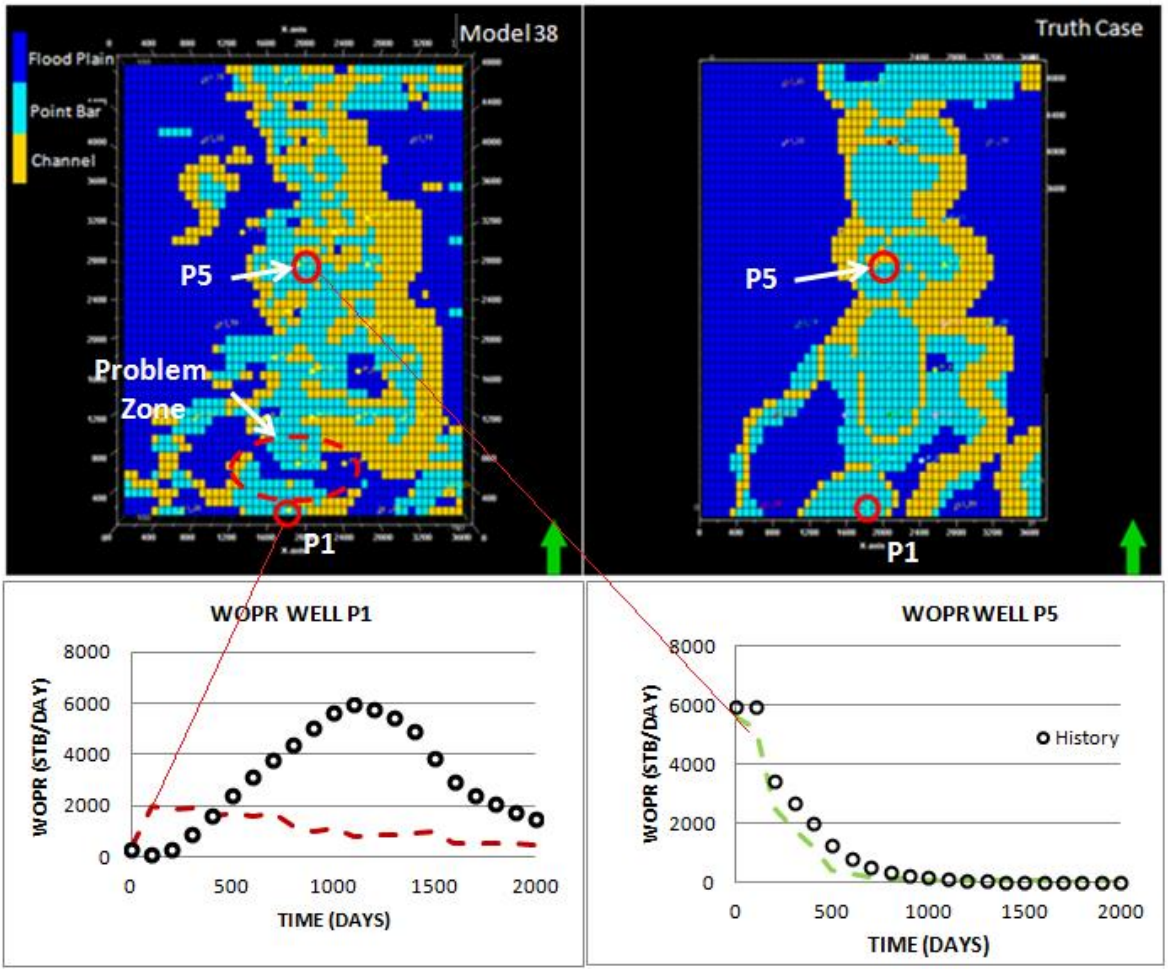

Figure 7.13: Visual and well oil production rate (WOPR) comparison between Model 38, obtained in Section 6.2.4 and the "Truth case". Wells P1 and P5 are highlighted with a red circle. The facies representations are showing layer 21 of the 3D cube. We can observe that production response of the Well P1 in Model 38 do not match the history data, due to te lack of facies connectivity. WOPR of Well P5 in Model 38 matches better the production history than well P1. There is a better facies connectivity surrounding well P5 than well P1.

In this section the problem addressed is focussed on the selection of a geomodel based on their sandbody connectivity, specifically related to sanbodies generated by fluvial meandering channels.

Facies model connectivity analysis has captured the attention of many authors that have proposed different methodologies to measure and analyse this important feature in reservoir modelling. Larue and Hovadik (2006) described the relationship between net to gross and reservoir connectivity and used this relationship to characterize the types of connectivity that can be found in a reservoir and the optimal well location in order to drain the reservoir. A different approach was shown by Renard *et al*. (2011) where they stochastically generated reservoir and interwell connectivity paths into reservoir facies models; these connectivity paths are then sampled and used as hard data during the facies modelling process.

Pardo-Igúzquiza and Dowd (2003) generated a computer program (CONNEC3D) that measures the facies connectivity. This program is based on a connectivity function $\tau(h)$ for different spatial directions and a number of connectivity statistics. Nurafza *et al*. (2006) presented a statistical approach to model connectivity of all sort of body sizes and aspects based on percolation theory.

In this section, an approach that includes some of the methodologies mentioned above is presented. Based on the possibility of stochastically generating multiple facies realizations, a code was introduced into the automatic history match workflow that measures the geobody connectivity over several facies realizations and selects a realization to be used for fluid flow simulation based on the degree of geobody connectivity, which would match better the production history.

In this thesis we used a simple technique that combines: (1) scanning the 3D facies realizations to evaluate the connection between cells of the same facies; (2) estimating the proportions of the permeable facies within the model which is equivalent to estimate the net to gross of the model and (3) counting the number of connected geobodies. This is based on the application of the percolation theory,

application available in the software SGeMS (Remy *et al*., 2009). SGeMS uses a method for calculating connected regions ("geobodies") in a hydrocarbon reservoir based on an algorithm which visits a cell in a facies model, assigning a geobody value and then the algorithm compares this cell with the neighbouring cells assigning the same geobody value to the cell that has the same value as the first visited cell. The algorithm continues the comparative process cell by cell and results in identification of all separated geobodies in the reservoir model grid.

A connectivity index (CI) is estimated by considering the facies connectivity in three axes (equations 7.3, 7.4 and 7.5) that can be used as parameters that measures the degree of connectivity of permeable facies.

Figure 7.14 is an illustration on how this technique measures the number of cells connected in the direction of a 2D grid axes (x, y). The code counts the number of cells of a sand facies that are in contact in the direction of the axes x, y and z, and adds all these number of cells, then the total number of porous facies cells in contact is divided by the total number of the grid in that specific direction (x, y or z).

Facies proportions (FP) are estimated dividing the number of grid cells with sand facies by the total number of cells of the grid this is equivalent to the net to gross (NTG) relationship. Net to gross is a very important geological factor in facies connectivity. Allen (1979) comparing outcrop information with well data (logs/cores) identify that NTG lower that 50% in well data, will represent a poor sand body connectivity within a reservoir. NTG larger than 50% in well-logs will increase the probability of sand body connectivity. A reservoir with a net to gross higher than 30% has facies connectivity larger than 90% (Larue and Hovadik, 2006). Bridge and Tye 2000 found that fluvial deposits with a net to gross larger than 70% indicates that all the channel deposits are connected.

Figure 7.15 highlights the facies proportions of the 2D grids showed in Figure 7.14.

The third factor used to estimate the connectivity index is the number of geobodies generated in a model. In geomodelling, a geobody is defined as the volume of interconnected cells that belongs to a facies, facies association, porosity or permeability groups (Deutsch, 1998). This was done following the described above algorithm realised in SGeMS (Remy *et al*., 2009). This algorithm is based on the percolation theory and is very similar to the methodology used by CONNECT3D (Pardo-Igúzquiza and Dowd, 2003). Figure 7.16 shows the number of geobodies identified by the SGeMS in the 2D grids shown in Figures 7.14 and 7.15.

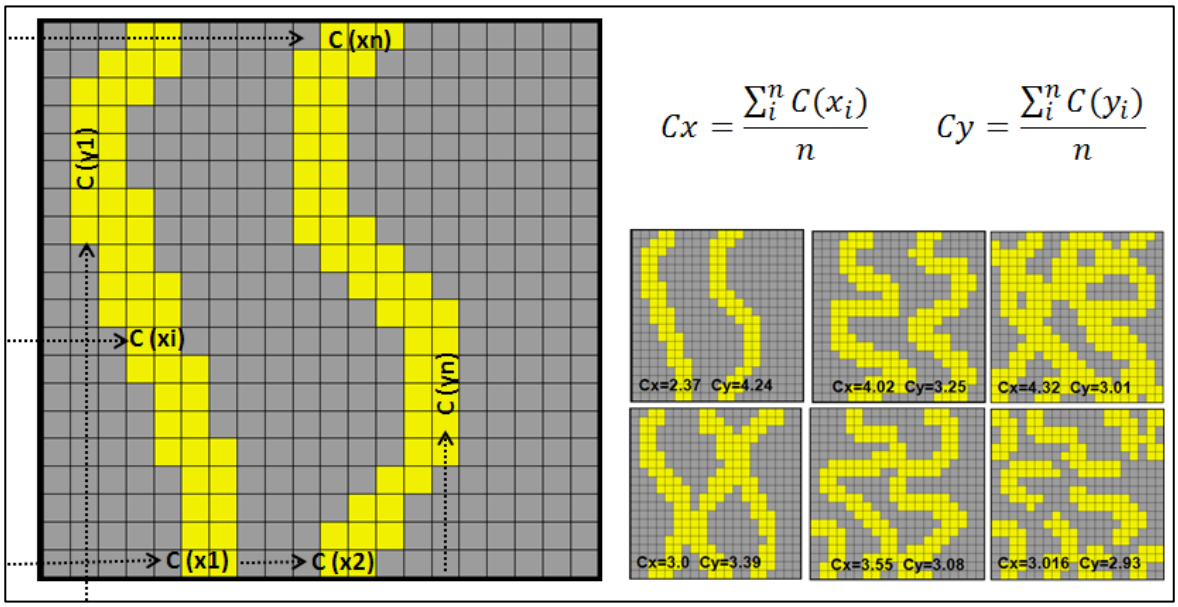

Figure 7.14: Illustration of how the code for connectivity index estimates the continuity (Cx and Cy) of permeable facies (yellow cells) in a 2D grid. We can observe six 2D grids with different measurements of continuity of permeable facies. The continuity is measured by adding the number of the connected porous facies cell ($C(x_i)$, $C(y_i)$) in an axis (x or y) and divided by the total number of cells n in an specific axis (x or y).

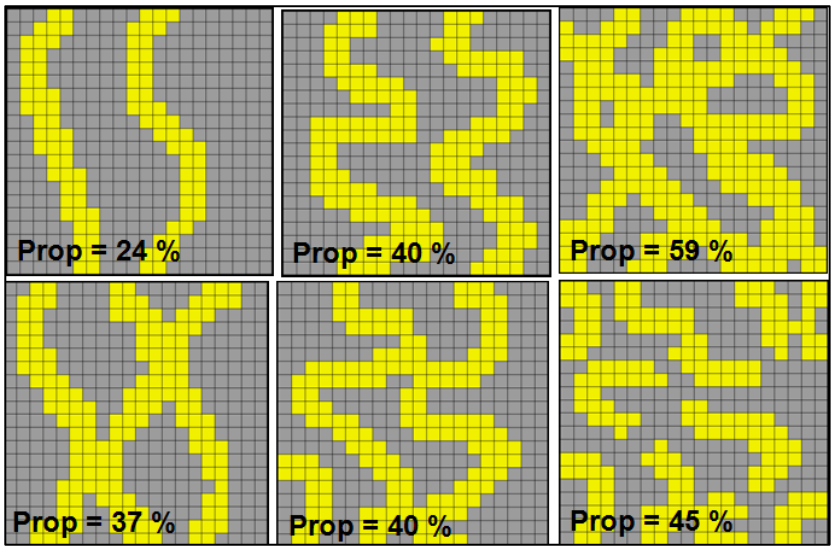

Figure 7.15: Permeable Facies Proportions (FP) of 2D facies models.

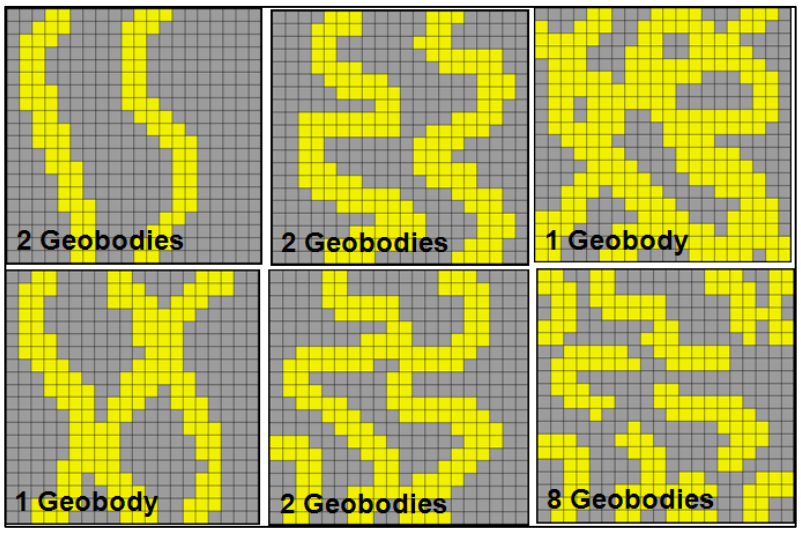

Figure 7.16: Number of channel geobodies of 2D facies models.

The connectivity index (CI) can be measured in the direction of the three axes (x, y and z) with the following equations:

$$CIx = \frac{Cx * FP}{NB} \qquad \textit{(eq. 7.3)}$$

$$CIy = \frac{Cy * FP}{NB} \qquad \textit{(eq. 7.4)}$$

$$CIz = \frac{Cz * FP}{NB} \qquad \textit{(eq. 7.5)}$$

where:

CI is the Connectivity Index, x, y and z represent the direction in which the CI was measured.

C is the facies continuity (measurement of how continuous a specific facies is in a single direction or axis), x, y and z represent the direction in which the facies continuity was measured.

FP is the facies proportion in a grid (number of cells of a specific facies divided by the total number of cells).

NB is the number of connected geobodies.

Figure 7.16 compares the connectivity indexes estimated using equations 7.3 and 7.4, for every 2D model.

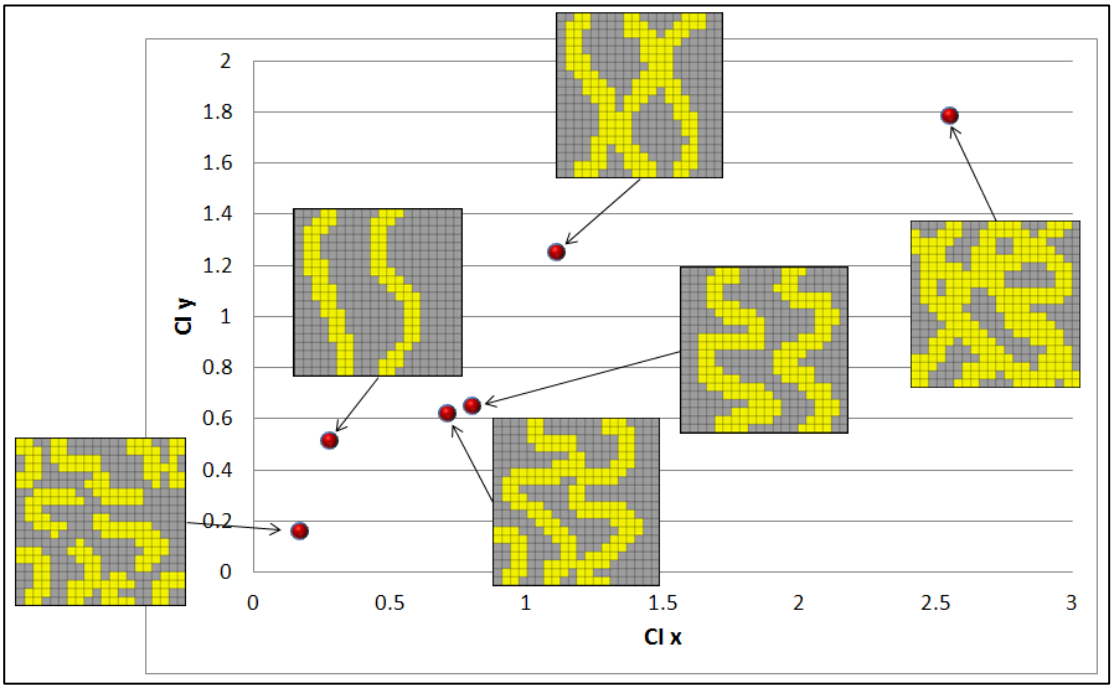

Figure 7.17: Connectivity Indexes calculated for the 2D facies models.

7.4.2 Application (Meandering channels)

The estimation of the connectivity index methodology was tested using the meandering fluvial unit from Stanford VI synthetic reservoir (Castro *et al*., 2005). The Connectivity Index (CI) was introduced into the automatic history matching framework, as another parameter to optimize with PSO, as illustrated in Figure 7.18.

After selecting a realistic combination of geomorphic parameters, a combination of connectivity indexes (CIx, CIy and CIz) are sampled, five facies realizations are generated and their connectivity indexes measured in direction of the x, y and z axes. These connectivity indexes are compared to the CI's sampled by PSO. Then the realization whose CI's are the closest to the CI's sampled is chosen for flow simulation taken further in history matching.

The setup for history matching and forecasting is the same as the setup shown in sections 7.3 and 7.2. The prior ranges for the connectivity indexes are given in Table 7.3.

History Match Set Up		
Geomorphic Parameters and Ranges	Chanel Width Channel Thickness Meander Amplitude Meander Wavelength	100 – 600 m 5 – 200 m 500 – 3000 m 500 – 3000 m
Connectivity Index	CIx CIy CIz	0.1 – 0.7 0.1 – 0.7 0.01 – 0.7

Table 7.3 Parameter used in history matching and their ranges for connectivity analysis.

Figures 7.19 and 7.20 illustrate a comparison of the forecast for oil production obtained with models that used multiple realizations with connectivity analysis and the models obtained using a single realization. In Figure 7.19, although, the P10-P90 range is wider in the forecast using the connectivity analysis than in the

forecast without it the P10-P90 range still accommodates the history data when using multiple realizations; while in the case of the models that did not use connectivity analysis history data is above the P10-P90 range. This means that the models obtained using multiple realizations match better the production behaviour of the field, which makes these models more reliable than the models that did not use multiple realizations. A wider P10/P90 range in the forecast with connectivity analysis is considered as more realistic.

Table 7.4 compares the computational time doing the history matching and forecasting of the models generated using connectivity analysis and models using a single facies realization. There is an increment in the computational time because 5 realizations are generated for each combination of model parameters. Also, the dimensionality of the sampled search space has increased by 3 extra connectivity parameters.

In Figure 7.21 we can observe the values of the connectivity indexes converging during the history match process. The connectivity indexes values are homing in close to the connectivity indexes of the truth case. CI´s converged close to the CI´s of the truth case. The largest CI is found in the y axis (North-South) which is parallel to the channel trend. There is better connectivity in the direction parallel to the channel than in the other directions. These results identify the models whose facies connectivity reproduces best the production history of a reservoir.

	Intelligent Priors	Intelligent Priors + Connectivity
History Matching	89 hs	112 hs
Forecasting	37 hs	45 hs

Table 7.4: Comparison of the time consumed by the models using connectivity analysis and models with no connectivity analysis.

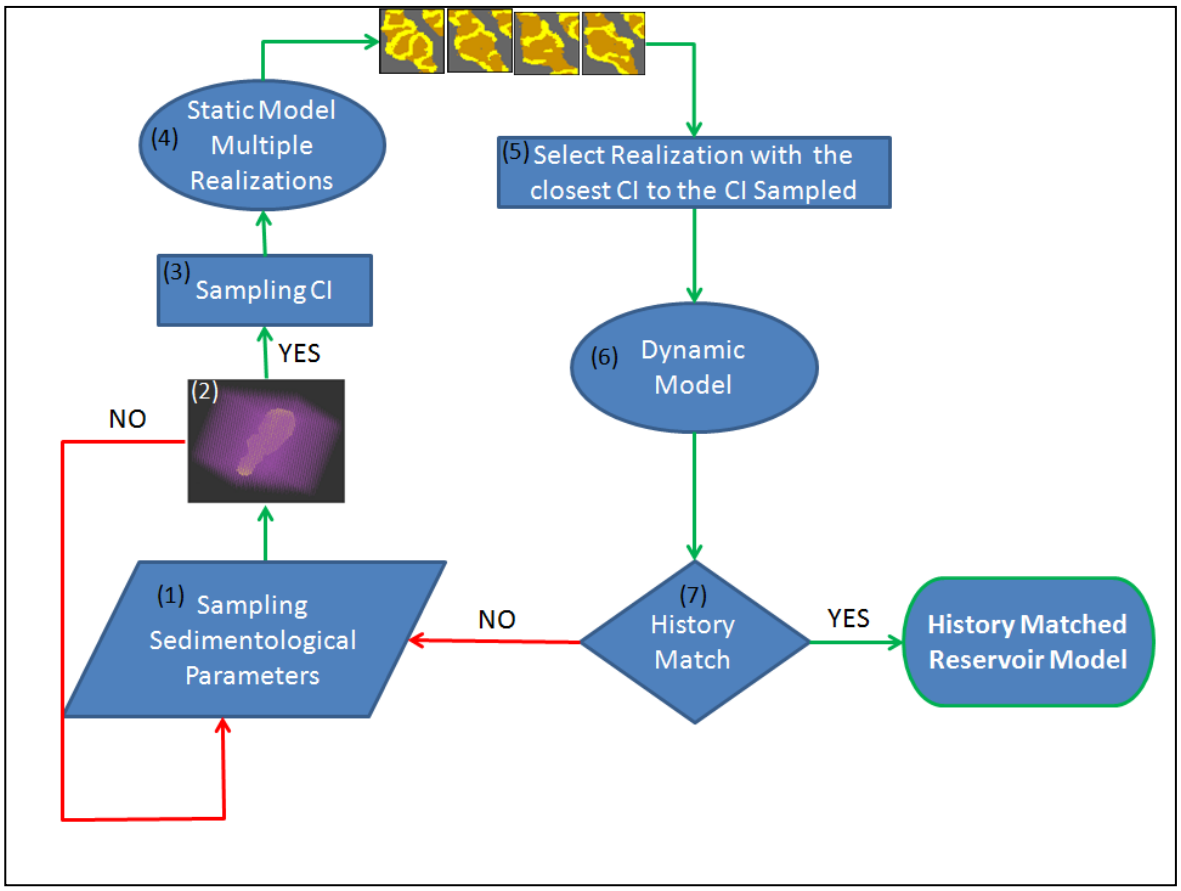

Figure 7.18: Workflow for automatic history matching including multiple facies realizations and Connectivity Index (CI) estimation. After sampling sedimentological parameters (channels width and thickness and meander wavelength and amplitude), the realism of the combination of these parameters is checked, a CI value is sampled as well, multiple realizations are obtained from the facies modelling and CI's are estimated a CI from each of the realizations. Then the CI of each realization is compared with the sampled CI, the realization with the CI closest to the sampled is chose to perform history matching.

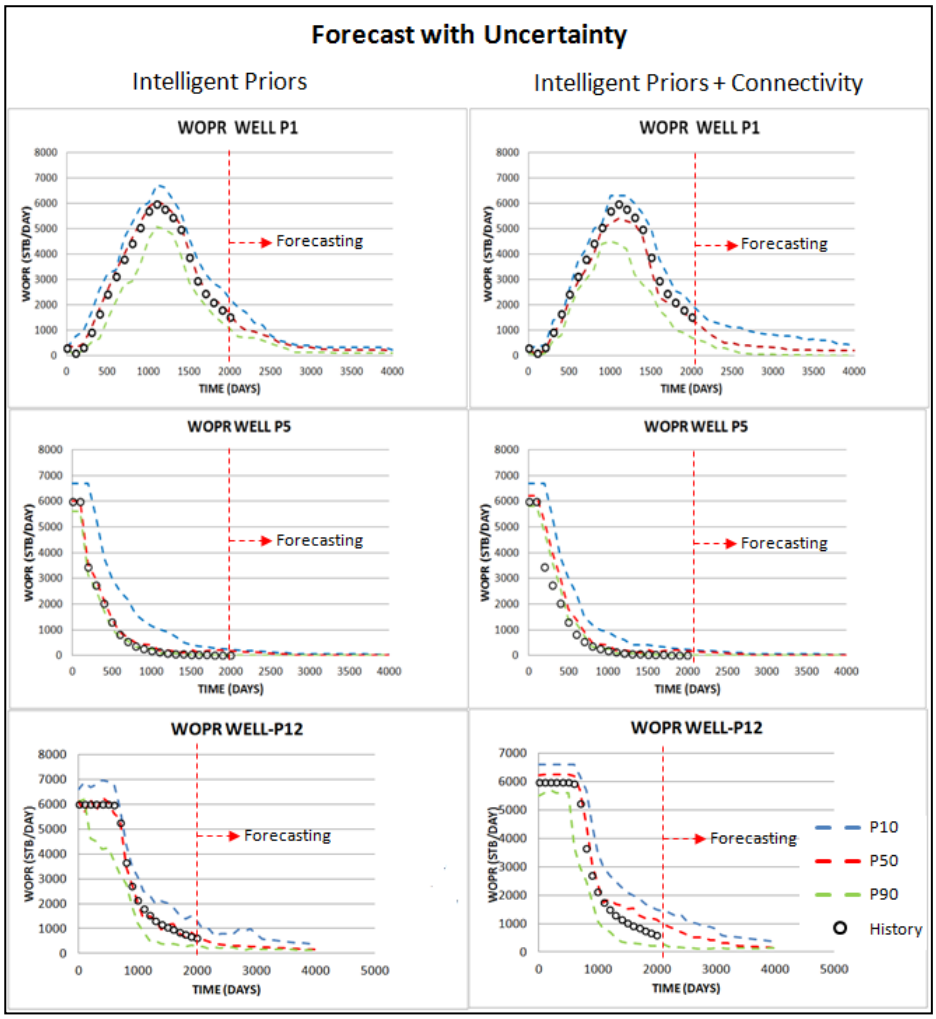

Figure 7.19: Comparison of oil production rate per well (WOPR) forecast between models generated with connectivity analysis and models generated without connectivity analysis (Section 6.2).

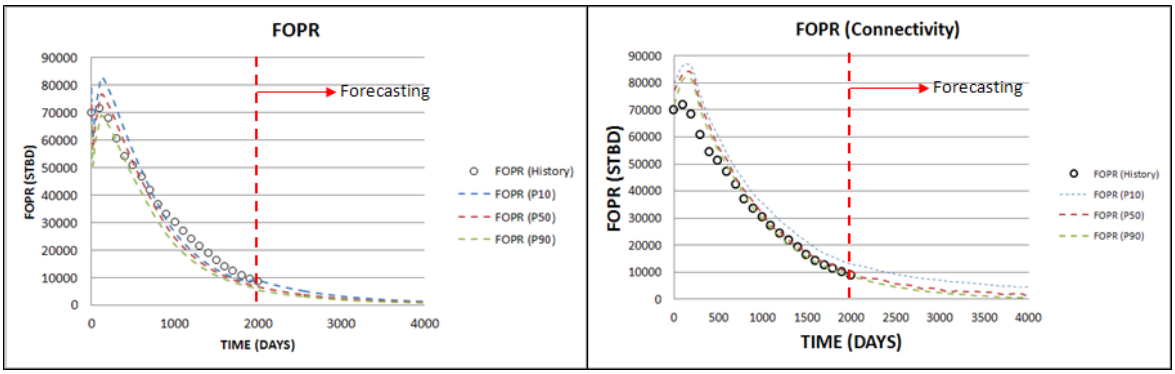

Figure 7.20: Comparison of Oil production forecast between models generated with connectivity analysis and models generated without connectivity analysis (Section 6.2).

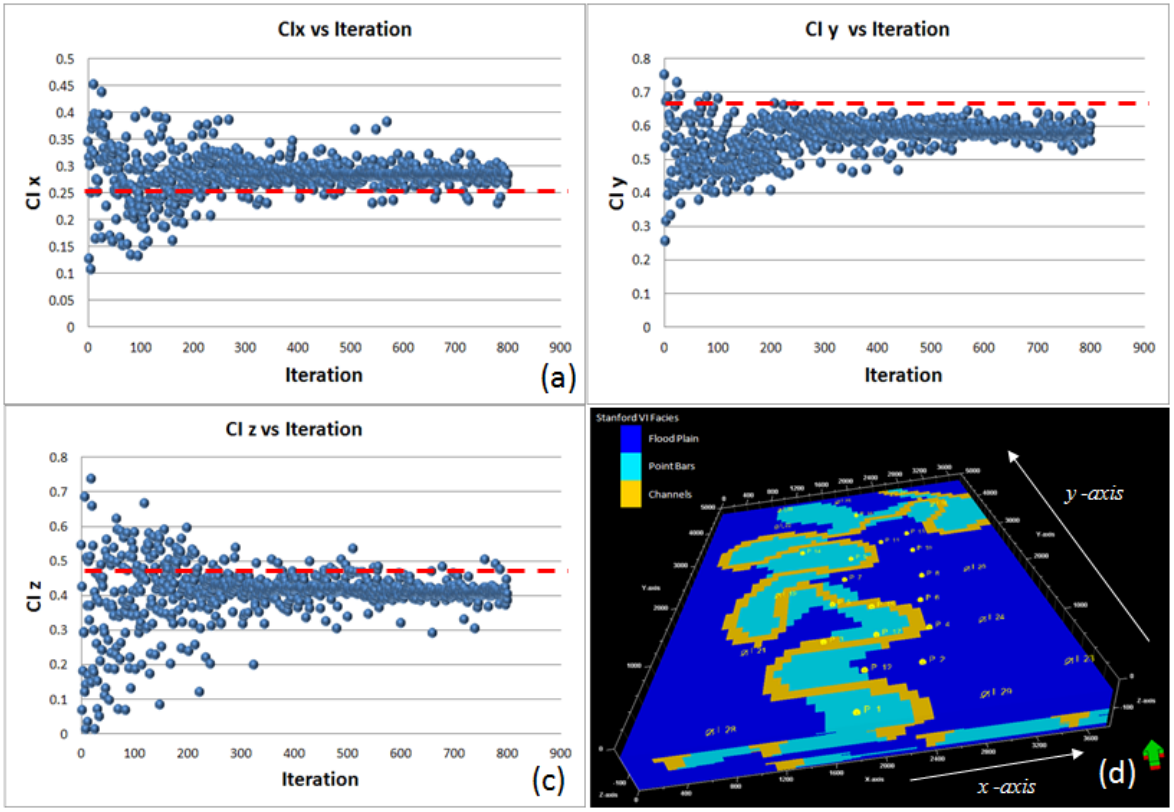

Figure 7.21: Connectivity Indexes convergences in for each axis (a), (b) and (c). “Truth Case” 3D representation highlighting the axes of the grid (d). Dashed red lines are the CI´s of the Truth Case. Note that the CI´s converge very close to the truth case CI index vales.

With this methodology, it is possible not only to select among many realizations the one with a connectivity index closer to the expected one, but also to identify which connectivity index represents best better the facies connectivity in the reservoir.

7.5 Facies modelling improvements within the automatic history workflow (Fluvial Meandering Channels Reservoir).

In previous sections of this chapter, some methodologies that improved the performance and realism of reservoir facies modelling have been introduced into

the history matching workflow. In this section, all the methodologies are applied to the history match process. Figure 7.22 is an illustration of the history matching workflow with the inclusion of multiple training images, vertical proportions and connectivity analysis. Intelligent prior information is used to control the realism in the combination of geomorphic parameters used to generate the facies models.

In order to be consistent with the applications of these improvements, the reservoir used is the fluvial meandering channel stratigraphic units of the Stanford VI synthetic reservoir (Castro *et al.,* 2005). Table 7.5 indicates the ranges used for the 19 uncertain parameters used in this case. History match and forecasting setups are the same as used in section 6.2.

Figure 7.23 is a compilation of the misfit evolution considering all the cases shown in this chapter, plus the misfit evolution obtained in Section 6.2: (a) misfit evolution using uninformative geological prior information; (b) using “Intelligent” prior information; (c) “Intelligent” priors plus Vertical Facies proportions; (d) “Intelligent” priors plus selecting multiple training images; (e) “Intelligent” priors plus Connectivity analysis and (f) including all the process (full workflow).

In Figure 7.23 we can observe that, for the cases b), d) and e), the history match process converges before the 600^{th} iteration while, for the case f) with the full workflow, the convergence appears to be after the 600^{th} iteration. This could be associated to the fact that the sampling for vertical proportion of facies is included in this case and, as observed in case c), there is not a clear convergence when sampling for vertical facies proportions.

The lowest misfit was obtained in case e), where the connectivity analysis was used to select from multiple realizations.

Figure 7.24 compares the forecasting of the Field Oil Production Rate (FOPR) between the different cases presented in this chapter. The results obtained using the full workflow case demonstrated a better match with the history data than in cases a) and b) and a lower range between P10 and P90 than in cases b) and c). We can observe as well that the full workflow has the lowest range P10-P90 (f).

Results in case e) are comparable to the results obtained in “d” although the history match is better in case e) than in case d) during the first 500 days of production data.

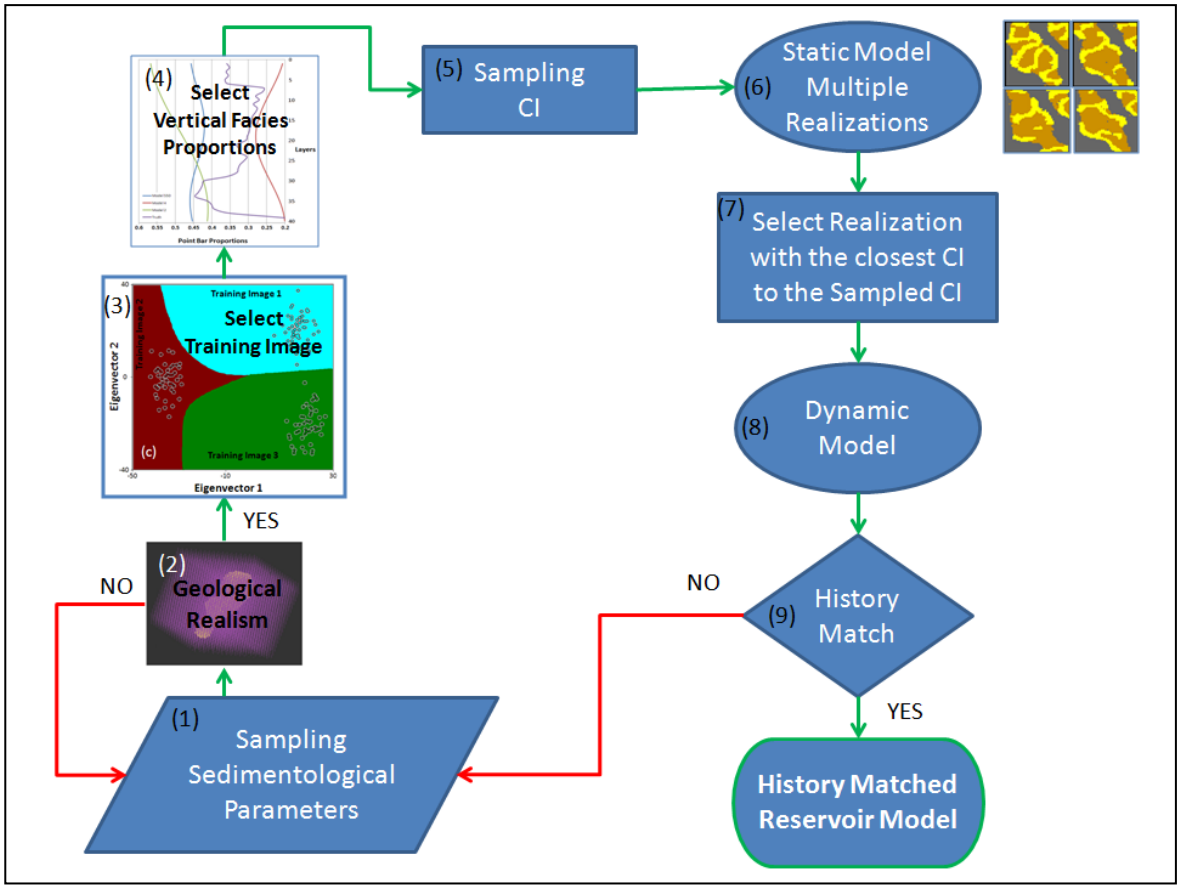

Figure 7.22 Full workflow for improving geological realism in reservoir facies models within the automatic history match framework (CI: Connectivity Index).

History Match Set Up		
Geomorphic Parameters and Ranges	Chanel Width Channel Thickness Meander Amplitude Meander Wavelength	100 – 600 m 5 – 200 m 500 – 3000 m 500 – 3000 m
eigenvalues	All 8 eigen values have the same range (-50 to 50)	
Vertical Proportion Parameters	j k $vp1$ $vp2$	0 – 1.6 0 – 25 0 – 0.8 0 – 0.8
Connectivity Index	CIx CIy CIz	0.1 – 0.7 0.1 – 0.7 0.01 – 0.7

Table 7.5: Ranges of the 19 parameters used in the full workflow for improving geological realism in reservoir facies models within the automatic history match framework.

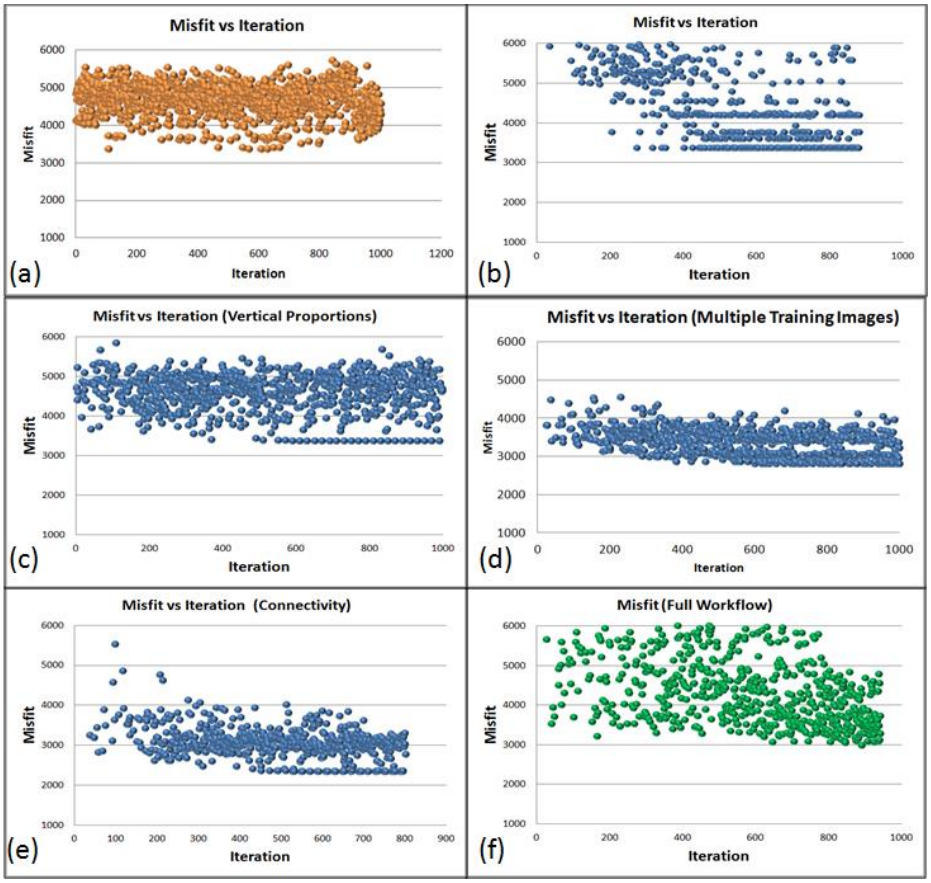

Figure 7.23 Evolution of the misfit during the history matching process: (a) using uninformative geological prior information; (b) using "Intelligent" prior information; (c) "Intelligent" priors plus Vertical Facies proportions; (d) "Intelligent" priors plus selecting multiple training images; (e) "Intelligent" priors plus Connectivity analysis and (f) including all the process (full workflow).

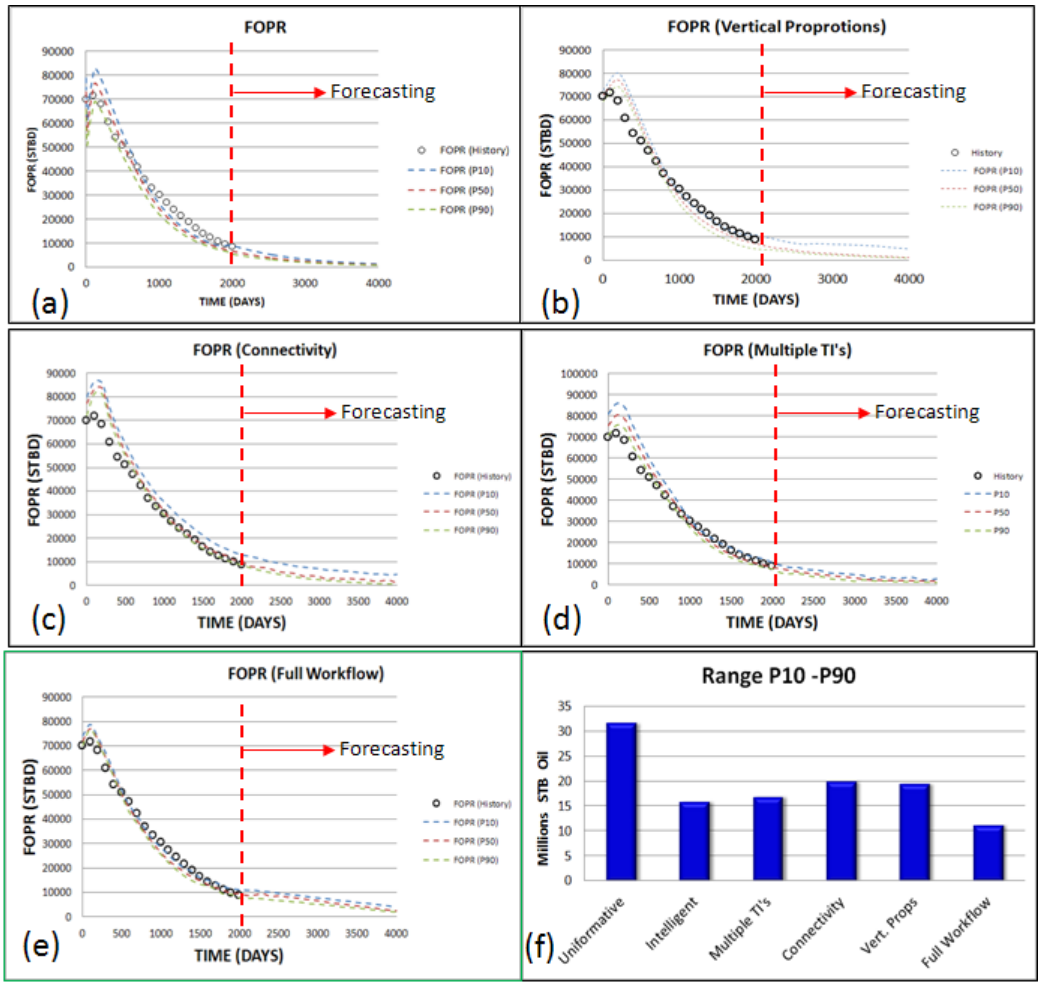

Figure 7.24: Comparing the forecast of the FOPR between the different cases, (a) using only "intelligent" geological prior information; (b) including Vertical facies proportions; (c) including connectivity analysis; (d) Multiple training images and (e) full workflow case; (f) is a comparison of the uncertainty ranges P10-P90 for each case.

In Figure 7.25 we can observe a comparison between the model with the lowest misfit obtained in the full-workflow case (Model 846) and the truth case as well as a comparison of their geomorphic parameters. It is important to highlight that the orientation of the channels in all the cases shown in this chapter where set North-South. Changes in orientation were not used as a parameter in this thesis since Arnold (2008) already had identified orientation as one of the most important geological parameters in history matching reservoir production.

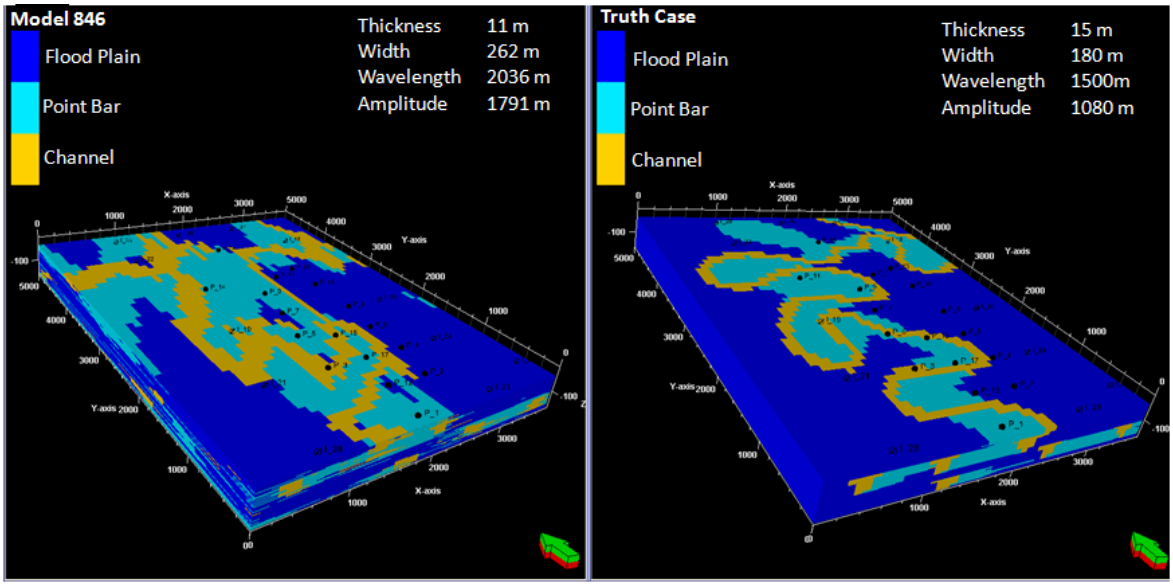

Figure 7.25: Comparison between the model with the lowest misfit in the full-workflow case and the truth case.

Figure 7.26 shows the values of the parameters obtained in the model with the lowest misfit in the "full-workflow" case. The training image used was Training Image 1, which is a representation of meandering channels. The connectivity index with the highest value was the one associated with the y-axis, this is actually consistent with the "truth" case, since the channel geobodies are oriented North-South (parallel to the y-axis). The curve of the vertical proportion of the point bars is very similar to the vertical proportions of point bars in the "truth" case although the values of point bars proportions is higher in model #846 than in the "truth case".

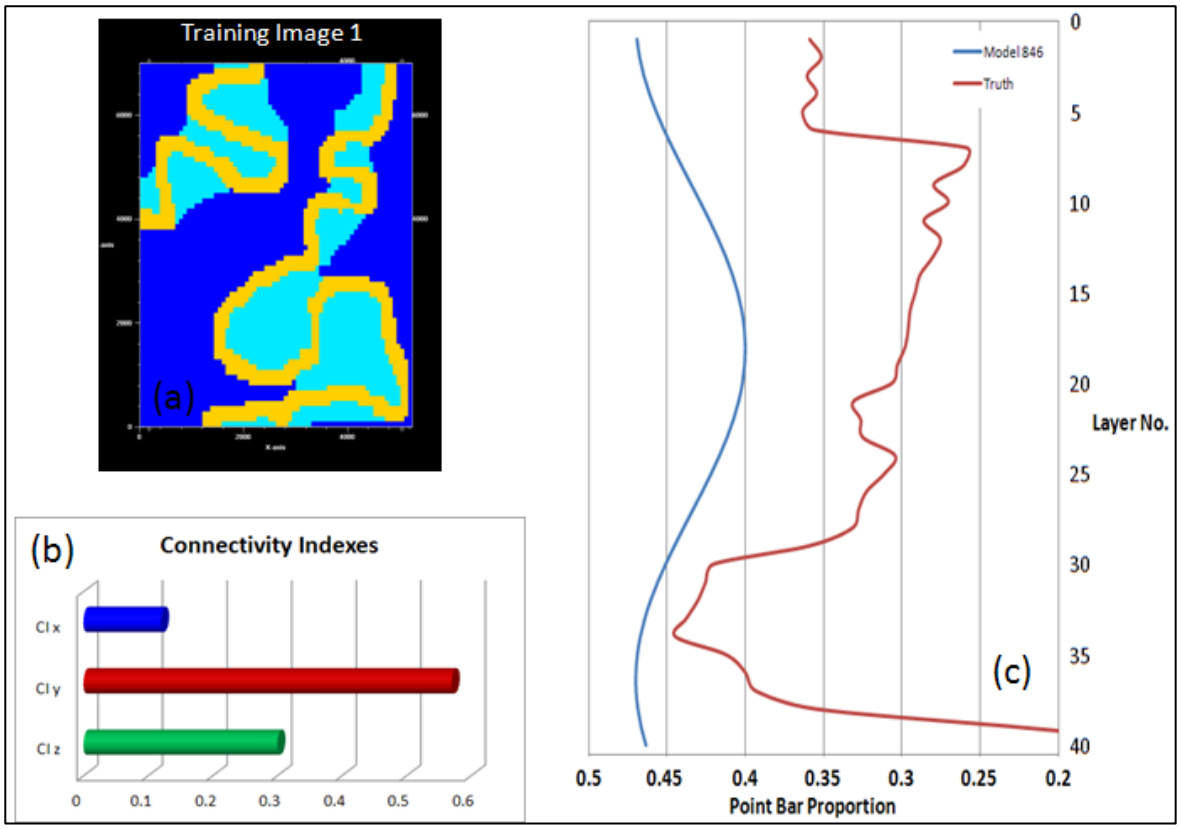

Figure 7.26: Parameters used in Model #846 (Lowest misfit) in the "full-workflow" case. (a) The model was built using Training image 1; the highest connectivity index was associated to the y axis; in (c) the vertical proportion curve for Point Bars compared to the Vertical proportions of the "truth case".

In Figure 7.27 we can observe the forecasting for 8 individual wells in the case of using the full workflow for history-matching. In some of the cases the range of P10-P90 is wide, but in most of the cases the forecasting does not show a high spread.

Table 7.6 indicates the time used for history matching and forecasting with uncertainty using the full workflow developed in this thesis.

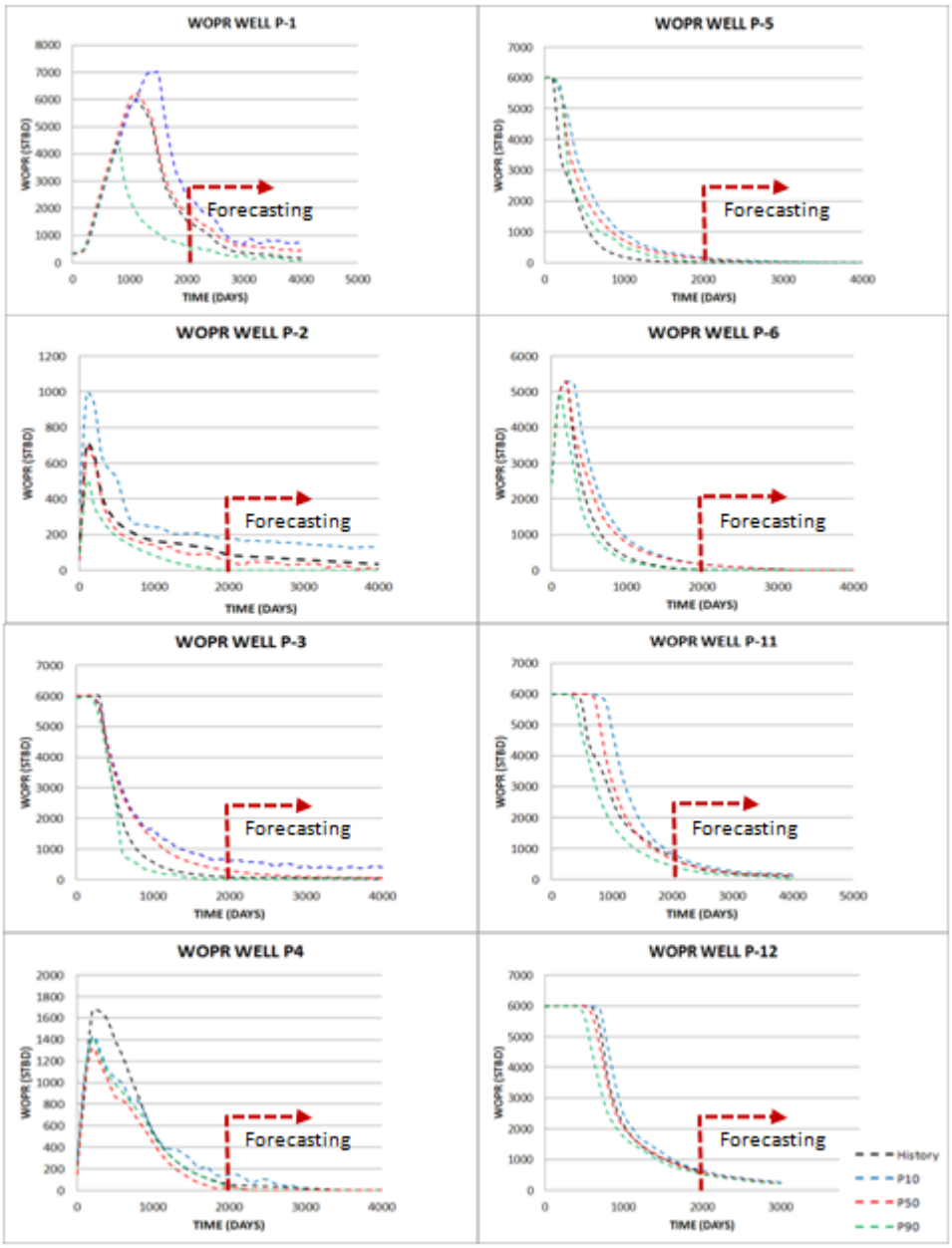

Figure 7.27: Production forecasting of 8 wells using the full workflow for history-matching.

	Intelligent Priors	Full Workflow
History Matching	89 hs	123 hs
Forecasting	37 hs	37 hs

Table 7.6: Comparison of the time consumed by the models using the full workflow analysis and models with no connectivity analysis.

7.6 Summary

We have seen in this chapter a series of improvements in the reservoir facies modelling process that were applied to the automatic history match workflow. All these improvements honour the fact that the geometry of the facies within the reservoir model is controlled by “intelligent” geological prior information that assures the realism of the facies geometry.

(1) The first expansion included in the automatic history match framework was the use of multiple training images. As mentioned in Section 7.2, training images used in Multiple Point Statistics are geological concepts. The importance of using multiple training images is that this allows the automatic history match process (Chapter 3) to use different geological concepts and generate models that are validated against the production data of a reservoir.

In this case, three different training images were used, representing deposits generated by meandering, anastomosed and low sinuosity channels. The results obtained show that the models with the lowest misfit were generated using the training images representing anastomosed and meandering channels, which are the concepts that are closer to the truth case in describing the geometrical relationships among the facies of meandering channels deposits. This methodology can be seen as a way to select from different sedimentological interpretations by various geoscientists which is a common issue in reservoir characterization.

(2) In Section 7.3, the inclusion of facies’ vertical proportions in fluvial deposits was describes (Section 5.4.1) with a periodic function. In this case, the parameters of a sinuous function (equations 7.1 and 7.2) were sampled by the adaptive sampling algorithm (PSO) in the automatic history-matching workflow (Section 3) to generate a sinuous curve of the vertical facies proportions. In the case of the Stanford VI, the vertical facies proportions do

not quite follow the sinuous behaviour, but the models that obtained the lowest misfit, have vertical facies proportion sinuous curves that were following the trends observed in the “truth” case, although the actual value of the facies proportions were not the same.

(3) The last feature included in the automatic history-match framework was the connectivity analysis. In pixel-based geostatistical models the geobody connectivity has been a known problem. The use of Multiple point statistics (Chapter 2) has improved the connectivity problem to a certain degree compared to geomodels based on two-points statistics. One way to tackle this problem is to generate multiple facies realizations using the same parameters, just varying the “seed”. This is not an efficient methodology unless the connectivity can be controlled by MPS parameters and optimized by the Connectivity Index. In this case a code that scans the facies realization and measures the connectivity of the geobodies by analysing the continuity of a geobody along the axes x, y and z, measuring the net to gross or facies proportion in a realization and estimating the number of geobodies in a facies model realization. A connectivity index was estimated then (see equations 7.3, 7.4 and 7.5) using the parameters mentioned here.

In the automatic history match process connectivity indexes (CI’s) in three directions (x, y and z) were sampled from uniform distributions. During the facies modelling process multiple realizations were obtained and the CI’s were estimated for each realization. These connectivity indexes were then compared to the CI’s previously sampled and corresponding to the best history match. The realization with the connectivity indexes most similar to the sampled CI´s was chosen to use in the history match process.

This methodology allows identifying the connectivity indexes and the connectivity anisotropy of a reservoir as well as selecting the realization that better honours the connectivity indexes selected. This avoids assigning high misfit to plausible models just because the facies model did not respect the geobody connectivity.

Finally, all these three techniques were used together in the automatic history-matching workflow, generating models that not only considers the realism of the facies geometry of fluvial meandering deposits, but also tests different geological concepts or interpretations, varies the vertical facies proportion based on a periodic function and analyses the connectivity of geobodies, all these process are run automatically and the output models are validated against production data.

Chapter 8

Summary and Conclusions

8.1 General view of the thesis

A summary of the results obtained in this thesis is outlined here, starting from the modelled inter-relationships between geomorphic parameters - used as intelligent sedimentological prior information in the automatic history-match workflow. Several improvements have been developed for facies modelling within the automatic history matching workflow.

In the recent developments of automatic history-matching, most of the attention has been paid to improve the sampling and optimization algorithms, as well as analysing the impact of the prior information of reservoir engineering parameter. Arnold (2008) developed various techniques to parameterize geological information and used these geological parameters in the framework of automatic history-matching. Arnold's (2008) work demonstrated the importance of considering the integration of geological parameters into the automatic history-match process and highlighted the impact of preserving realism of the geological models used in history matching.

This thesis is focused on presenting a methodology to preserve the realism of geological models and to introduce this methodology into the automatic history-matching framework.

The main point addressed in this work is related to keeping the realism of facies distribution and geometry of three depositional environments (fluvial meandering, deep-marine channels and deltaic systems).

In this thesis, machine learning techniques were used for compiling geomorphic parameters associated with each of the three considered sedimentary environment. These “intelligent” compilations of parameters were used as informative prior information, from which it was possible to sample within the Bayesian framework of automatic history matching (Chapter 3).

8.2 Thesis Conclusions

This Section is divided into two main parts; the first part is dedicated to major outcomes obtained from this work and their applications. The second part is dedicated to give more detail to the contributions obtained from this thesis.

8.2.1 Major Conclusions

1 A system that controls the geological realism of facies geometry in reservoir models was developed and included into the automatic history matching framework. The approach ensures that only realistic combinations of geomorphic parameters are considered for history matching, and therefore reducing computing time and avoiding history matching reservoir models with facies geometries not observed in nature.

2 The control of geological realism was based on generation of “intelligent” geological prior information within the inverse modelling loop of reservoir history matching. By using “intelligent” geological prior information it was possible to control the realism of multiple facies models.

3 Reservoir models developed for different depositional environments -- fluvial meandering channels, deltaic deposits and deep-marine channels -- can be automatically generated assuring the realism of their facies

geometries. Geomorphic parameters from these three depositional environments were compiled from an exhaustive review of published work. Machine Learning Techniques were used to identify the internal relationships between these geomorphic parameters. These relationships were used as "intelligent" prior information.

4 A methodology to assess geological interpretations that best match production data and reduces the uncertainty was proposed in the thesis. The use of multiple training images within the automatic history match process introduces the possibility of screening multiple geological interpretations/concepts, which is one of the largest uncertainties in reservoir modelling. Under the Bayes rule, sampling from multiple training images (prior information) provides the selection of the training image (geological concept) that generates facies models whose production responses matches better the production history, this was explained in Section 7.2.

5 The vertical distribution of facies proportions is directly associated with the evolution through time of a sedimentary system. The evolution of factors like the accommodation space changes and the source of sediments would affect the facies distributions, generating different stacking patterns. Based on the available reservoir data (cores, well-logs and seismic information) it is possible to interpret these sedimentation patterns but, as in any interpretation process, it is subject to large uncertainty involved. In Section 7.3 the changes in the vertical facies proportions were parameterized using a sinuous function and introduced into the automatic history matching workflow. Sampling from different sedimentary stacking patterns (distribution of vertical facies proportions) validated the stratigraphic evolution model with production data. This improvement of the automatic history matching workflow allows the use of different stratigraphic evolution patterns, which included the uncertainty associated with the interpretation of stacking patterns.

6 Assessing the connectivity of multiple realizations avoids discarding realistic geomodels and allows accounting for stochastic variability. Selecting from multiple facies realizations generated with the same combination of geomorphic parameters increases the possibility of finding a model that matches production history. This feature was introduced into the automatic history matching workflow in Section 7.4. The criterion to select from multiple realizations was the connectivity of geobodies, identified as a Connectivity Index (CI), because different realizations generated from a single set of parameters could have different degree of connectivity between geobodies'. The CI vector represents connectivity in three dimensions. CI components are sampled from a uniform distribution and compared to the CI across the multiple generated realizations. Then, the realization with the CI more similar to the sampled CI, is chosen to perform the history match process.

7 The inclusion of the CI into the automatic history match framework does not only reduce the possibility of discarding realistic combination of geomorphic parameters, but also allows validating the degree of connectivity of a specific facies in a determined sedimentary environment.

8.2.2 Detailed outcomes

1 The complex relationships between geomorphic parameters can be described by Multilayer Perceptron (MLP) and Support Vector Regression (SVR). These powerful tools can be used to identify relationships among different geological properties.

2 SVR demonstrated to be a more reliable technique when modelling the geomorphic parameters than MLP since the results obtained with MLP showed some unrealistic artefacts that were generated in areas with low data control. These artefacts were not observed in the results obtained with SVR.

3 All the geomorphic parameters are directly related as shown in Appendix E, with the use of Machine Learning it is possible to observe these relationships in a multidimensional space.

4 The use of One-Class SVM as the filter that controls the selection of geomorphic parameters for a reservoir model is a better option than using SVR since One-Class SVM can directly reject the combination of geomorphic parameters that is considered as unrealistic, since this is actually a classification problem rather than a regression problem.

5 One-Class SVM models as geological prior information for reservoir facies modelling reduced the uncertainty related to number of models used for history matching, and reduce the uncertainty in forecasting the production behaviour of the reservoir (Sections 6.2 and 6.3).

6 Multiple training images are related to multiple geological interpretations. This approach can be applied when there is a high degree of uncertainty in the sedimentary environment interpretation of a reservoir. Using multiple sedimentary environment interpretations (training images) as a parameter to sample within the automatic history match workflow allows the possibility of using multiple interpretations instead of being fixed to a single sedimentological interpretation. This saves time in building separate sets of models for every interpretation.

7 Plotting the fields where a training image or geological interpretation has validity using MDS and SVM, is useful not only for selecting the training image to build a reservoir model but for rejecting training images that could overlap fields of validity with other training images (Section 7.2).

8.3 Data used

The results obtained in this thesis were based on synthetic reservoirs. These results show that the techniques applied here can be applied in real cases offering a realistic and adequate representation of uncertainty in reservoir production forecast and saving computing time when using geological parameters in automatic reservoir history matching.

The fluid and reservoir engineering properties of the synthetic reservoirs used in this thesis were based on the properties of the Stanford VI Reservoir (Castro *et al.,* 2005). The three synthetic reservoirs were described in Chapter 6.

The "intelligent" geological prior information generated for the sedimentary environments studied in this thesis, was based in the collection of geomorphological data from published work, Appendices A, B and C show detailed tables with all the geomorphic parameters compiled.

The relationships between these geomorphic parameters were identified by using machine learning techniques, these relationships were used a the prior information controlling the realism of the facies models.

8.4 Codes used

Facies models were performed using the Multiple Point Statistics algorithm SNESIM (Strebelle, 2002) from the software of the Stanford University SGeMS (Remy *et al.,* 2009). The codes that control the realism of the combination of geological parameters and other features that improved the geological realism within the automatic history match process were written in R (Gentleman and Ihaka, 1997). The codes that connected all the programs involved in this thesis (SGEMS (Stanford University), ECLIPSE-100 (Schlumberger), R, Machine Learning codes and RAVEN (www.epistemy.com)) were written using Python (Lutz, 2010).

8.5 Future Work

This thesis is a step forward in controlling the geological realism of facies models and assessing geological uncertainty from different sources, within the process of automatic history matching. But still further work can be performed in order to improve the results obtained here and in other aspects related to geological realism in reservoir modelling.

8.5.1 Improvement of the work presented here

- It is necessary to run the workflow proposed in this thesis for controlling the realism of facies models and the application of features that asses the uncertainty in geological interpretation (multiple training images, vertical facies proportions and facies connectivity) in a real case, because working with real data would improve the workflow since coping with actual reservoir data usually includes the normal noise associated with data and features real heterogeneities of an actual reservoir.
- Increase the number of facies in the models presented here like crevasse splay deposits, coal seems, intra-channel clay plugs, etc. in order to increase the realism of the reservoir geology.
- Use a more flexible function instead of sine (e.g. kernel based function) for modelling vertical proportion distributions, since there is not a good match between the vertical facies proportions of the truth case in section 7.3 and the sinuous curve obtained from the automatic history matching process. Although the trends obtained from the models with the lowest misfit mimic the trend of the vertical facies proportions of the “truth” case.
- Generate automatic changes of vertical proportion curves in different areas of the reservoir in order to consider the spatial variability of this feature.
- Consider sampling the values of the geomorphic parameters in ranges that represent real changes in the facies geometry in order to avoid getting trapped in apparent local minima. Figure 8.1 is a representation

of a potential local minimum where the algorithm got trapped because of the resolution of the sampling. This cannot be controlled by RAVEN yet.

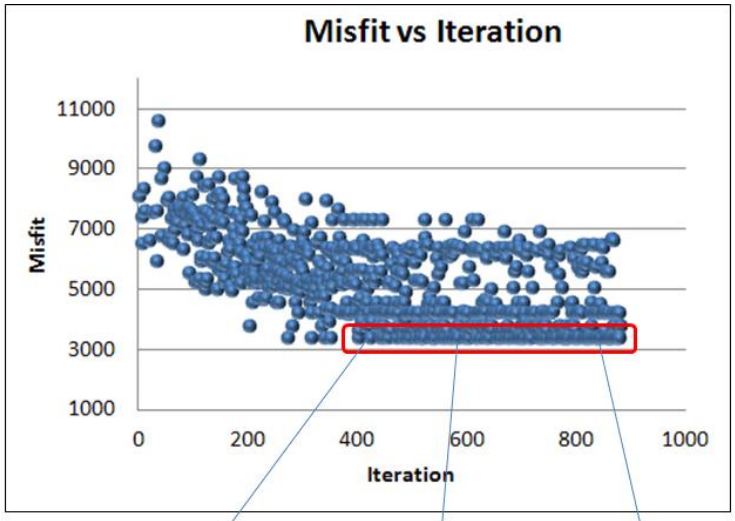

Model	317	637	838
Width	237.5728	237.5735	237.5777
Thickness	12.6329	12.6338	12.6406
Amplitude	888.7632	888.7633	888.7546
Wavelength	1240.8603	1240.8539	1240.8592

Figure 8.1 Apparent local minima (red square). Due to sampling values resolution.

- Optimization of the codes developed in this thesis will save computing time, some of the codes look very long and repetitive.

8.5.2 Other aspects related to geological realism

- Generating intelligent prior information related to petrophysical data, using Machine Learning Techniques will relate properties like porosity, permeability, grain size, burial depth and facies with diagenetic processes which are the factors that controls fluid flow and storage in reservoir.
- Generate intelligent geological prior information based on machine learning techniques for other depositional environments, like braided

fluvial channels, shore-face, estuarine, carbonates, lacustrine and volcanoclastics among others.

- Finding geological priors for faults throw and dip as well as fractures parameters like aperture, frequency and geometry, which should be related to the stress field that generated the fault-fracture system in a reservoir.
- Include the realistic geometry of the facies bounding surfaces like clinoforms and lateral acretionary surfaces which have a great impact on reservoir fluid flow (Deveugle, *et al.,* 2011).
- Incorporate the methodology applied in this thesis with techniques that integrate large datasets like Multiple Kernel Learning (MKL). Backhouse *et al.,* (2012) used MKL to integrate reservoir parameters from, well data, reservoir data, training images and production data in order to history match a reservoir. Intelligent sedimentological prior information can be integrated into the workflow presented by Backhouse *et al.* (2012) in order to work only with geologically realistic reservoir models.

References

Aanonsen, S., Naevdal, G., Oliver, D., Reynolds, A., and Valles, B. (2009) *The ensemble Kalman filter in reservoir engineering – a review*. SPE Journal, SPE 117274–PA, 14(3): 393–412.

Abreu, V., Sullivan, M., Pirmez, C. and Mohrig, D. (2003) *Lateral Accretion Packages (LAPs): An Important Reservoir Element in Deep-Water Sinuous Channels*. Marine and Petroleum Geology. 20: 632-648.

Alapetite, J., Leflon, B., Gringarten, E. and Mallet,J-L. (2005) *Stochastic Modelling of Fluvial Reservoirs.The YACS Approach*. SPE Annual Technical Conference and Exhibition. Dallas-Texas. SPE 97271, 5 pp.

Allen, G.P. (1997) *Sedimentology and Stratigraphy of Alluvial and Deltaic Reservoirs.* Maraven S.A. Internal Publication, Caracas. 98 pp

Allen, G.P., Laurier, D. and Thouvenenin, J. (1979). *Etude Sedimentologique du Delta de la Mahakam*: Paris TOTAL, Compagnie Francaise des Petroles, Notes e Memories 15, 156 pp.

Allen, J.R.L. (1965) *Finning upward cycles in alluvial successions*. Geological Journal. 4 (2): 229-246.

Allen, J.R.L. (1965b) *Late Quaternary Niger Delta, and Adjacent Areas: Sedimentary Environments and Lithofacies*. AAPG Bulletin. 49 (5) 547-600.

Allen, J.R.L. (1979) *Studies in fluviatile sedimentation: An elementary geometrical model for the connectedness of avulsion-related channel sand bodies*. Sedimentary Geology. 24 (3-4): 253-267.

Allen, J.R.L. (1982) *Sedimentary Structures. Their character and physical basis, Vol II.* Developments in Sedimentolgy 30B. Elsevier. The Netherlands. 663 pp.

Allen, J.R.L. (1983) *Studies in Fluviatile Sedimentation: bars, bar-complexes and sandstone sheets (low sinuosity braided streams) in the Brownstones (L.Devonian), Welsh Borders*. Sedimentary Geology. Vol 33, Pag. 237-93.

Allen, J.R.L. (1991) *The Bouma Division A and the Possible Duration of Turbidity Currents.* Journal of Sedimentary Petrology. 61: 291-295.

Anderson, M.P. (1997) *Characterization of Geological Heterogeneity*. In Dagan, G. and Neuman, S.P. (eds) Subsurface flow and transport: A stochastic approach. Cambridge University Press. Cambridge. 23-43.

Anterion, F., Eymard, R. and Karcher, B. (1989) *Use of Parameter Gradient for Reservoir History Matching.* SPE18433. Symposium of Reservoir Simulation. Houston, TX. 339-354.

Archie, G.E. (1942) *The electrical resistivity log as an aid in determining some reservoir characteristics*. Journal of Petroleum Technology. 5: 54-62.

Arnaud-Fassetta, G. (2003) *River Channel Changes in the Rhone Delta (France) Since the End of the Little Ice Age: Geomorphological Adjustment to Hydroclimatic Change and Natural Resource Management*. Catena 5 (2) 141-172.

Arnold, D.P. (2008) *Geological Parameterization of Petroleum Reservoir Models for Improved Uncertainy Quantifiaction*. PhD Thesis. Heriot-Watt University. UK. 229 pp.

Arps, J.J. (1944) *Analysis of Decline Curves*. AIME Houston Meeting Transactions. 228-247.

Asquith, G. and Krygowski, D. (2004) *Basic Well Log Analysis*. AAPG Methods in Exploration Series 16. AAPG, Oklahoma. 244 pp.

Backhouse, L., Demyanov, V. and Christie, M. (2012) *Integration and Selection of Geological Scenarios Through Multiple Kernel Learning to Improve The Prediction of Reservoir Properties*. Proceedings of the Ninth International Geostatistical Congress , Oslo. 8 pp.

Bahttachayra, B. and Solomatine, D.P. (2000) *Application of artificial neural networks in stage-discharge relationships*. Proccedings of the 4th International Conference on Hydroinformatics, Iowa City, USA. 1-7.

Bahttacharya, J.P. and Walker, R.G. (1992) *Deltas*. In Walker, R.G. and James, N.P. (eds) . Facies Models Response to Sea Level Change. Geological Association of Canada: 157-177.

Bastidas, L, Palacios, Z. and Rivas, F. (2008). *Deltaic Systems with Fluvial Dominion Interpretation using Artificial Neural Networks.* 12th WSEAS International Conference on SYSTEMS, Heraklion, Greece. 327-333.

Batycky, R.P., Seto, A.C. and Fenwick, D.H. (2007) *Assisted History Matching of a 1.4-Million-Cell Simulation Model for Judy Creek 'A' Pool Waterfloff/HCMF Using a Streamline Based Workflow*. SPE Paper 108701, Anaheim CA. 10 pp.

Baun, G. and Vail, P.R. (1988) *Sequence Stratigraphic Concepts applied to Paleogene Outcrops, Gulf and Atlantic Basins*. In Wilgus, C.K., Hastings, B.S., Posamentier, H., Van Wagoner, J., Ros, C.A. and Kendal, C.G. (eds) Sea Level changes an Integrated Approach. SEPM SpecialPublication, 42.

Belkin, M., Niyogi, P. and Sindhwani, V. (2006) *Manifold Regularization: A Geometric Framework for Learning from Labeled and Unlabeled Examples.* Journal of Machine Learning Research. 7: 2399-2434.

Besaw, L.E., Rizzo, D.M., Kline, M., Underwood, K.L., Doris, J.J., Morrissey, L.A. and Pelletier, K. (2009) *Stream classification using hierarchical artificial neural networks: A fluvial hazard management tool*. Journal of Hydrology. 373: 34-43.

Beucher, H., Galli, a., Le Loc'h, G. and Ravenne, C. (1993) Including a Regional *trend in Reservoir modelling using the Truncated Gaussian Method*. In Soares, A. editor, *Geostatistics-Troia*. Vol 1, 555-566.

Bishop, C.M. (1995) *Neural Networks for pattern recognition*. Oxford University Press, Oxford. 504 pp.

Borg, I., and Groenen, P. (1997). *Modern multidimensional scaling: theory and applications*. New York: Springer.

Bridge, J.S. (1975) *Computer Simulation of Sedimentation in Meandering Streams*. Sedimentology 22 (1): 3-43.

Bridge, J.S. (2003) *Rivers and floodplains, forms processes and sedimentary record*. Blackwell Science Ltd. ed. Oxford. 491 pp.

Bridge, J.S. and Mackey, S.D. (1993) *A theoretical study of fluvial sandstone body dimensions*. In: Flint, S. and Bryant I.D. The Geological Modelling of Hydrocarbon Reservoirs and Outcrop Analogues. International Association of Sedimentologists. Special Publication No. 15. Blackwell Scientific Publications. pag 213-236

Bridge, J.S. and Tye, R.S. (2000) *Interpreting the dimensions of Ancient Fluvial Channel Bars, Channels and Channel Belts from Wireline-Logs and Cores*. AAPG Bulletin. 84 (8): 1205-1228.

Brown, S. and Richards, P.C. (1989) *Facies and development of the Middle Jurassic Brent Delta near the northern limit of its progradation. UK, North Sea*. In Whateley, M.K.G. and Pickering, K.T. (eds.) Deltas Sites for Fossil Fuels. Geological Society Special Publication. No.41. Blackwell Scientific. Publications Oxford. 253-268.

Bujor, S., Thenin, D. and Perry, I. (2011) *Using a Three Dimensional Lithofacies Proportion Cube for More Realistic Reservoir Models: Case Study of a Steam Assisted Gravity Drainage (SAGD) Project in the Athabasca Oil Sands, NE Alberta, Canada*. Proceedings of the Gussow Geoscience Conference. Bannf, Alberta. 15 pp.

Buszewski, B. and Kowalkowski, T. (2006) *A New Model of Heavy Metal Transport in the Soil Using Nonlinear Artificial Neural Networks*. Environmental Engineering Science. 23(4): 589-595.

Brown, W. M., Gedeon, T. D., Groves D. I. and Barnes , R. G. (2000) *Artificial neural networks: a new method for mineral prospectivity mapping*. Australian Journal of Geosciences. 47 (4): 757-770.

Caers, J. (2005) *Petroleum Geostatistics*. Society of Petroleum Engineers. 88 pp.

Caers, J. and Hoffman, T. (2006) The Probability Pertubation Method: A New Look at Bayesian Inverse Modeling. Mathematical Geosciences. 38 (1): 81-100.

Callec, Y., Deville, E., Desaubliaux, G., Griboulard, R., Huyghe, P., Mascle, A., Mascle, G., Noble, M., Padron, C. and Schmitz, J. (2010) *The Orinoco Turbidite System: Tectonic Control on Sea-floor morphology and Sedimentation*. AAPG Bulletin. 49 (6): 869-887.

Carlston, C.W. (1965*) The relation of free meander geometry to stream discharge and its geomorphic implications*. American Journal of Science. 263: 864-885.

Carriquiry, J.D. and Sanchez, A. (1999) Sedimentation in the Colorado River Delta and Upper Gulf of California after Nearly a Century of Discharge Loss. Marine Geology. 158 (1): 125-145.

Carter, J.N., Ballester, P.J., Tavassoli, Z. and King, P.R. (2006) *Our Calibrated Model has Poor Predictive Value: An example from the Petroleum Industry*. Reliability Engineering and System Safety. 91: 1373-1381.

Castro, S. A., Caers, J. and Mukerji, T. (2005). *The Stanford VI Reservoir: 18th Annual Report.* Stanford Centre for Reservoir Forecasting. Stanford University. 73 pags.

Catuneanu, O. (2006) *Principles of Sequence Stratigraphy*. Elsevier. Amsterdam. 375 pp.

Challenor, P. and Tokmakian, R. (2011) *Modelling Future Climates.* In Christie, M., Cliffe, A., Dawid, P. and Senn, S. (eds.) Simplicity, Complexity and Modelling. Wiley. Chichester: 69-81.

Cherkassky, V. and Mulier, F.M. (2007) Learning from Data: Concepts, Theory and Methods. 2nd edition. Wiley and Sons Inc.

Cherpeau, N., Caumon, G., Caers, J., and Lévy, B. (2012) *Assessing the Impact of Fault Connectivity Uncertainty in Reservoir Studies using Explicit Discretization*. SPE Paper 148085-MS. 9 pp.

Chitale, S.V. (1970) *River Channel Patterns*. Journal of the Hydraulics Division. Proc. Am. Soc. Civ. Eng. HY1: 201-221.

Christie, M. (2011) *Uncertainty Quantification and Oil Reservoir Modelling*. In Christie, M., Cliffe, A., Dawid, P. and Senn, S. (eds.) Simplicity, Complexity and Modelling. Wiley. Chichester: 147-172.

Christie, M.A. (1996) *Upscaling for Reservoir Simulation*. Journal of Petroleum Technology. 48 (11): 1004-1010.

Christie, M.A. and Blunt, M.J. (2001) *Tenth SPE comparative solution project: A comparison of upscaling techniques.* SPE Reservoir Evaluation and Engineering, 4(4):308–317.

Christie, M., Demyanov, V. and Erbas, D. (2006) *Uncertainty Quantification for Porous Media Flow.* Journal of Computational Physics. 217: 143-158.

Christie, M.A., Glimm, J., Grove, J.W., Higdon, D.M., Sharp, D.H. and Wood-Schutz, M.M. (2005). *Error analysis and simulation of complex phenomena*. Los Alamos Science. 29:6-25.

Christie, M., Cliffe, A., Dawid, P. and Senn, S. (2011) *Simplicity, Complexity and Modelling*. Chapter 1: Introduction. Wiley. Chichester: 1-9.

Clemente, P. and Perez-Arlucea, M. (1993) *Depositional Architecture of the Cuerda Del Pozo Formation, Lower Cretaceous of the Extensional Cameros Basin, North-Central Spain*. Journal of Sedimentary Petrology. 63 (3): 437-452.
Clerc, M. (2006) Particles Swarm Optimization. London Uk. Wiley-Blackwell.

Coleman, J.M. and Wright, L.D. (1975) *Modern river deltas variability of processes and sand bodies*. In Broussard, M.L. (Ed.) Deltas, models for exploration. Houston Geological Society: 99-149.

Collobert, R. and Bengio, S. (2001) SVMTorch: Support vector machines for large-scale regression problems. Journal of Machine Learning Research. 1: 143-160.

Cortes, P. and Vapnik, V. (1995) *Support Vector Networks*. Machine Learning. Vol 20:273-297.
Correggiari, A., Cattaneo, A. and Tricardi, F. (2005) *The modern Po Delta System: Lobe Switching and Asymmetric Prodelta Growth*. Marine Geology. 222-233: 49-74.

Crane, R.C. (1983). *A Computer Model for the Architecture of Avulsion-controlled Alluvial suites*. PhD Thesis. The University of Reading, Department of Geology. Unpublished. 229 pp.

Culbertson, D.M., Young, L.E. and Brice, J.C. (1967) *Scour and fill in alluvial channels.* U.S. Geological Survey. Open file report 58 pp.

Curtis, D.M. and Picou, E.B. (1980) *Gulf Coast Cenozoic: A Model for the Application of Stratigraphic Concepts to Exploration on Passive Margins*. American Association of Petroleum Geologists, Memoir 6: 243 – 268.

Dabrio-Gonzalez, C.J. (1984) Sedimentacion en Costas Siliciclasticas, Deltas y Mares Someros. Ciclo de Seminario de Sedimentologia Vol. 1. Instituto Geologico y Minero de España: 131-191.

Dake, L.P. (2002) *Fundamentals of Reservoir Engineering*. Elsevier. Amsterdam. 443 pp.

Damuth, J.E., Flood, R.D., Kowsmann, R.O., Belderson, R.H. and Gorini, R.A. (1988*) Anatomy and Growth Pattern of Amazon Deep-Sea Fan as Revealed by Long-Range Side-Scan Sonar (GLORIA) and High-Resolution Seismic Studies*. AAPG Bulletin. 72 (8): 885-911.

Darman, N.H., Pickup, G. and Sorbie, K.S. (2002) *A Comparison of Two-Phase Dynamic Upscaling Methods Based on Fluid Potentials*. Computational Geosciences. 6 (1): 5-27.

Datta-Gupta, A. (2000) *Streamline Simulation: A Technology Update. Distinguish Author Series*. Journal of Petroleum Technology. 68-74

Davies, W.M. (1899) *The geographical cycle*. The Geographical Journal. 14 (5): 481-504.

de Marsily, G., Lavedan, G., Boucher, M., Fasanino, G. (2004) Interpretation of Interference Tests is a Well Field using Geostatistics Techniques to fit the Permeability distribution in a Reservoir Model. In Verly, G., David, M., Journel,

A.G. and Marechal, A. Geostatistics for Natural Resources Characterization 182: 831-849.

Demicco R. V. (1998) *CYCOPATH 2D-- a two-dimensional forward model of cyclic sedimentation on carbonate platforms*. Computers and Geosciences. 24 (5): 405-423.

Demyanov, V., Christie, M., Kanevski, M. and Pozdnoukhov, A. (2012). *Reservoir Modelling Under Uncertainty – A Kernel Learning Approach.* IX International Geostatistics Congress. Oslo, extended abstract.

Demyanov, V., Pozdnoukhov, A., Kanevski, M. and Christie, M. (2008). *Geomodelling of a Fluvial System with Semi Supervised Support Vector Regression*. VII International Geostatistics Congress. Santiago de Chile: 627-636.

Demyanov, V., Subbey, S. and Christie, M. (2004) *Uncertainty Assessment in PUNQ-S3 -Neighbourhood Algorithm framework for geostatistical modelling*. 9thEuropean Conferenceon the Mathematics of Oil Recovery, Cannes, France.

Deutsch, C. V. (1998) *Fortran programs for calculating connectivity of three-dimensional numerical models and for ranking multiple realizations*. Computers & Geosciences 24 (1): 69–76.

Deutsch, C. V. (2002) *Geostatistical Reservoir Modeling*. Oxford University Press. New York. 376 pp.

Deveugle, P.E.K., Jackson, M.D., Hampson, G.J., Farrel, M.E., Sprague, A.R. Stweart, J. and Calvert, C.S. (2011) *Characterization of stratigraphic architecture and its impact on fluid flow in a fluvial dominated deltaic reservoir analogue: Upper Cretaceous Ferron Sandstone Member, Utah*. AAPG. Bulletin, 95: 693-727.

Doyen, P.M., Psalia, D.E. and Strandenes, S. (1994) *Beyesian Sequential Indicator Simulation of Channel Sands from 3D Seismic Data in The Oseberg Field, Norwegian North Sea*. SPE 69th Technical Conference. New Orleans. SPE-28382. 15 pp.

Doyle, J.D. and Sweet, M.L. (1995) Three-Dimensional distribution of Lithofacies, Bounding Surfaces, Porosity and Permeability in a Fluvial Sandstone – Gypsy Sandstone of Northern Oklahoma. AAPG Bulletin. 79 (1): 70-96.

Duane, S., Kennedy, A.D., Pendleton, B.J. and Roweth, D. (1987) *Hybrid Monte Carlo.* Physics Letters B, 195 (2): 216-222.

Duda, R.O. and Hart, P.E. (1973) *Pattern Classification and Scene Analysis.* John Wiley and Sons.

Dupre, W.R. and Thompson, R. (1979) *The Yukon Delta a Model for Deltaic Sedimentation in an Ice-Dominated Environment*. Offshore Technology Conference. Paper 3434: 657-664.

Durlofsky, L.J. (1998) Coarse Scale Methods of Two-Phase Flow in Heterogeneous Reservoirs: Volume Averaged Equations and their Relationship to Exisisting Upscaling Techniques. Computational Geosciences. 2 (2): 73-92.

Dury, G.H. (1967) *Some channel characteristics of the Hawkesbury river, New South Wales*. Australian Geographical Studies, 5: 135-149

Ehsani, A.H. and Quiel, F. (2008) *Geomorphometric feature analysis using morphometric parameterization and artificial neural networks*. Geomorphology, 99 (1-4): 1-12.

Engelbrecht, A. (2005) *Fundamentals of Computational Swarm Intelligence*. Chichester, England, UK: John Wiley & Sons.

Erbas, D. (2007) *Sampling Strategies for Uncertainty Quantification in Oil Recovery Prediction*. PhD Thesis. Heriot-Watt University.

Erbas, D. and Christie, M. (2007) *Effect of Sampling Strategies on Prediction Uncertainty Estimation.* SPE Reservoir Simulation Symposium, Houston, Texas. SPE 106229. pag 1-8.

Ergo Online Database: *www.fugro-robertson.com/ergo*

Ethridge, F.G. and Schumm, S.A. (2007) *Fluvial Seismic Geomorphology: a view from the surface*. In Davis, R.J., Posamentier, H.W., Wood, L.J. and Cartwright, J.A. (eds). Seismic Geomorphology, Application to Hydrocarbon Exploration and Production. Geological Society Special Publication 277.: 205-223.

Evensen, G. (2007) Data Assimilation: The Ensemble Kalman Filter. New York. Springer.

Fan J. and Gijbels I. (1996) *Local Polynomial Modelling and Its Applications.* Monographs on Statistics and Applied Probability 66. London, Chapman and Hall.

Ferguson, R.I. (1975) *Meander irregularity and wavelength estimation*. Journal of Hydrology. 26 (3-4):315-333.

Fielding, C.R. and Crane, J. (1987) *An Application of Statistical Modelling to the Prediction of Hydrocarbon Recovery Factors in Fluvial Reservoir Sequences*. In Ethridge, F.G., Flores, R.M. and Harvey, M.D. (eds). Recent Developments in Fluvial Sedimentology. SEPM Special Publication 39: 321-327.

Fielding, C.R., Trueman, J. and Alexander, J. (2006) *Holocene Depositional History of the Burdekin River Delta of Norteastern Australia: A model for a Low Accommodation , High-Stand Delta.* Journal of Sedimentary Research 76: 411-428.

Fisk, H.N. (1961) *Bar-finger Sands of the Mississippi Delta*. In Peterson, J.A. and Osmond, J.C. (eds.) Geometry of Sandstone bodies. American Association of Petroleum Geologists. Tulsa. 29-50.

Fisk, H.N, Kolb, C.R., McFarlan, E. and Wilbert, L.J. (1954) *Sedimentary Framework of the Modern Mississippi Delta*. Journal of Sedimentary Research. 24: 76-99.

Foix, N., Allard, J.O., Paredes, J.M. and Giacosa, R.E. (2012) *Fluvial styles, Palaeohydrology and Modern Analogues of and Exhumed, Cretaceous Fluvial System. Cerro Basino Formation, Cañadón Asfalto Basin, Argentina*. Cretaceous Research. 34: 298-307.

Foresti, L. (2011) *Kernel-Based Mapping of Meteorological fields in complex orography*. PhD Thesis. University of Lausanne. Unpublished. 182 pp.

French, J.R. (1993) *Numerical simulation of vertical marsh growth and adjustment to accelerated sea-level rise, North Norfolk, U.K.* Processes and Landforms. 18 (1): 63-81.

Galloway, W.E. (1975) *Processes Framework for Describing the Morphological and Stratigraphic Evolution of Deltaic Depositional Systems.* In: Broussard, M.L. (ed.) Deltas, Models for Exploration. Houston Geological Society, 87–98.

Gavalas, G.R., Shah, P.C., Seinfeld, J.H. (1976) *Reservoir History Matching by Bayesian Estimation*. Society of Petroleum Engineers Journal. Vol. 16 (6): 337-350.

Gelman, A. (2002) *Prior Distribution*. In El-Shaarawi, A.H. and Piegorsch, W.W. (eds) Encyclopedia of Environmetrics.. Vol 3: 1634-1637. John Wiley and Sons, Ltd. Chichester.

Gentleman, R. and Ihaka, R. (1997) *R*. Statistics Department of the University of Auckland. http://www.r-project.org

Gibbling, M.R. (2006) Width and thickness of fluvial channel bodies and valley fills in the *geological record: A Literature compilation and classification*. Journal of Sedimentary Research. 76: 731-770.

Giosan, L., Constantinescu, S., Clift, P.D., Tabrez, A.R., Danish, M. and Inam, A. (2006) *Recent Morphodynamics of the Indus Delta, Shore and Shelf.* Continental Shelf Research. 26: 1668-1684.

Gomez, S., Gosselin, O. and Barker, J.W. (2001) *Gradient-Based History Matching with a Global Optimization Method*. Society of Petroleum Engineers Journal. Vol 6 (2): 200-208.

Google Earth. www.earth.google.co.uk

Govindaraju, R.S. (2000a) *Artificial neural networks in hydrology. I Preliminary Concepts*. Journal of Hydrologic Engineering. 5 (2): 115-123.

Govindaraju, R.S. (2000b) *Artificial neural networks in hydrology. II Hydrologic Applications*. Journal of Hydrologic Engineering. 5 (2): 124-137.

Gross, L.J. and Small, M.J. (1998) *River and floodplain process simulation for subsurface characterization*. Water Resources Research. 34: 2365–2376.

Guardiano, F. and Srivastava, R.M. (1993) *Multivariate Geostatistics: Beyond Bivariate Moment.* In Soares, A. (ed.) Geostatistics-Troia. 1: 133-144. Kluwer Academic Publications.

Hair, J. F., Anderson, T. E., Tatham, R. L. and Black, W. C. (1998). *Multivariate data analysis*. Upper Saddle River, NJ: Prentice Hall.

Hajizadeh, Y., Christie, M. and Demyanov, V. (2009) *Application of Diferential evolution as a New Method for Automatic History Matching*. International Petroleum Conference and Exhibition, Kuwait. SPE-127251. 13 pp.

Hajizadeh, Y., Christie, M. and Demyanov, V. (2011) *Ant Colony Optimization for History Matching and Uncertainty Quantification of Reservoir Models*. Journal of Petroleum Science and Engineering. 77: 78-92..

Harding, T.P. and Lowell, J.D. (1979) Structural Styles, Their Plate Tectonic Habitats and Hydrocarbon Traps in Petroleum Provinces. AAPG Bulletin. V. 63 (7): 1016-1058.

Hardle, W (1989*). Applied Nonparametric Regression*. Cambridge University Press. Cambridge. 409 pp.

Harris, P.T., Pattiaratchi, C.B., Keene, J.B., Dalrymple, R.W., Gardner, J.V., Baker, E.K., Cole, A.R., Mitchell, D., Gibbs, P. and Schroeder, W.W. (1996) *Late Quaternary, Deltaic and Carbonate Sedimentation in the Gulf of Papua Foreland Basin Response to Sea-Level Change*. Journal of Sedimentary Research. 66 (4): 801-819.

Hastie, T., Tibshirani, R. and Friedman, J. (2009) *The Elements of Statistical Learning. Data Mining, Inference and Prediction*. Springer. New York. 745 pp.

Hauge, R., Syversveen, A.R. and MacDonnald, A. (2006) *Objects Models with Vector Steering. Mathematical Geology*. 38 (1): 17-32.

Haykin, S. (1999) Neural Networks: A Comprehensive Foundation. Macmillian College Publishing Company, NY. 842 pp.

Helland-Hansen, W., Stell, R., Nakayama, K. and Kendall, C.G. (1989) Review and computer modelling of the Brent Group Stratigraphy. In Whateley, M.K.G. and Pickering, K.T. (Eds.) *Deltas Sites for Fossil Fuels*. Geological Society Special Publication. No.41. Blackwell Scientific. Publications Oxford. 237-252.

Hodgetts, D., Drinkwater, N.J., Hodgson, J., Kavanagh, J., Flint, S.S., Keogh, K.J. and Howell, J.A. (2004) Three-dimensional geological models from outcrop data using digital data collection techniques: an example from the Tanqua Karoo depocentre, South Africa. In Curtis, A. and Woods, R. (eds) Geological Prior Information: Informing Science and Engineering. Geological Society of London. Special Publications, 239: 57-75.

Hoffman, B. T. and Caers, J. (2006) *History Matching by jointly perturbing local facies proportions and their spatial distributions: Application to a North Sea Reservoir.* Journal of Petroleum Science and Engineering 57: 257-272.

Holland, J. (1975) Adaptation in Natural and Artificial Systems. University of Michigan press. Ann. Arbor., MI 1, no. 97 : 5 pp.

Holland, S.M. (2008) *Non-metric Multidimensional Scaling (MDS)*. University of Georgia, Athens. 7 pp. http://strata.uga.edu/software/pdf/mdsTutorial.pdf

Honarkhah, M.L. and Caers, J. (2012) *Direct non-stationary Multiple-Point Modeling by Distance Based Pattern Simulation*. IX International Geostatistical Congress. Oslo. Extended Abstract.

Höök, M., Hirsch, R. and Aleklett, Kjell (2009) *Giant Oil Fields Decline Rates and their Influence on World Oil Production*. Energy Policy. 37 (6): 2262-2272.

Howard, A.D. and Hemberger, A.T. (1991) *Multivariate characterization of meandering*. Geomorphology. 4:161-186.

Hu, L.Y. (2000) Gradual Deformation and Iterative Calibration of Gaussian-related Stochastic Models. *Mathematical Geology* 32 (1): 87-108.

Hu, L.Y., Le Ravalec, M., Blacc, G., Roggero, F., Noteinger, B., Haas, A. and Corre B. (1999) Reducing Uncertainties in Production Forecasts by Constraining Geological Modeling to Dynamic Data. SPE-56703. SPE Annual Technical Conference and Exhibition. Houston 8 pp.

Hyne, N.J, Cooper, W.A. and Dickey, P.A. (1979) *Stratigraphy of Intermontane Lacustrine Delta, Catatumbo River, Lake Maracaibo, Venezuela*. AAPG, Bulletin. 63 (11) 2042-2057.

Jaynes, E.T. (1968) *Prior Probabilities*. IEEE Transactions on Systems Science and Cybernetics. 4 (3): 227-241.

Johnson, D.P. (1982) *Sedimentary Facies of an Arid Zone Delta: Gascoyne Delta, Western Australia.* Journal of Sedimentary Research 52 (2): 547-563.

Jones, R. R., McCaffrey, K. J. W., Wilson, R. W. and Holdsworth, R. E. (2004) *Digital field data acquisition: towards increased quantification of uncertainty during geological mapping*. In Curtis, A. and Wood, R. Geological Prior Information:

Informing Science and Engineering. Geological Society Special Publication No. 239, 43-56.

Journel, A.G. (1983) *Non-parametric estimation of spatial Distribution*. Mathematical Geology, 15 (3): 445-468.

Journel, a. and Alabert, F. (1989) *Non-Gaussian Data Expansion in the Earth Sciences*. Terra Nova. 1: 123-134.

Kanevski, M.F. (1999) *Spatial Predictions of Soil Contamination Using General Regression Neural Networks*. Int. Journal of Systems Research and Information Systems. 8 (4): 241-256.

Kanevzski, M., Demyanov, V. and Maignan M. (1997) *Mapping of soil contamination by using artificial neural networks and multivariate geostatistics*. Lecture Notes in Computer Science. 1327:1125-1130.

Kanevzski, M., Pozdnoukhov, A. and Timonin, V. (2009) *Machine learning for spatial environmental data. Theory, applications and software*. EPFL Press. Lausanne Switzerland. 377 pp.

Kanevzski, M. and Maignan M. (2004) *Analysis and modelling of spatial environmental data*. EPFL Press. Lausanne Switzerland. 288 pp.

Kathrada, M. (2009) *The Flexi-PSO: Towards a more flexible Particle Swarm Optimizer.* OPSEARCH. 46 (1) 52-68.

Kennedy J. and Eberhart, R. (1995) Particle Swarm Optimization. Proceedings of the IEEE International Conference of Neural Networks. Vol. 4 : 1942-1948. New Jersey. IEEE Service Center.

Krassenberg, D., Tornqvist, T.E. and Bridge, J.S. (2001) *Conditioning a process based model of sedimentary architecture to well data*. Journal of Sedimentary Research. 71 (6): 868-879.

Kroonenberg, S.B., Rusakov, G.V. and Svitoch, A.A. (1997) *The Wandering of the Volga Delta: a Response to Rapid Caspian Sea-Level Change*. Sedimentary Geology. 107: 189-209.

Kruskal, J. B. (1964) *Multidimensional scaling by optimizing goodness of fit to a nonmetric hypothesis*. Psychometrika, 29, 1-27.

Lallier, F., Caumon, G., Borgomano, J., Viseur, S., Fournier, F., Antoine, C. and Gentilhomme, T. (2012) *Relevance of the stochastic stratigraphic well correlation approach for the study of complex carbonate settings: application to the Malampaya buildup (Offshore Palawan, Philippines).* The Geological Society of London Special Publication 370 (1): 265-275.

Lampert, C.H. (2009) *Kernel Methods in Computer Visions*. Foundations and Trends in Computer Graphics and Vision. 4 (3): 193-295.

Langbein, W.B. and Leopold, L.B. (1966) *River – Meanders theory of minimum variance*. U.S. Geol. Survey, Prof. Pap. 422-H. 15 pp.

Lange, K., Cordua, K.S., Frydendall, J., Hansen, T.M. and Mosegaard, K. (2011) *A Frequency Matching Method for Generation of a Prior Sample Model from Training Images*. In Marschallinger, R. and Zobl, F. (eds): Mathematical Geosciences at the Crossroads of Theory and Practice, Proceedings of the IAMG-2011 conference, September 5-9 2011, Salzburg, Austria:8 pp.

Larue, D.K. and Hovadik, J. (2006) *Connectivity of channelized reservoirs: a modelling approach*. Petroleum Geoscience. 12: 291-308.

LeBlanc, R. (1972) *Geometry of Sandstone Reservoirs*. In: Underground Waste Management and Environmental Implications. American Association of Petroleum Geologists Memoir 18: 133-189.

Lee, J.A. and Verleysen, M. (2007) *Nonlinear dimensionality reduction.* Springer. New York. 308 pp.

Leeder, M. R. (1973) *Fluviatile finning upward cycles and the magnitude of palaeochannels*. Geological Magazine (110) 265-276.

Leopold, L.B. and Maddock, J.T. (1953) *The hydraulic geometry of stream channels and some physiographic implications.* U.S. Geol. Surv. Prof. Papers 252.

Leopold, L.B. and Wolman, M.G. (1957) *River Channel Patterns: Braided ,Meandering and Straight*. U.S. Geol. Surv. Prof. Papers 282-B: 39-85.

Leopold, L.B. and Wolman, M.G. (1960) *River Meanders*. Bulletin of the Geological Society of America. 71: 769-794.

Leopold, L.B., Wolman, M.G. and Miller, J.P. (1964) *Fluvial Processes in Geomorphology*. Freeman and Co. San Francisco. 511 pp.

Liu, N., Betancourt, S. and Oliver D.S. (2001) *Assessment of Uncertainty Assessment Methods.* SPE-71624. Annual Technical Conference. New Orleans. 15 pp.

Liu, N. and Oliver D.S. (2005) *Ensemble Kalman Filter for Automatic History-Matching of Geologic Facies .* Journal of Petroleum Science and Engineering. 47: 147-161.

Liu, Y. (2006) *Using the Snesim Program for Multiple-point Statistical Simulation* Computers and Geosciences. 32 (10): 1544-1563.

Lorenz, J.C., Heinze, D.M., Clark, J.A. and Searls, C.A. (1985) *Determination of Widths of Meander-Belt Sandstone Reservoirs from vertical Downhole Data, Mesa Verde Group, Piceance Creek Basin, Colorado*. AAPG Bulletin, Vol. 69 (5): 710-721.

Lutz, M. (2009) *Learning Python.* O'Reilly . Sebastopol. CA. 1163 pp. www.python.org

Martinesen, O.J. (1990) *Fluvial intertidal dominate deposition in the Namurian (Carboniferous) of northern England*. Sedimentology. V. 37: 1099-1113.

Massonnat, G.J. (2000) *Can we sample the complete Geological Uncertainty Space in Reservoir Modelling Uncertainty Estimates?.* SPE paper 38746. SPE Journal. 5 (1): 46-59.

Matheron, G. (1963) *Principles of Geostatistics*. Economic Geology. (58): 1246-1266.

Matheron, G. (1971) *The Theory of Regionalized Variables and its Applications*. Le Cahier du Centre de Morphologie Mathématique de Fontainebleau. No 5. École Nationale Supérieore des Mines de Paris. 218 pp.

Mathew, W.H. and Shepard, F.P. (1962) *Sedimentation of Fraser River Delta, British Columbia*. AAPG Bulletin. 46 (8): 1416-1438.

Mattax, C.C. and Dalton, R.L. (1999) Reservoir Simulation, SPE Monograph Series. Society of Petroleum Engineers. Richardson. Texas. 173 pp.

Maucec, M., Yarus, J.M., Shi, G., Chambers, R.L. (2012) *Grid-less Modelling of Reservoir Properties with Maximum Continuity Field Interpolation*. IX International Geostatistical Congress. Oslo. Extended Abstract.

Miall, A.D. (2006) *Reconstructing the architecture and sequence Stratigraphy of the preserve fluvial record as a tool for reservoir development: A reality check.* American Association of Petroleum Geologists Bulletin, Vol. 90, No. 7, pag. 989-1002.

Miall, A.D. (1996) *The Geology of Fluvial Deposits. Sedimentary Facies, Basin Analysis, and Petroleum Geology*. Springer. 582 pp.

Mial A.D. (1994) *Reconstructing Fluvial Macroforms Architecture from two-dimensional outcrops: Examples from the Castlegate Sandstone, Book Cliffs Utah.* Journal of Sedimentary Research. B64: 146-158.

Miall A.D. (1992) *Alluvial Deposits*. In Walker R.G. and James N.P. (eds.) Facies Models Response to Sea Level Change. Geological Association of Canada. 119-142.

Miall, A.D. (1991) *Hierarchies of architectural units in clastic Rocks and their relationship to sedimentation rate.* In Miall, A:D. and Tye, N. (eds.) The three-dimensional facies architecture of terrigenous clastic sediments and its implication for hydrocarbon discovery and recovery: SEPM, Concepts in Sedimentology and Paleontology, 3: 6-12.

Miall, A.D. (1985) *Architectural-element analysis: a new method of facies analysis applied to fluvial deposits*. Earth Science Reviews. 22: 261-308.

Miall, A.D. (1976) *Facies Models 4. Deltas*. In Walker R. (eds) Facies Model Geoscience Canada Vol. 3 (3): 215-227.

Milliken, W.J., Emanuel, A.S. and Chakravarty, A. (2001) Application of 3D streamline simulations to Assist History Matching. SPE Journal 502-508.

Mohamed, L. (2011) *Novel Sampling Techniques in Reservoir History Matching Optimization and Uncertainty Quantification in Flow Prediction*. PhD Thesis. Heriot-Watt University. UK. 377 pp.

Mohamed, L., Christie, M. and Demyanov, V. (2010) *Comparison of Stochastic Sampling Algorithms for Uncertainty Quantification*. SPE Journal March. 31-38.

Moscariello, A. (2005) *Exploration potential of the mature Southern North Sea basin margins: some unconventional plays based on alluvial and fluvial fan sedimentation models*. Geological Society. London. Petroleum Geology Conference Series. 6: 595-605.

Muñoz-Marí, J., Bovolo, F., Gómez-Chova, L., Bruzzone, L. and Capms-Valls, G. (2009) *Semisupervised One-Class Support Vector Machines for Classification of Remote Sensing Data*. IEE Transactions on Geoscience and Remote Sensing. 10 pp.

Mutti, E. and Ricci Lucchi, F. (1972) *Le Torbiditi dell' Appenino Settentrionale: introduzione all' analisi di facies*. Mem. Societa Geol. Ital. 11: 161-199.

North, C.P. (1996) *The prediction and Modeling of Subsurface Fluvial Stratigraphy.* In Carling, P.A. and Dawson, M. R. (eds.) Advances in Fluvial Dynamics and Stratigraphy. John Wiley & Sons Ltd. New York. 395-508.

Nurafza, P.R., King, P.R. and Masihi, M. (2006) *Facies Connectivity Modelling and Field Study*. SPE Paper 100333, Europec/EAGE Conference. Viena. 12 pp.

Okano, H. (2006) *Quantification of uncertainty in coarse-scale relative permeability for reservoir production forecast*. PhD Thesis Heriot-Watt University UK.

Okano, H., Pickup, G. and Christie, M. (2006) *Quantification of Uncertainty due to Sub-grid Heterogeneity in Reservoir Models.* SPE-Paper 100226-MS. 11pp.

Olariu, C. and Bhattacharya, J.P. (2006) *Terminal Distributary Channels and Delta Front Architecture of River Dominated Delta Systems.* Journal of Sedimentary Research. 76: 212-233.

O'Sulivan, A. (2004) *Modelling simulation error for improved reservoir prediction*. PhD Thesis Institute of Petroleum Engineering Heriot-Watt University, Edinburgh UK.

O'Sulivan, A. and Christie, M. (2005) *Solution Error Models : a New Approach for Coarse Grid History Matching*. SPE 93268. Proceedings of the SPE Reservoir Simulation Symposium. Houston, Texas, USA.

Panin, N. (2003) The *Danube Delta. Geomorphology and Holocene Evolution: a Synthesis*. Geomorphologie: relief, processus, environment. 9 (4): 247-262.

Pantin, H.M. (1979) *Interaction between velocity and effective density in turbidity flow: phase-plane analysis, with criteria with autosuspension*. Marine Geology. 31: 59-99.

Pardo-Igúzquiza, E. And Dowd, P.A. (2003) *CONNEC3D: a computer program for connectivity analysis of 3D random set models*. Computers & Geosciences. 29: 775-785.

Park, H., Scheidt, C., Fenwick, D., Boucher, A. and Caers, J. (2013) *History Matching and Uncertainty Quantification of facies models with multiple geological interpretations*. Computational Geosciences :1-13

Park, R.G. (1997) Foundations of Structural Geology. Chapman and Hall. Abingdon. 202 pp.

Peaceman, D.W. (1977) *Fundamentals of Numerical Reservoir Simulation*. Elsevier. Amsterdam. 176 pp.

Pezzetta, J.M. (1973) *The St. Clair River Delta: Sedimentary Characteristics and Depositional Environments*. Journal of Sedimentary Petrology. 43 (1): 168-187.

Pirmez, C. and Imran, J. (2003) *Reconstruction of Turbidity Currents in Amazon Channels*. Marine and Petroleum Geology. 20: 823:849.

Platt, J. (1999) *Probabilistic outputs for support vector machines and comparison to regularized likelihood methods*. In Smola, Bertlett, Schölkopf and Schuurmans (eds) Advances in Large Margin Classifiers. MIT Press.

Pondrelli, M., Rossi, A.P., Platz, T., Ivanov, A., Marinangeli, L. and Baliva, B. (2011) *Geological, Geomorphological, Facies and Allostratigraphic maps of the Eberswalde Fand Delta*. Planetary and Space Science. 59: 1166-1178.

Posamentier, H.W. (2005) *Application of 3D seismic visualization techniques for seismic stratigraphy, seismic geomorphology and depositional systems analysis: examples from fluvial to deep-marine depositional environments*. Geological Society of London. Petroleum Geology Conference Series. Pag. 1565-1576.

Posamentier, H.W. (2003*) D*epositiona*l elements associated with a basin floor channel-levee system: case study from the Gulf of Mexico.* Marine and Petroleum Geology. 20:677-690.

Posamentier, H.W. and Kolla, V. (2003) *Seismic Geomorphology and Stratigraphy of Depositional Elements in Deep-Water Settings*. Journal of Sedimentary Research. V 73 (3): 367-388.

Press, W., Teufolsky, S., Vetterling, W. and Flannery, V. (1988) Numerical Recipes in C: The Art of Scientific Computing. New York. Cambridge University Press.

Pyles, D.R., Jennette, D., Tomasso, M., Beaubouef, R.T. and Rossen C. (2010) *Concepts learned from a 3D outcrop of a Sinuous Slope Channel Complex: Beacon Channel Complex, Brushy Canyon Formation, West Texas, USA.* Journal of Sedimentary Research. 80: 67-96.

Qi, L., Carr, T.R. and Goldstein, R.H. (2007) *Geostatistical Three-Dimensional Modelling of Oolite Shoals, St Louis Limestone, South East Kansas.* AAPG Bulletin, 91 (1): 69-96.

Ramon J.C. and Cross, T.A. (1997) *Characterization and Prediction of Reservoir Architecture and Petrophysical Properties in Fluvial Channel Sandstones, Middle Magdalena Basin. Colombia.* Ciencia, Tecnologia y Futuro. 1: 19-46.

Rasmussen, E.S., Vangkilde-Pedersen, T. and Scharling, P. (2007) *Prediction of reservoir sand in Miocene deltaic deposits in Denmark based on high-resolution seismic data*. Geological Survey of Denmark and Greenland Bulletin 13: 17–20.

Ravane, C., Galli, A., Doligez, B., Beucher, H. and Eschard, R. (2002) *Quantification of Facies Relationships Via Proportion Curves*. Quantitative Geology and Geostatistics. 12: 19-39.

Remy, N., Boucher, A. and Wu , J. (2009) *Applied Geostatistics with SGEMS*. Cambridge. 264 pp.

Renard, P. and Allard D. (2011) *Connectivity Metrics for Subsurface Flow and Transport*. Advances in Water Resources. 51: 168-196.

Renard, P., Straubhaar, J. and Caers, J. (2011) *Conditioning Facies Simulations with connectivity Data*. Mathematical Geoscience. 43: 879-903.

Rhoads, B.L. (1992) *Statistical models of fluvial systems*. Geomorphology. 5: 433-455.

Rivas, D., Rojas, T., Chacartegui, F., Rey, O., Delgado, M. Alezones, R., and Cortiula, B. (1997) *Modelo Sedimentológico de un Sistema Deltaico de Flujo Estacional en Clima Tropical Desértico. Delta del Río Mitare, Estado Falcón, Venezuela.* Memorias del I Congreso Latinoamericano de Sedimentología. Isla de Margarita, Venezuela Vol II. Sociedad Venezolana de Geólogos: 209-216.

Robinson, J.W. and McCabe, P.J. (1997) *Sandstone-Body and Shale-Body Dimensions in a Braided Fluvial System: Salt Wash Sandstone Member (Morrison Formation), Garfield County, Utah*. AAPG Bulletin. 81 (8): 1267-1291.

Roggero, F. and Hu L. Y. (1998) Gradual Deformation of Continuous Geostatistical Models for History Matching. Proceedings of the Annual Technical Conference and Exhibition. SPE -49004: 27-30. New Orleans.

Rojas, T., Demyanov, V., Christie, M. and Arnold, D. (2011) *Use of Geological Prior Information in Reservoir Facies Modelling.* In Marschallinger, R. and Zobl, F. (eds): Mathematical Geosciences at the Crossroads of Theory and Practice, Proceedings of the IAMG-2011 conference, September 5-9 2011, Salzburg, Austria: 266-285.

Rogers ,S.J., Fang, J.H., Karr, C.L. and Stanley, D.A. (1992) *Determination of lithology from well-logs using neural networks*. American Association of Petroleum Geologists Bulletin. 76 (5) 731-739.

Rosgen, D.L. (1994) *A classification of natural rivers*. Catena 22: 169-199.

Saggaf, M.M., Nebrija, Ed L. (2000) Estimation of Lithologies and Depositional Facies from Wire-line Logs. AAPG Bulletin. 84 (10):1633-1646.

Saito, Y., Wei, H., Zhou, Y., Nishimura, A., Sato, Y. and Yokota, S. (2000) *Delta Progradation and Chenier Formation in the Huanghe (Yellow River) Delta, China*. Journal of Asian Earth Sciences. 18: 489-497.

Sambridge, M. (1999a) *Geophysical inversion with a Neighbourhood Algorithm –i. Searching a Parameter Space*. Geophysical Journal International, 138 (2): 479-494.

Sambridge, M. (1999b) *Geophysical inversion with a Neighbourhood Algorithm –ii. Appraising the Ensemble*. Geophysical Journal International, 138 (3): 727-746.

Schilthuis, R.J. (1936) *Active Oil and Reservoir Energy*. Transactions AIME. 118. 35-52.

Schölkopf, B. and Smola, A.J. (2002) *Learning with Kernels: Support Vector* Machines, Regularization, Optimization and Beyond. MIT Press. 644 pp.

Schölkopf, B., Williamson, R.C., Smola, A.J., Shawe-Taylor, J., and Platt, J. (2000) *Support Vector Method for Novelty detection*. In Solla, S.A., Leen., T.K. and Muller K.R. (eds). Advances in Neural Information Processing Systems 12, MIT Press: 582-588.

Schölkopf, B., Platt, J., Shawe-Taylor, J., Smola, A.J. and Williamson, R.C. (2001) *Estimating the support of a high-dimensional distribution*. Neural Computation, 13: 1443-1471.

Schumm, S.A. (1963) *Sinuosity of Alluvial Rivers on the Great Plains*. 74: 1089-1100.

Schumm, S.A. (1967) *Meander Wavelength of Alluvial Rivers*. Science. 157: 1549-1550.

Schumm, S.A. (1968) *River adjustment to altered hydrologic regime. Murrumbidgee River and paleochannels*, Australia. US Geological Survey Professional Paper-598, 65 pp.

Schumm, S.A. (1972) *Fluvial Paleochannels. In J.K. Rigby and W.K. Hamblin (Eds.) Recognition of Ancient Sedimentary Environments.* Society of Economic Paleontologists and Mineralogists. Special Publication 16: 98-107.

Schumm, S.A. (1985) *Patterns of Alluvial Rivers.* Annual Reviews of Earth and Planetary Sciences. 13: 5-17.

Seifert, D. and Jesen, J.L. (2002) *Using Sequential Indicator Simulation as a Tool in Reservoir Description: Issues and Uncertainties*. Mathematical Geology. 31, (5): 527-550.

Seier, A., Evensen, G., Skjervheim, J.A., Hove, J. and Vabo, J.B. (2011) *Using the EnKF for History Matching and Uncertainty Quantification of Complex Reservoir Models.* In Biegler, L., Biros, G., Ghattas, O., Heinkenscholss, M., Keyes, D., Mallick, B., Tenorio, L., van Bloemen Wanders, B. and Willcox, K. (eds.) Computational Methods for Large Scale Inverse Problems and Quantification of Uncertainty.

Serrano-Suarez, B.E. (2003) *The Sinu River Delta on the Northwestern Caribbean Coast of Colombia: Bay infilling Associated with Delta Development.* Journal of South American Earth Sciences.16 (7) 623-631.

Sestine, G. (1989) *Nile Delta a Review of Depositional Environments and Geological History.* In Whateley, M.K.G. and Pickering, K.T. (eds) Deltas Sites and Traps for Fossil Fuels. Geological Society of London, Special Publications. 41: 99-127.

Shang, J.Q., Ding, W., Rowe, R.K. and Josic, L. (2004) *Detecting heavy metal contamination in soil using complex permittivity and artificial neural networks*. Canadian Geotechnical Journal. 41 (6): 1054-1067.

Shanley, K.W. and McCabe, P.J. (1994) *Perspective on the Sequence Stratigraphy of Continental Strata*. AAPG Bullentin. 78 (4): 544-568.

Shepard, R. N. (1962). *The analysis of proximities: multidimensional scaling with an unknown distance function*. Psychometrika, 27, 125-139; 219-246.

Shi, Y. and Eberhart, R. (1998) *A modified particle swarm optimiser.* In: Proceedings of the IEEE International Conference on Evolutionary Computation, IEEE Press, pp. 69–73, Piscataway, NJ, USA.

Slater, G.E. and Durrer, E.J. (1971) *Adjustment of Reservoir simulation Models to Match Field Performance*. Society of Petroleum Engineers Journal. Vol.11 (3) 295-305.

Smith, D.G. and Smith, N.D (1980) *Sedimentation in anastomosing river systems: examples from alluvial valleys near Banff, Alberta*. Journal of Sedimentary Petrology. 50: 157-164.

Smith, R. and Moller, N. (2003) *Sedimentology and reservoir modelling of the Ormen Lange field, mid Norway*. Marine and Petroleum Geology. 20 (6-8): 601-613.

Smola, A.J. and Schölkopf, B. (2004) A tutorial in support vector regression. Statistics and Computing. 14: 199-222.

Sollich, P. (2002) *Bayesian Methods for Support Vector Machines: Evidence and Predictive Class Probabilities*. Machine Learning. 46: 21-52.

Southard, J.B. and Mackintosh, M.E. (1981) *Experimental tests of autosuspension.* Earth Surface Processes and Landforms. 6: 103-111.

Stow, D.A.W. (1994) *Deep-Sea Processes of Sediment Transport and Deposition.* In Pye, K. (ed) Sediment Transport and Deposition Processes. Blackwell Scientific Publications. Oxford. 257-291.

Stow, D.A.W., Reading, H.G. and Collinson, J.D. (1996) *Deep Seas*. In H.G. Reading (Ed.) Sedimentary environments: Processes, Facies and Stratigraphy. Blackwell Science. London. 395-453.

Strebelle, S. B. and Journel, A. G. (2001) *Reservoir Modelling Using Multiple Point Statistics*. Society of Petroleum Engineering Annual Technical Conference and Exhibition New Orleans-Lousiana. SPE-71324, 11 pp.

Strebelle, S.B. (2002) *Conditional Simulations of Complex Geological Structures Using Multiple Point Statistics.* Mathematical Geology, V.34 (1): 1-21.

Suganthan, P. (1999) Particle *swarm optimiser with neighbourhood operator*. In: Proceedings of the Congress of Evolutionary Computation, IEEE Press, 3, pp. 1958–1962, Washington D.C., USA.

Sun, N.Z. (1994) *Inverse Problem in Ground Water Modelling (Theory and Application on Transport of Porous Media)*. Dordrecht, The Netherlands: Kluwer Academic Publishers. 337 pp.

Suzuki, S. and Caers, J. (2008) *A Distance-Based*. Prior Model Parameterization for Constraining Solutions of Spatial Inverse Problems. Mathematical Geosciences. 40: 445-469.

Suzuki, S. and Caers, J. (2006) *History Matching with an Uncertain Geological Scenario*. SPE Paper 102154. San Antonio, TX. 17 pp.

Suzuki, S., Caumon, G. and Caers, J. (2008) *Dynamic Data Integration for Structural Modelling: Model Screening Approach Using a Distance Based Model Parameterization*. Computational Geoscience. 12: 105-119.

Svirsky, D., Rayazanov, A., Pankov, M., Corbett, P.W.M. and Posysoev, A. (2004) *Hydraulic Flow Units Resolve Reservoir Description Challenges in a Siberian Oil Field*. SPE paper 87056-MS. Kuala Lumpur. 15 pp.

Swan, A.R.H. and Sandilands, M. (1998) Introduction to Geological Data Analysis. Blackwell Science. Oxford. 446 pp.

Tavassoli, Z., Carter, J. and King, P. (2004) *Errors in history matching.* Society of Petroleum Engineers Journal. SPE-86883. Vol. 9 (3): 352-361.

Tarantola, A. (2005) *Inverse Problem Theory and Methods for Modelling Parameters Estimation*. Society for Industrial and Applied Mathematics. Philadelphia. 342 pp.

Tarantola, A. (1987) *Inverse Problem Theory. Methods for Data fitting and Model Parameter Estimation*. Amsterdam, The Netherlands: Elsevier Science Publishers. 342 pp.

Teichert, C. (1958) *Concept of Facies*. AAPG Bulletin. 42: 2718-2744.

Thiele, M.R., Batycky, R.P. and Fenwick, D.H. (2000) *Streamline Simulation for Modern Reservoir-Engineering Workflows.* Distinguish Author Series. Journal of Petroleum Technology. 64-70.

Thomas, K., Hellums, L. and Reheis, G. (1972) A *Nonlinear Automatic History Matching Technique for Reservoir Simulation Models*. SPE 3475, 46th Annual Fall Meeting, New Orleans. 508-514.

Torgerson, W. S. (1952). *Multidimensional scaling: I. Theory and method*. Psychometrika, 17: 401-419.

Vapnik, V.N. (1995) *The Nature of Statistical Learning Theory*. Springer, New York. 315 pp.

Vapnik, V.N. (1998) *Statistical Learning Theory*. Wiley, New York. 736 pp.

van den Berg, J. H. (1995) *Prediction of alluvial channel pattern of perennial rivers.* Geomorphology. 12: 259-279.

Verwer, K., Kenter, J. M. A., Maathuis, B. and Della Porta, G. (2004). *Stratal patterns and lithofacies of an intact seismic-scale Carboniferous carbonate platform (Asturias, northwester Spain): A virtual outcrop model.* In Curtis, A. and Wood, R. Geological Prior Information: Informing Science and Engineering. Geological Society Special Publication No. 239, 29-41.

Viseur, S., Shtuka, A. and Mallet, J.L. (2001) *Stochastic Object-Based Simulation of Channels Constrained by High Resolution Seismic Data*. Proceedings from IAMG 2001. Cancun, Mexico. 11 pp.

Walford, H.L., White, N.J. and Sydow, J.C. (2005) *Solid Sediment Load History of the Zambezi Delta*. Earth and Planetary Science Letters. 238: 49-63.

Warne, A.G., Meade, R.H., White, W.A., Guevara, E.H., Gibeaut, J., Smyth, R.C., Aslan, A. and Tremblay, T. (2002) *Regional Controls on Geomorphology, Hydrology and Ecosystem Integrity in the Orinoco Delta, Venezuela*. Geomorphology 44: 273-307.

Whateley, M.K.G. and Pickering, K.T. (1989) *Deltas: Sites and Traps for Fossil Fuels*. Geological Society Special Publication. No.41. Blackwell Scientific. Publications Oxford. 360.pp.

Webster R. and Oliver, M. (2001) *Geostatistics for Environmental Scientists*. John Wiley & Sons, LTD. Chichester. 271 pp.

Wickelmaier, F. (2003) *An Introduction to MDS*. Sound Quality Research Unit. Aalborg University, Denmark. 26 pp.

Wijns, C., Poulet, T., Boschetti, F., Dyt, C. and Griffiths, C.M. (2004). *Interactive inverse methodology applied to stratigraphic forward modelling.* In Curtis, A. and Woods, R. (eds) Geological Prior Information: Informing Science and Engineering. Geological Society of London. Special Publications, 239: 147-156.

Williams, G.P. (1986) *River Meander Channel Size*. Journal of Hydrology, 88: 147-164.

Williams, M.A. and Keating, J.F. (1998) *The Stratigraphic Method: A Structured Approach to History-Matching Complex Simulation Models*. SPE Reservoir Evaluation and Egineering. SPE 38014: 169-176.

Wonham, J.P., Jayr, S., Mougamba, R. and Chuilon, P. (2000) *3D Sedimentary evolution of a Canyon fill (Lower Miocene-age) from Mandrove Formation, offshore Gabon*. Marine and Petroleum Geology. 17: 175-197.

Wood, L. J. and Mize-Spansky, K.L. (2009) *Quantitative Seismic Geomorphology of a Leveed-Channel System Offshore Eastern Trinidad and Tobago, Northeast South-America*. AAPG Bulletin. 93 (1):101-125.

Wood, R. and Curtis, A. (2004) *Geological Prior Information, and its application to geoscientific problems*. In Curtis, A. and Woods, R. (eds) Geological Prior Information: Informing Science and Engineering. Geological Society of London. Special Publications, 239: 1-14.

Wyllie, M.R.J. and Rose, W.D. (1950) *Some theoretical considerations relative to the quantitative evaluation of the physical characteristics of reservoir rock from electric log data*. Journal of Petroleum Technology. 189 105-110.

Wynn, R.B., Cronin, B.T. and Peakall, J. (2007) *Sinuous Deep-Water Channels: Genesis, Geometry and Architecture*. Marine and Petroleum Geology. 24: 341-387.

Yesilnacara, E. and Topal, T. (2005) *Landslide susceptibility mapping: A comparison of logistic regression and neural networks methods in a medium scale study, Hendek region (Turkey)*. Engineering Geology. 79(3-4): 251-266.

Zaitlin, B.A., Dalrymple, R.W. and Boyd, R. (1994) *The Stratigraphic Organization of Incised-Valley Systems Associated with Relative Sea-Level Change*. In Dalrymple, R.W., Boyd, R. and Zaitlin, B.A. (eds) Incised Valley Systems origin and Sequence Stratigraphy. SEPM Special Publication 51.

Zeller, J. (1967) *Meandering Channels in Switzerland.* In symposium of river morphology. International Association of Science Hydrology. Publication 75: 174-186.